Development of synthetic cooperative consortia using genetic engineering and adaptive laboratory evolution in yeasts.

Dissertation

zur Erlangung des Doktorgrades

der Naturwissenschaften

vorgelegt beim Fachbereich Biowissenschaften

der Johann Wolfgang Goethe-Universität

in Frankfurt am Main

von

Leonardo Javier Beltrán Guzmán

aus Quito, Ecuador

Frankfurt am Main, 2023

D 30

Vom Fachbereich Biowissenschaften der

Johann Wolfgang Goethe - Universität als Dissertation angenommen.

Dekan: Prof. Dr. Sven Klimpel

Gutachter: Prof. Dr. Eckhard Boles
Prof. Dr. Claudia Büchel

Datum der Disputation:

Contents

List of Figures

List of Tables

Chapter: 1 Introduction

1.1   Biotechnology for production of goods of interest

The use of microorganisms for industrial purposes is not novel. For centuries or even millennia, microorganisms have been employed during empirical methods for the production of cheese, yogurt, bread, and fermented beverages, converting raw materials into valuable goods. However, the advent of genomic technologies represented a new era for microbial production, allowing for careful tuning of metabolic pathways or even the incorporation of foreign genes into host organisms.

This innovation facilitated the creation of substances that were not conventionally part of their metabolic processes, thereby causing a revolutionary impact on the industry, such as the production of human insulin from bacterial and yeast cultures (Goeddel et al. 1979). Nowadays, goods of great relevance to our society, such as energy, materials, chemicals, and even drugs, find in biotechnological processes new avenues for production in cleaner, safer, and environmentally responsible ways (Ajikumar et al. 2010; Hansen et al. 2009; Schrader et al. 2009; Stalidzans & Dace 2021; H. Zhang, Pereira, et al. 2015).

The production processes of primary and secondary metabolites, as well as enzymes and compounds of pharmaceutical interest, have been improved by the use of mutations and recombinant DNA processes (Adrio & Demain 2010). For instance, by employing random mutagenesis and specific plasmid expression systems (Kirchner & Tauch 2003), the gram-positive bacterium *Corynebacterium glutamicum* has been extensively used for production of the amino acids L-glutamate and L-lysine, reaching in many cases levels of industrial relevance (Adrio & Demain 2010; Chinen et al. 2007; Q. Liu et al. 2008; Sahm et al. 2000).

However, easily reaching high production is not the norm in biotechnological production. Metabolic transformation processes do not always render the expected results regarding production, which frequently negatively affects organism physiology (Van Dien 2013). After a complex pathway transformation, optimisation protocols often prioritise addressing toxic intermediate molecules or low enzymatic activity. This involves identifying bottlenecks and creating iterative design-build-test-learn cycles. (S. Y. Lee & Kim 2015; Wu et al. 2016).

Another frequently explored concept to improve low-production titers is the metabolic

burden caused by engineered pathways. This concept represents "the proportion of the resources a host cell – either energy molecules of carbon building blocks – that are used to construct and operate engineered pathways" (Glick 1995; Wu et al. 2016). Detrimental examples have been described for *Azotobacter vinelandii* and *Pseudomonas putida*, in which increasing plasmid copy number expression has compromised critical features of these organisms, such as the ability to fix nitrogen or to produce siderophores, respectively, (Glick et al. 1986; Glick 1995; Y. Hong et al. 1991). However, the increasing complexity of the metabolic pathways employed makes it difficult to predict or even identify metabolic burden effects, opening the possibility of misidentifying them as effects derived from toxic intermediate or low enzyme activity.

1.2 Use of consortia in synthetic biology

As an alternative to address the constraints mentioned above, efforts to develop engineered systems are increasingly focusing on developing and using microbial consortia (Brenner et al. 2008; Darvishi et al. 2022). In nature, microbial life is found only as part of complex communities, which allows these entities to display more robust properties than what its members would exhibit as individuals, such as environmental endurance or the use of complex carbon sources (Fierer 2017; McCarty & Ledesma-Amaro 2019; Stenuit & Agathos 2015). This success is attributed to the compartmentalisation of complex functions into multiple organisms, a process known as division of labour (Brenner et al. 2008), and to a communication system between members of a consortium, either by exchanging metabolites or responding to signal molecules (Brenner et al. 2008; Campbell et al. 2015; Keller & Surette 2006).

Many attempts have been made to employ this concept for production. For instance, single-species consortia employing *E. coli* have been developed for the production of n-butanol (Saini et al. 2015) or amino benzoic acid (H. Zhang & Stephanopoulos 2016) from glucose, the production of flavonoids from a mixture of glycerol and *p*-coumaric acid (J. A. Jones et al. 2016), or allowing the use of complex substrates such as xylose in mixture with glucose for the production of muconic acid (H. Zhang, Li, et al. 2015). Single-species consortia using *Pichia pastoris* allowed for the production of the statins monacolin-J and lovastatin from methanol (Y. Liu et al. 2018). However, better examples of the potential of this approach are mixed domain consortia, such as *Clostridium phytofermentans* and *Saccharomyces cerevisiae*, which allow the transformation of α-cellulose into ethanol, *Trichoderma reesei* and *E. coli* for the production of isobutanol from cellulosic biomass (Minty et al. 2013) or a consortia employing *Lactobacillus plantarum* and *S. cerevisiae*

for improved riboflavin secretion (Konstantinidis et al. 2021).

Although there have been significant production enhancements shown through certain approaches, such as a 970-fold increase in flavonoids and a 15-fold increase in amino benzoic acid reported in studies from J. A. Jones et al. 2016 and H. Zhang and Stephanopoulos 2016, respectively, there are still limitations that must be addressed to achieve further progress in microbial production (Lindemann et al. 2016). One major obstacle in applying this technology is achieving and maintaining a proper microbial ratio among the populations used (Jawed et al. 2019). Studies have shown that factors such as differences in doubling time, response to toxic by-products, substrate competition, and even culture volume can affect consortia configuration and impact the overall performance (Shou et al. 2007; K. Zhou et al. 2015). To address this issue, some have suggested fine-tuning during inoculation as an alternative to reach desired microbial ratios. However, population fluctuations can make it challenging to achieve consistent results (Jawed et al. 2019; J. A. Jones & Koffas 2016; Z. Li et al. 2019).

1.2.1   Types of consortia

Microbial consortia are ubiquitously found in nature. Every population interacts with each other to achieve resilience to environmental conditions and relative stability that allows them to obtain such endurance (Brenner et al. 2008; McCarty & Ledesma-Amaro 2019). Among the most relevant kinds of natural microbial interactions (see Figure 1.1), only commensalism, predation, and cooperation have been explored due to their potential for developing stable populations systems.

1.2.1.1   Commensalism

Commensalism represents the classic approach, arranging the transformation process in sequential order; this feature allows the degradation of complex or even toxic compounds, distributing the labour of further metabolite disposal to other consortia members. The literature describes many interesting examples of this approach, such as the production of the copolymer poly(3-hydroxybutyrate-co3-hydroxyvalerate) from sucrose, utilising a consortium including *Bacillus subtilis* and *Ralstonia eutropha* (Bhatia et al. 2018).

However, incompatibility among the strains limits this sort of mixed consortia, which might require different environmental conditions for optimal operation (H. Zhang & Wang 2016). Single species consortia have been employed to bypass this limitation, as the full consortia will share equal optimal conditions (Jawed et al. 2019). For instance, narin-
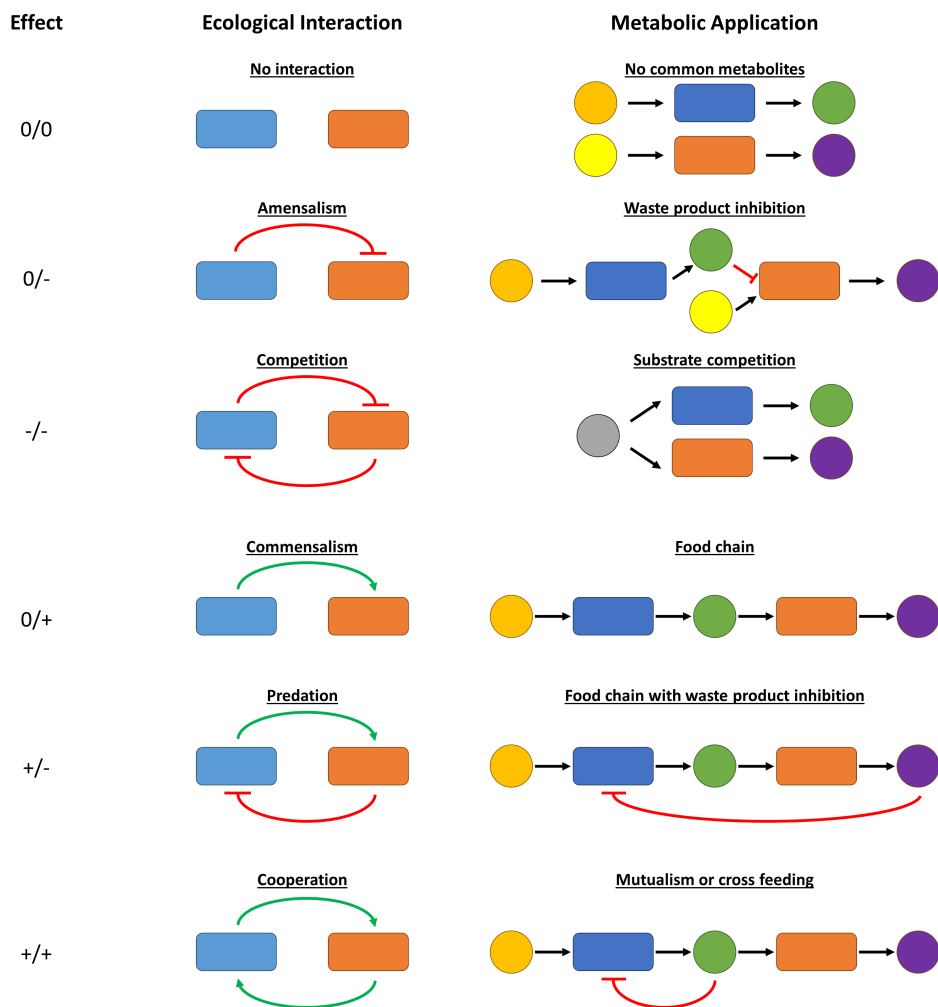
Figure 1.1: Microbial interaction motifs. Schematic representation of the principal motifs behind microbial interactions. Positive (+), negative (-) or neutral (0) effects are described for each one of the interaction systems. Rectangular figures describe microbial populations, while circular marks represent either substrates or metabolites produced by microbial species. Green and red arrows represent stimulating or inhibitory interactions, respectively. Adapted from Grosskopf and Soyer 2014 and Sgobba and Wendisch 2019.

genin production using a consortium with *E. coli* that would first produce tyrosine and *p*-coumaric acid for a subsequent transformation into naringenin by the second strain (Ganesan et al. 2017). However, this approach limits the exploitation of the metabolic potential of specific chassis organisms. A more in-depth discussion and examples about these types of consortia can be found in Jawed et al. 2019 and Sgobba and Wendisch 2019.

Additionally, the chemical nature of intermediate molecules might present limitations to the trafficking process, preventing its mobility between consortia conformant strains, forcing the design and implementation of membrane transport proteins (Jawed et al. 2019; K. Zhou et al. 2012).

1.2.1.2 Predation

Predation represents an interesting approach for reaching controllable consortia popula-
tions. Quorum sensing mechanisms are chemical communication systems that allow mi-
croorganisms to establish a cell-cell communication system. Usually, they convey infor-
mation regarding extracellular conditions or intracellular physiological status to prompt
quick response and adaptation (Camilli & Bassler 2006). Balagaddé et al. 2008 engi-
neered a single species consortia using *E. coli* that recreated a predator-prey system
using this signalling mechanism. The predator strain carried a constitutive suicide gene,
an effect rescued by a quorum-sensing molecule (antidote) secreted by the prey strain,
effective only under a specific cell density. However, predator strains at its time produce
another quorum-sensing molecule (poison) that triggers the expression of a suicidal gene
in the prey strain. In this way, a consortium dominated by the prey strain would eventu-
ally rescue the predator, affecting its survival and producing oscillation cycles depending
on their cell densities.

Balagaddé et al. 2008 discovered that if the consortium starts at a specific high cell den-
sity, oscillations between populations are avoided as quorum sensing modules act simul-
taneously rather than intermittently. However, they also describe that such engineered
stabilisation attempts will eventually be disrupted due to natural selection mutations
that will disrupt the original design (Balagaddé et al. 2008).

Increasing the size of the consortia to utilise more than two strains has also been ex-
plored to achieve better stability in the long term, e.g. a "rock-paper-scissor" system
employing interaction between three *E. coli* strains (Liao et al. 2019). Although this
approach proved more effective for achieving consortia stability, its application for pro-
duction purposes grows unappealing due to the complexity of networks required to reach
an efficient division of metabolic labour among the participant strains.

1.2.1.3 Cooperation

Cooperative systems allow for an alternative that avoids the above-discussed limita-
tions. Using strains whose survival depends on mutual collaboration establishes a cross-
feeding regimen that promotes survival and stability among conformant strains while
taking advantage of their engineered or natural metabolic capacities (McCarty & Ledesma-
Amaro 2019).

For instance, a cooperative consortium between *Sporomusa ovata* and *Citrobacter amalo-
naticus Y19* was devised to convert CO into acetate, employing the natural CO oxidising

capacity of *C. amalonaticus Y19* to produce CO_2 and H_2, byproducts that later were used by *S. ovata* to produce acetate and biomass (C. R. Lee et al. 2018). This elegant configuration reportedly allowed better production titers in consortia than what these individual organisms could achieve alone (C. R. Lee et al. 2018).

Aiming for a stable system that allows for tunable conformant species proportions, Kerner et al. 2012 engineered a cooperative system using two *E. coli* strains auxotrophic for tyrosine and tryptophan, respectively. In response to specific inducer signals, these strains modulated their amino acid secretion to feed their companion strain, allowing for a continuous tuning capacity.

After engineering key auxotrophies, Sgobba et al. 2018 engineered an *E. coli-C. glutamicum* consortia able to convert starch into lysine, cadaverine and pipecolic acid. The *E. coli* faction auxotrophic for lysine but able to secrete *α*-amylase would convert starch into glucose, allowing its usage for itself and also feeding the *C. glutamicum* faction, that besides cadaverine and pipecolic acid, would provide the lysine required by the *E. coli* to supplement for its auxotrophy.

This kind of elegant consortia maximises the metabolic capacities of highly efficient organisms such as *C. glutamicum* for the production of amino acids, but it leaves little space for product or substrate diversification as genetic modifying tools or extensive knowledge about metabolic pathways are insufficient among many microorganisms of industrial interest.

1.2.2 Game theory

Cooperative behaviours can establish an efficient division of labour, resulting in a relatively stable population representation in a co-culture (McCarty & Ledesma-Amaro 2019). The stability primarily depends on the adequate production of exchange molecules that would complement the auxotrophies of both parties (Cavaliere et al. 2017; Konstantinidis et al. 2021).

However, dependency on the availability of common goods for a system's survival is a controversial topic in evolutionary biology, as it predicts that organisms will choose to exploit common resources while cutting out expenditures related to their production (West et al. 2007). These "cheater" cells would possess a competitive advantage against cooperator strains, allowing them to invade and take over the population (Hummert et al. 2014; Sanchez et al. 2013; West et al. 2006).

(A)

	Cooperate	Defect
Cooperate	*b-c* / *b-c*	*b* / *-c*
Defect	*-c* / *b*	*0* / *0*

(B)

Round	🟢	🔴	Payoff
1st	C	D	*-c / b*
2nd	D	D	*0 / 0*
3rd	C	C	*b-c / b-c*
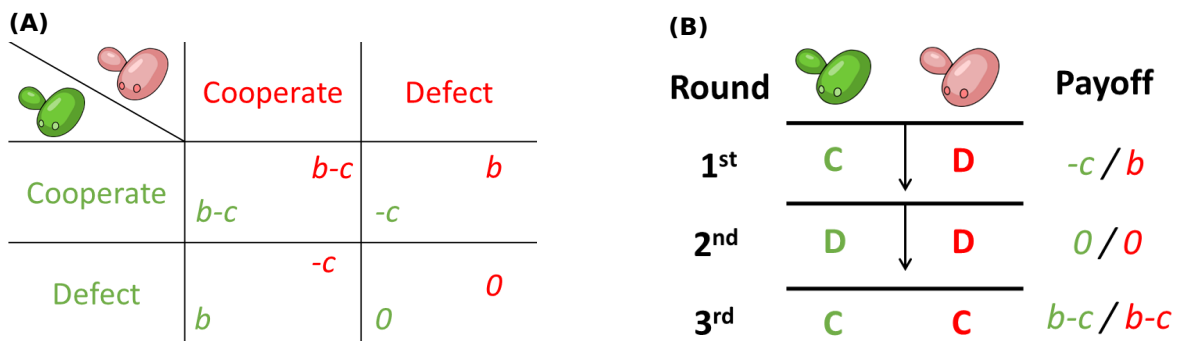
Figure 1.2: Schematic representation of the Prisoner's Dilemma (PD). Game players are represented in different colours. **(A)** Basic PD arrange, when both players cooperate, both incur in a cost (c) but receive a benefit (b), establishing a balance rewards of b-c, which symbolises the best scenario in the system. However, when one cooperates and the other defects, the cooperating party just performs the cost, while the defecting player only receives the benefit. While this is the best scenario for defectors, is the worst for cooperators. If both parties defect, neither will receive a benefit but also, no one will incur in any cost, generating a zero (0) reward balance. While this last is the worst scenario in the system, it represents its most stable point, as either player's reward can be decreased by the sole action of the other player (Nash equilibrium). **(B)** Representation of rewards obtained after three PD iterations. Individual behaviours are described for each player as C (cooperate) and D (defect). Payoffs column describes individual players' rewards according to the specified colour code. Adapted from Doebeli and Hauert 2005.

This scenario is often called the "tragedy of the commons", where public goods produced through communal effort are exploited by individuals who do not contribute to their production. As a result, cooperation that could lead to better rewards for all is replaced by selfish exploitation that provides short-term gains at the expense of the community (Hardin 1968; MacLean & Gudelj 2006; West et al. 2007).

Game theory scenarios have been used to better understand the success of cooperative consortia in nature, trying to reconcile how the search for individual interests matches the interest of a group.

The Prisoner's Dilemma (PD) is maybe the most recurrent scenario trying to address cooperation in biology (see figure 1.2). In its most straightforward format, it involves two players in a cooperative system, and both are given two options: to cooperate or defect. If both choose to defect, both will receive a reward lower than what they would have received if they decided to cooperate. However, if just one cooperates and the other defects, the last would receive the largest reward and the cooperator the lowest possible recompense. An equilibrium state is reached when neither player can improve their gains by alone changing its behaviour, which is reached with both players defecting, granting them both a low reward, but higher than what they would obtain if they cooperate and the other part cheat (Nash 1950; Stewart & Plotkin 2012) (see figure 1.2A).

The application of this principle to biological systems would mean the failure of any cooperation, as parties would avoid the risk that cooperative behaviours are met with defection from the other player. However, the ever-adapting nature of biological systems allows for different scenarios of the PD to explain cooperation, as it would involve iterative cycles permitting the parties to respond to the outcomes of the previous round (Kraines & Kraines 2000). It has been proposed that a "Win-stay Lose-Switch" like strategy, together with iterative PD rounds, could help explain the origin of cooperation in biological systems (Doebeli & Hauert 2005; Kraines & Kraines 2000).

This means that when a party receives a high payoff during a PD cycle, it will retain the same behaviour for the next cycle. However, if the payoff is low, it will change its behaviour irrespective of what it was in that cycle, eventually producing and sustaining a cooperation-cooperation panorama (see figure 1.2B).

Greig and Travisano 2004 provided a practical approximation to this theory while studying the secretion of sucrose invertase in cultures of *S. cerevisiae*. They propose that the high variability in the *SUC* family genes (Carlson & Botstein 1983) is the product of a constant adaptation to environmental conditions. Under abundant sucrose (composed of glucose and fructose subunits) and single sugars panorama, cells with healthy or carrying multiple *SUC* genes will prosper. However, when monosaccharides availability increases, *suc* strains will become fitter by being able to benefit from freely accessible resources until they are depleted, a moment in which activation or duplication of *SUC* genes will become again advantageous.

The researchers suggested similarities between this system and the PD, as the monosaccharides produced after invertase secretion represented a common good that, when abundant, could be exploited by "cheater" cells. Cells are encouraged to become better adapted to the prevailing scenario, leading to silencing or deleting *SUC* copies, even allowing for copy number variations of the *SUC2* gene. However, when sucrose is prevalent, the incentive runs in the opposite direction, promoting invertase secretion, which is enhanced after activating or increasing copies of *SUC*. In this way, a positive reward (plenty of monosaccharides) would sustain the same behaviour, while a negative reward (starvation) would encourage a change (Greig & Travisano 2004).

However, this interpretation of data has also been disputed by several groups, proposing different explanations for this and other interactions among microorganisms (Doebeli & Hauert 2005; Gore et al. 2009; Hummert et al. 2014; Schuster et al. 2008). This discussion shows the vastness of the field and how much is still to be described behind

the evolution of cooperation among biological systems.

Interestingly, it has been proposed that yeast, particularly *S. cerevisiae*, can produce and secrete nutrients in concentrations enough to supplement the growth of auxotrophic neighbouring cells, creating heterogeneous colonies that feed from nutrient pools (Campbell et al. 2015). This report portrays nutrient production and secretion as a naturally occurring phenomenon, disregarding the metabolic burden placed upon producer cells, which would also differ for more 'expensive' produced goods. Recent evidence has reduced the scope of these freely exchanged metabolites (Aulakh et al. 2023), but the limited variety of molecules and naturally produced titers that can sustain these synergistic communities would still restrict their potential use in industry.

1.3 Genetic engineering of yeasts for cooperative consortia

Previously, it was mentioned that the utilisation of biological tools for converting raw materials into valuable products while implementing more gentle and eco-friendly processes signifies a paradigm shift in industrial production (Ajikumar et al. 2010; Stalidzans & Dace 2021; H. Zhang, Pereira, et al. 2015). However, the full potential of microorganisms' capabilities is often hindered by our understanding of their physiology, metabolism, and genetic capabilities (S. Y. Lee & Kim 2015; McCarty & Ledesma-Amaro 2019).

Model organisms offer an alternative for introducing heterologous pathways in hosts where there is a better understanding of their metabolisms and genetic modification capabilities. In this regard *S. cerevisiae* stands out as a widely used eukaryotic model organism which requires relatively simple handling conditions, with well-established genetic modification tools that offer robustness for industrial production processes (M. Li & Borodina 2015; McCarty & Ledesma-Amaro 2019). These reasons have turned *S. cerevisiae* into a favourite organism for the production of fine chemicals and heterologous proteins (Brückner et al. 2018; Fathi et al. 2021; Garces Daza et al. 2023; Hou et al. 2012; Mafakher et al. 2010; R. S. K. Walker & Pretorius 2018).

These features have also fuelled the use of *S. cerevisiae* during the research of synthetic consortia, providing valuable insights into the development and regulation of cross-feeding systems and population control processes. Shou et al. 2007 demonstrated that such cooperative systems can be created relatively simply after punctual modifications to create complementary profiles among the participating strains. This rationally

designed system based on the exchange of lysine and adenine successfully sustained its development across a wide range of initial cell density conditions, producing a relatively stable cell proportion state after 200 h of fermentation (Shou et al. 2007). Later, these results were complemented by studying how the system responds to the invasion of cheater strains, suggesting that consortia survival depends on an "adaptive race" that favours fast growth, leaving to chance if cooperators or cheaters would succeed in taking over the population (Waite & Shou 2012). However, it is unclear what prevents that after a cooperator strain has won an initial race stage, it finds its prevalence challenged by fitter descendants that conserving favourable mutations eliminates overproducing variants.

More recently, it has been proposed that *S. cerevisiae* can naturally develop and sustain cooperative consortia by exchanging nutrients without the need for genetically engineered overproducing mutations (Aulakh et al. 2023; Campbell et al. 2015). These would consolidate *S. cerevisiae* as an attractive model for developing cooperative consortia, exploiting its resilience to harsh conditions and its already naturally occurring metabolite exchange systems. However, the current range of molecules in this exchange system limits its practicality for production processes,

1.4   Adaptive laboratory evolution

The natural capacities of *S. cerevisiae* have consolidated this microorganism as an attractive host for the production of valuable goods. However, disciplines such as genetic and metabolic engineering have allowed to expand the range of its capacities, allowing the use of a broader substrate base such as xylose (Osiro et al. 2019) or arabinose (J. Becker & Boles 2003) and production of non-native compounds such as trans-cinnamic acid (Gottardi, Knudsen, et al. 2017), taxadiene (Nowrouzi et al. 2020) or compounds of pharmaceutical interest such as cannabinoids (Luo et al. 2019), proving to be fundamental assets for biotechnology development. Nevertheless, process optimisation based only on these tools can be tedious and extensive, requiring detailed knowledge of every enzymatic step, especially when cells are subjected to multiple modifications (Shepelin et al. 2018; Wegner et al. 2015).

Adaptive laboratory evolution (ALE) complements the previously mentioned disciplines as a way to harness the mutation capacity and short replication times of microorganisms to improve adaptation to environmental conditions (Dragosits & Mattanovich 2013; Portnoy et al. 2011). Microorganisms cultivated for prolonged periods during subse-
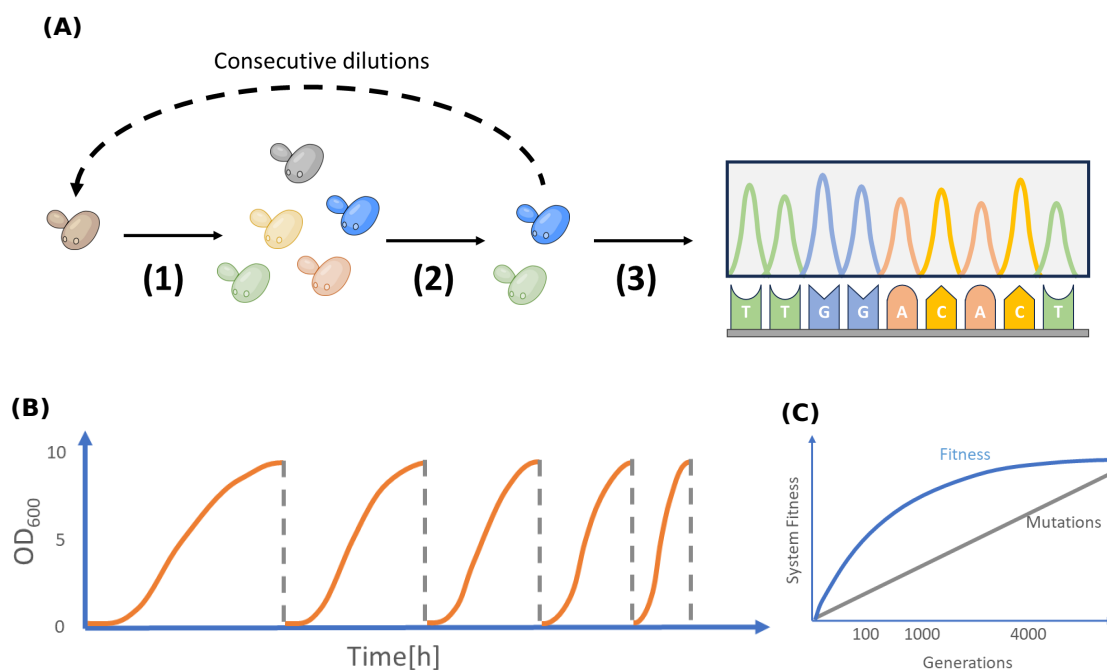
Figure 1.3: Adaptive laboratory evolution representation. **(A)** Basic representation of different steps depicting an adaptive laboratory evolution process. (1) Initial culture generates genetic diversity after initial divisions. (2) Selective conditions favour more advantageous mutations, allowing these mutants to overcome the culture. (3) Genetic analysis of mutants will reveal favourable mutations responsible for their improved fitness. Dashed line represents iterative cycles in which better-adapted strains are used for consecutive dilutions, optimising the generation of favourable mutations. **(B)** Graphical model of consecutive dilutions during an ALE experiment; with each passage, the time required for culture saturation gets shorter. **(C)** Conceptual representation of the mutation's accumulation across generations and the fitness improvement during an ALE experiment. Adapted from Shepelin et al. 2018 and Dragosits and Mattanovich 2013.

quent dilutions and under specific stress conditions can potentially select for randomly occurring mutations that offer a better adaptation under such environments (Dragosits & Mattanovich 2013; Shepelin et al. 2018).

ALE implementation process can be divided into three stages: first, a diverse gene pool is generated in the initial population; second, after exposing the population to selective conditions during cultivation, more advantageous mutations tend to lead the better-adapted mutants to dominate the culture; third, the population is analysed to isolate individual mutants and establish a relationship between identified mutations and the improved phenotype observed. Iterative repetition rounds of the first and second steps can contribute to accumulating favourable mutations, further enhancing the evolved strain's fitness with each round (see figure 1.3).

The identified mutations can later be back-engineered into clean background strains for consecutive ALE experiments or to complement further genetic engineering processes (Shepelin et al. 2018). In this way, it is possible to achieve counterintuitive modifications that affect strain's performance by modification spanning multiple pathways (S. Lee &

Kim 2020)

This approach has been successfully employed in yeast research, for example, during improved production of organic acids such as succinic (Otero et al. 2013), and muconic acid (Leavitt et al. 2017), which after a genetic engineering step were evolved to produce mutant prototrophic strains for the precursor employed, effectively improving cell fitness and overall production. During a glucose-xylose co-fermentation study, mutations obtained after sequencing of evolved strains proved valuable not only for reproducing the observed phenotype but for the development of more efficient strains while combined with previously known favourable mutations (Papapetridis et al. 2018). A more extensive compilation of the application of adaptive laboratory evolution for producing industrial-relevant compounds in common and uncommon organisms can be found in S. Lee and Kim 2020 work.

However, ALE effectiveness depends on precisely applying an adequate selective pressure during fermentation (Shepelin et al. 2018). This feature makes ALE a promising tool for improving our understanding of how *S. cerevisiae* metabolite exchange occurs during co-culture development. It may even allow us to extend this understanding beyond previously described interactions and towards other pathways of industrial interest.

1.5   Central carbon metabolism

The development of cooperative consortia demands that each party produce enough components to sustain its own growth and for the production of the molecules to be exchanged. Carbohydrates such as glucose or fructose store the chemical energy and build molecules that yeast utilises to maintain its internal metabolic processes and growth. The import of these molecules into yeast cells is done via facilitated diffusion aided by a family of hexose transporters involving 20 members, which present different affinities for their substrates, allowing a fine-tuning for import mechanisms based on extracellular nutrient availability (Compagno et al. 2014; Kaniak et al. 2004; Sabina & Johnston 2009).

Once inside the cell, sugars are oxidised in a multi-step process called glycolysis that produces two molecules of pyruvate and energy in the form of two molecules of ATP and NADH per glucose molecule (Compagno et al. 2014) (see figure 1.4). First, a hexokinase transfers a phosphate group from an existing ATP to the hexoses producing glucose-6-phosphate (G6P) or fructose-6-phosphate (F6P) from glucose and fructose, respectively (Compagno et al. 2014; Dickinson & Schweizer 2004). These molecules are interconverted between each other by the action of the phosphoglucose isomerase
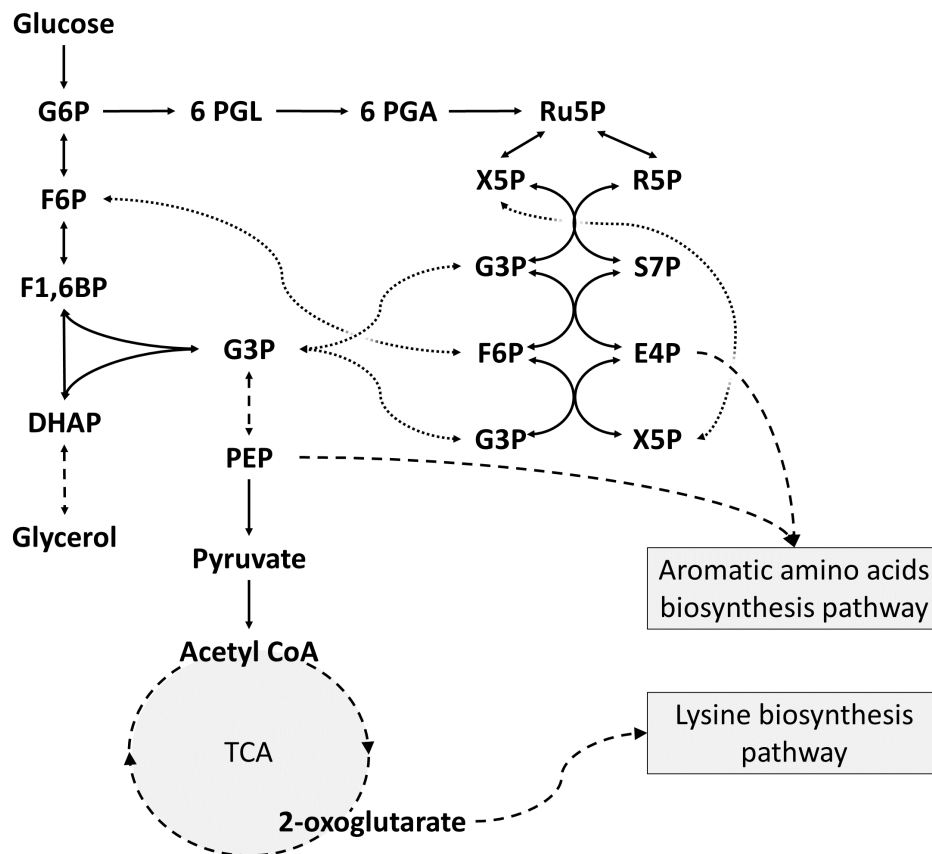
Figure 1.4: Representation of basic carbon metabolism in yeast. Depiction of glycolysis and the pentose phosphate pathway in yeast. Straight lines indicate single reactions, while dashed lines represent multiple reaction processes. Arrowheads represent the directionality of the transformations. Dotted lines represent similar molecules produced at different points in the pathways. Precursors for the aromatic amino acid and lysine biosynthesis pathways are indicated. G6P, glucose-6-phosphate; F6P, fructose-6-phosphate; F1,6BP, fructose-1,6-biphosphate; DHAP, dihydroxyacetone phosphate; G3P, glyceraldehyde-3-phosphate; PEP, phosphoenolpyruvate; 6PGL, 6-phosphogluconolactone; 6PGA, 6-phosphogluconate; Ru5P, ribulose-5-phosphate; X5P, xylulose-5-phosphate; R5P, ribose-5-phosphate; S7P, sedoheptulose-7-phosphate; E4P, erythrose-4-phosphate; TCA, tricarboxylic acid cycle. Adapted from Dickinson and Schweizer 2004.

Pgi1p (Aguilera 1986; Boles et al. 1993). Another ATP molecule is used to phosphorylate F6P into fructose-1,6-biphosphate (F1,6BP) (Dickinson & Schweizer 2004), which later on is divided by the aldolase Fba1p into dihydroxyacetone phosphate (DHAP) and glyceraldehyde-3-phosphate (G3P) (Lobo 1984). While these molecules are interconvertible by the action of Tpi1p (Compagno et al. 2001), just G3P is required for continuing the pyruvate production (Compagno et al. 2014; Dickinson & Schweizer 2004).

The G3P oxidation process is catalysed by the glyceraldehyde-3-phosphate dehydrogenase family, which reduces a NAD^+ producing a NADH and a 1,3-biphosphoglycerate molecule (McAlister & Holland 1985), whose energy-rich phosphate group is used by the phosphoglycerate kinase Pgk1p, to regenerate an ATP and 3-phosphoglycerate (Hitzeman et al. 1980). During the next step of glycolysis, this molecule is converted by the

phosphoglycerate mutase Gpm1p (Rodicio et al. 1993) into 2-phosphoglycerate which is substrate mainly for the enolase Eno2p producing phosphoenolpyruvate (PEP) (Entian et al. 1987; McAlister & Holland 1982).

The pyruvate kinase uses this central molecule's high-energy phosphate group to re-cover another ATP molecule producing pyruvate (Pearce et al. 2001). This molecule represents a central branch-point for cell metabolism, as it may be fermented into ethanol or oxidised via the tricarboxylic acid cycle (TCA) (Dickinson & Schweizer 2004).

Pyruvate consumption through the TCA cycle is energetically more favourable than fermentation; however, *S. cerevisiae* shows a preference for its fermentative consumption even when oxygen is available (Pronk et al. 1996). In this way, cytosolic pyruvate is first converted into acetaldehyde by the pyruvate decarboxylases Pdc1p, Pdc5p, and Pdc6p (Hohmann 1991; Kellermann et al. 1986; Seeboth et al. 1990) releasing a CO_2. The acetaldehyde is then reduced by alcohol dehydrogenases Adh1p, Adh3p, Adh4p, and Adh5p, into ethanol regenerating the NAD^+ used during glycolysis (Dickinson & Schweizer 2004; Piškur & Compagno 2014; Young & Pilgrim 1985).

The major oxidative degradation of pyruvate requires first that it is transported into the mitochondria, which convert it into acetyl-CoA to be later incorporated into the TCA cycle. This transformation is performed by the pyruvate dehydrogenase complex composed of five subunits: PDA1 (E1α), PDB1 (E1β), LAT1 (E2), LPD1 (E3) and PDX1 (protein X) (Dickinson & Schweizer 2004). Additionally, pyruvate can also enter the TCA cycle in the form of oxaloacetate, which is formed from pyruvate by the pyruvate carboxylases Pyc1p and Pyc2p (Stucka et al. 1991; M. E. Walker et al. 1991). This process helps to replenish the oxaloacetate pool for this cycle (Dickinson & Schweizer 2004).

The TCA cycle is the cell's most significant carbon oxidation system, generating crucial precursors for cellular compounds and the biosynthesis of several amino acids. For example, lysine biosynthesis derives from one of its intermediate molecules, 2-oxoglutarate (Feller et al. 1999), that is produced after the sequential transformation of citrate into isocitrate (Cupp & McAlister-Henn 1991; Gangloff et al. 1990; Haselbeck & McAlister-Henn 1991, 1993; Piškur & Compagno 2014). Initial citrate is produced after the condensation of acetyl-CoA and oxaloacetate catalysed by citrate synthases Cit1p and Cit3p (Graybill et al. 2007; Kim et al. 1986).

Parallel to glycolysis, *S. cerevisiae* possesses another carbon metabolic pathway of great importance for its production of reducing potential and cell building blocks production,

the pentose phosphate pathway (PPP) (see figure 1.4) (Bertels et al. 2021; Dickinson & Schweizer 2004). The PPP is described to encompass two branches: an oxidative irreversible that generates NADPH molecules, allowing the cell to cope with oxidative stress and a second non-oxidative reversible branch that provides precursors for nucleotides and aromatic amino acids (Bertels et al. 2021).

The first reaction of the oxidative branch begins from G6P, which is converted to 6-phosphogluconolactone (6PGL) by the glucose-6-phosphate dehydrogenase Zwf1p (Nogae & Johnston 1990). This step is of particular interest in yeast physiology as it is a primary source of NADPH, providing reducing power for the synthesis of lipids and amino acids and aiding in the control of reactive oxygen species by allowing the regeneration of reduced glutathione (Bertels et al. 2021).

The conversion of 6PGL into 6-phosphogluconate (6PGA) is considered to be catalysed in yeast by the 6-phosphogluconolactonases Sol3p and Sol4p (Bertels et al. 2021; Brown et al. 2006; Stanford et al. 2004), which is later converted into ribulose-5-phosphate (Ru5P) by the 6-phosphogluconate dehydrogenases Gnd1p and Gnd2p yielding also an NADPH (Dickinson & Schweizer 2004; Lobo & Maitra 1982).

Metabolism of R5uP can then follow two directions, epimerization to xylulose-5-phosphate (X5P) by the ribulose-5-phosphate 3-epimerase, Rpe1p, or isomerization to ribose-5-phosphate (R5P) by the ribose-5phosphate ketolisomerase, Rki1, (Miosga & Zimmermann 1996). The following steps of the PPP are characterised by joint reactions between these two products or their byproducts in each step. First the transketolases Tkl1p and Tkl2p convert X5P and R5P into G3P and sedoheptulose-7-phosphate (S7P), respectively (Fletcher et al. 1992; Sundström et al. 1993), products that then can be converted by the transaldolase Tal1p into F6P and erythrose-4-phosphate (E4P) (Schaaff et al. 1990). Finally, a Tkl1p and Tkl2p transketolases mediated activity can transform the X5P and E4P into G3P and F6P and vice versa (Dickinson & Schweizer 2004).

It is important to highlight that the F6P, G3P or X5P produced during the PPP are not compartmentalised and can openly be integrated into glycolysis or into different reactions across the PPP (see figure 1.4) (Bertels et al. 2021). In this manner, the PPP is of great importance for cell physiology as it provides NADPH, a required cofactor of a multitude of reactions; ribose skeletons, needed for synthesis of histidine, purine and ribo- and deoxynucleotides; and also for the production of E4P which together with the glycolysis intermediate molecule PEP, acts as precursor for the aromatic amino acids tyrosine, phenylalanine and tryptophan (Dickinson & Schweizer 2004).

Interestingly, in spite that the carbon flow into PEP is higher than into E4P, less of this flow ends in the production of aromatic amino acids, as the fermentative degradation of pyruvate diverts most of it, allowing just a 1% of the flow to reach this pathway (Blank et al. 2005). This particular feature of yeast has motivated central carbon metabolism rewiring attempts, for example, disrupting the oxidative branch of the PPP by deleting the G6P dehydrogenase Zwf1p and overexpressing the transketolase Tkl1p to reverse the flow in the non-oxidative branch from F6P and G3P into E4P and X5P (Curran et al. 2013), or a less successful attempt that combined the G6P dehydrogenase Zwf1p deletion with a down-regulation of the major pyruvate kinase Pyk1p seeking to increase the PEP cellular pool (Gold et al. 2015).

1.5.1 Aromatic amino acids biosynthesis

S. cerevisiae represents an interesting organism for the biotechnological production of aromatic compounds, allowing a safer and less pollutant production process than its traditional petroleum and even plant-derived alternatives for the cosmetic, plastic, agrochemical and pharmaceutic industries (Brückner et al. 2018; Gottardi, Grün, et al. 2017; Gottardi, Knudsen, et al. 2017; Gottardi, Reifenrath, et al. 2017; Hansen et al. 2009; H.-N. Lee et al. 2018; Weber et al. 2012).

The first step of this pathway consists of the condensation of PEP and E4P into 3-deoxy-D-arabino-heptulosonate-7-phosphate (DAHP), a process that in yeast is performed by the DAHP synthases Aro3p and Aro4p. Interestingly, these isozymes display a differentiated feed-back regulatory effect to the pathway end products: Aro3p for phenylalanine and Aro4p for tyrosine, with Aro3p displaying a better affinity for both substrates (Hartmann et al. 2003).

The next step in the aromatic amino acid pathway is performed by the penta-functional Aro1p, which converts DAHP into 5-enolpyruvylshikimate-3-phosphate (EPSP): first, the cyclisation of the molecule produces 3-dehydroquinate; second, the introduction of a double bond creating 3-dehydroshikimate; third, an NADPH is consumed to produce shikimate to later on be phosphorylated to shikimate-3-phosphate by the consumption of an ATP, compound that would be finally converted into EPSP (Gottardi, Reifenrath, et al. 2017). These series of transformations highlights the role of the intermediate 3-dehydroshikimate as an essential precursor for valuable molecules such as *cis-cis* muconic acid (Brückner et al. 2018; Curran et al. 2013) and vanillin (Hansen et al. 2009).

The chorismate synthase Aro2p performs the transformation of EPSP into chorismate,
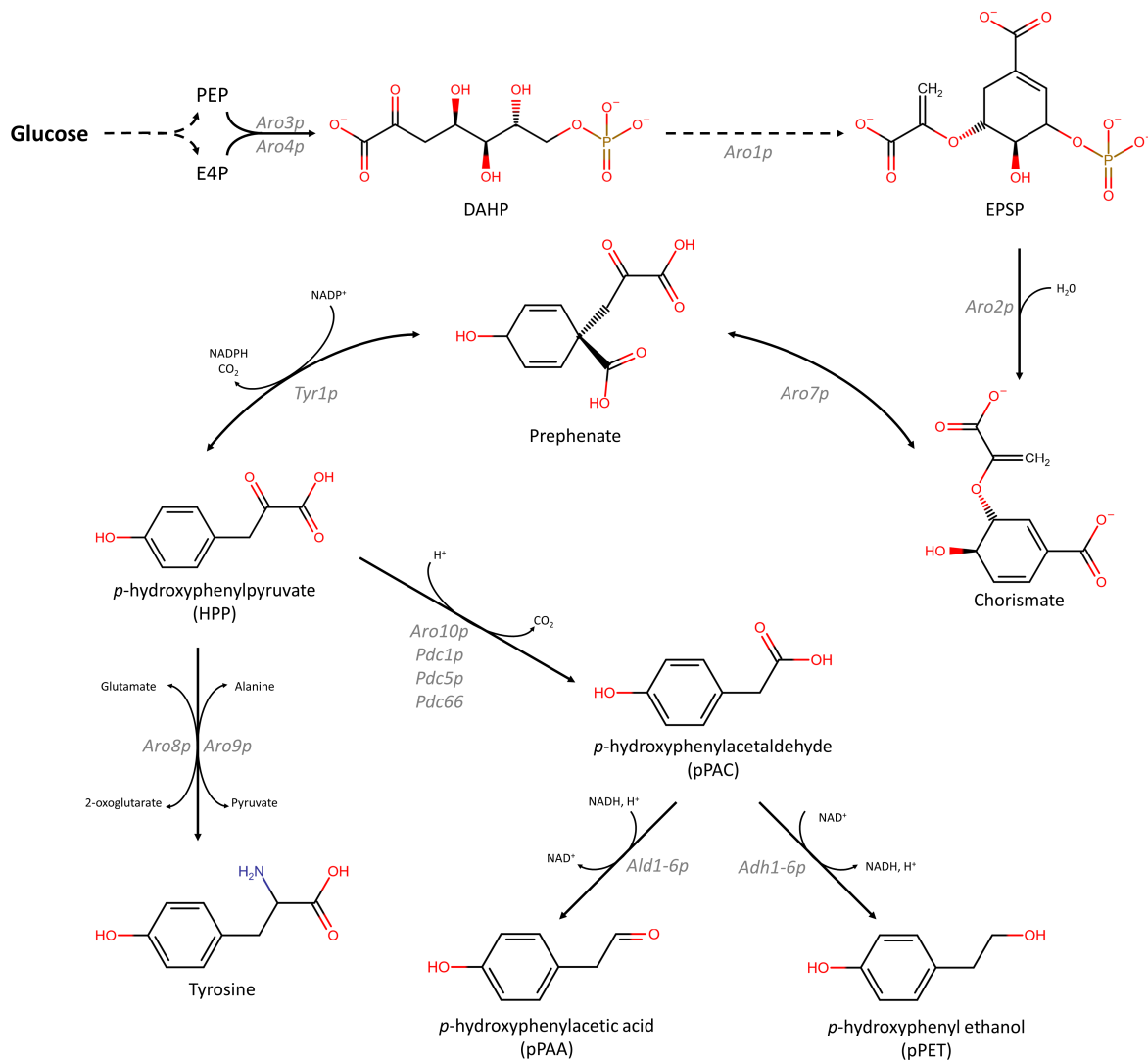
Figure 1.5: Schematic representation of tyrosine biosynthesis pathway and its degradation into the Ehrlich pathway. Single-head and double-head arrows depict one-direction and reversible reactions, respectively. The grey text represents the names of the principal genes involved in described reactions. Dashed lines represent several steps of enzymatic reactions. PEP, phosphoenolpyruvate; E4P, erythrose-4-phosphate; DAHP, 3-deoxy-D-arabinoheptulosonate-7-phosphate; EPSP, 5-enolpyruvylshikimate-3-phosphate. Adapted from Reifenrath et al. 2018.

which is a branching point that divides the tryptophan biosynthesis pathway from the tyrosine and phenylalanine biosynthesis pathway (Gottardi, Reifenrath, et al. 2017; D. G. Jones et al. 1991; Quevillon-Cheruel et al. 2004).

The tryptophan biosynthesis pathway begins with the conversion of chorismate into anthranilate, a reaction that is catalysed by the anthranilate synthase complex composed of two subunits Trp2p and Trp3p (Zalkin et al. 1984). This step has also shown to be feedback inhibited by the pathway's end product, tryptophan (Prantl et al. 1985). Then, a phosphoribosylation of anthranilate is performed by the action of Trp4p, producing phosphoribosyl anthranilate (Furter et al. 1986; Furter et al. 1988). The phosphoribosyl anthranilate isomerase Trp1p catalyses an internal rearrangement producing, after

a reduction reaction, carboxyphenylamino-1-deoxy-ribulose 5-phosphate (Braus 1991). This molecule is then decarboxylated by Trp3p, which, besides forming part of the anthranilate synthase complex, display also an indole-3-glycerolphosphate synthase activity, producing indol-3-glycerol phosphate (Braus 1991; Paluh & Zalkin 1983; Prantl et al. 1985). Finally, the Trp5p tryptophan synthase separates the indole group, precipitating it with a serine to produce tryptophan and G3P (Braus 1991; Moye & Zalkin 1985; Zalkin & Yanofsky 1982).

On the other branch, biosynthesis of tyrosine and phenylalanine continues with the chorismate mutase Aro7p, which rearranges the enolpyruvyl side-chain to produce prephenate (Ball et al. 1986). This enzyme shows a feedback inhibitory effect for tyrosine and an enhancement response upon tryptophane concentrations (Braus 1991). The removal of this regulatory effect has also been exploited to improve carbon flow into aromatic compound synthesis (Luttik et al. 2008).

Prephenate is the last common molecule for the tyrosine and phenylalanine biosynthesis pathway. Phenylalanine synthesis continues with the prephenate dehydratase Pha2p, which produces phenylpyruvate, the direct precursor of this aromatic amino acid (Braus 1991; Maftahi et al. 1995). On the other hand, prephenate can also be converted into hydroxyphenylpyruvate (HPP) after a reduction catalysed by the prephenate dehydrogenase Tyr1p (Mannhaupt et al. 1989; Reifenrath & Boles 2018; Urrestarazu et al. 1998). Finally, a transamination catalysed by the aminotransferases Aro8p and Aro9p generates phenylalanine and tyrosine from the oxo-acids phenylpyruvate and hydroxyphenylpyruvate, respectively (Hassing et al. 2019; Iraqui et al. 1999; Urrestarazu et al. 1998).

1.5.1.1 Ehrlich pathway

The Ehrlich pathway allows the degradation of several amino acids, producing fusel alcohols or acids with organoleptic properties of increasing interest for the beverage and pharmaceutical industries (Cordente et al. 2019). Just branch-chain (leucine, valine, isoleucine), sulfur-containing (methionine), and aromatic (tryptophan, phenylalanine, tyrosine) amino acids are processed by it, producing fusel alcohols that, except phenylethanol, are considered unpleasant in higher concentrations (Cordente et al. 2019; Hazelwood et al. 2008; Wang et al. 2017).

It comprises three reactions performed by a variety of enzymes, which process a broad spectrum of molecules (see figure 1.5). The first step consists of a transamination of the amino acid to produce its respective α-keto acids. In *S. cerevisiae* this reaction is

performed principally by the Aro8p and Aro9p amino transferases, however Bat1p and Bat2p have also been shown to contribute to this activity (Cordente et al. 2019; Hazelwood et al. 2008). It is important to highlight the broad substrate specificity of these enzymes; for instance, Aro8p has been reported to utilise glutamate, phenylalanine, tyrosine, 2-oxoglutarate and 2-ketoadipate, among others, placing it as a link between the aromatic amino acid and lysine biosynthesis pathway (Bulfer et al. 2013; Iraqui et al. 1998; Karsten et al. 2011). The second reaction involves a decarboxylation of the α-keto acids producing the respective fusel aldehydes, a reaction also catalysed by enzymes with broad substrate specificity such as Pdc1p, Pdc5p, Pdc6p which also play an essential role during glycolysis, but most importantly by Aro10p (Iraqui et al. 1999; Kneen et al. 2011; Vuralhan et al. 2003). The final step consists of the degradation of the fusel aldehyde into its higher alcohol form by alcohol hydrogenases, highlighting the role of the enzymes Adh1p-Adh6p, or into a fusel acid form by aldehyde dehydrogenases, mainly Ald1p, Ald2p, Ald3p, Ald4p, Ald5p, Ald6p (Cordente et al. 2019; Hazelwood et al. 2008).

The ratio distribution between the acid and alcohol fused forms depends on the cell's redox status; for instance, an anaerobic fermentation has been described to favour fusel alcohol production (Vuralhan et al. 2003). This shift in the ratio has been described to help the cell to oxidise the excess of NADH formed during fermentation, allowing it to maintain its redox balance (Hazelwood et al. 2008)

Higher alcohols, particularly the ones derived from aromatic amino acid degradation through the Ehrlich pathway, play an essential role as quorum sensing molecules (QSMs), allowing a cell-to-cell communication system used to evaluate and adjust their response to environmental conditions such as nutrient availability or cell density (Jagtap et al. 2020). Phenylethanol, tryptohol, and to a lesser extent *p*-hydroxyphenyl ethanol (pPET), the higher alcohol forms from phenylalanine, tryptophane and tyrosine, respectively, have been shown to play a significant role in inducing morphological adaptations towards mycelium or filamentous growth forms under low nutrients availability (H. Chen & Fink 2006; Gimeno et al. 1992; Padder et al. 2018).

1.5.2 Lysine biosynthesis

Lysine is considered an essential amino acid for mammals, widely regarded as necessary for proper muscular and immunological development (Roy et al. 2000; Shelton et al. 2008; Zhao et al. 2004). Its assimilation from vegetable sources is frequently insufficient due to its low concentrations, a reason that has motivated its production from different microbial sources (Isogai et al. 2021). Currently, lysine industrial production uses the
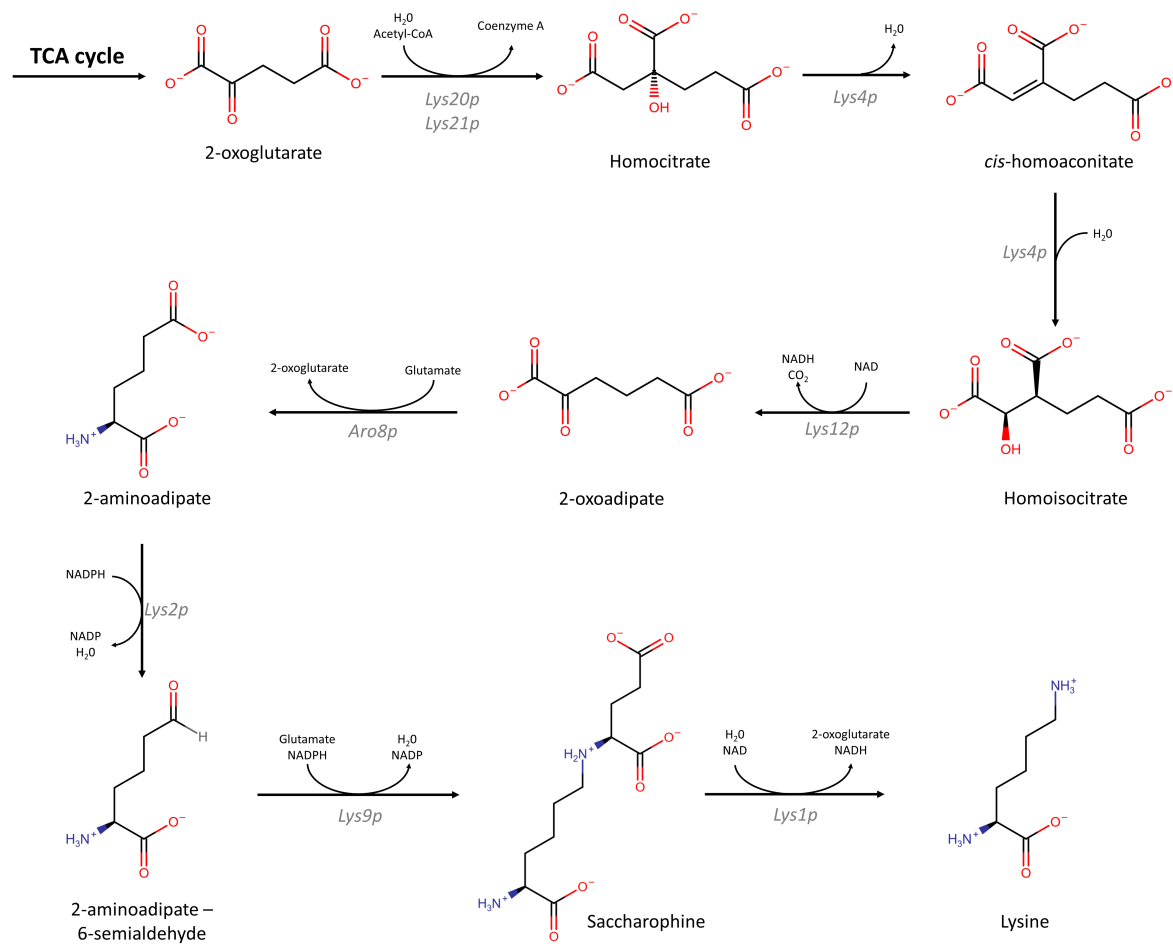
Figure 1.6: Schematic representation of lysine biosynthesis pathway. Single-head arrows depict one-way reactions. Grey text represents the names of the enzymes recognised to catalyse respective reactions.

bacteria *Corynebacterium glutamicum*; however *S. cerevisiae* is gaining attention as a producing platform mainly due to its "Generally recognised-as-safe" status. As a result, achieving high-level lysine production with this yeast represents an exciting prospect for developing premium products, such as yeast extract and livestock feed enriched with lysine (Isogai et al. 2021) (see figure 1.6).

Lysine biosynthesis in yeast begins with the conversion of 2-oxoglutarate from the TCA cycle into homocitrate, in a process catalysed by the homocitrate synthases Lys20p and Lys21p (Feller et al. 1999; Ramos et al. 1996). The homocitrate formation is also the limiting step in this pathway as both homocitrate synthases present a lysine feedback inhibitory effect (Maragoudakis et al. 1967; Sinha et al. 1971). Several groups have exploited alleviation of this regulatory effect to increase lysine production in *S. cerevisiae* (Feller et al. 1999; Isogai et al. 2021).

The second and the third steps in the pathway are performed by the homoaconitase Lys4p, which converts homocitrate into *cis*-homoaconitate and then to homoisocitrate,

similar to the aconitase reaction in the TCA that transforms citrate into isocitrate (Zabriskie & Jackson 2000). The subsequent transformation of homoisocitrate into 2-oxoadipate is performed by the homocitrate dehydrogenase Lys12p, which is NAD^+ dependent (Strassman & Ceci 1965; Zabriskie & Jackson 2000).

The fifth step for lysine biosynthesis involves an aminotransferase reaction to produce 2-aminoadipate. Interestingly, Aro8p has been suggested as the responsible enzyme for catalysing this reaction, based on the high affinity demonstrated towards 2-oxoadipate as substrate (Karsten et al. 2011). The enzyme Lys2p reduces 2-aminoadipate to produce 2-aminoadipate-6-semialdehyde (ASA) in a reaction that consumes a NADPH (Sinha & Bhattacharjee 1971). However, Lys2p activity depends on Lys5p as a post-translational modificatory catalyst, performing a phosphopantetheinylation that sets Lys2p into its catalytic form (Ehmann et al. 1999).

The subsequent saccharopine production is catalysed by the saccharopine reductase Lys9p, using ASA as a substrate while consuming a glutamate and a NADPH molecule (Andi et al. 2006; E. E. Jones & Broquist 1966; Ramos et al. 1988; Storts & Bhattacharjee 1987). The final step of the lysine biosynthesis pathway is catalysed by the saccharopine dehydrogenase Lys1p, which performs a cleavage of saccharopine, producing oxoglutarate and lysine, while regenerating an NADH molecule (Borell et al. 1984; Ogawa & Fujioka 1978; Ramos et al. 1988; Zabriskie & Jackson 2000).

Notably, the regulation of this pathway is not only performed during the initial step by the homocitrate synthases as a response to high lysine concentrations. It has been reported that the pathway's intermediate molecule ASA acts as a co-inducer for the transcriptional factor Lys14p, promoting transcription of several pathway genes such as *LYS20*, *LYS21*, *LYS5*, *LYS9* and *LYS1* (B. Becker et al. 1998; Borell et al. 1984; Feller et al. 1994; Ramos et al. 1988).

1.6   Amino acid transport

Optimal cell growth and development depend on proper amino acid homeostasis; consequently, the *de novo* synthesis, metabolic conversion, and transport processes are strictly regulated.Some small non-ionized molecules such as oxygen, carbon dioxide or weak acids and bases are naturally permeable across biological membranes; however, larger ionised or hydrophilic molecules such as carbohydrates and amino acids are not (Gabba et al. 2020). In this regard, specialised proteins distributed across the membrane play a vital role in the traffic of molecules to help sustain homeostasis.

Amino acid traffic across the membrane is carried out under an active transport modality, in which the involved transporters use the energy available from electrochemical gradients, allowing movement of solutes against the concentration gradient (Forrest et al. 2011). Such a transport mechanism is modulated by the proton motive force, which considers the membrane potential ($\Delta\Psi$) and the pH gradient (ΔpH) as a motor force for molecules movement (Bianchi et al. 2019). This feature allows the use of extracellular pools for building up intracellular amino acid concentrations, even in prototrophic strains, as importing is energetically less demanding than *novo* synthesis processes (Bianchi et al. 2019; Campbell et al. 2015; Wagner 2005). Imported amino acids, besides for protein construction, can be used as nitrogen source (Godard et al. 2007) and carbon source, as long as they are not degraded into the Ehrlich pathway (Hazelwood et al. 2008).

Among the yeast amino acid transporters expressed in the cellular membrane, two main groups can be established based on the specificity of their activity: broad- and narrow-spectrum types. Among these classes, it is not uncommon to find overlapping substrate specificity profiles; in fact, this redundancy allows the cell to react to specific environmental conditions (Bianchi et al. 2019).

Two permeases have been described to display a broad specificity, Gap1p and Agp1p. Gap1p, or general amino acid permease, displays a high affinity for all the amino acids. It is expressed mainly under low nitrogen conditions (Grenson et al. 1970; Jauniaux & Grenson 1990; Risinger et al. 2006), also playing the role of "nutrient sensor" for the cell (Donaton et al. 2003; Van Zeebroeck et al. 2009, 2014). The second broad spectrum permease Agp1p imports all naturally occurring amino acids except for arginine and lysine (Andréasson et al. 2004; Düring-Olsen et al. 1999).

The category of narrow-spectrum transporters includes many permeases with various substrate specificities; however, this bibliographical revision will focus mainly on the transporters that facilitate tyrosine and lysine import due to their relevance for the present project.

1.6.1 Lysine import mechanism

Lysine import has been reported to be facilitated by three narrow-spectrum permeases: Can1p, Vba5p, and Lyp1p. However among them Lyp1p highlights as the most efficient with K_m between 10 and 25 μM, in comparison with Can1p with reported K_m of 150 to 250 μM (Ghaddar et al. 2014; Grenson 1966; Grenson et al. 1966; Sychrova & Chevallier 1993; Sychrova et al. 1993). Overexpression of Vba5p has been reported to increase

lysine and arginine import; however, its deletion produced no significant difference for lysine import, which has motivated its recognition as a lysine importer but of limited relevance (Shimazu et al. 2012).

Active transport of lysine mediated by Lyp1p has been described to be more importantly influenced by membrane potential than for the pH gradient, producing highly asymmetric K_m values for the inward and outward transport, which contributes to the apparent unidirectionally of lysine flow (Bianchi et al. 2016). This contributes to the predominant role of Lyp1p in the yeast transport of lysine, allowing the building up of relatively high levels.

1.6.2   Tyrosine import mechanism

Tyrosine import has been described to be mediated by multiple narrow-spectrum permeases such as Tat1p, Tat2p, Bap2 and Bap3 (Bianchi et al. 2019; Kanda & Abe 2013; Regenberg et al. 1999; Schmidt et al. 1994). However, these transporters have also been related to traffic of other aromatic and neutral amino acids with a variety of affinities (Bajmoczi et al. 1998; Bianchi et al. 2019; Düring-Olsen et al. 1999; Sáenz et al. 2014). Tat3p has also been described to transport tyrosine for yeast, but this gene is absent in laboratory *S. cerevisiae* strains (Omura et al. 2007). However, the most crucial tyrosine permease seems to be Tat1p (Kanda & Abe 2013; Schmidt et al. 1994).

As previously stated, the proton motive force that drives the traffic of amino acids across the membrane is influenced by the membrane potential and the pH gradient. However, these elements do not promote the movement of all amino acids equally, causing one or the other to act more influentially over the substrate movement according to the charge they present. Assuming a transport stoichiometry of 1:1 among substrate and proton molecules, Bianchi et al. 2019 suggest that membrane potential and pH gradient will exert an equal motive force on neutral substrates such as aromatic amino acids. However, the role of the membrane potential will be twice as significant for transporting basic amino acids such as lysine. This projection suggests that the intracellular accumulation of amino acids is influenced by their charge, with the accumulation of basic amino acids being two orders of magnitude higher than that of neutral amino acids (Bianchi et al. 2019; Henderson et al. 2019).

1.7   Transport regulation

Yeast can modulate its behaviour and growth according to available nutrients (Broach 2012). This fine-tuning response is possible by rapidly modulating their protein membrane transporters in response to particular nutrient circumstances (Bianchi et al. 2016, 2019; Grenson et al. 1966; Tamayo Rojas et al. 2021). In this sense, yeast exhibits an efficient membrane transporter casting system and highly selective degradation mechanisms to rapidly respond to the quantity and quality of environmental nutrients (Broach 2012; Van Belle & André 2001).

Degradation of membrane transporter relies on the ubiquitination system to mark proteins to be internalised, with the E3 ubiquitin ligase Rsp5p usually conjugating ubiquitin proteins to the targeted substrates (Finley et al. 2012; Lauwers et al. 2010). This ligase contains WW domains, which can directly interact with PPx(Y/F) motifs in substrate proteins; however, many of its substrates, including many membrane permeases, do not possess such motifs (Finley et al. 2012). In this context, the interaction between Rsp5p and the α-arrestins is required for proper interaction with the transporter proteins as ubiquitination substrates (Finley et al. 2012; Ivashov et al. 2020).

There are 14 identified α-arrestins (arrestin-related trafficking adaptors) recognized in yeast, Art1p-Art10p, Bul1p-Bul3p, and Spo23p, which provides the PPx(Y/F) motif that allows for Rsp5p interaction (Babst 2020; Becuwe et al. 2012; MacGurn et al. 2012; Nikko & Pelham 2009; O'Donnell & Schmidt 2019). However, just Art1p and Art2 (Tat2p, Mup1p, Can1p, and Lyp1p), and with a weaker activity Art8 (Tat2p) have been reported to interact with membrane amino acid transporters (Nikko & Pelham 2009).

Art1p and Art2p present a shared coverage but base their activity on different metabolic cues. The internalisation of Mup1p, Can1p, and Lyp1p has been reported to be mediated by Art1p for substrate-induced endocytosis (high substrate concentrations). At the same time, Art2p covers the opposite setting, being required for starvation-induced endocytosis (low substrate concentrations) (Gournas et al. 2017; Ivashov et al. 2020; Lin et al. 2008; MacGurn et al. 2011; Nikko & Pelham 2009). The internalisation of Tat2p under starvation conditions is reported to be also mediated by Art2p; however, under a substrate-induced scenario, both α-arrestins Art1p or Art2p can mediate the process (Nikko & Pelham 2009).

This cue-dependent response has been described to derive from specific acidic patches at the N- and C-terminus of the transporter proteins, which interact with positive patches

in the arrestin C-domains and PY motifs, precisely directing in the Rsp5p mediated ubiquitination to nearby lysine residues (Ivashov et al. 2020).

In the event of an amino acid shortage, TORC1 complex (target of rapamycin complex 1) will become inactivated, consequently removing the repression it exerts on the kinase Npr1p, which will result in the phosphorylation of Art1p utterly preventing any further interactions with it (S. Lee et al. 2019; MacGurn et al. 2011). At the same time, under low amino acid levels, the kinase Gcn2p will be activated, leading to the phosphorylation of eIF2α, resulting in a widespread decrease in translation activity, except for the translation of the transcription factor Gcn4 (Hinnebusch 2005). Gcn4p is a major inducer for amino acid biosynthesis genes (Natarajan et al. 2001), which is also believed to promote transcription of Art2p, eventually leading to the formation of the Art2p-Rsp5p complex (Ivashov et al. 2020). This complex can then fully interact with the acidic patches at the C-terminus of membrane proteins, leading to their ubiquitination and eventual internalisation (Ivashov et al. 2020).

On the other hand, high amino acid levels will reactivate the TORC1 complex, repressing Npr1p, which prompts the activation of the α-arrestin Art1p (MacGurn et al. 2011). Complementary, Ppz phosphatases will act at the plasma membrane level, dephosphorylating the Npr1p-dependent phosphorylation sites on Art1p, causing a complementary activation of this arrestin (S. Lee et al. 2019). Increased levels of Art1p will promote the formation of the Art1p-Rsp5 complex, leading to its interaction with the N-terminus of transporter proteins (Ivashov et al. 2020). Moreover, increased nutrient levels inhibit the Gcn2p kinase, thereby preventing the promotion of Gcn4p translation and suppressing Art2p induction (Ivashov et al. 2020).

As previously described, the TORC1 Complex acts as a major regulator system, allowing the cell to react according to multiple stress environmental cues such as carbon sources, nitrogen availability, temperature or redox conditions (Loewith & Hall 2011; Urban et al. 2007). Nitrogen availability, in particular, is communicated to TORC1 by a GTPases system, which modifies the GTP/GDP status of the Gtr1p and Gtr2p proteins, switching it between an activated or deactivated status.

When amino acid levels are high, TORC1 is activated by a specific configuration of Gtr1p-Gtr2p, which involves Vam6p and Lst4p-Lst7p modifying Gtr1p and Gtr2p, respectively, into their active forms: Gtr1p^{GTP}-Gtr2p^{GDP} (Binda et al. 2009; Péli-Gulli et al. 2015). Meanwhile, under low amino acid conditions, a switch in the GTP/GDP modifications of Gtr1p and Gtr2p is produced, rendering an inactive Gtr1p^{GDP}-Gtr2p^{GTP} configuration.
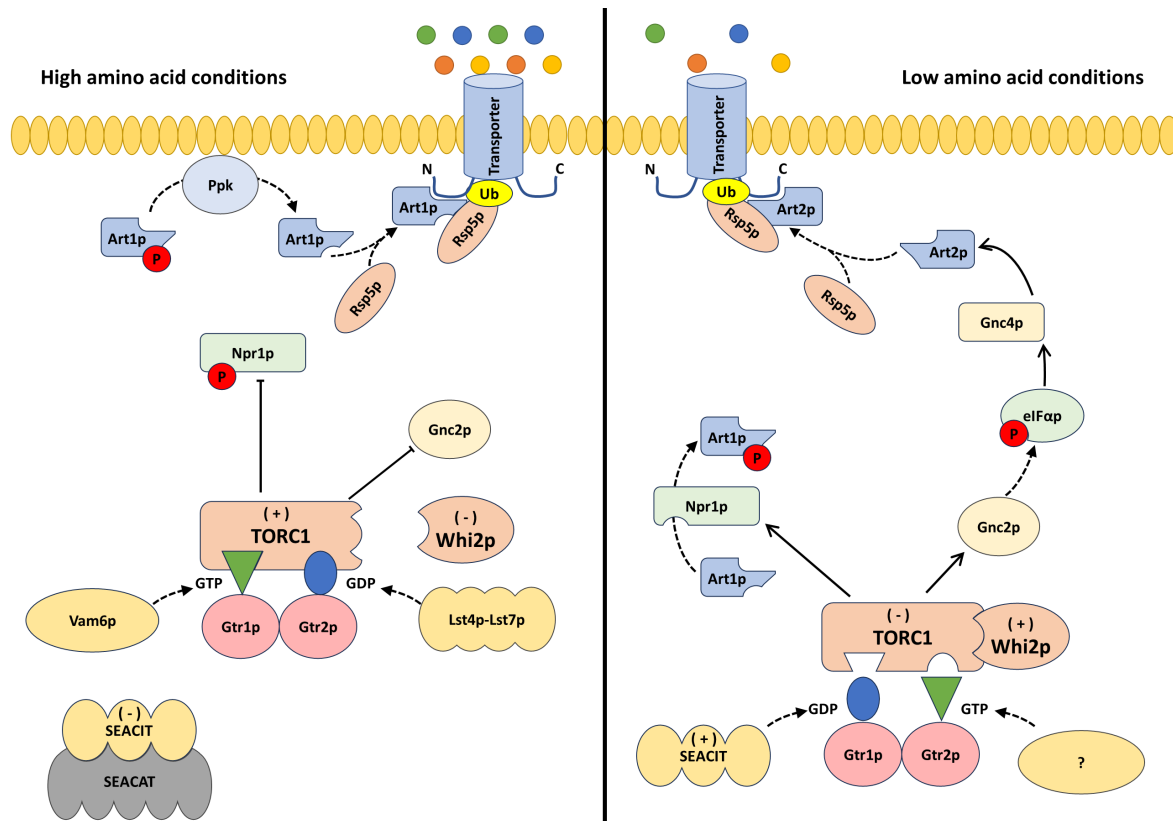
Figure 1.7: Model for amino acid transporters regulation mechanisms mediated by arrestins. General representation of molecular mechanisms described for the regulation of TORC1 complex and subsequent regulation of membrane transporters based on arrestin interaction. Straight lines represent inducing or inhibitory effects, and dashed lines denote chemical modifications. Left and right panels represent high and low amino acid panoramas, respectively. Transporter proteins represent Tat2p, Mup1p, Can1p, or Lyp1p. Adapted from Teng and Hardwick 2019, and Ivashov et al. 2020.

This process is mediated by the SEACIT complex, composed of Iml1p, Npr2p, and Npr3p, which modify the status of Gtr1p into a deactivated state, while the modifying agent of Gtr2p remains to be described (Panchaud et al. 2013a). The SEACAT complex, consisting of Sea2p, Sea3p, Sea4p, Seh1p, and Sec13p, has been observed to suppress SEACIT regulation, leading to an activated TORC1 in response to amino acid levels, most relevantly to leucine. Nevertheless, the precise mechanisms underlying this regulation are yet to be elucidated (Panchaud et al. 2013b; Teng & Hardwick 2019).

However, this SEACIT-Grt regulatory pathway is not the only one described to regulate TORC1 activity. X. Chen et al. 2018 described this function for the gene *WHI2*, which was previously related to producing small-size cells during the initiation of the cell cycle (Carter & Sudbery 1980). Phenotype analysis of *fis1*Δ mutants reveal that consistently these strains developed a premature stop codon in the gene *WHI2*, which rescues the *fis1* related detrimental effect (Cheng et al. 2008). Subsequent studies demonstrated that Whi2p act as a negative regulator of TORC1 specifically in response to low amino acid conditions, particularly to low leucine, in a SEACIT-Grt independent manner but requiring

interaction with Psr1p, Psr2p, or both phosphatases (X. Chen et al. 2018; Teng et al. 2018). Consequently, a nonfunctional Whi2⁻ phenotype has been related to a bypass on the regulatory effects imposed by TORC1 in response to poor media conditions (Cheng et al. 2008; J. Hong & Gresham 2014; Teng & Hardwick 2019; Van Leeuwen et al. 2016). However, specific details about this regulation process are still to be defined.

1.8 Aim of this study

Biotechnological processes offer better production conditions for a wide variety of goods of industrial interest. The production of aromatic compounds, for example, involves molecules of great value for cosmetic, plastic, agrochemical and pharmaceutic industries (Brückner et al. 2018; Gottardi, Grün, et al. 2017; Gottardi, Knudsen, et al. 2017; Gottardi, Reifenrath, et al. 2017; Hansen et al. 2009; H.-N. Lee et al. 2018; Weber et al. 2012). However, the yield of such processes frequently prevents a proper implementation that would allow the replacement of traditional production processes (Van Dien 2013).

Numerous rational engineering approaches have been attempted to enhance metabolic pathways associated with desired products. Unfortunately, genetic modifications and heterologous pathway expression often lead to a higher metabolic burden on the producing organisms, ultimately leading to reduced production levels and fitness (S. Y. Lee & Kim 2015; Wu et al. 2016).

This project utilised adaptive laboratory evolution to better understand the development of synthetic cooperative consortia, using *S. cerevisiae* as a model organism. Specifically, a synthetic cooperative consortium was developed around the exchange of lysine and tyrosine, which was subjected to adaptive laboratory evolution aiming to induce mutations that would improve the system's fitness either by enhanced production or upgraded stress resistance. Consequently, the mutant strains isolated after the evolution rounds were sequenced to identify relevant variations that could be related to the growth and production phenotypes observed.

The insights derived from this project are expected to contribute to further developing synthetic cooperative consortia with utilitarian purposes.

Chapter: 2 Materials and Methods

This section will present the protocols used during the development of this project. Conditions described were used for all the experiments unless explicitly described.

2.1 Chemicals and enzymes

2.1.1 Chemicals and reagents

The list of the chemicals and reagents used in this project is presented in table 2.1. If not declared explicitly, any other compound employed was acquired from Roth.

Table 2.1: List of chemicals and reagents used in this project.

Compound	Producer
Acetonitril	Roth
Adenine	Roth
Amino acids	Roth
Amonium sulfat	DB
Bacterial Trypton	Difco
Bacteriological Peptone	Oxoid
Carbenicillin	Roth
Chloramphenicol	Roth
ClonNAT (Nourseothricin)	WERNER BioAgents
DNA Ladder Gene Ruler 1kb Plus	Thermo Fisher Scientific
dNTPs	NEB
EDTA	Roth
Geneticin (G418)	Merck
Glucose	Roth
Hygromycin B	Roth
Kanamycin sulfate	Roth
KH_2PO_4	Roth
Lithium acetate	Roth
Loading Buffer Dye, Purple (6x)	NEB
p-Coumaric acid	Roth
p-Hydroxyphenyl ethanol	Sigma Aldrich
PEG-4000	Roth
SDS	Roth
Sheared Salmon Sperm DNA	Ambion
Tris-HCl	Roth
Uracil	Sigma Aldrich
Yeast Extract	Difco
Yeast Nitrogen Base (YNB) without Amino Acids and Ammonium Sulfate	Difco

2.1.2 Enzymes and kits

Table 2.2 presents the list of enzymes and supplements used in this project.

Table 2.2: List of enzymes used in the project.

Enzymes	Producer
DreamTaq, including buffer	NEB
Phusion DNA polymerase, incl. buffer	NEB
Q5 DNA polymerase, incl. buffer	NEB
Restriction enzymes, incl. buffer	NEB
T7 DNA ligase	NEB

The commercial kits used in this project are presented in table 2.3

Table 2.3: List of commercial kits employed in the project.

Description	Producer
GeneJET Genomic DNA Purification Kit	Thermo Fisher Scientific
GeneJET Plasmid Miniprep Kit	Thermo Fisher Scientific
NucleoSpin Gel and PCR Clean Up	Macherey-Nagel

2.1.3 Solutions

Protocols for the preparation of the solutions used in this project are described below.

2.1.3.1 Frozen competent cell solution

A 10 mL stock volume of frozen competent cell (FCC) solution was prepared by dissolving 1 mL of DMSO into 8 mL of water using a 0.2 μm nylon membrane for sterilisation, and supplemented with 1 mL of autoclaved 50% glycerin. The resulting solution presented a 5% glycerin and 10% DMSO (v/v) concentration.

2.1.3.2 Transformation solution

A large volume of transformation mix was prepared in advance and kept at 4°C until required.

A volume of 26 mL of sterile PEG 4000 in a 50% concentration (w/v) was supplemented with 3.6 mL of lithium acetate 1.0 M sterile. The mix was supplemented with 1 mL of Sheared Salmon Sperm DNA in a concentration of 2mg mL^{-1} dissolved in a 10 mM TRIS-HCl, 1 mM EDTA, ph 8.0 solution, to a final volume of 30.6 mL of transformation solution.

2.2 Equipment

A list of the equipment used in this project is presented in table 2.2.

Table 2.4: List of equipment used in the project.

Devices	Manufacturer
Agarose gel-electrophoresis chambers	Neolab
Cell electroporator, Gene Pulser	Bio-Rad
Cell growth quantifier Aquila	Aquila Biolabs
Fluorescence spectrophotometer CLARIOstar Plus	BMG LABTECH
Incubator Multitron Standard,	Infors HT
Nanodrop 1000 spectrophotometer	Thermo Fisher Scientific
PCR cycler - Labcylcler triple block	SensoQuest
pH-meter	765 Calimatic Knick
Pipette, 0.1-2.5 μL	Eppendorf
Pipette, 100-1000 μL	Eppendorf
Pipette, 10-100 μL	Eppendorf
Pipette, 2-20 μL	Eppendorf
Shaker	Infors HT
Spectrophotometer Ultrospec 2100 Pro	Amersham Bioscience
Thermomixer Comfort	Eppendorf
Vibrax VXR Basic	IKA
HPLC system - BioLC	
Pump system - LPG-3400SD	Thermo Scientific
Autosampler - WPS-3000SL	Thermo Scientific
Column Oven - TCC-100	Thermo Scientific
Degasser - SRD3400	Thermo Scientific
Wavelength Detector - VWD-3400RS	Thermo Fisher Scientific
Columns	
Zorbax Eclipse Plus C18 Rapid Resolution (4.6 x 150mm 0.5μm)	Agilent
Zorbax SB-C8 Rapid Resolution (4.6 x 150mm 3.5μm)	Agilent

2.3   Media and supplements

The present section presents the base recipes for the media used in this project. Solid media preparation used a 2% (w/v) agar concentration when required.

2.3.1   LB media for bacterial culture

The nutritionally rich Luria-Bertani broth (LB-medium) was used for general bacterial culture. Preparation was done according to the recipe in table 2.5.

Table 2.5: Composition of LB media. pH was adjusted to 7.5 with NaOH.

Component	Final concentration
Tryptone	10 g L^{-1}
Yeast Extract	5 g L^{-1}
NaCl	5 g L^{-1}

2.3.2   YPD media for *S. cerevisiae* culture

The Yeast Peptone media supplemented with glucose (YPD) was used for the general yeast culture in this project.

Table 2.6: Composition of YPD media. Carbon source was added after autoclaving the media.

Component	Final concentration
Bacto Peptone	20 g L^{-1}
Bacto Yeast Extract	10 g L^{-1}
Carbon source (Glucose)	20 g L^{-1}

2.3.3   SCD media for *S. cerevisiae* culture

Standard minimal complete media supplemented with glucose (SCD) was used during evolution processes as well as for the evaluation of phenotype of evolved mutants and engineered strains. According to experimental requirements, media composition was adjusted to lack or include specifically required nutrients, whose supplementation was performed according to section 2.3.6.

Table 2.7: Composition of synthetic complete media (SCD). pH was adjusted to 6.3 with KOH. Carbon source was added after autoclaving.

Component	Final concentration
Yeast Nitrogen Base w/o Amino Acids and Ammonium Sulfate	1.7 g L^{-1}
Ammonium sulfate	5 g L^{-1}
20x Amino acid mix	50 m L^{-1}
Carbon source (Glucose)	20 g L^{-1}

2.3.4   SMD media for *S. cerevisiae* culture

The Standard Minimum Media supplemented with glucose (SMD) was employed as a reduced media during an evolution process as well as to evaluate mutants derived from this process. This base recipe was adjusted according to strain requirements following the supplementation nutrient table presented in section 2.3.6.

Table 2.8: Composition of synthetic minimum media (SMD). Prior to autoclaving, the pH was set to 6.3 using KOH. Media was buffered with sterile KH$_2$PO$_4$ to a final concentration of 20 mM. Buffer and the carbon source were added after autoclaving the media.

Component	Concentration
Yeast Nitrogen Base w/o Amino Acids and Ammonium Sulfate	1.7 g L^{-1}
Ammonium sulfate	5 g L^{-1}
Carbon source (Glucose)	20 g L^{-1}

2.3.5 Antibiotic supplementation

The use of dominant markers during selection allowed to detect positive transformants as well as to maintain an active selection on bacterial cultures later on processed for plasmid extraction. Stock and working concentrations used are described below.

Table 2.9: Antibiotic supplementation for media preparation. All solutions need to be sterile filtrated using a 0.2 μm nylon membrane.

Component supplement	Stock solution	Final concentration
Carbenicillin	60 mg mL^{-1} in 50% (v/v) ethanol	60 μg mL^{-1}
Chloramphenicol	34 mg mL^{-1} in 70% (v/v) ethanol	34 μg mL^{-1}
ClonNAT (Nourseothricin)	100 mg mL^{-1} in ddH$_2$O	100 μg mL^{-1}
Geneticin (G418)	200 mg mL^{-1} in ddH$_2$O	200 μg mL^{-1}
Hygromycin B	200 mg mL^{-1} in ddH$_2$O	200 μg mL^{-1}
Kanamycin sulfate	50 mg mL^{-1} in ddH$_2$O	50 μg mL^{-1}

2.3.6 Extra nutrients supplementation

When required, base media was supplemented with amino acids or uracil according to concentrations established in following sections.

2.3.6.1 Amino acids mix

An amino acid and nitrogenated bases mix concentrated by 20 fold was prepared and supplemented during the preparation of SCD media.

Table 2.10: Amino acid composition of 20x media solution. Stock solution was sterile autoclaved and kept 4°C until usage.

Compound	mg L^{-1}	Concentration in 20x mix (mM)	Final concentration in media (mM)
Adenin	224	1.657663	0.082883
Arginin	768	4.408726	0.220436
Methionin	768	5.147453	0.257373
Isoleucin	1152	8.780488	0.439024
Phenylalanin	960	5.811138	0.290557
Valin	1152	9.837746	0.491887
Threonin	1152	9.672544	0.483627

2.3.6.2 Supplement solutions

Supplement solutions were used during the media preparation process to complement specific auxotrophies. The concentrations employed for each one of them are described below.

Table 2.11: Supplement solutions preparation. Once sterile, solutions were stored at 4°C until needed. Solutions marked with * were stored at room temperature. As stocks were stored sterile, they were added as needed before or after base media sterilization.

Compound	mg L^{-1}	Stock concentration	mL used per L of media	Media final concentration (mM)
Uracil*	1.2	10.70606	16	0.171297
Histidin	2.4	15.4685	8	0.123748
Tryptophan	2.4	11.75146	8	0.094012
Leucin	3.6	27.4453	16	0.439125
Tyrosine*	0.45	2.483	20	0.08
Lysine	3.235	19.7	32	0.394

2.4　Microbial strains and plasmids

2.4.1　Microbial strains

A list of the microbial strains used is presented in table 2.12.

Table 2.12: List of strains used in the project.

Strain - Alias	Genotype	Comment	Reference
Escherichia coli			
DH10B	F⁻ *mcr*A Δ(*mrr-hsd*RMS-*mcr*BC) φ80*lac*ZΔM15 Δ*lac*X74 *rec*A1 *end*A1 *ara*D139 Δ(*ara-leu*)7697 *gal*U *gal*K λ⁻ *rps*L(Str^R) *nup*G	-	Thermo Scientific
Saccharomyces cerevisiae			
CEN.PK 113-5D	*MATa ura3-52*	-	EUROSCARF, Frankfurt
CEN.PK 113-7D	*MATa*	-	EUROSCARF, Frankfurt
K1	*Unknown in full, evolved from K0*	Strain obtained after evolution of K0.	This study
LBGY001 - WT	*MATa, ste3Δ::kanMX, ura3-52*	Deletion of *STE3* with KanMX marker using homologous recombination.	This study
LBGY002	*MATa, ste3Δ::KanMX, tyr1Δ ura3Δ::TDH3p-GFP-ENO1t-Hyg,*	Integration of into eGFP and Hygromicin into *URA3* locus using homologous recombination into LBGY001.	This study
LBGY003	*MATa, ste3Δ::KanMX, lys1Δ, ura3Δ::TDH3p-mRuby-ENO1t-Hyg*	Integration of into mRuby2 and Hygromicin into *URA3* locus using homologous recombination into LBGY001.	This study
LBGY004 - K0	*MATa, ste3Δ::kanMX, tyr1Δ, ura3Δ::TDH3p-GFP-ENO1t-Hyg, pyk2Δ::LYS21^{fbr}*	Integration of *LYS21^{fbr}* into *PYK2* locus into LBGY002.	This study
LBGY005 - Y0	*MATa, ste3Δ::kanMX, lys1Δ, ura3Δ::TDH3p-mRuby-ENO1t-Hyg, pyk2Δ::ARO3^{fbr}::ARO4^{fbr}*	Integration of *ARO3^{fbr} ARO4^{fbr}* into *PYK2* locus into LBGY003.	This study
LBGY015	*MATa, ste3Δ::kanMX, lys1Δ, ura3Δ::TDH3p-mRuby-ENO1t-Hyg, pyk2Δ::ARO3^{fbr}::ARO4^{fbr}, lys9$^{(1013CTΔ::0)}$*	Strain Y0 with mutated version of *lys9* employing CRISPR/Cas9 assisted strategy.	This study

Table 2.12 – continued from previous page

Strain - Alias	Genotype	Comment	Reference
LBGY019	*MATa, ste3Δ::kanMX, lys1Δ, ura3Δ::TDH3p-mRuby-ENO1t-Hyg, pyk2Δ::ARO3^{fbr}::ARO4^{fbr}, art2(614TΔ::0)*	Strain Y0 with mutated version of *art2* employing CRISPR/Cas9 assisted strategy.	This study
LBGY034	*MATa, ste3Δ::kanMX, ura3-52, [2u, URA3, pTDH3-TAL-ENO1t]*	Transformation of plasmid LBGV062 into LBGY1.	This study
LBGY035	*MATa, ste3Δ::kanMX, lys1Δ, ura3Δ::TDH3p-mRuby-ENO1t-Hyg, pyk2Δ::ARO3^{fbr}::ARO4^{fbr}, [2u, URA3, pTDH3-TAL-ENO1t]*	Transformation of plasmid LBGV062 into Y0.	This study
LBGY036	*Unknown in full, based on Y0 - ura3Δ::TDH3p-mRuby-ENO1t-Hyg, [2u, URA3, pTDH3-TAL-ENO1t]*	Transformation of plasmid LBGV062 into Y1.	This study
LBGY037	*Unknown in full, based on Y1 - ura3Δ::TDH3p-mRuby-ENO1t-ClNAT, [2u, URA3, pTDH3-TAL-ENO1t]*	Transformation of plasmid LBGV062 into Y1.2.	This study
LBGY038	*Unknown in full, based on Y1.2 - ura3Δ::TDH3p-mRuby-ENO1t-ClNAT, [2u, URA3, pTDH3-TAL-ENO1t]*	Transformation of plasmid LBGV062 into Y2.	This study
LBGY040	*MATa, ste3Δ::KanMX, tyr1Δ ura3Δ::TDH3p-GFP-ENO1t-Hyg, [2u, URA3, GFPdropout]*	Transformation of plasmid SiHV005 into LBGY001.	This study
LBGY041	*MATa, ste3Δ::KanMX, tyr1Δ ura3Δ::TDH3p-GFP-ENO1t-Hyg, [2u, URA3,pCCW12p-DOD-PGK1t / pTDH3-CYP76AD1-ENO1t]*	Transformation of plasmid LBGV063 into LBGY001.	This study
LBGY042	*MATa, TRP1, ura3, leu2, his3, [2u, URA3,pCCW12p-DOD-PGK1t / pTDH3-CYP76AD1-ENO1t]*	Transformation of plasmid LBGV063 into MRY08.	This study
LBGY043	*MATa, TRP1, aro4Δ::pHXT7-ARO1-CYC1t, ura3Δ::pTPI1-ARO4^{fbr}-ARO4t_pHXT7-ARO3^{fbr}-CYC1t, aro10Δ, [2u, URA3,pCCW12p-DOD-PGK1t / pTDH3-CYP76AD1-ENO1t]*	Transformation of plasmid LBGV063 into MRY17.	This study
LBGY044	*MATa, ste3Δ::kanMX, lys1Δ, ura3Δ::TDH3p-mRuby-ENO1t-Hyg, pyk2Δ::ARO3^{fbr}::ARO4^{fbr}, [2u, URA3,pCCW12p-DOD-PGK1t / pTDH3-CYP76AD1-ENO1t]*	Transformation of plasmid LBGV063 into Y0.	This study
LBGY045	*Unknown in full, based on Y0 - ura3Δ::TDH3p-mRuby-ENO1t-Hyg, [2u, URA3,pCCW12p-DOD-PGK1t / pTDH3-CYP76AD1-ENO1t]*	Transformation of plasmid LBGV063 into Y1	This study
LBGY046	*Unknown in full, based on Y1 - ura3Δ::TDH3p-mRuby-ENO1t-ClNAT, [2u, URA3,pCCW12p-DOD-PGK1t / pTDH3-CYP76AD1-ENO1t]*	Transformation of plasmid LBGV063 into Y1.2.	This study
LBGY047	*Unknown in full, based on Y1.2 - ura3Δ::TDH3p-mRuby-ENO1t-ClNAT, [2u, URA3,pCCW12p-DOD-PGK1t / pTDH3-CYP76AD1-ENO1t]*	Transformation of plasmid LBGV063 into Y2.	This study
LBGY051	*Unknown in full, based on Y1 - ura3Δ::TDH3p-mRuby-ENO1t-ClNAT, whi2Δ*	Deletion of *WHI2* into Y1.2 employing CRISPR/Cas9 assisted strategy.	This study
LBGY052	*MATa, ste3Δ::kanMX, lys1Δ, ura3Δ::TDH3p-mRuby-ENO1t-Hyg, pyk2Δ::ARO3^{fbr}::ARO4^{fbr}, whi2Δ*	Deletion of *WHI2* into K0 employing CRISPR/Cas9 assisted strategy.	This study
LBGY053	*Unknown in full, based on K0 - ura3Δ::TDH3p-mRuby-ENO1t-Hyg, pyk2Δ::ARO3^{fbr}::ARO4^{fbr}, Whi2*	Reparation of *whi2* into K1 employing CRISPR/Cas9 assisted strategy.	This study

Table 2.12 – continued from previous page

Strain - Alias	Genotype	Comment	Reference
LBGY054	*Unknown in full, based on Y1.2 - ura3Δ::TDH3p-mRuby-ENO1t-Hyg, pyk2Δ::ARO3^{fbr}::ARO4^{fbr}, Whi2*	Reparation of *whi2* into Y2 employing CRISPR/Cas9 assisted strategy.	This study
LBGY060	*MATa, ste3Δ::kanMX, lys1Δ, ura3Δ::TDH3p-mRuby-ENO1t-Hyg, pyk2Δ::ARO3^{fbr}::ARO4^{fbr}, asr1(311GΔ::0)*	Strain Y0 with mutated version of *ars1* employing CRISPR/Cas9 assisted strategy.	This study
LBGY061	*MATa, ste3Δ::kanMX, lys1Δ, ura3Δ::TDH3p-mRuby-ENO1t-Hyg, pyk2Δ::ARO3^{fbr}::ARO4^{fbr}, lys9$^{(1013CTΔ::0)}$, lys2Δ::0*	Strain LBGY015 with a full *LYS2* deletion by employing a CRISPR/Cas9 assisted strategy.	This study
LBGY062	*MATa, ste3Δ::kanMX, lys1Δ, ura3Δ::TDH3p-mRuby-ENO1t-Hyg, pyk2Δ::ARO3^{fbr}::ARO4^{fbr}, lys9$^{(1013CTΔ::0)}$, lys14Δ::0*	Strain LBGY015 with a full *LYS14* deletion by employing a CRISPR/Cas9 assisted strategy.	This study
LBGY063	*MATa, ste3Δ::kanMX, lys1Δ, ura3Δ::TDH3p-mRuby-ENO1t-Hyg, pyk2Δ::ARO3^{fbr}::ARO4^{fbr}, lys9$^{(1013CTΔ::0)}$, lys20Δ::0, Lys21Δ::0*	Strain LBGY015 with full *LYS20* and *LYS21* deletions by employing a CRISPR/Cas9 assisted strategy.	This study
LBGY064	*MATa, ste3Δ::kanMX, ura3-52, aro10Δ::0*	Strain LBGY001 with a full *ARO10* deletion by employing a CRISPR/Cas9 assisted strategy.	This study
LBGY065	*MATa, ste3Δ::kanMX, lys1Δ, ura3Δ::TDH3p-mRuby-ENO1t-Hyg, pyk2Δ::ARO3^{fbr}::ARO4^{fbr}, aro10Δ::0*	Strain Y0 with a full *ARO10* deletion by employing a CRISPR/Cas9 assisted strategy.	This study
LBGY066	*Unknown in full, based on Y0 - ura3Δ::TDH3p-mRuby-ENO1t-Hyg, aro10Δ::0*	Strain Y1 with a full *ARO10* deletion by employing a CRISPR/Cas9 assisted strategy.	This study
LBGY067	*Unknown in full, based on Y1 - ura3Δ::TDH3p-mRuby-ENO1t-Hyg, aro10Δ::0*	Strain Y1.2 with a full *ARO10* deletion by employing a CRISPR/Cas9 assisted strategy.	This study
LBGY068	*Unknown in full, based on Y1.2 - ura3Δ::TDH3p-mRuby-ENO1t-ClNAT, aro10Δ::0*	Strain Y2 with a full *ARO10* deletion by employing a CRISPR/Cas9 assisted strategy.	This study
LBGY079	*MATa, ste3Δ::kanMX, lys1Δ, ura3Δ::TDH3p-mRuby-ENO1t-Hyg, pyk2Δ::ARO3^{fbr}::ARO4^{fbr}, [CEN.ARS, URA3, Kan, LYP1::GFP]*	Transformation of plasmid LBGV117 into Y0.	This study
LBGY080	*MATa, ste3Δ::kanMX, lys1Δ, ura3Δ::TDH3p-mRuby-ENO1t-Hyg, pyk2Δ::ARO3^{fbr}::ARO4^{fbr}, art2(614TΔ::0), [CEN.ARS, URA3, Kan, LYP1::GFP]*	Transformation of plasmid LBGV117 into LBGY019.	This study
LBGY089	*MATa, ste3Δ::kanMX, lys1Δ, ura3Δ::TDH3p-mRuby-ENO1t-Hyg, pyk2Δ::ARO3^{fbr}::ARO4^{fbr}, art2Δ*	Deletion of *ART2* into Y0 employing CRISPR/Cas9 assisted strategy.	This study
LBGY090	*MATa, ste3Δ::kanMX, lys1Δ, ura3Δ::TDH3p-mRuby-ENO1t-Hyg, pyk2Δ::ARO3^{fbr}::ARO4^{fbr}, lys9Δ*	Deletion of LYS9 into Y0 employing CRISPR/Cas9 assisted strategy.	This study
LBGY095	*MATa, ste3Δ::kanMX, lys1Δ, ura3Δ::TDH3p-mRuby-ENO1t-Hyg, pyk2Δ::ARO3^{fbr}::ARO4^{fbr}, lys9Δ, [CEN.ARS, URA3, Kan, pTDH3, LYS9, ENO1t]*	Transformation of plasmid LBGV119 into LBGY090.	This study
LBGY096	*MATa, ste3Δ::kanMX, lys1Δ, ura3Δ::TDH3p-mRuby-ENO1t-Hyg, pyk2Δ::ARO3^{fbr}::ARO4^{fbr}, lys9Δ, [CEN.ARS, URA3, Kan, Spacer]*	Transformation of plasmid LBGV120 into LBGY090.	This study
LBGY097	*MATa, ste3Δ::kanMX, lys1Δ, ura3Δ::TDH3p-mRuby-ENO1t-Hyg, pyk2Δ::ARO3^{fbr}::ARO4^{fbr},[CEN.ARS, URA3, Kan, pTDH3, LYS9, ENO1t]*	Transformation of plasmid LBGV119 into Y0.	This study

36

Table 2.12 – continued from previous page

Strain - Alias	Genotype	Comment	Reference
LBGY098	*MATa, ste3Δ::kanMX, lys1Δ, ura3Δ::TDH3p-mRuby-ENO1t-Hyg, pyk2Δ::ARO3^{fbr}::ARO4^{fbr},[CEN.ARS, URA3, Kan, Spacer]*	Transformation of plasmid LBGV120 into Y0.	This study
MRY08	*MATa, TRP1, ura3, leu2, his3*	Negative control strain for tyrosine production.	Reifenrath and Boles 2018
MRY17	*MATa, TRP1, aro4Δ::pHXT7-ARO1-CYC1t, ura3Δ::pTPI1-ARO4^{fbr}-ARO4t_pHXT7-ARO3^{fbr}-CYC1t, aro10Δ*	Positive control strain for tyrosine production.	Reifenrath and Boles 2018
Y1	*Unknown in full, evolved from Y0*	Strain obtained after evolution of Y0.	This study
Y1.2	*Unknown in full, based on Y1 hygΔ::ClNAT*	Strain Y1 carrying a ClNAT dominant marker instead of Hygromicin.	This study
Y2	*Unknown in full, evolved from Y1.2*	Strain obtained after evolution in Y1.2.	This study

2.4.2 Plasmids

The development of this work involved the development and use of several plasmids, which are described in table 2.13.

Table 2.13: List of plasmids employed in this project.

Strain - Alias	Genotype	Comment	Reference
JTV19	*[pTPI1-Aro4^{fbr}-ARO4t,pHXT7-Aro3^{fbr}-CYC1t,pFAB1-Aro1K1370A-tRKI1,KanMX,2μ,Amp-ColE1]*	Plasmid for overexpression of Aromatic amino acid pathway.	Reifenrath and Boles 2018
LBGV003	*[pROX3-CAS9-CYC1t,pSNP52-GuideSeq TRY1-SUP4t,Hyg,AmpR-ColE1]*	CRISPR/Cas9 plasmid targeting *TYR1*, derived from pRCC-H.	This study
LBGV004	*[CenArs,URA3,p-Lys21^{fbr}-LYS21t, pBR322,AmpR]*	Expression plasmid carrying *LYS21^{fbr}* with native promotor and terminator.	This study
LBGV006	*[ConLS,pTDH3,GFPEnvy,ENO1t,ConRE-Hyg,URA3'Hom,KanR-ColE1,Ura5'Hom]*	Integration plasmid for GFP into *URA3* locus.	This study
LBGV007	*[ConLS,pTDH3,mRuby2-ENO1t,ConRE,Hyg,URA3'Hom,KanR-ColE1,Ura5'Hom]*	Integration plasmid for mRuby2 into *URA3* locus.	This study
LBGV022	*[ConLS',gfp dropout-ConRE',URA3,CenArs,KanR-ColE1]*	Backbone expression centromeric plasmid with *URA3* marker.	This study
LBGV026	*[pROX3-CAS9-CYC1t,pSNP52-GuideSeq Lys1-SUP4t,Hyg,AmpR-ColE1]*	CRISPR/Cas9 plasmid targeting *LYS1*, derived from pRCC-H.	This study
LBGV052	*[Mj.DOD,ClmR-ColE1]*	*DOD* from *Mirabilis jalapa* entry plasmid into GoldenGate system.	This study
LBGV053	*[Bv.CYP-76AD1,ClmR-ColE1]*	*CYP-76AD1* from *Beta vulgaris* entry plasmid into GoldenGate system.	This study

Table 2.13 – continued from previous page

Strain - Alias	Genotype	Comment	Reference
LBGV054	*[Rs.TAL,ClmR-ColE1]*	*TAL* from *Rhodobacter sphaeroides* entry plasmid into GoldenGate system.	This study
LBGV060	*[pCCW12p-Mj.DOD-PGK1t,AmpR-ColE1]*	Expression unit assambly for *DOD* into GoldenGate system.	This study
LBGV061	*[pTDH3-Bv.CYP76AD1-ENO1t,AmpR-ColE1]*	Expression unit assambly for *CYP-76AD1* into GoldenGate system.	This study
LBGV062	*[2μ, URA3, pTDH3-TAL-ENO1t,AmpR-ColE1]*	Expression plasmid for *TAL* using SiHV005 as backbone.	This study
LBGV063	*[2μ, URA3,pCCW12p-DOD-PGK1t,pTDH3-CYP76AD1-ENO1t,KanR-ColE1]*	Multi expression plasmid carrying LBGV060 and LBGV061 expression units.	This study
LBGV071	*[pROX3-CAS9-CYC1t,pSNP52-gfp dropout-SUP4t,ClNAT,AmpR-ColE1]*	CRISPR/Cas9 backbone plasmid carrying a GFP dropout for BsaI digestion. It carries a *ClNAT* selection marker.	This study
LBGV072	*[pROX3-CAS9-CYC1t,pSNP52-gfp dropout-SUP4t,Hyg,AmpR-ColE1]*	CRISPR/Cas9 backbone plasmid carrying a GFP dropout for BsaI digestion. It carries a Hyg selection marker.	This study
LBGV073	*[pROX3-CAS9-CYC1t,pSNP52-GuideSeq ART2-SUP4t, ClNAT,AmpR-ColE1]*	CRISPR/Cas9 plasmid targeting *ART2* derived from LBGV071.	This study
LBGV074	*[pROX3-CAS9-CYC1t,pSNP52-GuideSeq ASR1-SUP4t,ClNAT,AmpR-ColE1]*	CRISPR/Cas9 plasmid targeting *ASR1* derived from LBGV071.	This study
LBGV082	*[LYP1,ClmR-ColE1]*	*LYS1* entry plasmid into GoldenGate system. Stop codon removed.	This study
LBGV083	*[pROX3-CAS9-CYC1t, pSNP52-GuideSeq WHI2-SUP4t,Hyg,AmpR-ColE1]*	CRISPR/Cas9 plasmid targeting *WHI2* derived from LBGV072.	This study
LBGV084	*[pROX3-CAS9-CYC1t, pSNP52-GuideSeq WHI2-SUP4t,ClNAT,AmpR-ColE1]*	CRISPR/Cas9 plasmid targeting *WHI2* derived from LBGV071.	This study
LBGV085	*[pROX3-CAS9-CYC1t,pSNP52-GuideSeq whi2 for K1-SUP4t,ClNAT,AmpR-ColE1]*	CRISPR/Cas9 plasmid targeting *whi2* from K1, derived from LBGV071.	This study
LBGV086	*[pROX3-CAS9-CYC1t,pSNP52-GuideSeq whi2 for Y2-SUP4t,Hyg,AmpR-ColE1]*	CRISPR/Cas9 plasmid targeting *whi2* from Y2,derived from LBGV072.	This study
LBGV093	*[pROX3-CAS9-CYC1t,pSNP52-GuideSeq ARO10 -SUP4t,Hyg,AmpR-ColE1]*	CRISPR/Cas9 plasmid targeting *ARO10* derived from LBGV072.	This study
LBGV094	*[pROX3-CAS9-CYC1t,pSNP52-GuideSeq LYS2 -SUP4t;ClNAT,AmpR-ColE1]*	CRISPR/Cas9 plasmid targeting *LYS2* derived from LBGV072.	This study
LBGV095	*[pROX3-CAS9-CYC1t,pSNP52-GuideSeq LYS14 -SUP4t,ClNAT,AmpR-ColE1]*	CRISPR/Cas9 plasmid targeting *LYS14* derived from LBGV072.	This study
LBGV107	*[pROX3-CAS9-CYC1t,pSNP52-GuideSeq LYS20/21 -SUP4t,ClNAT,AmpR-ColE1]*	CRISPR/Cas9 plasmid targeting *LYS20* and *LYS21* derived from LBGV072.	This study
LBGV117	*[CenArs,URA3, LYP1::GFP,AmpR-ColE1]*	Expression plasmid for *LYP1::eGFP* derived from SRV096 (UCP). *LYP1::eGFP* cassette integrated by homologous recombination.	This study
LBGV118	*[LYS9,ClmR-ColE1]*	*LYS9* entry plasmid into GoldenGate system.	This study

Table 2.13 – continued from previous page

Strain - Alias	Genotype	Comment	Reference
LBGV119	*[CenArs, URA3, Kan, pTDH3-LYS9-ENO1t,AmpR-ColE1]*	Expression plasmid carrying *LYS9* derived from LBGV022.	This study
LBGV120	*[CenArs,URA3,Kan,Spacer,AmpR-ColE1]*	Empty expression plasmid derived from LBGV022.	This study
pRCC-H	*[pROX3-CAS9-CYC1t,pSNP52-GuideSeq empty-SUP4t,Hyg,AmpR-ColE1]*	CRISPR/Cas9 backbone plasmid. It carries a Hyg selection marker.	Generoso et al. 2016
pRCC-N	*[pROX3-CAS9-CYC1t,pSNP52-GuideSeq empty-SUP4t,ClNAT,AmpR-ColE1]*	CRISPR/Cas9 backbone plasmid. It carries a ClNAT selection marker.	Generoso et al. 2016
pUG6K	*[pTEF-KanMX-tTEF,AmpR-ColE1]*	Expression plasmid for KanMX.	This study
SARV03	*[pROX3-CAS9-CYC1t,pSNP52-GuideSeq PKY2-SUP4t,ClNAT,AmpR-ColE1]*	CRISPR/Cas9 plasmid targeting *PKY2*, derived from pRCC-N	Prof. Boles group, Frankfurt
SiHV005	*[2μ, URA3, eGFP,AmpR-ColE1]*	Backbone expression episomal plasmid with *URA3* marker .	Prof. Boles group, Frankfurt
SRV096	*[CenArs,URA3,AmpR-ColE1]*	Stable low copy expression plasmid for microscopy images.	Tamayo Rojas et al. 2021
YCplac33	*[CenArs,URA3,pBR322,AmpR]*	Low copy expression plasmid	Gietz and Akio 1988

Plasmid Libraries

Name	Comment	Manufacturer
MoClo-YTK - (Kit 1000000061)	Set of 96 plasmids used for the hierarchical assembly of single and multigene constructs for *S. cerevisiae*	Addgene

2.5 Oligonucleotides

Oligonucleotides used in this project were acquired from Biomers and originally provided in a lyophilised state. Each vial was resuspended with sterile double distilled water to a 100 μM concentration as a stock concentration. After resuspension, vials were submitted to an activation protocol by two cycles of heating at 90°C for 2 min and centrifuged at max speed for 1 min. This intended to ensure proper denaturation of oligos. Activated vials were either stored at -20°C until required or used to prepare a working stock vials by a 1:10 dilution.

Table 2.14: List of oligonucleotides used in the project. Once reconstituted to a 100μM concentration, vials were kept at -20°C until usage.

Primer name	Sequence	Comment
LBGp001	TAAATTTGTG TAGGAAAGGC AAAATACTAT CAAAATTTTC TTCGTACGCT GCAGGTCGAC	Integration of KanMX into *STE3* locus.
LBGp002	TACTCCTAGT CCAGTAAATA TAATGCGACA CTCTTGTGGC ATAGGCCACT AGTGGATCTG	Integration of KanMX into *STE3* locus.
LBGP003	ATTTGGCCGT TATCACGGAG	Test integration of kanMX into *STE3* locus.

Table 2.14 – continued from previous page

Primer name	Sequence	Comment
LBGP004	TCTGCCTTGG CCCAAATATC	Test integration of kanMX into *STE3* locus.
LBGP005	TTCCAGATGG TGCTGGAATG	Test integration of kanMX into *STE3* locus.
LBGP006	AAGTAGGCAC ATCCCTTACG	Test integration of kanMX into *STE3* locus.
LBGp019	TGGAATGCAA TCAAATCAAG AGTCGACCGA TTGAACTTGA ATTTGACGGA TGATCAAATC	Upstream *LYS21* locus amplification for strain s288c.
LBGp020	GATTTGATCA TCCGTCAAAT TCAAGTTCAA TCGGTCGACT CTTGATTTGA TTGCATTCCA	Insetion of Q364R into *LYS21* for strain s288c.
LBGp021	ACGCCAAGCT TGCATGCCTG CAGGTCGACT CTAGAGGATC ACAAACGCTT GACGGAAGAC	Insetion of Q364R into *LYS21* for strain s288c.
LBGp022	CGACGTTGTA AAACGACGGC CAGTGAATTC GAGCTCGGTA TGGATGACTG GGTGAAAGTG	Downstream *LYS21* locus amplification for strain s288c.
LBGp023	TCACCGGGTT CTGTGCATTC	Sequencing primer for *LYS21*.
LBGp024	CCCGTCTTCA AGCTAGATGC	Sequencing primer for *LYS21*.
LBGp031	GGATTTTACG CTGGGTTCGC GTTTTAGAGC TAGAAATAGC AAGTTAAAAT AAGG	CRISPR guide for pRCC-H targeting *LYS1*.
LBGp032	CGCGAACCCA GCGTAAAATC CGATCATTTA TCTTTCACTG CGGAG	CRISPR guide for pRCC-H targeting *LYS1*.
LBGp034	CTGCGATTTC AGCGACAAAG	Amplification of *LYS1* locus.
LBGp035	CGGAGGAAGA GGATTATGAG	Amplification of *LYS1* locus.
LBGp036	CTGCCACTGA CTGATCCTTG	Sequencing primer for *LYS21*.
LBGp037	GAGAGGGTGA ACAATTTGCC	Sequencing primer for *LYS21*.
LBGp040	TCTGCCTAAT ACCGACGTTG ATTTGCCCCC CTTGTCCGCC ATTTAAACTG TGAGGACCTT AATAC	Amplification of ARO3^{fbr}-ARO4^{fbr} cassette from JTV16 and integration into *PYK2*.
LBGp041	AATGGACAAT TAAATAAAAT TAAGTAAAAA AAATAAGGAC GGTACCGGCC GCAAATTAAA GCCTTC	Amplification of ARO3^{fbr}-ARO4^{fbr} cassette from JTV16 and integration into *PYK2*.
LBGp042	TCTGCCTAAT ACCGACGTTG ATTTGCCCCC CTTGTCCGCC ACAAACGCTT GACGGAAGAC	Amplification of *LYS21^{fbr}* cassette from LBGV004 and integration into *PYK2*.
LBGp043	AATGGACAAT TAAATAAAAT TAAGTAAAAA AAATAAGGAC TGGATGACTG GGTGAAAGTG	Amplification of *LYS21^{fbr}* cassette from LBGV004 and integration into *PYK2*.
LBGp097	GATCGACGCA AAGATCACAC CAAG	CRISPR guide for SIHV190 targeting *LYS9*.
LBGp098	AAACCTTGGT GTGATCTTTG CGTC	CRISPR guide for SIHV190 targeting *LYS9*.
LBGp145	TGCATGCCTG CAGGTCGACT CTAGAGGATC TGACAGTAAA TTAGGAGTTC TGTGTGCAC	Amplification of *ASR1*.
LBGp146	AAACGACGGC CAGTGAATTC GAGCTCGGTA TGCCTTAGTA AGTGAGAAAT ATGGCAAG	Amplification of *ASR1*.
LBGp189	CTTAGAGGTC TCAGATCTTT AACCGCTAGA GGTCTCCGTT TTGAGACCGA CGTCCTG	CRISPR guide for LBGV71 targeting *ART2*.
LBGp190	CAGGACGTCG GTCTCAAAAC GGAGACCTCT AGCGGTTAAA GATCTGAGAC CTCTAAG	CRISPR guide for LBGV71 targeting *ART2*.
LBGp191	CTCTATCAGC GATAGTGCTA CTAC	Amplification of *ART2* locus.
LBGp192	CTATAACTGC TATGCTGTAA GAGAC	Amplification of *ART2* locus.
LBGp193	CTTAGAGGTC TCAGATCATT TCTTTCGTTA GTTGTTTGTT TTGAGACCGA CGTCCTG	Amplification of *ARS1* locus.
LBGp194	CAGGACGTCG GTCTCAAAAC AAACAACTAA CGAAAGAAAT GATCTGAGAC CTCTAAG	Amplification of *ARS1* locus.
LBGp203	CGTCTCGTCG GTCTCATATG GGCAGGTTTA GTAACATAAT AACGTCCAAT	Forward oligo to crate a GG part 3a with *LYP1*.
LBGp205	GAACAGCAAC AGCAACAGAA CTCAC	Amplification of *WHI2* from 61-699 bp.
LBGp206	TTTCTGTTGT TGCTGTTGTT GCTTT	Amplification of *WHI2* from 61-699 bp.
LBGp207	CTTAGAGGTC TCAGATCTCA AACTGAAATT ACTCCTGGTT TTGAGACCGA CGTCCTG	CRISPR guide to attack *whi2* mutation in K1.

Primer name	Sequence	Comment
LBGp208	CAGGACGTCG GTCTCAAAAC CAGGAGTAAT TTCAGTTTGA GATCTGAGAC CTCTAAG	CRISPR guide to attack *whi2* mutation in K1.
LBGp209	CTTAGAGGTC TCAGATCAAC GGTCCAAAAA ACACCTGGTT TTGAGACCGA CGTCCTG	CRISPR guide to attack *whi2* mutation in Y2.
LBGp210	CAGGACGTCG GTCTCAAAAC CAGGTGTTTT TTGGACCGTT GATCTGAGAC CTCTAAG	CRISPR guide to attack *whi2* mutation in Y2.
LBGp213	CGAAAAGAAC AGAAAGCGCA AGAAGACAAC TCCTTCACAC TTAGGAAAGA CACAATATGT AACAGTATGG TTTCTTGGTA TCCCCTCTTT	Oligo donor for *WHI2* deletion.
LBGp214	AAAGAGGGGA TACCAAGAAA CCATACTGTT ACATATTGTG TCTTTCCTAA GTGTGAAGGA GTTGTCTTCT TGCGCTTTCT GTTCTTTTCG	Oligo donor for *WHI2* deletion.
LBGp221	CGTTTTCTCG GATGGGTTTC CTCCTTGATT AATGCTGCAT	Oligo for *LYP1* amplification removing undesired Bsa restriction site.
LBGp222	ATGCAGCATT AATCAAGGAG GAAACCCATC CGAGAAAACG	Oligo for *LYP1* amplification removing undesired Bsa restriction site.
LBGp225	TCCCATTAAA AATAAGGGAA AAGAGAA	Amplify *WHI2* locus.
LBGp226	TTCCTTCTTC ATGTGCTTTG AGACA	Amplify *WHI2* locus.
LBGp237	CGTCTCAGGT CGGTCTCAAG AACCTGCAAC AGCAGCCCAG AATTTCTCCC ATAAATTC	Reverse oligo to crate a GG part 3a with *LYP1*.
LBGp238	CTTAGAGGTC TCAGATCAAC GGTGACTGTG AATGTTGGTT TTGAGACCGA CGTCCTG	CRISPR guide for LBGV71 targeting *LYS2*.
LBGp239	CAGGACGTCG GTCTCAAAAC CAACATTCAC AGTCACCGTT GATCTGAGAC CTCTAAG	CRISPR guide for LBGV71 targeting *LYS2*.
LBGp240	TAATTATTGT ACATGGACAT ATCATACGTA ATGCTCAACC TAGTGAGTAA CTCTGTGATA TCTCTCTATA ATTAGCAGTT	Oligo donor for *LYS2* deletion.
LBGp241	AACTGCTAAT TATAGAGAGA TATCACAGAG TTACTCACTA GGTTGAGCAT TACGTATGAT ATGTCCATGT ACAATAATTA	Oligo donor for *LYS2* deletion.
LBGp242	CTTAGAGGTC TCAGATCCTA AGCTCGTTCA AACTAGGGTT TTGAGACCGA CGTCCTG	CRISPR guide for LBGV71 targeting *LYS14*.
LBGp243	CAGGACGTCG GTCTCAAAAC CCTAGTTTGA ACGAGCTTAG GATCTGAGAC CTCTAAG	CRISPR guide for LBGV71 targeting *LYS14*.
LBGp244	TATATCAATC TACAGGCAAA ATTATTACGT AAACAGACAA TATTGCCAGA AAACAGATCT TATACCAAAA TGATGAGAGA	Oligo donor for *LYS14* deletion.
LBGp245	TCTCTCATCA TTTTGGTATA AGATCTGTTT TCTGGCAATA TTGTCTGTTT ACGTAATAAT TTTGCCTGTA GATTGATATA	Oligo donor for *LYS14* deletion.
LBGp254	GAATGGCAAA GTGGTGATAG AGTTCATA	Amplify *LYS2* locus.
LBGp255	ACTGATTATT CGATTTTCTT CTTGCTGA	Amplify *LYS2* locus.
LBGp256	TATTGTTATG GAAGGTTTAG TGCTGGAG	Amplify *LYS14* locus.
LBGp257	ATAGGCCGAT TAGAATGCTT ATTGTTCT	Amplify *LYS14* locus.
LBGp260	CTTAGAGGTC TCAGATCAAG ACAATATTCC CACGGTAGTT TTGAGACCGA CGTCCTG	CRISPR guide for LBGV71 targeting *LYS20-LYS21*.
LBGp261	CAGGACGTCG GTCTCAAAAC TACCGTGGGA ATATTGTCTT GATCTGAGAC CTCTAAG	CRISPR guide for LBGV71 targeting *LYS20-LYS21*.
LBGp262	ATAACAAACA AAGGAAGGAC CCTGTATTGT TTTCCTAAAG CGTTCCCAAA CCATTACATT ATGTTCTTTC ACTTATTACA	Oligo donor for *LYS20* deletion.
LBGp263	TGTAATAAGT GAAAGAACAT AATGTAATGG TTTGGGAACG CTTTAGGAAA ACAATACAGG GTCCTTCCTT TGTTTGTTAT	Oligo donor for *LYS20* deletion.
LBGp264	GAATTTTCTC TTCGGTAGTG GACGA	Amplify *LYS20* locus.
LBGp265	TTCTTCTTTT AATGCGTATC GGACA	Amplify *LYS20* locus.

Table 2.14 – continued from previous page

Primer name	Sequence	Comment
LBGp266	GTGCAACGAC AACCCAAGTA ATTGTATACT TTAACAAACC TTTCATTATA TATATAGTAC ACATATTTCA AACATACACA	Oligo donor for *LYS21* deletion.
LBGp267	TGTGTATGTT TGAAATATGT GTACTATATA TATAATGAAA GGTTTGTTAA AGTATACAAT TACTTGGGTT GTCGTTGCAC	Oligo donor for *LYS21* deletion.
LBGp268	AGATATGGCA CTTCTCTTTC CGTTG	Amplify *LYS21* locus (used with LBGP024).
LBGp269	CAAAAACAAA AAGTTTTTTT AATTTTAATC AAAAAAGATC TATGGGCAGG TTTAGTAAC	Forward oligo for *LYP1* integration into SRV096 (UCP).
LBGp270	CAGGACAATT GAGTTATATT AACGTATTAT ATATTTTAAT ATAAGAAGAA ATGTATCAAA AGGTTTATCA TACGTAACAG	Oligo donor for *LYS9* deletion.
LBGp271	CTGTTACGTA TGATAAACCT TTTGATACAT TTCTTCTTAT ATTAAAATAT ATAATACGTT AATATAACTC AATTGTCCTG	Oligo donor for *LYS9* deletion.
LBGp272	TCAATAAAGG GTATTGAGAA TTTCCAATGG	Amplify *LYS9* locus (used with LBGP090).
LBGp273	AGAGAAGAAC AAGCAAGATT TTTCCCTACC CCTATTGGGC GAATTATTCT ACGATAATTA TATATATAGA GCCACTGCAT	Oligo donor for *ART2* deletion.
LBGp274	ATGCAGTGGC TCTATATATA TAATTATCGT AGAATAATTC GCCCAATAGG GGTAGGGAAA AATCTTGCTT GTTCTTCTCT	Oligo donor for *ART2* deletion.
LBGp275	CTCCACTTTC CCGCCTATAT TTCTA	Amplify *ART2* locus.
LBGp276	AGCATGTAGT CAACAAAAAG GGAGT	Amplify *ART2* locus.
LBGp288	CGTCTCGTCG GTCTCATATG GGAAAGAACG TTTTGTTG	Forward oligo to crate a GG part 3 with *LYS9*.
LBGp289	CGTCTCAGGT CGGTCTCAGG ATTTAAGCCA CTGTCTTTTC CTTTAG	Reverse oligo to crate a GG part 3 with *LYS9*.
MRP194	TGTCGGTATG TAATAGGTTA GTGG	Amplification of *ARO10* locus.
MRP195	AATTTGGCGG CCTTTTATAG TTC	Amplification of *ARO10* locus.
MRP193	TAAAGTTTAT TTACAAGATA ACAAAGAAAC TCCCTTAAGC AAACTTGTGG GCGCAATTAT AAAACACTGC TACCAATTGT	Donor oligo for *ARO10* deletion.
MRP202	GAATTACAAG AATACCGTAG CACTTG	Amplification of *TYR1* locus.
MRP203	CGAACGGTCA CTAGAATGAC TC	Amplification of *TYR1* locus.
MRP199	CTGAAAGAAA AATATGCCTC AGCTAAATTC GAACTGGTGA ATCCATGATA AATCATTCAT AAAAGATGAT TTAGAATTTG	Donor oligo for *TYR1* deletion.
SiHP060	GGGCGGATTA CTACCGTT	Check *URA3* integration upstream.
SiHP061	GTAATGTTAT CCATGTGGGC	Check *URA3* integration upstream.
SiHP062	AGAGCACTTG AATCCACTGC	Check *URA3* integration downstream.
SiHP063	GATTTGGTTA GATTAGATAT GGTTTC	Check *URA3* integration downstream.
SiHseq001	TCCTGGCCTT TTGCTGG	Sequencing primer for pYTK001 derived plasmids.
SiHseq002	GGACTCCTGT TGATAGATC	Sequencing primer for pYTK001 derived plasmids.
SRP344	AAGCGTGACA TAACTAATTA CATGACTCGA GTTATTTGTA CAATTCGTCC ATTC	Reverse oligo for *LYP1* integration into SRV096 (UCP).

2.6 Synthetic DNA

Codifying sequences ordered in the present project were acquired from Twist Biosciences. Table 2.15 presents the list of acquired genes.

Table 2.15: Synthetic genes used in this project. Genes used codon optimisation strategies to improve protein synthesis efficiency.

CDS name	Protein	Organism
CYP76AD1	Tyrosine hydroxylase	Beta vulgaris
DOD	DOPA dioxygenase	Mirabilis jalapa
TAL	Tyrosine ammonia-lyase	Rhodobacter sphaeroides

The online tool JCat (Grote et al. 2005) was selected for the codon optimisation process of the acquired genes, but due to constraints during the synthesis problems, just the *DOD* from *Mirabilis jalapa* was processed using this algorithm. The *CYP76AD1* from *Beta vulgaris* and the *TAL* from *Rhodobacter sphaeroides* were codon optimised using a Geneious software strategy that randomises them by avoiding codons presenting a low threshold usage.

2.7 Microbial culture processes

This section will define the different microbial culture regimens employed for the present project.

2.7.1 Bacterial culture

Bacterial strain cultures used LB media supplemented with relevant antibiotics in accordance with the selection markers present on plasmids. Antibiotic concentrations were presented in section 2.3.5.

Positive clones were screened after overnight incubation at 37°C utilising LB-agar plates supplemented with relevant antibiotics. The selection process was based on the displayed phenotype, discriminating between green or white colonies depending on the presence of fluorescent proteins on the plasmids.

Once positive clones were selected, liquid cultures were prepared, inoculating cells from one colony into 5 ml of LB media supplemented with relevant antibiotics at 37°C for approximately 18 h before processing as required.

2.7.2 Yeast culture

Three main kinds of media were used for yeast cultivation: YPD, SCD and SMD. Liquid cultivations were performed in shake flasks of 100 or 300 mL using a shaking speed of 180 h at 30°C.

Prior to the preparation of experimental cultures, biomass originated during preculture was washed with double distilled sterile water two times using centrifugation rounds of 3,000 xg for 2 minutes.

2.7.2.1 Yeast single culture

Single culture fermentation refers to cultures done with just one strain, analysing the relative performance of this strain under a defined genotype and media. Experiments on overproducer strains for a given amino acid were performed in media lacking that amino acid. For each fermentation, the preculture used the same media that would be employed in the experiment, using a volume from 30 to 50 mL for approximately 48 h.

Fermentations used 300 mL flasks with 30 ml of media, inoculated to an OD of 0.2 OD_{600} unless otherwise specified. The Aquila CGQ sensor was used to detect increases in cell density during fermentation.

2.7.2.2 Yeast co-culture cultivation

Co-culture fermentation refers to cultures using two strains with complementary phenotypes around the exchange of lysine and tyrosine. In this sense, media used for co-culture experiments always lacked lysine and tyrosine. Preculture of individual strains was performed for 48 h in media lacking the amino acid each one overproduced.

Shaking flasks of 300 mL with 30 ml of media were used for fermentations. Unless otherwise specified, strains were inoculated to an individual OD of 0.2 OD_{600}. Monitoring of changes in the culture's cell density was performed using the Aquila CGQ system.

2.7.2.3 Aquila CGQ sensor

The CGQ system allows non-invasive monitoring for microbial proliferation in liquid media. Biomass growing into a transparent glass flask is exposed to light pulses, which are scattered after interacting with the microorganisms. A sensor collects the back-scattered light transforming it into a signal that, in this way, produces an estimation of the culture's density at any given time (Bruder et al. 2016).

Nevertheless, the arbitrary units (a.u.) in which the equipment assesses biomass density cannot be directly related to more universally used methods such as OD_{600}, as these values depend on the sensor used, the transparency of the media, the cell size and the quality of the shaking flasks used (lack of scratches). In this sense, this sensor was used to establish the time point of the beginning of the growth phase of each fermentation, rather than to establish differences in biomass yield.

Record files collected from each experiment were normalised to the lowest registry for each flask experiment. Later on, an arbitrary value of 100 a.u. was added to each registry to compensate for the original biomass signal at the beginning of the experiment. Finally, a sampling reduction process was performed on the processed values for better data handling during the graphic production process. This process involved sampling every 20 registries for fermentations up to 72 h long or every 100 values for longer fermentations.

Unless specified otherwise, all experiments were performed at least in triplicates using shaking flasks of 300 mL capacity, using 30 mL media.

2.8 Molecular biology methods

2.8.1 Yeast DNA extraction

Yeast genomic DNA extraction for PCR processes was performed with modifications as described by Lõoke et al. 2011.

Briefly, one colony from a culture no older than 30 h or 100 μL of a yeast liquid culture in early exponential phase were resuspended in 100 μL of a 200 mM lithium acetate 1% SDS solution, vortexing vigorously to disrupt cell clumps. Vials were incubated at 70°C for 10 min, followed by the addition of 300 μL of 96% ethanol to precipitate DNA. The supernatant was discarded after a 15,000 xg centrifugation for 3 min, and the white precipitate was washed again using 500 μL of 70% ethanol by pipetting to disrupt the pellet completely. Using the previous settings, the supernatant was thoroughly discarded after a new centrifugation step. The remaining ethanol was dried by incubating vials with the lead open at 42°C for 45 min.

Once completely dry, cell pellets were resuspended with 50 μL of double distilled water, disrupting the cell pellet by pipetting. Vials were incubated at room temperature for 1 h to allow precipitated DNA to be resuspended in water. Finally, cell debris was precipitated

by centrifuging the vials at 15,000 xg for 1 min.

The supernatant obtained could be successfully used to prepare PCR reactions, and if long-term storage was required, it was stable for up to three months after carefully transferring it into a clean vial.

2.8.2 Bacterial plasmid extraction

Following bacterial cultivation in selective media, plasmid extraction was performed by using the GeneJET Plasmid Miniprep Kit following the manufacturer's recommendations, except for the plasmid final elution, which was performed using 50 μL of sterile double-distilled water.

2.8.3 Polymerase chain reaction

The ability to increase the amount of a given DNA sequence is a tool of paramount importance in molecular biology. This section will present the techniques used to this end, according to the different enzymes used and pursued ends. Annealing temperatures for the oligos employed during amplification reactions were obtained using the NEB temperature calculator tool.

2.8.3.1 High-fidelity DNA amplification

High-fidelity DNA amplification techniques were employed when the obtained oligo sequence needed to be conserved for further down processes such as cloning or sequencing. To this end, Q5 or Phusion high-fidelity DNA polymerase were used according to manufacturer recommendations.

Table 2.16: High-fidelity DNA amplification protocol.

Component	Stock concentration	Working concentration	Volume used
Polymerase compatible buffer	5x	1x	10 μL
dNTPs	10 mM	200 μM	1 μL
Primer forward	10 μM	500 nM	2.5 μL
Primer reverse	10 μM	500 nM	2.5 μL
High fidelity polymerase (Q5 or Phusion)	2,000 U mL^{-1}	1 U	0.5 μL
Template	variable	20ng	variable

After the amplification, reactions were supplemented with Loading Buffer Dye, Purple to a 1x concentration, and analysed via electrophoresis using a 1% agarose gel. Prior to further use of the obtained amplicons in cloning or sequencing processes, the remaining volume of the PCR reaction was purified using the NucleoSpin Gel and PCR Clean

Up kit according to manufacturer recommendations, except for the elution, which was performed in 30 μL of sterile double distilled water.

Table 2.17: High-fidelity thermal cycling protocol. The second step was repeated for 35 cycles.

Step	Temperature	Duration	Function
1	98°C	30 sec	Initial denaturation of DNA
2	98°C	10 sec	Denaturation of DNA
	50-72°C	20 sec	Primers annealing
	72°C	30 sec per kb	DNA elongation
3	72°C	5 min	Final DNA elongation

2.8.3.2 Splicing overlap PCR

The splicing over PCR technique was employed to merge DNA fragments that shared homology sections between them. Individual fragments were added as templates into a high-fidelity DNA amplification reaction, using the forward primer of the desired upstream fragment and the reverse primer for the downstream fragment relative to the desired construct. In this way, initial amplification would produce partial products that eventually would anneal with each other, allowing further amplification rounds to produce the complete constructs.

2.8.3.3 DreamTaq DNA polymerase

DreamTaq amplification was employed to evidence correct genomic integration into the desired locus. Amplicons generated based on this technology were directly revealed in agarose gels at 1% via electrophoresis.

Table 2.18: Dream-Taq DNA amplification protocol.

Component	Stock concentration	Working concentration	Volume used
DreamTaq green buffer	10x	1x	1.25 μL
dNTPs	10 mM	200 μM	1 μL
Primer forward	10 μM	500 nM	2.5 μL
Primer reverse	10 μM	500 nM	2.5 μL
DreamTaq DNA polymerase	5 U mL^{-1}	1.75 U	0.35 μL
Template	variable	20ng	variable

Table 2.19: DreamTaq thermal cycling protocol. The second step was repeated for 40 cycles.

Step	Temperature	Duration	Function
1	95°C	30 sec	Initial denaturation of DNA
2	95°C	10 sec	Denaturation of DNA
	50-72°C	20 sec	Primers annealing
	72°C	60 sec per kb	DNA elongation
3	72°C	5 min	Final DNA elongation

2.8.4   Enzymatic digestion

When required, correct plasmid assembly was evaluated via enzymatic digestion of obtained oligos prior to Sanger sequencing processes. The endonucleases employed were chosen so that the digested fragments produced would be of different sizes for easier identification during the electrophoresis process. A final reaction volume of 10 μL, including 500 ng of DNA, 0.5 μL per restriction enzyme per sample, was prepared using the adequate digestion buffer. Samples were digested at 37°C for at least 1 h and were supplemented with 3 μL of Loading Buffer Dye, Purple prior to being resolved in a 1% agarose gel for fragments analysis using electrophoration.

2.8.5   Electrophoresis

The extension of the DNA fragments generated in this project was evaluated using agarose gel electrophoresis. This technique allows the characterisation of DNA fragments based on their molecular weight by exposing them to an electric field that, due to the negative charge of DNA's phosphate groups, forces molecules to migrate towards a positive pole. Consequently, smaller fragments will migrate across the agarose gel faster than large ones, allowing a relative characterisation of their sizes.

The DNA samples were loaded into a 1% agarose gel prepared in 1x TAE-buffer (TRIS 40 mM and EDTA 1 mM to a pH of 8 adjusted with acetic acid) and exposed to a 120 to 150 V until a good band separation could be obtained approximately 40 min. For estimation of fragments size 7 μL of DNA Ladder Gene Ruler 1kb Plus, previously supplemented with loading buffer to a 1x concentration, was loaded next to the DNA lines.

2.8.6   Sanger sequencing

Candidate oligos were sequenced using Sanger technology to evaluate the correct DNA amplicons or plasmids sequence. These processes were performed by hiring sequencing services from Mycrosynth®. According to the service supplier, 15 μL reaction tubes were produced per sequencing order, including around 600 ng of plasmid DNA or 200 ng of cleaned PCR product and 20 μM of sequencing primer.

The ABI files generated after sequencing were analysed using Geneious software (Biomatters 2019).

2.8.7   Yeast transformation

Precultures of the desired strain were prepared using 50 mL of YPD liquid media until the early exponential phase, meaning an OD_{600} range between 0.8 till 3.0 using the conditions described in section 2.7.2. Once that point was reached, cells were collected and washed two times using 25 mL and 0.5 mL of double distilled water, respectively. The pellet was dissolved in a given volume of sterile double distilled water, such that aliquots of 50 μL carry 5 OD_{600} equivalent units. If cells were required for a future transformation, FCC (see section 2.1.3.1) was used for resuspension. Aliquots were stored at -80°C for up to 8 months. Prior to usage, frozen vials were thawed at room temperature for 2 min.

A volume of 306 μL of transformation solution (see section 2.1.3.2) was supplemented with 54 μL of DNA mix to be transformed. For plasmid transformation, around 1 μg of DNA were employed, while for linear DNA, 500 ng of annealed oligos were used.

Previously prepared cell aliquots were centrifuged at 3,000 xg for 2 min to remove supernatant. The prepared transformation mix was used to gently resuspend the cell pellet by slowly pipetting the volume up and down. The cell suspension was submitted to a heat shock at 42°C for 45 min, followed by centrifugation at 3,000 xg for 2 min to remove the supernatant.

If transformants selection would be based on an auxotrophy marker, the cell pellet was resuspended in 100 μL of sterile double distilled water and directly plated on the selective media. While, if dominant markers were used, a regeneration process was performed by resuspending cells in 3 mL of YPD media without selection and incubating them at 30°C for 4 h in a shaker at 180 rpm. After this period, cells were recovered, centrifuged as previously described and plated into selective media.

Plates incubation was performed at 30°C for 4 days or until visible colonies could be appreciated.

2.8.8   Preparation and transformation of *E. coli* cells.

Competent cells preparation

A 400 mL LB preculture from one colony of DH10B *E. coli* strain was growth until and OD_{600} cell density of around 0.6. The culture was split into eight aliquots, 50 mL each and incubated in an ice bath completely submerged for 30 min.

The cell pellet was recovered by centrifuging it at 4,000 xg for 15 min at 4°C, these condi-

tions were used for all centrifugation steps required during the preparation of competent *E. coli* cells. Three serial cell concentration processes were performed after subsequently resuspending the obtained cell pellets up to a volume of 25 mL and concentrating in one vial the cells proceeding from two aliquotes until all biomass was contained in one vial.

The obtained cell pellet was washed in 4 mL of steril 10% (w/v) glycerol ice cold. The cell pellet was distributed in 50 μL aliquots after resuspending it in ice cold 4 mL of steril 10% (w/v) glycerol. Prepared aliquots were stored at -80°C until needed.

Transformation

For transformation of competent *E. coli* cells, a vial of previously prepared competent cells were defrosted at room temperature for 2 min and supplemented with approximately 20 ng of the required plasmid DNA. The mixture was transferred and evenly distributed to an electroporation cuvette of 2 mm gap size.

Condensation formed was wiped, and an electric pulse of 2.5 kV was applied using a Gene Pulser set with a resistance of 200 Ω and capacitance of 25 μF. Cells were resuspended using 1 mL of LB media and recovered in a regular 1.5 mL microtube at 37°C for 45 min. After centrifuging cells at 4,500 xg for 3 min, the supernatant was partially removed, leaving a volume of approximately 200 μL used for cell resuspension. Positive transformant selection was performed using LB-agar plates supplemented with the appropriate selection marker and incubated at 37°C overnight as described in section 2.7.1.

2.8.9 GoldenGate assembly

The modular hierarchical assembly strategy developed by M. E. Lee et al. 2015, commonly known as the GoldenGate system was used during the development of plasmids in this project. This system is based on single-mix reactions that exploit the use of ligases, type II restriction enzymes and precisely designed cut sites to assemble plasmids, allowing a wide variety of expression systems. In this way, the system allows an easy exchange of promoters, terminators, CDS, selection markers and even the generation of multi-expression plasmids.

The system employs three different plasmid levels: The first level, described as a part plasmid, allows the handling of single oligonucleotide units without expression components. CDS, which were not originally part of this toolkit, were introduced into the system at this stage. The second level involves the hierarchical assembly of expression units,

described as cassette plasmids, which includes promotor, CDS and terminator regions and other structural connector pieces, selection markers and replication ori regions as needed. The last level, named multigene plasmid, allows the assembly of multiple expression units in one single plasmid.

Table 2.20: GoldenGate thermal cycling protocol. Consecutive digestion and ligation process referred to in the second step was performed 15 times if the reaction involved less than 5 components, otherwise, 25 cycles were employed.

Step	Temperature	Duration	Function
1	37°C	10 min	Initial digestion
2	37°C	1.5 min	Digestion
	16°C	3 min	Annealing and ligation
3	37°C	5 min	Final digestion
4	50°C	5 min	Ligase inactivation
5	80°C	10 min	Restriction enzyme inactivation

The assembly of plasmids in the present project, unless stated otherwise, were developed using this system following the original guidelines and recommendations proposed by M. E. Lee et al. 2015 in the original paper with minor modifications such as the use of the restriction enzyme Esp3I instead of its BsmbI because of its better performance at lower temperatures and the use of the optimised BsaI-HFv2 instead of the original BsaI.

The temperature cycling program and reaction preparation protocol are presented in tables 2.20 and 2.21, respectively.

Table 2.21: GoldenGate thermal cycling protocol. The consecutive digestion and ligation process referred to in the second step was performed 15 times if the reaction involved less than five components; otherwise, 25 cycles were employed.

Components	Stock	Working concentration	Volume used
T4 DNA ligase buffer	10x	1x	1 μL
Type II endonuclease (BsaI HFv2/Esp3I)	10,000-20,000 U mL^{-1}	5-10 U	0.5 μL
T7 DNA ligase	3'000,000 U mL^{-1}	1,500 U	0.5 μL
CRISPR/Cas9 vector backbone	variable	12 $f$mol	variable
Annealed oligos	1 μM	12 $f$mol	0.2 μL

2.8.10 Homologous recombination integration

The homologous recombination machinery in yeast was exploited during the genomic integration of oligonucleotides, mutation insertion and plasmid construction strategies.

Homology regions to a desired target with an extension of 40 bp were introduced via PCR up and down-stream of genes of interest, which later on were transformed into strains as described in section 2.8.7. The availability of these homologous overhangs was supposed to promote recombination processes in yeast, allowing the production of

the desired modifications or assembly of plasmids. Integration plasmids constructed via GoldenGate system employed homology regions of 300 bp, initially available in the system.

The selection of positive transformants was performed based on selection markers employed during the process and via PCR confirmation to verify that integration occurred in the desired locus.

2.8.11 CRISPR/Cas9 construction and usage

The CRISPR/Cas9 plasmids used in the presented work are derived from the vectors developed by Generoso et al. 2016 with minor modifications. The original strategy for introducing the CRISPR-guide sequence was modified to exhibit an eGFP dropout to be replaced by the desired guide after a GoldenGate assembly process.

The CRISPR-guides for this project were designed using CRISPOR web tool (Concordet & Haeussler 2018), and cloned following the protocol previously described in section 2.8.9, employing a BsaI-HFv2 GoldenGate strategy. Positive colonies were screened first based on the absence of eGFP expression and by sequencing the guide and gRNA structures.

The versatility of this system even allowed for the design of targeted plasmids for introducing punctual mutations by employing donor oligos with down to one nucleotide of difference in the CRISPR-guide sequence. In later sections, this approach is referred to as CRISPR/Cas9-assisted strategy.

2.9 Evolved strains separation

Strains isolation after the evolution rounds used the genetic markers integrated into the parental strains. If no dominant marker could be used, the separation was done based on the engineered auxotrophies of parental strains.

A sample from the colony or 30 μL of the liquid media containing the strains to be separated were diluted 500 μL of sterile water, and vortexed vigorously for 10 sec. A volume of 30 μL was then plated in a YPD agar plate supplemented with G418 and incubated at 30°C for 48 h or until the development of colonies could be spotted.

Observed colonies were individually stamped into selective media plates to discriminate the lineage of the colony, i.e. media with different antibiotic selections for dominant markers discrimination or plates with and without the exchange metabolites. An addi-

tional plate with non-selective media was used after the colonies were seeded into the selective media as a positive control for sample viability. If a colony grew in more than one selective media was considered still to be a co-culture and discarded from further analysis.

Colonies that suggested being single descendants from a parental strain were re-spread into three consecutive, non-selective, YPD agar plates to ensure that any mixed population from the same parental strain would be separated.

2.10 Quantification methods

2.10.1 Optical density determination

The optical density (OD) of cultures using a $\lambda=600$, referred to as OD_{600}, was employed as an indicator of the biomass density at a given time point. The measurements were performed in a Spectrophotometer Ultrospec 2100 Pro (Amersham Bioscience), blanked with double distilled water. A linear relation between biomass cell density and the OD_{600} values obtained from the equipment were considered to exist up to a value of 0.3; samples that exceeded this value were diluted accordingly.

2.10.2 Fluorescence tracking

The integrated fluorescent markers in the strain were utilised as indicators to establish the relative proportion of the cells at a given time.

Fluorescence determinations were performed using a fluorescence spectrophotometer from CLARIOstar Plus BMG LABTECH. Optical settings for the GFP channel used excitation and emission ranges of 455 to 495 nm and 495 to 535 nm, respectively. The dichroic filter was set to 491.2 with a focal height of 6.4 mm and a gain of 2,087. For the mRuby channel, excitation and emission ranges of 544 to 574 nm and 585 to 615 nm were used, respectively. The value for the dichroic filter was set to 579.5 with a gain of 2,753 and a focal height of 6.2 mm. Data collection for both channels used spiral scan mode with a diameter of 4 mm in 96 well plates with flat and clear bottoms. Shaking frequency during measurements used orbital mode with a frequency of 500 rpm adding 20 sec of shaking before reads. All data processing performed used raw values.

First, calibration lines using each strain at different OD_{600} were produced to establish a relation between the fluorescence's arbitrary units and known cell density values. This analysis proved the lack of cross-signal contamination between both channels.

Samples processing was performed as follows: at established time points, aliquots of approximately 1 mL were recovered from each flask to establish the OD_{600} cell density values as described in section 2.10.1. The supernatant was discarded after centrifuging the vials at 3,000 xg for 5 min. Cell pellets were washed two times with double distilled water using centrifugation cycles of 3,000 xg for 2 min. Cell pellets were resuspended in water using a variable volume that was adjusted aiming for a vial OD_{600} value of around 0.2.

Fluorescence analysis was conducted in technical triplicates using a volume of 200 μL per well in 96 well plates with flat and clear bottoms. Technical replicas per experiment were averaged, and this value was used to estimate the proportion of cells per population at that given time point. Partial populations were added to establish the total cell density of the vial. This allowed the estimation of the proportional conformation of both populations in the culture.

Nevertheless, it is important to highlight that these estimations were done in washed and diluted samples, which prevents a relation can be constructed between the original OD_{600} values measured before washing and values obtained after adding both population's individual OD_{600} titters.

2.10.3   High-performance liquid chromatography determinations

Metabolite secretion into culture media was monitored via high-performance liquid chromatography (HPLC). The analysis employed an HPLC+ focused system Dionex UltiMate 3,000 equipped with an RS variable wavelength detector. Equipment operation and data analysis were conducted using Chromeleon software version 6.8 from Thermo Scientific.

Samples from the culture were centrifuged at 3,000 xg for 5 min and supernatants aliquots were recovered for HPLC determination. Before measurement, all samples were supplemented with acetonitrile to a final concentration of 20%.

2.10.3.1   Determination of *p*-hydroxyphenyl ethanol

Determination of *p*-hydroxyphenyl ethanol was performed according to the protocol provided by Reifenrath and Boles 2018. Briefly, eluent A (8 mM KH_2PO_4, pH 2.4) and eluent B (100% acetonitrile) were used in the gradient program described in table 2.22 at 40°C. Detection of *p*-hydroxyphenyl ethanol was achieved using a wavelength of 215 nm while using an Agilent Zorbax SB-C8 column (4.6 $\times$ 150 mm, 3.5 μm) with an injection volume of 25 μL.

Table 2.22: HPLC program for quantification of *p*-hydroxyphenyl ethanol. Protocol was adapted from Reifenrath and Boles 2018.

Time (min)	Flow (mL min$_{-1}$)	Eluent B(%)
0	1	0
5	1	0
25	1	10
28	1	30
33	1	30
35	1	0
40	1	0

2.10.3.2 Determination of *p*-coumaric Acid

Determination of *p*-coumaric acid together with *p*-hydroxyphenyl ethanol used a protocol adapted from Gottardi, Reifenrath, et al. 2017. An isocratic program using 80% of eluent A (0.1% of formic acid in ddH$_2$O) and 20% of B eluent (0.1% of formic acid in acetonitrile) in an Agilent Zorbax SB-C8 column (4.6 × 150 mm, 3.5 μm) using a steady flow rate of 1 mL min^{-1} and a temperature of 40°C allowed the detection of *p*-coumaric acid and *p*-hydroxyphenyl ethanol at wavelengths of 310 nm and 214 nm, respectively using an injection volume of 25 μL.

2.10.3.3 Tyrosine determination

Determination of tyrosine together with *p*-hydroxyphenyl ethanol was performed using a protocol modified from Hassing et al. 2019. A gradient protocol involving eluent A (20 mM KH$_2$PO$_4$, pH 2.4) and eluent B (100% acetonitrile) were used in a Zorbax Eclipse Plus C18 Rapid Resolution (4.6 x 150 mm 0.5 μm) column according to conditions described in table 2.23 at 40°C with an injection volume of 5 μL. Detection of both metabolites was achieved at a wavelength of 215 nm.

Table 2.23: HPLC program for quantification of tyrosine and *p*-hydroxyphenyl ethanol. Protocol was adapted from Hassing et al. 2019.

Time (min)	Flow (mL min$_{-1}$)	Eluent B(%)
0	0.8	1
4.5	0.8	7.8
6	1.2	10
9.5	1.2	14
10	0.8	15
13	1.2	19
16	1.2	23
18	0.8	25
22	0.8	30
25	0.8	1
30	0.8	1

2.11　Whole genome sequencing process

2.11.1　Genomic DNA extraction

The genomic DNA extraction was performed using the GeneJET Genomic DNA Purification Kit, according to the manufacturer's recommendations. Genomic DNA concentration from each extracted sample was measured using a Nanodrop 1000 spectrophotometer from Thermo Scientific, and its quality, as well as RNA purity, were evaluated by electrophoresis in an agarose gel.

2.11.2　Genomic library construction and high-throughput DNA sequencing

Once the genomic DNA has been extracted, library preparation and High-throughput DNA Sequencing processes were performed by hiring services from Novogene Co., Ltd.

The methods reported by the company begin with an agarose gel electrophoresis to check for integrity and purity of the genetic material, followed by a Qubit® 3.0 fluorometer quantitation to establish if all samples had concentrations above 500 ng, allowing library construction. Samples were sliced randomly into approximately 350 bp fragments before using the NEBNext® DNA Library Prep Kit for library preparation according to its instructions. Briefly, fragment ends were repaired by 5' phosphorylation and dA-tailing. NEBNext adapters were ligated to the fragments, which were subsequently PCR enriched using P5 and P7 oligos and subsequently purified. Fragments size was assessed using Agilent® 2,100 bioanalyser at a 1 ng/uL and via quantitative real-time PCR (qPCR). Samples with concentrations above 2 nM of an appropriated insert size (between 300 and 500 bp size) were considered suitable for Illumina® high-throughput sequencing.

Libraries qualified were pooled accordingly to expected data production and real concentration. The Illumina® sequencing platform performed the pair-end sequencing with a read length of PE150 at each end.

Raw data collected by the sequencing process was stored in two FASTQ files per strain (separate data sets for forward and reverse reads) and cleaned according to the company quality standard using internal proprietary software to eliminate reads with adapters contamination or low-quality reads (undetermined bases content higher than 10% or Q_{phred} score equal or lower than 5).

2.12 Bioinformatic analysis

Bioinformatic analysis and processes such as pairing data sets, further data sets cleaning, mapping of data sets versus a reference genome, detection of sequences variations and identification of low and high coverage areas, as well as the generation of consensus sequences were done using Geneious Prime software (Biomatters 2019).

Once files were received, quality control was performed using FastQC software (Andrews 2018) to confirm they were fitted for further processing. The files validation process was based on the lack of alarm signals on the FastQC analysis for both reads of the same strain data set, especially regarding the absence of over-represented reads that could suggest the presence of adapter sequences.

The generated FASTAQ files contained information regarding the quality of each read as ASCII characters. These values are used to generate the Q_{phred} scores according to the equation $Q_{phred}=-10\log_{10}(e)$, producing a logarithmic estimation of the likelihood of a base being called incorrectly (Ewing & Green 1998).

The relation between the likelihood of a base being called correctly, the Phre score and the Q_{phred} score can be found in the table 2.24

Table 2.24: Q_{phred} score and related error rates

Phred score	Error base	Right base	Q-score
10	1 in 10	90%	Q10
20	1 in 100	99%	Q20
30	1 in 1,000	99.90%	Q30

Files that were not properly cleaned by Novogene Co., Ltd were processed using the BBDuk plugin (Bushnell 2015) to remove low-quality reads with Q_{phred} scores of less than 20 on both ends and minimum overlaps of 20 base pairs. The slicing process was performed after both data sets, forward and reverse reads, were paired together.

Paired and clean data sets were mapped using the Genious mapper algorithm, with Low-Medium Sensitivity using up to five consecutive iterations to emphasise variations in findings and avoid further trimming.

The reference genomes required for the data sets mapping process were developed from a CEN.PK 113-7D *de-novo* assembled genome (Salazar et al. 2017) including all the known modifications relative to the analysed strain. Once the analysis of parental strains produced consensus genomes, they were used as reference genomes for the evolved strains mapping processes. High and low coverage areas were defined as regions with

coverage above or below two standard deviations from the coverage media, merging similar annotations that were less than 50 base pairs apart from each other.

Variations on the analysed genomes were defined with a minimum representation frequency of 0.5 when working with haploid strains. Variations across the genomes were detected, with particular emphasis on non-synonymous and no silent variants inside coding regions. Additionally, variations inside low-coverage areas were dismissed as sequencing artefacts.

Consensus sequences were generated setting a threshold of 50% for the highest quality so that a variation would be accepted when the sum of all quality data for that variation is higher than the 50% of all variations values in that position.

Once generated, the variations data per strain were used to conduct individual analysis into the mapping files, using information relative to coverage and variant relative frequency to validate possible mutations.

2.13   Copy number variation

The possible existence of partial or total chromosomal duplications as an evolutionary product was explored using the CNVpytor tool (Suvakov et al. 2021). It allows the detection of copy number variations (CNV) based on whole genome sequencing data, particularly on the read depth of aligned reads.

The ".bam" files required for the analysis were obtained from the mapping process performed in the Genious platform during the whole genome sequencing analysis of each strain. Individual mask files were created according to the specification of the CNVpytor development team, specifying the chromosomal length for each strain, values that were also obtained from the Geneious analysis. Histogram analysis and GC correction per strain were performed using a threshold of 1,000 base pairs as the smallest extension searched for an area with copy number variations.

Chapter: 3 Results

The present project aimed to obtain a better understanding behind the conformation and evolution of synthetic cooperative (syntrophic) consortia, seeking to elucidate if the selective pressure produced mutations of industrial interest. Such a cooperative system was constructed around the exchange of two amino acids while employing the baker's yeast *Saccharomyces cerevisiae* as an experimental model.

After two rounds of adaptive laboratory evolution, isolated strains were tested for improved system fitness, meaning an enhanced tolerance to stress conditions or upgraded metabolite production.

An analysis of the most relevant mutations is presented, focusing on the growth performance variations and changes in metabolite production.

3.1 Mating prevention strategy

The synthetic co-cultures built in this project were constructed upon the model organism *S. cerevisiae*, particularly on the popular strain CEN.PK 113-5D, defined as a *MATa* type, auxotrophic for uracil (van Dijken et al. 2000).

The development of multiple strains co-cultures required the implementation of a mechanism to prevent any mating process. In this sense, the *STE3* gene that encodes for the *factor a* pheromone receptor on *MATalpha* cells was deleted (Hagen et al. 1986). Consequently, if an accidental induction of the *HO* gene would occur, cells switching mating types could not interact with the *factor a* pheromone secreted by *MATa* cell types, effectively preventing the mating process (Haber 2012; Ho et al. 2017).

By this approach, the strain LBGY001 was obtained, constituting the basis for all experiments performed in this work. Seeking to simplify the nomenclature, it will be referenced in the following sections as the wild-type (WT) strain.

3.2 Development of auxotrophic strains for syntrophic consortia

The development of a cooperative consortium requires an active metabolite exchange between the counterparts (Shou et al. 2007). In this sense, complementary phenotypes were devised around the exchange of the amino acids lysine and tyrosine. Both amino

acids come from well-studied metabolic pathways, with the capacity for generating auxotrophic and overproducing phenotypes by modification of single genes (Brückner et al. 2018; Cai et al. 2021; Ehmann et al. 1999; Feller et al. 1999; Hartmann et al. 2003).

Mixed co-cultures are described to present individual populations on uneven and dynamic proportions (Shou et al. 2007). To monitor these variations, two different fluorescence markers were devised to be integrated into the conforming strains. Vectors LBGV006 and LBGV007 carrying *eGFP* or *mRuby2* genes for cytoplasmic expression, respectively, were developed. Both of them target the *URA3* locus for the integration and employ *hygromycin* as dominant marker (see section 2.8.10).

In order to develop the synthetic cooperative consortia, amino acid auxotrophies were produced using the wild-type strain LBGY001 as a basis. A lysine auxotrophic strain was produced after a partial deletion of the gene *LYS1* by using a CRISPR/Cas9-assisted strategy, as described in section 2.8.11. The enzyme Lys1p catalyses the transformation of saccharopine to lysine during the last step in the lysine biosynthesis as described in figure 1.6. As result of this partial deletion, a 372 amino acid protein was shortened to just 14 residues of extension, effectively producing a lysine auxotrophic strain. The vector LBGV007 was also transformed into this strain to achieve an *mRuby2* cytoplasmic expression for future tracking processes. The produced strain was renamed LBGY002.

The planned tyrosine auxotrophy was achieved similarly by partially deleting the gene *TYR1* (Reifenrath & Boles 2018) employing a CRISPR/Cas9-assisted strategy. The resulting protein presented just 65 of its original 453 residues, producing a tyrosine auxotrophic strain. A cytoplasmic eGFPp expression was achieved in this strain by integrating the plasmid LBGV006. The obtained strain was renamed LBGY003.

3.3 Overproducing mechanisms

After introducing the desired auxotroph phenotypes, it was necessary to devise overproducing mechanisms to enable mutual feeding of the auxotrophic strains. To this end, the lysine and tyrosine biosynthesis pathways were studied, looking for enzymes whose performance is negatively regulated by the amount of free amino acid available. The search criteria were limited by the availability of reported mutations that produced a feedback-resistant phenotype on those genes. Finally, integration into the *PYK2* locus was considered as an expression platform for these overproducing variants.

3.3.1 Overproduction of aromatic amino acids

Inside the aromatic amino acids pathway, tree genes fulfilled the described criteria: *ARO3*, *ARO4* and *ARO7*, but just the first two have an impact on the total carbon flow into the pathway. In contrast, *ARO7* would favour prephenate and its subsequent byproducts formation. Both proteins, Aro3p and Aro4p, catalyse the first step in the aromatic amino acid pathway, the transformation of erythrose-4-phosphate (E4P) and phosphoenolpyruvate (PEP) into 3-deoxy-D-arabino-heptulosonate-7-phosphate (DAHP) (Figure 1.5). These isozymes show inhibition by different end products of the aromatic amino acid pathway, Aro3p being inhibited by phenylalanine and Aro4p by tyrosine (Hartmann et al. 2003; Schnappauf et al. 1998). Thanks to the remarkable similarity between both genes, feedback-resistant variants have been successfully developed following the same principle: a replacement of the lysine residue by a leucine in the loop between β6a and β6b regions of the protein. This correspond to a K229L for Aro4p and K222L for Aro3p (Brückner et al. 2018; Hartmann et al. 2003). Based on this criteria, the variants *ARO3*^{K222L} and *ARO4*^{K229L} were chosen for the overproduction of tyrosine as part of the aromatic amino acid biosynthesis pathway. In pursuit of clarity and simplicity for future references, both variants will be referred to as *ARO3*^{fbr} and *ARO4*^{fbr} respectively. It was expected that using these mutations would allow increased production of all aromatic amino acids.

While tyrosine is the only relevant aromatic amino acid for this project's development, the previously described mutations would potentially cause an increased production for all of them. This unnecessary and costly activity was used as a metabolic burden filter, allowing adaptive laboratory evolution to produce better adaptation strategies for these mutations, either repressing unnecessary resources expenditure or targeting improved tyrosine production.

Once the overproducing variants were defined, their integration into the *PYK2* locus was performed. A cassette from the previously developed plasmid JTV19 (see section 2.4.2) carrying the construct $_pTPI1$:*ARO4*^{fbr}:*Aro4*$_t$::$_pHXT7$:*ARO3*^{fbr}:*CYC1*$_t$ (Reifenrath et al. 2018) was amplified, including relevant homologous regions upstream and downstream for the integration locus mentioned above. The strain LBGY003 was chosen for the integration of this cassette by using a CRISPR/Cas9-assisted integration strategy, effectively producing a lysine auxotrophic and aromatic amino acids overproducer strain (see figure 3.2) labelled as LBGY005. Considering that this strain will be used for future adaptive laboratory evolution processes, it will be described as Y0 in reference to the

amino acid it produces and the number of evolution rounds it has experienced.

3.3.2 Overproduction of lysine

Following a similar approach, the homocitrate synthases isozymes Lys20p and Lys21p are highlighted as candidates for lysine overproduction. They catalyse the conversion of 2-oxoglutarate to homocitrate as the first step of the lysine biosynthesis pathway. While *LYS20* is described to play a principal role in substrate transformation, reported mutations in this gene were less successful in alleviating the regulatory feedback effect of lysine than the reported mutation on *LYS21*. A Q366R on *LYS21* produce a tenfold lysine accumulation in contrast with fourfold accumulation observed for feedback resistance mutations in the gene *LYS20* (Feller et al. 1999). Based on this criteria, the variant $LYS21^{Q366R}$ was considered for the overproduction of lysine and will be referred to as $LYS21^{fbr}$.

In order to achieve the overproduction of this amino acid, first a $LYS21^{fbr}$ variant needed to be generated. A wild-type copy of *LYS21* from *S. cerevisiae* strain S288C was amplified into two fragments, using primers to introduce the variant mentioned above. Regions of 500pb upstream and 300bp downstream were included to conserve *LYS21*'s native promoter and terminater regions. Once produced, the fragments were cloned into a linearised YCplac33 vector and assembled using homologous recombination (see section 2.8.10), creating the plasmid LBGV004.

Once obtained, the plasmid was used as a template for the $LYS21^{fbr}$ amplification, including homology regions for the integration into the *PYK2* locus. The integration of this cassette into an LBGY002 strain using a CRISPR/Cas9-assisted strategy yielded a tyrosine auxotrophic, lysine overproducer strain (see figure 3.2) labelled as LBGY004. Following the same principle previously applied for the aromatic amino acids overproducer strain, the strain LBGY004 was renamed K0 as it will be used for further evolutionary processes.

3.4 Synthetic cooperative consortia development

Aiming to develop a syntrophic consortium around the exchange of tyrosine and lysine, two strains (K0 and Y0) were developed, presenting complementary phenotypes. A graphical representation of this consortium is depicted in figure 3.1.

To establish if the overproducing mechanisms would be enough to sustain the active metabolite exchange between both populations, proof of concept tests were performed in SCD plates lacking one amino acid: lysine or tyrosine. The missing amino acid was
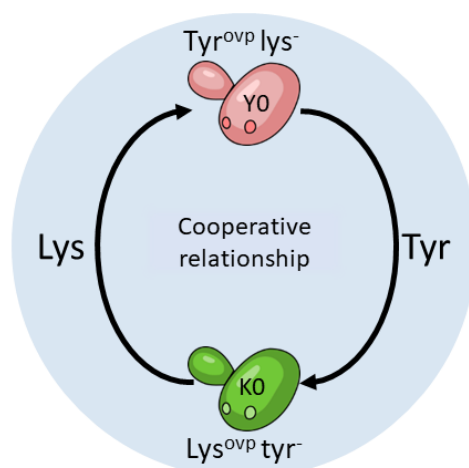
Figure 3.1: Representation of a syntrophic consortium around the exchange of lysine and tyrosine. Red cell represents the Y0 strain, carrying a mRuby2 fluorescent protein. Green cell represents the K0 strain, bearing an eGFP fluorescent marker. Black arrows represent the amino acid production. "ovp" refers to overproducer phenotype.

used to establish if an overproducer strain could secrete this metabolite in sufficient amounts to sustain the growth of a sensor strain, which would be auxotroph for that amino acid.

Volumes of 20 μL of OD_{600} 1 of washed cell suspension solutions were plated in respective areas of selective media. After five days of growth, the results in figure 3.2 suggest that only the lysine overproduction mechanism can successfully sustain the growth of lysine auxotrophic cells. Figure 3.2A shows sensor strain's growth restricted to the regions closer to the overproducer strain cultures. This phenomenon could not be observed in figure 3.2B, where despite good growth of the tyrosine overproducer strain, no hints of growth can be appreciated for the sensor strain.

(A)   **(B)**
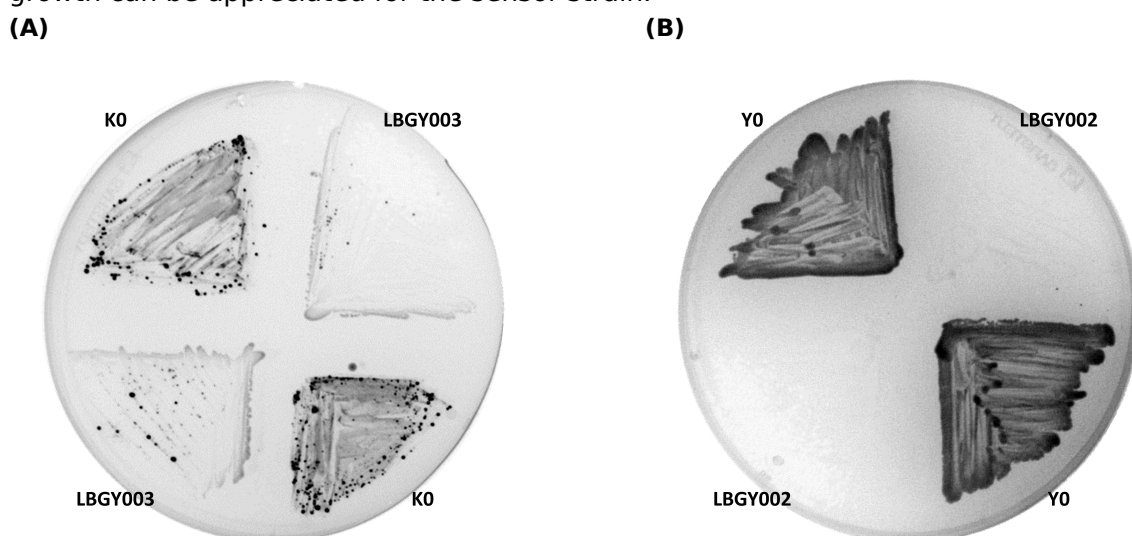
Figure 3.2: Overproduction test using SCD plates. **(A)** Evaluation of lysine overproduction by the strain K0 in an SCD-lys plate, using the lysine auxotrophic LBGY003 strain as sensor. **(B)** Assessment of tyrosine overproduction performance by the strain Y0 in an SCD-tyr plate, the tyrosine auxotrophic strain LBGY002 was used as sensor.
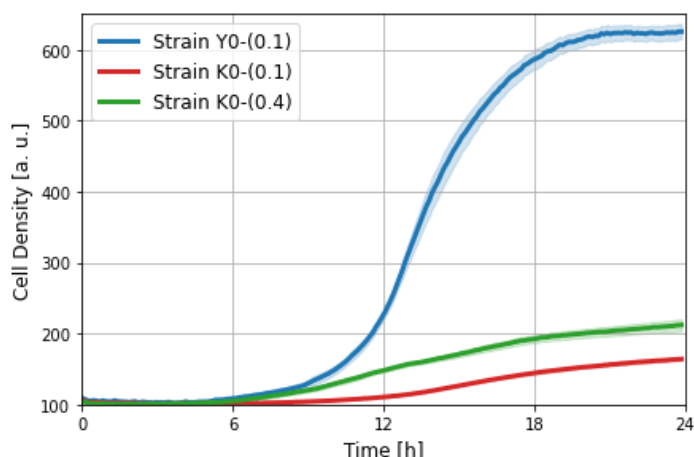
Figure 3.3: Growth performance test for amino acid overproducing strains. Depiction of growth profile demonstrated by the strains K0 and Y0 under different cell density values. The starting OD_{600} titers used are described in brackets next to the strain name. Continuous lines and shaded areas represent mean and standard error, respectively. The experiment used SCD media depleted of lysine for K0 or tyrosine for Y0 cultures.

The reported variants used for tyrosine overproduction have been reported as efficient in several works, in which they demonstrated to increase the carbon flow into the aromatic amino acid pathway (DeLoache et al. 2015; Gottardi, Reifenrath, et al. 2017; Jakočiūnas et al. 2015; Reifenrath & Boles 2018; Reifenrath et al. 2018). In this sense, a new test was performed using liquid SCD-tyr-lys media as a growing platform to evaluate the efficient cooperation of the strains.

First, it was necessary to establish the best conditions to help the co-culture develop effectively. A growth test was performed using pure cultures of both strains in different cell density concentrations, starting from 48 h preculture.

This test aimed to establish the lag phase extension time for both strains, suspecting that close to equal conditions would allow synchronised growth during co-cultivation. Cultures were prepared after 48 h of preculture. Results presented in figure 3.3 suggest that strain Y0 presents a shorter lag phase than K0 but that this difference is reduced when a higher cell density concentration for the latter one is used. It is suggested that by using an OD_{600} value of 0.4 for the strain K0, its lag phase matches the one observed for a Y0 culture of OD_{600} value of 0.1.

Low cell density (a.u.) titers reached by the strain K0 are due to the relatively low tyrosine concentration in the SCD media but also to the cell density determination system used by the Aquila CGQ sensor employed during this project. A more detailed description of the nature of this determination is presented in the section 2.7.2.3.

Consequently, a co-culture experiment was devised using uneven cell proportions be-
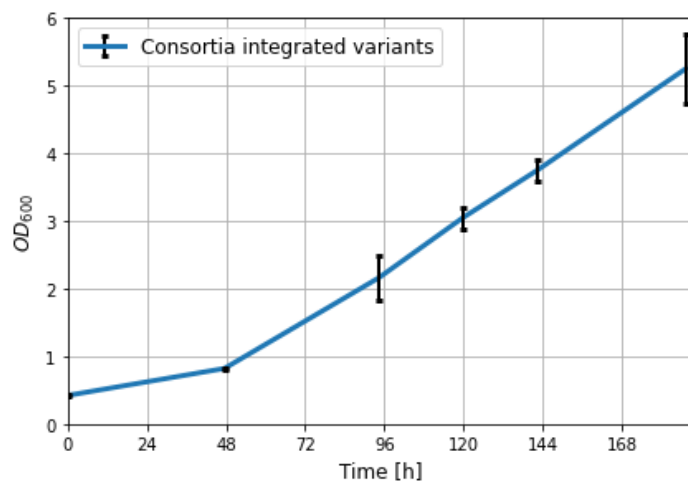
Figure 3.4: Synthetic cooperative consortia development. Co-culture developed with the strains Y0 and K0 tyrosine and lysine donors, using SCD-tyr-lys media and a cell proportion ratio of 1:4, respectively. Bars in black represent OD_{600} standard deviation at each time point.

tween the parties, a 1:4 ratio between the strains Y0 and K0, respectively, using an OD_{600} of 0.1 as base concentration.

The performance of this co-culture is presented in figure 3.4, where it can be appreciated that the applied configuration successfully allowed the co-culture to grow, suggesting that the engineered modifications integrated into their genomes were enough to sustain cooperation.

3.5 Consortia adaptive laboratory evolution

The successful establishment of developing co-cultures suggested that the metabolite exchange was sufficient to sustain growth under the tested conditions. The relatively slow growth observed in this first co-cultured set a base level for developing and improving the system's fitness.

Adaptive laboratory evolution offers an alternative for improving a strain's performance using naturally occurring mutations. This is achieved by exposing the culture to stress conditions directly related to the desired feature. Consequently, naturally occurring mutations that represent an advantage under set conditions would be positively selected (see section 1.4).

After defining the best conditions for co-culture development, an adaptive laboratory evolution process was started using as the initial point the successful consortia presented in figure 3.4, which used a Y0, K0 ratio of 1:4 with a final OD_{600} value of 0.5. A diagram for the existing cooperation between these strains was presented in figure 3.1.

Once co-cultures reached the near end of the exponential growth phase, they were used to seed a new fermentation using again SCD media lacking both exchange metabolite with an initial OD_{600} of 0.5. An OD_{600} value of 5 was defined to indicate the near end of the exponential growth phase considering the upcoming media nutrients depletion, such as ammonium, uracil and glucose.

This process was defined as "passage", and each replica went through 10 passages before the adaptive laboratory evolution process could be finished. The subsequent inoculum dilutions were expected to increase the selective pressure as efficient metabolite production and uptake are paramount for consortia growth.

3.5.1 Mutants isolation

Upon completing the adaptive laboratory evolution process, a screening strategy for isolating mutants of interest was applied. Assuming that the evolved consortia would include cells with improved production or uptake processes, samples from the cultures were plated in agar plates lacking both exchange metabolites.

Briefly, 30 μL of a 1:200 dilution from each replica flask passage ten were plated into SCD-tyr-lys plates. After two weeks of incubation at 30°C, one of the replica plates presented the development of a big colony that contrasted with the small colonies observed in the rest. A sample of this colony was resuspended into 500 μL of sterile water, from which 30 μL was used to seed a second SCD-tyr-lys plate to evaluate if the fast growth phenotype of this big colony could be replicated. After five days of culture, the new plate presented plenty of small colonies, suggesting that cells isolated from the first strain could promote the development of cooperative co-cultures in the new plate.

A sample from one of the colonies on this last plate was processed to isolate single strains using the engineered auxotrophies built into the parental strains. A detailed description of the protocol is presented in section 2.9.

This approach allowed the identification of ten lysine auxotrophic strains, which were assumed to derive from Y0 and anticipated to overproduce tyrosine, while 25 colonies demonstrated to be tyrosine auxotrophic and considered descendants of the strain K0 and expected to overproduce lysine. Five colonies failed to grow on any media used for this screening, even in YPD used as control.

All the suspected tyrosine overproducer strains and ten suspected lysine overproducer strains were provisionally renamed with an asterisk and an Arabic numeral.

3.5.2 Evolved cell analysis

Preliminary phenotypic analyses were performed in these strains to identify the most interesting candidates for subsequent genetic studies.

3.5.2.1 Tyrosine overproducer descendants

As previously described, the industrial relevance of many derivatives from the aromatic amino acid pathway was one of the principal reasons to consider tyrosine as an exchange molecule for this project. In this manner, it was expected that descendants from the lysine auxotrophic and tyrosine overproducer strain Y0 could present improved tyrosine titers. For initial assessment, the readily detectable degradation product of tyrosine, *p*-hydroxyphenyl ethanol (pPET) from the Ehrlich Pathway (see figure 1.5) was used (more details available in section 2.10.3.1).

(A)

(B)   **(C)**
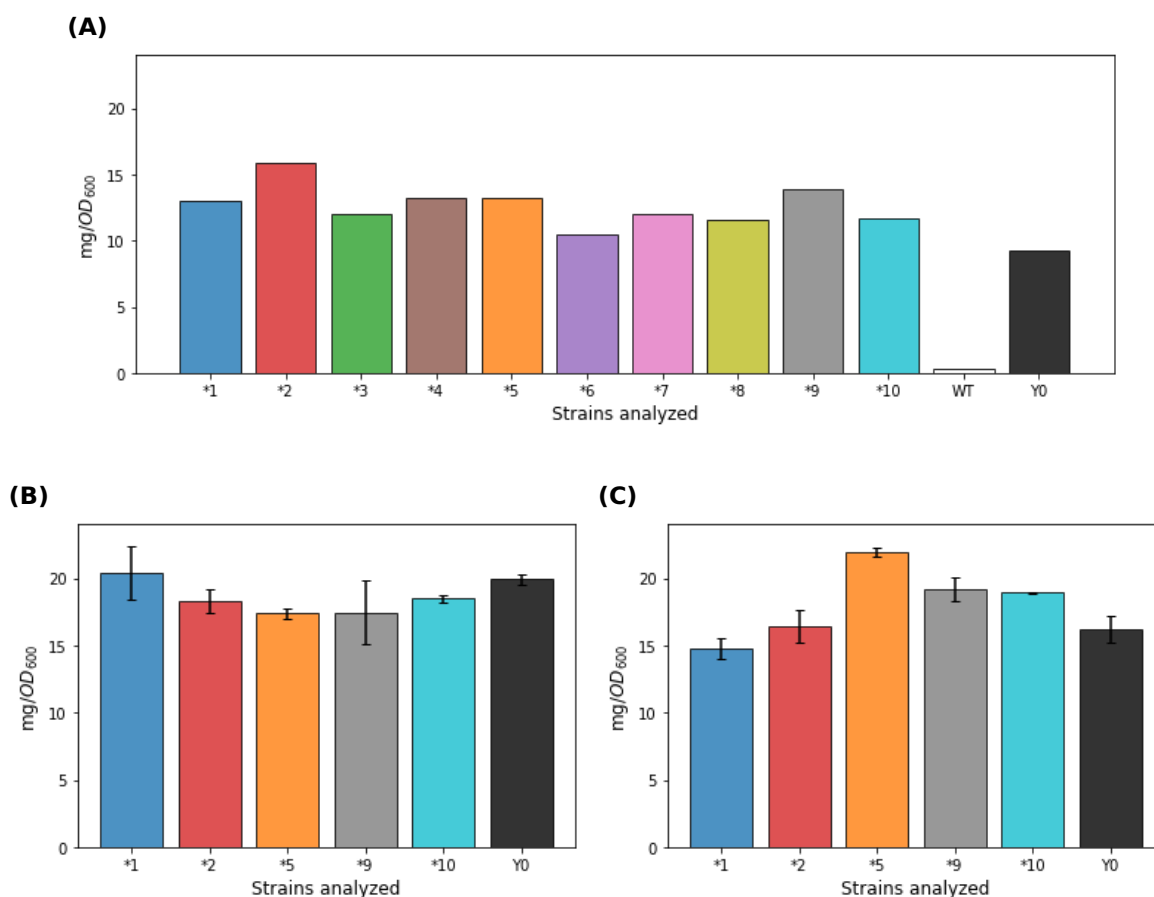
Figure 3.5: Production of pPET in evolved strains. **(A)** Metabolite production screening in all evolved strains isolated after the first evolution round using single replicas. Figures **(B)** and **(C)** show titers obtained from the best producers chosen after the first screening in two independent measurements using triplicates. Data suggest that increased production is not consistent across experiments. Determinations were done after 48 h of growth in SCD-tyr media. Bars represent the mean of measured values with respective standard deviations.
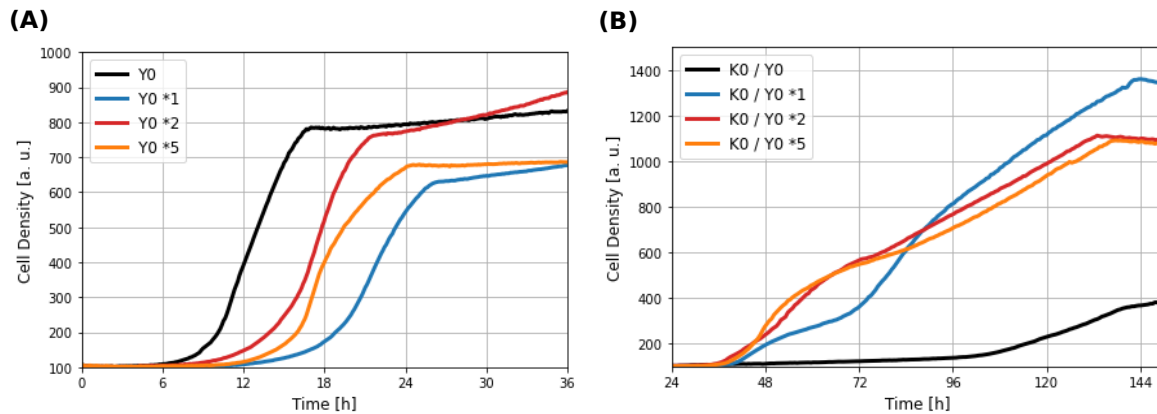
Figure 3.6: Growth analysis of Y0-derived strains. **(A)** Growth under single fermentation conditions using SCD-tyr media. **(B)** Growth in consortia conditions using the strain K0 as lysine donor in a ratio 1:1 in SCD-tyr-lys media. Analysis was performed using single repetitions.

Initial screening performed in all ten obtained strains suggested minor production improvements on pPET titers compared with the original strain Y0. Nevertheless, obtained titers show significant fluctuation between experiments (Figure 3.5B and 3.5C), which forced the subsequent analysis to be conducted among randomly chosen strains. For this purpose, the strains *1, *2 and *5 were selected as representatives from this evolutionary process.

The growth performance of the elected evolved strains was established under single and co-culture conditions (see section 2.7.2.1 and 2.7.2.2, respectively). These strains demonstrated a later growth than the parental strain Y0 under single growth conditions (Figure 3.6A), but they performed significantly better when cultivated under consortia conditions (Figure 3.6B). The observed performance appeared puzzling, as improved growth under co-culture conditions could not be explained as improved individual fitness.

3.5.2.2 Lysine overproducer descendants

As obtaining an increased lysine production was not the main focus of this project, evolved descendants from the K0 strain were assessed solely on their ability to complement growth under consortia conditions. A co-culture fermentation was prepared for ten of the isolated K0 descendant strains using the originally engineered Y0 strain as tyrosine donor. Results are presented in figure 3.7.

The analysis focused on identifying strains that promoted early co-culture development, displaying consistent high cell density titers. Strains with interesting growth patterns, such as *5 or *10, failed to show both treads, displaying a later development but reaching high cell density titers, or vice-versa. In this sense, it was considered that the K0-

(A)

(B)
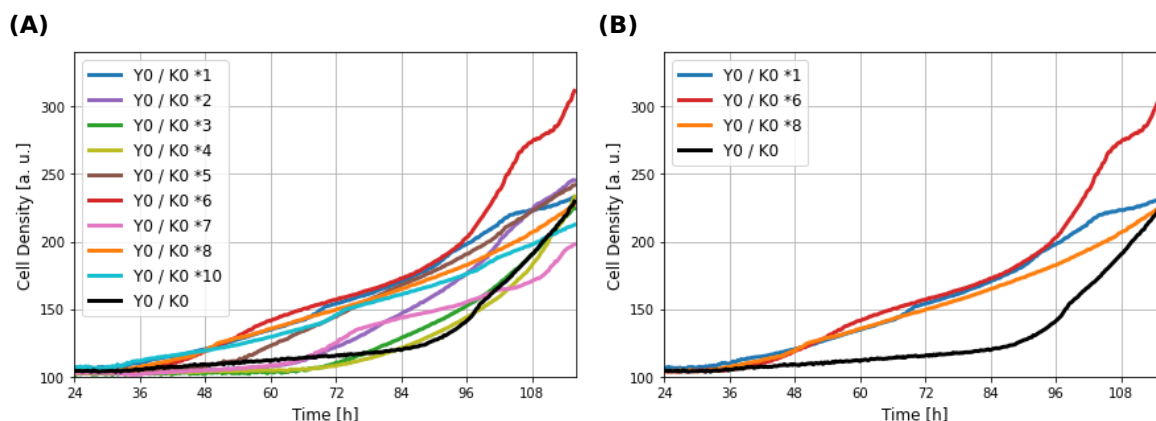
Figure 3.7: Growth analysis of K0-derived strains. Figure **(A)** shows all strains growing under consortia conditions. Figure **(B)** collects the growth of just the chosen strains for subsequent studies. The strain Y0 is used as tyrosine donor for all comparisons. Analysis was conducted using single replicas in SCD-tyr-lys media.

descendant strains *1, *6 and *8 presented a faster and better-sustained growth, reason for which they were selected for further analysis.

3.6 Second adaptive laboratory evolution process

A new adaptive laboratory evolution process was devised to stress the metabolites' exchange conditions further. This process explored a similar approach to the first evolution round, i.e. a consortium forced to exchange metabolites to supplement their auxotrophies but introducing a third party that would consume one metabolite but provide nothing in return. The third strain was conceived as a parasite that would deplete the media of one of the produced metabolites, compromising the system's survival unless production is sufficient to supply the requirements of the cooperator and the parasitic strains.

3.6.1 Strain development

For the configuration of this new adaptive laboratory evolution round, the chosen tyrosine-producing strain would be combined with two tyrosine auxotrophic strains, from which just one would provide the lysine required to sustain the co-culture growth as shown in the figure 3.8.

It was expected that as a result of this competition, the population of the lysine donor strain would be diminished in favour of the parasitic strain, compromising this amino acid availability and, consequently, limiting the tyrosine producer population and the co-culture survival. We anticipated that this stress would allow the emergence of better-fitted strains, either for amino acid uptake or for its production. It would likely provide mutations with potential applications in yeast biotechnology.
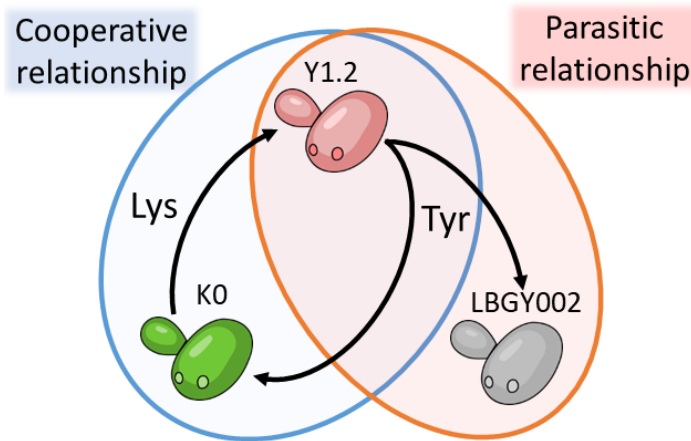
Figure 3.8: Second evolution diagram. A cooperative system is established between a lysine overproducer tyrosine auxotrophic strain (green) and a lysine auxotrophic tyrosine overproducer cell (red), that provide each other with amino acid they can not synthesise. However, a parasitic strain (grey), auxotrophic for tyrosine, consumes this metabolite without providing any nutrients to the media. Black arrows represent metabolite production and exchange flow.

3.6.1.1 Tyrosine donor for the second evolution process

Considering the programmed challenges for the consortium's survival during the second evolutionary process, it was estimated that using a strain with enhanced performance under co-culture conditions would improve the chances of a new consortium's successful growth. In this sense, one of the strains derived from the first evolution round was chosen for this process, the strain *1. This strain was renamed Y1, indicating the amino acid it produces and the evolutionary process it was obtained from. It was used as the basis for the tyrosine production process (strain performance shown in figure 3.6B).

To simplify the subsequent separation of tyrosine-producer-evolved strains after the evolutionary process, the use of a specific dominant marker for this strain was considered. The *hygromycin* resistance gene present in Y1 was replaced by the dominant marker *nourseothricin (clonNAT)* (see section 2.8.10), allowing for more straightforward discrimination of strains after evolution. This dominant marker was not employed as a discrimination agent during co-culture fermentations. In this manner, the strain Y1.2 was generated. The replacement of the above-mentioned selection marker was the only engineered difference between the strains Y1 and Y1.2.

3.6.1.2 Lysine donor for the second evolution process

The originally engineered strain K0 was chosen as lysine donor. The election was motivated by previous co-culture experiments, which proved that this strain could produce sufficient lysine to sustain consortium development (see figure 3.2A). Additionally, this

strain presented the benefit of an unevolved genome that excluded the presence of mutations that would improve uptake or trafficking processes.

3.6.1.3 Parasitic strain for the second evolution process

The parasitic strain used for the second evolution process was planned to compete with K0 for the tyrosine pool without providing lysine to the system. The best alternative was the strain LBGY002, which presented a tyrosine auxotrophy but lacked any engineered or evolved mechanism for lysine overproduction or tyrosine uptake.

3.6.2 Second evolution configuration

The second evolution process started with a mix of the strains Y1.2, K0, and LBGY002 in a proportion 2:2:1, respectively, for a total initial OD_{600} of 0.5, using triplicates. The effect of the parasitic strain in the co-culture was unknown, which was the reason that motivated the use of larger OD_{600} cell densities for the cooperating partners (Y1.2 and K0) than what was used for the first evolution (see section 3.5). Accordingly, the parasitic strain was kept as just one-fifth of the total cell density in the co-culture.

Another challenge programmed for this evolution round was to use SMD media solely supplemented with uracil to compensate for the auxotrophy of the strains (see reference 2.3.4). Consequently, this challenge forced the strains to produce previously freely available metabolites. As a transition process, the first passage was performed in SCD-tyr-lys, to allow for an easy increase in biomass. Since then, the fermentations used SMD with supplemented uracil to compensate for the strains' uracil auxotrophy. New passages were done after seven days of fermentation.

3.6.3 Clone isolation from the second evolution round

After the tenth passage was finished, each replica was diluted to an OD_{600} value of $1 \bullet 10^{-4}$ from which 50 μL were spread on YPD agar plates for a subsequent screening process (see section 2.9).

Selection based on dominant markers discrimination was possible for this evolution round. Colonies resistant to ClonNAT but sensitive to hygromycin were considered descendants from Y1.2. Meanwhile, colonies that presented the opposite phenotype were classified as descendants from K0 or LBGY002 strains. Time constraints prevented further studies into the phenotype changes the lysine producer and parasitic strains experimented, so the analysis focused solely on the descendants from the Y1.2 strain.

The isolation process produced 21 colonies with a phenotype consistent with descendants from the strain Y1.2, resistant to ClonNAT but sensitive to Hygromicin selection.

Each newly isolated tyrosine-producer strain was named after the fermentation flask they were obtained from (F1, F2, F3), plus the colony number on the original selective screening plate presided by a capital C.

(A)
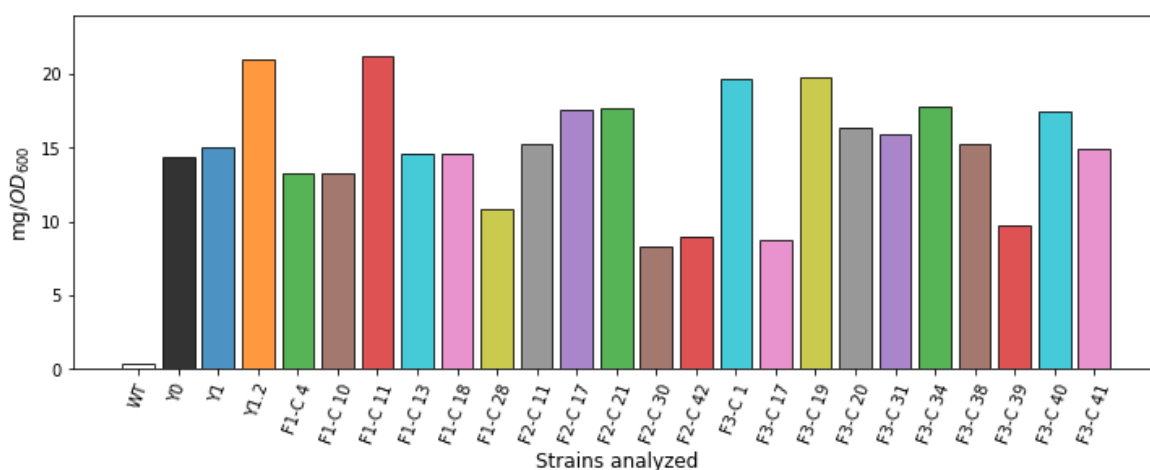
(B)
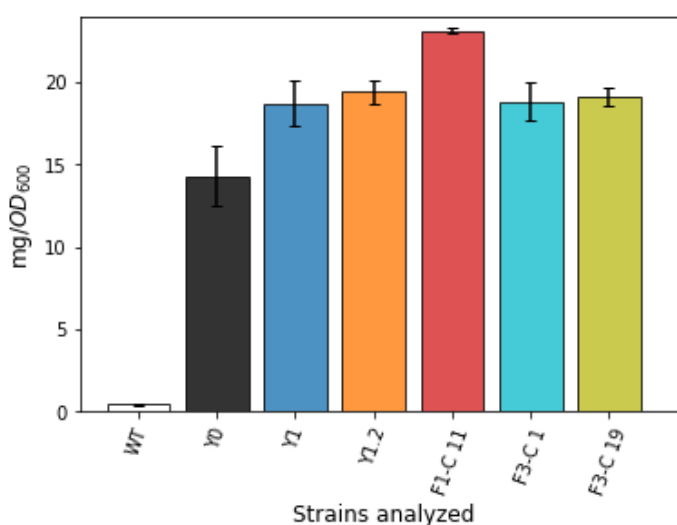
Figure 3.9: pPET production from strains obtained after the second evolution process. Production titers of pPET are normalised to the OD$_{600}$ cell density values of the culture. **(A)** Production ratios from all suspected tyrosine overproducer strains isolated after the second evolution in single replicates. **(B)** Displays means of production ratios with respective standard deviations of the considered best-producing strains in triplicates. Cultures used SCD-tyr media.

3.6.4 Analysis of isolated clones

A preliminary screening for pPET production was performed on the Y1.2 descendent, similar to the screening performed on the strains isolated after the first evolution process (see section 3.5.2.1).

This analysis suggested the strains F1-C 11, F3-C 1 and F3-C 19 as the most interesting producers (see figure 3.9).

The performance of these strains under single-growth and co-culture conditions was also evaluated (see figure 3.10). Similarly to the results obtained after the first evolution (see figure 3.6), strains derived from the second evolution presented a growth defect when compared to the original engineered strain Y0, showing longer lag phases under single-growth conditions. Nevertheless, they all perform better than the originally engineered strain under co-fermentation conditions. These results suggest that evolution produced mechanisms to favour growth under co-culture rather than in single-growth fashion.

In particular, the strain F1-C 11, which showed the highest pPET production ratio with shorter lag phases under single and co-culture conditions than the remaining isolated strains, was considered the most interesting strain produced after the second evolution round. Due to its exciting performance, the strain was renamed Y2, indicating the amino acid it produces and the evolution round it was isolated from and used for posterior analysis.

The evidenced growth difference between Y1 and Y1.2 is also noticeable, suggesting that the latter presents better growth under single-growth conditions but worse during co-culture cultivation. This feature will be commented on in more detail in subsequent sections.

(A)

(B)
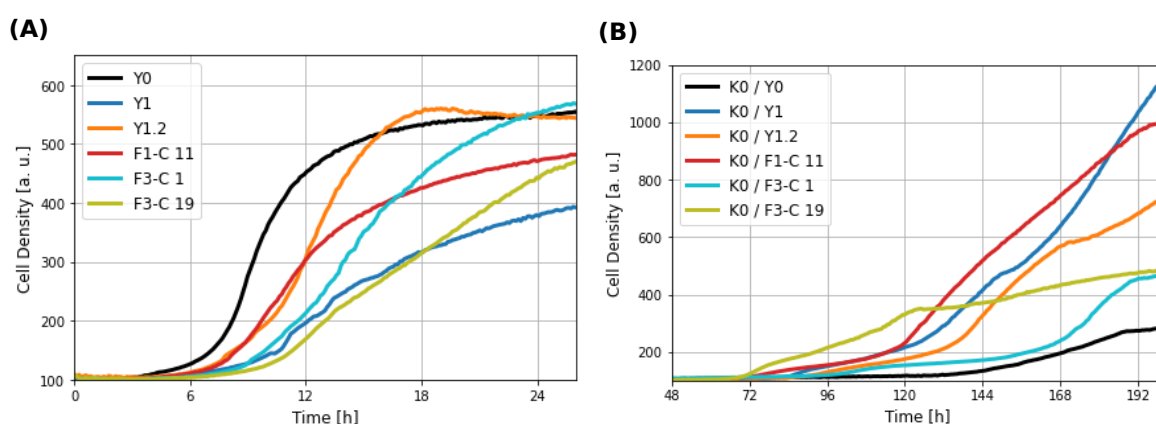
Figure 3.10: Growth performance of the best strains produced after second evolution process. An OD_{600} value of 0.2 was used for each fermentation.**(A)** Growth pattern under single-growth fermentation using SCD-tyr media. **(B)** Growth profile under co-cultivation using K0 as lysine donor and a 1:1 proportion in SCD-tyr-lys media. For each strain, employed an OD_{600} value of 0.1.

3.7 Whole genome sequencing analysis

Adaptive laboratory evolution did produce strains that grew better under co-culture conditions, so to discover the generated mutations that could explain the observed phenotypes, a whole genome sequencing analysis was conducted for the selected strains derived from Y0 (*1, *2, *5) and K0 (*1, *6, *8) together with the strain Y2. The parental strains Y0, K0 and Y1.2 were also included as references for the genome analysis of their evolved progeny. Genomic DNA samples extracted from the evolved and parental strains were sent to Novogene Co., Ltd to sequence via Illumina technology (detailed description in section 2.11).

The quality control report of the company indicated that files presented a Q30 score higher than 90% (see table 3.1). As described in section 2.12, files that were not properly cleaned by Novogene Co., Ltd, i.e. K0, K0 *1, K0 *6, K0 *8, Y1.2 and Y2 were cleaned up using the BBDuk plugin (Bushnell 2015) on Geneious Prime (Biomatters 2019), to remove short and low quality reads. Analysis on FastQC software (Andrews 2018) revealed no alarm sign on both data set files for the same analysed strains, so data processing was performed as described in section 2.12.

The genomic sequence of each parental strain was used during the mapping process of their respective derived evolved strains. For the analysis of the strains Y0 and K0, the reference genomes were produced based on the CEN PK113-7D genome published by Salazar et al. 2017. Prior to the mapping process, all reference genomes used for the analysis were incorporated with the genetic modifications engineered in the analysed strains, i.e. overproducing genes, auxotrophies, fluorescence proteins and respective dominant markers. (See description in 3.3 and 3.6.1.1). This modification tried to improve the mapping process and reduce false positive results, as the analysis would not

Table 3.1: Whole genome sequencing quality report. **Strain** and **Raw reads** indicate the strain name and the number of reads obtained for each one. **Error** represents the percentage of expected erroneous raw reads for each strain. Q-scores **Q20(%)** and **Q30(%)** represent raw read quality estimations. They describe the percentage of bases that are expected to be correctly called with an error of 0.1 or 0.01, respectively (see table 2.24). **GC(%)** describe the proportion of G and C nitrogenated bases present in the reads per strain.

Strain	Raw reads	Error(%)	Q20(%)	Q30(%)	GC(%)
Y0	3'731,666	0.03	97.11	91.94	38.31
Y0 *1 (Y1)	3'277,897	0.03	97.09	91.91	37.83
Y0 *2	3'619,884	0.03	96.39	90.4	38.36
Y0 *5	2'958,087	0.03	96.97	91.68	37.97
Y1.2	13'658,018	0.03	97.19	92.06	37.85
Y2	12'976,972	0.03	97.41	92.58	38.81
K0	12'924,868	0.03	96.92	91.55	37.87
K0 *1 (K1)	10'913,210	0.03	97.08	91.84	38.85
K0 *8	13'331,370	0.03	97.24	92.24	37.95
K0 *6	12'861,494	0.03	97.25	92.27	38.07

be directed to report modifications already described but unknown variations produced during the evolution process. In this sense, for the analysis of the strain Y1.2, the previously defined genome for strain Y1 was used and the dominant marker was manually curated to match the expected genotype.

As discrimination criteria to eliminate false positive results, just variations reported in all three analysed strains were considered. Also, the annotations with a variant frequency below 80% or localised in a low coverage area were excluded. Results are depicted in Table 3.2.

As depicted in the figures 3.6B and 3.7B, all the clones chosen for the sequencing analysis presented improved performance under co-culture conditions, which suggested that evolution might have produced beneficial features among lysine and tyrosine producer populations.

Interestingly, neither of the strains analysed produced mutations clearly related to their respective over-expressing pathways, which fails to explain the improved growth under co-culture conditions. Nevertheless, the obtained variations could still play roles in different processes, such as amino acid import and control of metabolic stress.

As consequence of the improved performance under co-culture conditions, the following mutation analysis will focus on variants common to all clones of each population, e.g., shared mutations for all tyrosine-evolved producers. Section 3.11 presents a detailed analysis of the detected mutations.

Table 3.2: Relevant mutations found during whole genome analysis. [*]Approximate values estimated by Geneious Prime.

Strain	Chromosome	Product	Nucleotide Change	CDS Position	Protein Effect	Variant Frequency	Variant P-Value *
Y0 *1	2	Art2	T Deletion	615	Frame Shift	100	1.60E-185
Y0 *2	2	Art2	T Deletion	615	Frame Shift	100	0
Y0 *5	2	Art2	T Deletion	615	Frame Shift	100	0
Y0 *1	10	Gef1	G ->T	1,116	Substitution L ->F	100	2.50E-205
Y0 *2	10	Gef1	G ->T	1,116	Substitution L ->F	100	6.30E-179
Y0 *5	10	Gef1	G ->T	1,116	Substitution L ->F	97.7	2.80E-145
Y0 *1	14	Lys9	CT Deletion	1,013	Frame Shift	100	0
Y0 *2	14	Lys9	CT Deletion	1,013	Frame Shift	100	2.50E-188
Y0 *5	14	Lys9	CT Deletion	1,013	Frame Shift	100	3.20E-149
Y0 *1	16	Asr1	G Deletion	311	Frame Shift	100	4.00E-168
Y0 *2	16	Asr1	G Deletion	311	Frame Shift	100	2.50E-172
Y0 *5	16	Asr1	G Deletion	311	Frame Shift	100	1.60E-125
Y1.2	9	Bcy1	C ->A	1,056	Substitution K ->N	100	0
Y2	7	She10	(TG)3 ->(TG)2	1,031	Frame Shift	100	0
Y2	12	Ski2	C ->G	1,217	Substitution G ->A	100	0
Y2	15	Whi2	(T)7 ->(T)6	227	Frame Shift	100	0
K0 *1	2	Cdc27	(TTA)20 ->(TTA)21	1,099	Insertion ->N	100	1.60E-20
K0 *6	2	Cdc27	(TTA)20 ->(TTA)21	1,099	Insertion ->N	88.6	0.00E+00
K0 *8	2	Cdc27	(TTA)20 ->(TTA)21	1,099	Insertion ->N	95.3	0
K0 *1	9	Dal81	(G)3 ->(G)2	2,339	Frame Shift	100	0
K0 *6	9	Dal81	(G)3 ->(G)2	2,339	Frame Shift	100	0
K0 *8	9	Dal81	(G)3 ->(G)2	2,339	Frame Shift	100	0
K0 *1	15	Whi2	G ->T	535	Truncation	100	0
K0 *6	15	Whi2	G ->T	535	Truncation	100	0
K0 *8	15	Whi2	G ->T	535	Truncation	100	0

3.8   Copy number variation analysis

Data generated during the whole genome sequencing analysis were also used to search for partial or total chromosomal duplications that might add more information to the observed behaviour of the evolved strains. In this sense, the files produced after the mapping process were examined using the CNVpytor tool (Suvakov et al. 2021) and establishing a threshold of 1,000 base pairs as the minimum length for the analysis of duplicated or deleted areas (Binning size).

Briefly, the algorithm uses the read-depth information from the mapping file, combines adjacent areas according to the binning size established, compensates the read-depth signal based on the CG content, and adjusts the extension of the segment accordingly to the mean difference of the read-depth signal of surrounding areas. Areas with copy number variations (CNV) are called based on their read-depth signal, making it possible to detect duplications or deletions.

Variations located in telomeric regions, across several strains and presenting an extension of around 20,000 base pairs or less were considered false positive calls, probably caused by an over-representation produced during the genome sequencing.

Table 3.3: CNV results analysis. Findings are presented organised by **Strain**, **CNV type** and **Chromosome**. **Region** describes the chromosome section in which the variation has been detected, expressed in base pairs. **CNV size** shows the extension of the affected area. **CNV level** indicates the read-depth signal of each called bin normalised to 1, which does not directly indicate the number of copies. While the **e-val1** and **e-val2** values refer to p-values, the first calculated from a t-test between the read-depth statistic between the region and globally, and the second to the probability that the read-depth statistics found are in the tail of a Gaussian distribution. Both p-values are corrected, multiplied by the genome size and divided by the minimum size of combined adjacent areas.

Strain	CNV type	Chromosome	Region	CNV size	CNV level	e-val1	e-val2
K0 *1	duplication	5	493,001-574,000	81,000	2.0295	0.00E+00	0.00E+00
K0 *1	duplication	9	1-440,000	440,000	2.333	0.00E+00	6.78E-230
K0 *6	duplication	5	493,001-574,000	81,000	2.0646	0.00E+00	0.00E+00
K0 *6	duplication	9	313,001-440 000	127,000	2.1583	0.00E+00	2.62E-197
K0 *8	duplication	2	4,001-634 000	630,000	2.0613	0.00E+00	0.00E+00
K0 *8	duplication	5	493,001-574,000	81,000	2.1253	0.00E+00	0.00E+00
K0 *8	duplication	5	1-117,000	117,000	2.2157	0.00E+00	0.00E+00
K0 *8	duplication	9	1-440,000	440,000	2.4747	0.00E+00	0.00E+00
Y0 *1	duplication	14	511,001-765,000	254,000	1.9552	0.00E+00	1.03E-03
Y0 *1	duplication	14	2,001-509,000	507,000	1.8936	0.00E+00	0.00E+00
Y0 *2	duplication	2	4,001-289,000	285,000	2.1926	0.00E+00	0.00E+00
Y0 *2	duplication	4	472,001-857,000	385,000	2.1612	0.00E+00	2.40E-34
Y0 *2	duplication	14	512,001-557,000	45,000	2.1029	0.00E+00	1.92E-09
Y0 *2	duplication	14	2,001-509,000	507,000	2.1837	0.00E+00	1.77E-259
Y0 *5	duplication	2	636,001-793,000	157,000	2.0345	0.00E+00	0.00E+00
Y0 *5	duplication	2	4,001-632,000	628,000	2.515	0.00E+00	0.00E+00
Y0 *5	duplication	4	472,001-858,000	386,000	2.0014	0.00E+00	2.07E-174
Y0 *5	duplication	9	1-439,000	439,000	2.0929	0.00E+00	2.87E+09
Y0 *5	duplication	13	482,001-913,000	431,000	2.0687	0.00E+00	7.10E-66
Y0 *5	duplication	13	1-478,000	478,000	2.042	0.00E+00	0.00E+00
Y0 *5	duplication	14	512,001-557,000	45,000	1.9749	0.00E+00	1.32E-22
Y0 *5	duplication	14	2,001-509,000	507,000	2.0111	0.00E+00	0.00E+00
Y1.2	duplication	3	158,001-179,000	21,000	2.15	1.52E-11	3.52E-158
Y2	duplication	3	158,001-177,000	19,000	2.0719	0.00E+00	0.00E+00

Results obtained are displayed in the table 3.3, in which no deleted sections could be identified. Every tyrosine and lysine producer strain obtained after the first evolution presented at least some chromosomal alteration type, whose sizes are above 45,000 till the full chromosomal length. Interestingly, each evolved group presented just one common variation among its strains, i.e., all evolved-lysine producers presented abnormalities on chromosome IX, and all tyrosine-evolve producers on chromosome XIV.

A graphical representation of read-depth signal data obtained from the samples is presented in figures 3.12 and 3.11. These representations suggest that the strains K0 *1 and K0 *8 might present three copies of a fragment from chromosome IX. Meanwhile, a segment of chromosome II seems to be present in three copies for the strain Y0 *5.

Findings from graphical data representation regarding precise multiple copy numbers cannot always be correlated with the information presented in table 3.3 as they both slightly differ in the information they depict. Graphical models are constructed on the basis of the read-depth signal, which could provide a better representation when a fragment is present in more than two copies, but at the same time, makes it more sensitive to artefacts, noise or false positive signals. Meanwhile, the data presented in the table are produced after a statistical analysis that seeks to exclude fragments whose properties fail to be significantly different from the properties of surrounding areas, risking the erroneous exclusion of positive areas.

In addition to the previously described similarities, strains Y1.2 and Y2 share a similar duplicated area, whose size is close to the exclusion boundary previously discussed and is not located in a telomeric region. This area close to 20,000 base pairs is located around 38,000 base pairs away from the *CEN3* locus in chromosome III, additionally including an ARS element, particularly *ARS310*, which might suggest that this section is present as an extrachromosomal array.

Genes included in this section are described in table 3.4, but no gene with a clear role related to the observed phenotype can be found. Just the gene *RHB1* has been suggested to play some role in lysine uptake, producing increased thialysine sensitivity when deleted (Urano et al. 2000). This effect suggests that it exerts a negative uptake regulation effect, a mechanism expected to be enforced after a gene duplication event. However, lysine auxotrophic strains would require an improved lysine uptake system, i.e. release of restrictions to transport, which would be the opposite of what a duplication of *RHB1* would achieve.

These findings, together with the absence of the duplication of this area in strain Y1 (the
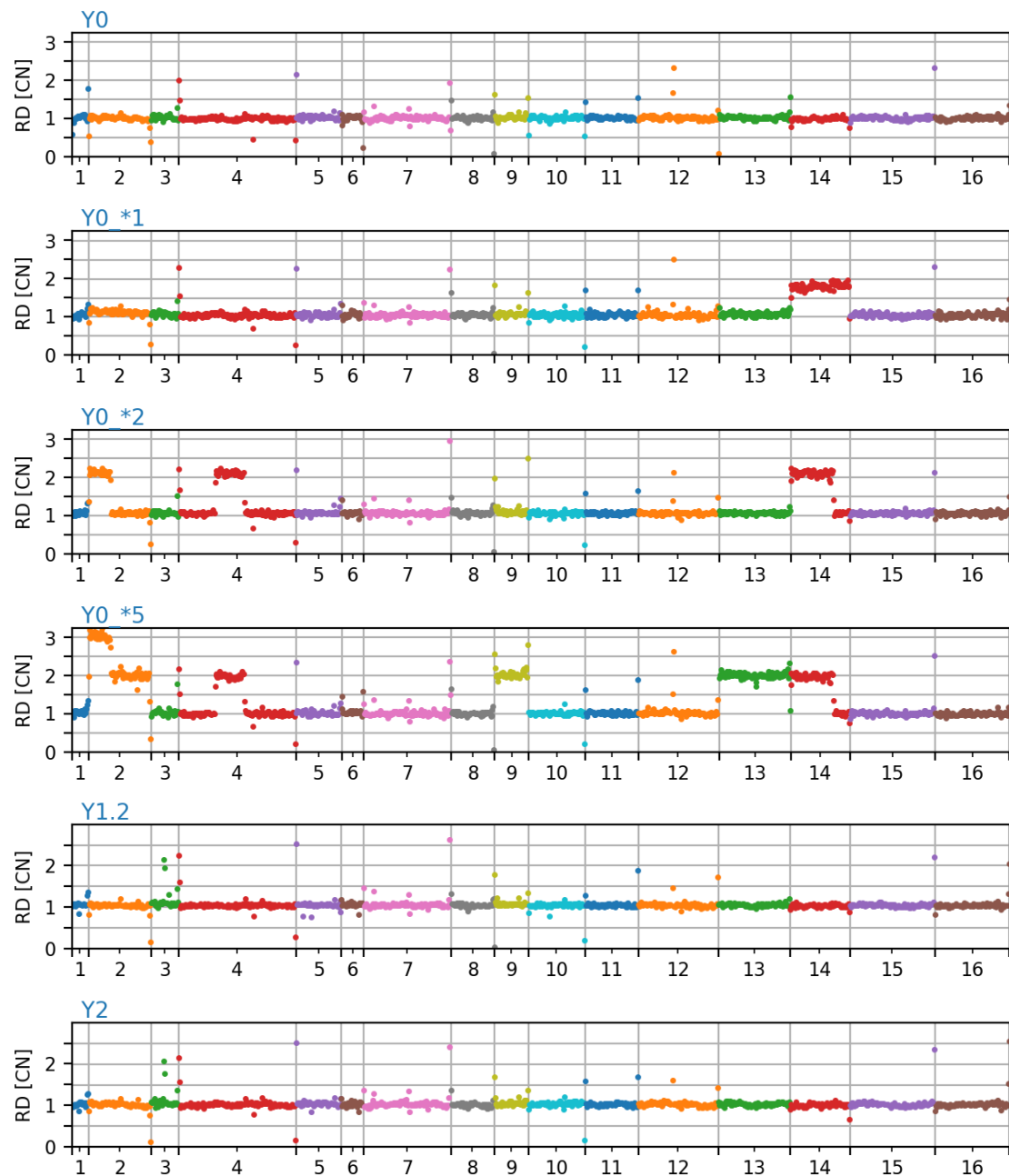
Figure 3.11: CNV analysis of the tyrosine producer strains. Graphical representation of the copy number of each bin, estimated on the base of its read-depth signal (RD [CN]). Coloured dots represent a bin unit grouped per chromosome.

direct predecessor of strain Y1.2), led to the consideration of this area as a false positive. Therefore, it was discarded from further analysis.

Among the tyrosine producer strains obtained after the first evolution, just one chromosomal alteration was common for all the strains, a duplication of chromosome XIV, which for the strain Y0 *1 was presented as a complete chromosomal duplication. Interestingly, this complete duplication was lost in its daughter strain Y1.2. This difference will be discussed in section 3.9.1 for its possible role in discrepancies between the be-
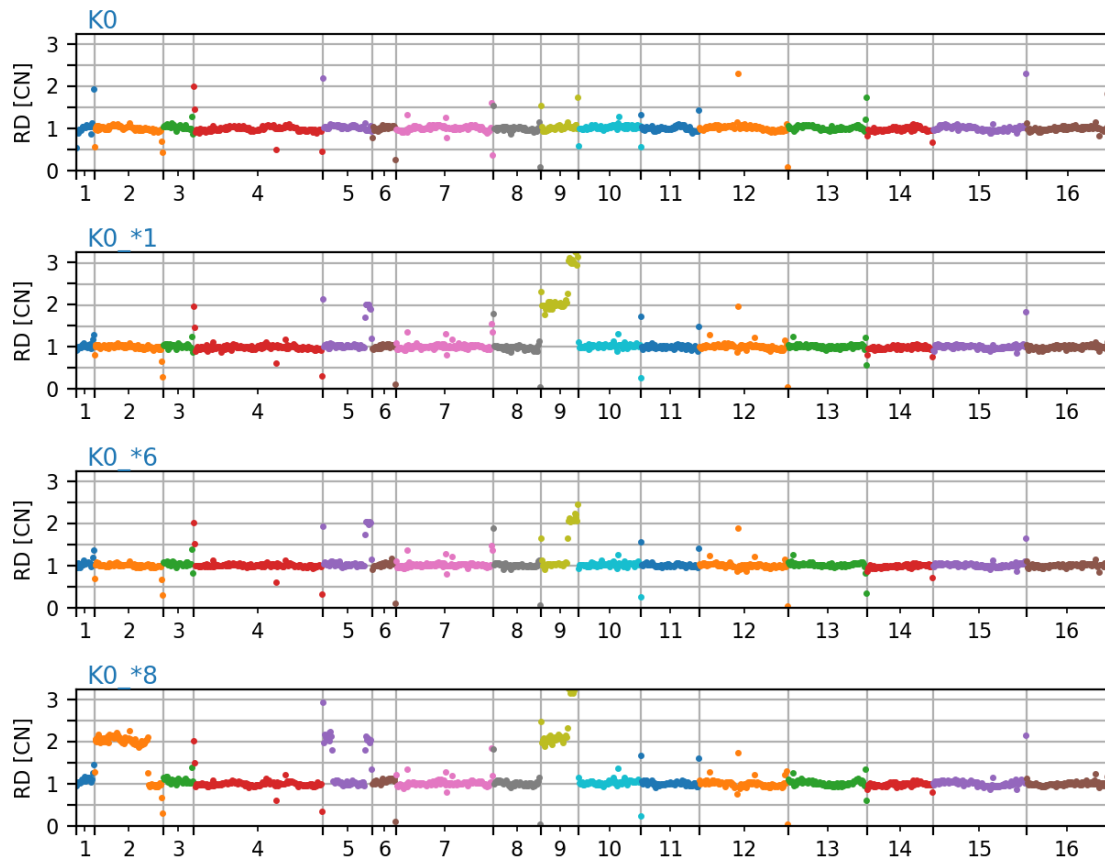
Figure 3.12: CNV analysis of the tyrosine producer strains. Graphical representation of the copy number of each bin, estimated on the base of its read-depth signal (RD [CN]). Coloured dots represent a bin unit grouped per chromosome.

haviour of these two closely related strains. It was also remarkable that the analysis of strain Y2 showed no relevant chromosomal alterations, although this strain arose after an evolutionary process.

Among the lysine-producing strains, highlight the presence of common alterations areas in the telomeric regions on chromosome V and chromosome IX. However, as improved lysine production was not the main focus of this research, a more detailed analysis of the impacts of these possible duplications was not included in the present work.

3.9 Strains growth performance analysis

With both evolutionary processes concluded and after the relevant strains had been isolated and sequenced, conducting a more detailed analysis of the strain's phenotype was important.

Adaptive laboratory evolution showed to have produced changes in the development of evolved strains in single-culture and co-culture performance, as initially depicted in

Table 3.4: Genes inside a possibly duplicated area for strains Y1.2 and Y2. Description of genes located in a section of chromosome III for strains Y1.2 and Y2. Relative location, as well as described function are provided.

Gene	Length (bp)	Beginning position	End position	Function	Reference
MAK32	1,092	161,007	162,098	Contributes for structural stability of dsRNA	Wickner et al. 1986
PET18	648	162,182	162,829	Required for growth at high temperatures	Kawakami et al. 1992; Toh-e and Sahashi 1985
MAK31	267	163,000	163,266	Required for maintenance of virus-like RNA plasmid, disruption produces a temperature-sensitive phenotype and reduced N-terminal acetylation capacity.	Polevoda and Sherman 2001; Toh-e and Sahashi 1985
HTL1	237	163,490	163,726	Required for growth under high temperatures, involved in the functioning of the RSC Chromatin remodelling Complex.	Romeo et al. 2002; Lu et al. 2003
HSP30	999	164,279	165,277	Protein induced as a response to thermal shock, glucose limitation, or stress induced by weak organic acids. Exerts an energy-protective role by limiting the proton-pumping ATPase activity.	Piper et al. 1997; Panaretou and Piper 1992
SLM5	1,479	168,914	170,392	Participates in aspargine-tRNA ligation.	Landrieu et al. 1997
NPP1	2,229	172,282	174,510	Participate in the extracellular nucleotide phosphate hydrolysis. Activity is enhanced during phosphate starvation to promote extracellular phosphate importing.	Kennedy et al. 2005
RHB1	630	175,541	176,170	GTPase involved in lysine and arginine transport. Null mutants show hypersensitivity to thialysine, a lysine toxic analogue.	Urano et al. 2000

figure 3.6 and 3.10 for tyrosine producing strains and in figure 3.7 for lysine producer strains. In every case, evolved strains present a relatively early increase in cell density signal during co-culture growth compared to non-evolved parental strains' performance. However, it remains unclear if this shortened lag phase is related to increased production of the exchange molecules, as pPET titers produced from tyrosine-evolved strains remained inconsistent across multiple fermentations (figures 3.5 and 3.9B).

The following sections will explore different features observed among the tyrosine-producer-evolved strains.

3.9.1 Growth analysis of strain Y1.2

During the performance analysis on the tyrosine producer strains obtained after the second evolution, the behaviour of strain Y1.2 was spotlighted as unusual. Considering the strain as a direct descendant from Y1, it was expected to perform similarly to its parental strain during single and co-culture fermentation. However, previously presented figure 3.10A depicts a Y1.2 strain that grew faster than its counterpart Y1 in single culture. It also presents a slightly different growth under co-culture conditions (figure 3.10B), which motivated further analysis of its growth performance.

A new co-culture fermentation using duplicates and equal OD_{600} values of 0.1 for both
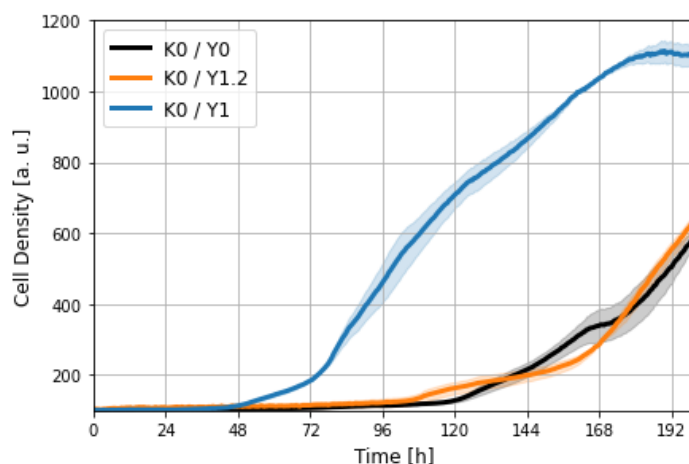
Figure 3.13: Growth performance comparison between strain Y1.2 and parental strains. Presented comparison used 72 h precultures with initial OD_{600} of 0.1 per strain using the strain K0 as lysine donor. Strong lines represent the mean of cell density using duplicates, and the shaded area the standard error at each time point. Fermentation was performed in SCD-tyr-lys media.

lysine and tyrosine donor strains (figure 3.13), demonstrated that the strain Y1.2 presented a much slower growth pattern than the strain Y1. Actually, the growth pattern observed by strain Y1.2 is closer to that demonstrated by the unevolved parental strain Y0.

As previously discussed, strain Y1.2 is directly derived from the evolved strain Y1, differing only in the dominant markers it uses and mutations that could have spontaneously occurred during the engineering process.

The genome sequencing analysis conducted on strain Y1.2 revealed just one miss-sense variation inside a coding region for this strain. The mutation on the gene *BCY1* refers to a 352K>N substitution, producing a lysine to aspargine change in the protein but otherwise not affecting the normal 417 amino acid extension of this protein. This gene has been described to encode for a regulatory subunit of the cyclic AMP-dependent kinase protein, which upon disruption fails to inhibit the AMP-dependent protein kinase activity, starvation and heat-shock increase sensitivity as well as the inability to grow on many carbon sources (Toda et al. 1987). In this sense, this protein's compromised activity seems irrelevant for the phenotype observed in the strain Y1.2. This mutation is also present in the strain Y2, as its evolved descendent; nevertheless, the strain Y2 presents a significantly better growth than Y1.2 (discussed in further detail in figure 3.14).

Another important difference between Y1.2 and its parental strain Y1 is the duplication loss in chromosome XIV (as discussed previously in section 3.8). This could suggest that an increased copy number of some genes or set of genes inside the first 509,000 base
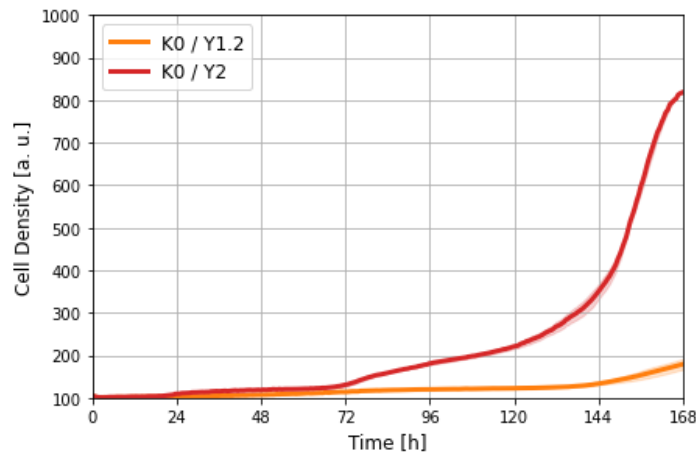
Figure 3.14: Performance comparison of Y1.2 and Y2 strains. The experiment employed precultures of 48 h using an initial OD_{600} of 0.2 per strain. Data is presented as the cell density average of triplicates in the strong line with standard error as a shaded area. The experiment used SCD-tyr-lys media.

pairs of chromosome XIV could be at least in part responsible for its performance under co-culture conditions (see duplicated areas information in table 3.3).

A new bioinformatic analysis aiming to detect mutations during evolution was repeated for chromosome XIV of the tyrosine-producing strains Y1 (previously designated as Y0 *1), Y0 *2 and Y0 *5, establishing as the frequency lower limit to call new variants as 20% (see section 3.7). The new settings seek to identify variations that, if existing in one of the two copies, would be represented in a frequency ranging from 25% to 50% of the reads for that position. Considering that all three evolved strains produced after the first evolution present a fast-growing phenotype on co-culture cultivation (see fig 3.6B), the analysis aimed to detect common variations present in all three strains.

Interestingly, the results in table 3.5 show no common mutation among the evolved strains, except for the one in *LYS9*. Nevertheless, the deletion on *LYS9* is located outside the duplicated area common for all strains, restricted to the first 509,000 nucleotides of chromosome XIV. Also, the lack of reported variations for chromosome XIV of the strain Y2, suggests that its favourable performance under co-culture growth (see 3.14) is not dependent or caused by mutations in this section.

These results suggest that the distinctive performance of the strain Y1.2, compared to strain Y1, could be related not to a variation in chromosome XIV genes but to the effect of a duplicated gene or set of genes in this section. Given the number of genes in this chromosomal section, it was not feasible for the development of this project to study the possible role of multiple gene copy numbers inside this section further.

Table 3.5: Report of mutation announced in duplicated areas of chromosome XIV. Analysis of mutations reported in the area possibly duplicated inside chromosome XIV. Lower frequency threshold is set to 20% to detect variations present in one of the possible multiple copies of respective genes. *Approximate values estimated by Geneious Prime.

Strain	Product	Chromosomal Location	Nucleotide Change	CDS Position	Protein Effect	Variant Frequency	Variant P-Value *
Y0 *1	App1	436,599	G ->T	473	Substitution G ->V	24.30%	2.10E-09
Y0 *5	App1	436,944	G ->T	466	Substitution D ->Y	23.20%	1.80E-08
Y0 *5	App1	436,953	G ->T	475	Substitution D ->Y	26.30%	2.80E-10
Y0 *1	Dcp2	391,669	C ->A	2,493	Substitution L ->F	24.00%	7.30E-07
Y0 *1	Dcp2	391,678	C ->A	2,484	Substitution L ->F	32.50%	1.50E-16
Y0 *1	Dcp2	391,681	C ->A	2,481	Substitution L ->F	22.10%	2.00E-13
Y0 *1	Dcp2	391,702	C ->A	2,460	Substitution Q ->H	21.40%	4.80E-09
Y0 *5	Dcp2	392,015	C ->G	2,499	Substitution K ->N	27.00%	8.90E-10
Y0 *5	Dcp2	392,021	C ->A	2,493	Substitution L ->F	25.00%	3.90E-16
Y0 *5	Dcp2	392,026	T ->A	2,488	Substitution I ->F	22.50%	7.50E-14
Y0 *5	Dcp2	392,030	C ->A	2,484	Substitution L ->F	31.00%	9.50E-15
Y0 *5	Dcp2	392,033	C ->A	2,481	Substitution L ->F	25.00%	1.60E-25
Y0 *1	Kri1	44,810	C ->G	52	Substitution E ->Q	21.40%	4.00E-07
Y0 *1	Lys9	702,818	Deletion	1,013	Frame Shift	100.00%	0
Y0 *2	Lys9	703,151	Deletion	1,013	Frame Shift	100.00%	2.50E-188
Y0 *5	Lys9	703,169	Deletion	1,013	Frame Shift	100.00%	3.20E-149
Y0 *1	Nar1	187,445	C ->G	1,189	Substitution A ->P	25.70%	3.80E-16
Y0 *1	Nar1	187,448	C ->G	1,186	Substitution A ->P	20.50%	3.40E-12
Y0 *1	Nar1	187,451	T ->G	1,183	Substitution T ->P	23.70%	8.60E-10
Y0 *5	Nar1	187,797	C ->G	1,189	Substitution A ->P	36.50%	5.60E-25
Y0 *5	Nar1	187,800	C ->G	1,186	Substitution A ->P	29.60%	2.10E-13
Y0 *5	Nar1	187,803	T ->G	1,183	Substitution T ->P	35.20%	1.20E-13
Y0 *1	Pms1	464,421	C ->A	2,608	Substitution L ->I	30.10%	2.30E-17

3.9.2   Growth of lysine producer strains

As previously described in section 3.5.2.2, the three lysine-producer strains isolated after the first evolution presented favourable growth under consortia conditions. This feature was exploited to better study variations on the tyrosine producer strains.

Figure 3.15 compares such different consortia's growth. The presence of an evolved lysine producer strain promotes faster growth, regardless of the lysine producer used, representing a convenient effect for analysing tyrosine producer strains.

Based on this improved co-culture performance, future analysis on co-culture development will use the strain K1 as lysin-donor.

3.9.3   Role of parasitic strain in fermentation

The successful development of co-culture during the second evolution motivated further exploration of possible system constraints derived from the parasitic strain's presence.

The effect of an increasing population of the parasitic strain LBGY002 can be observed in figure 3.16. Results suggest that adding a parasitic strain improves co-culture growth no

(A)   **(B)**
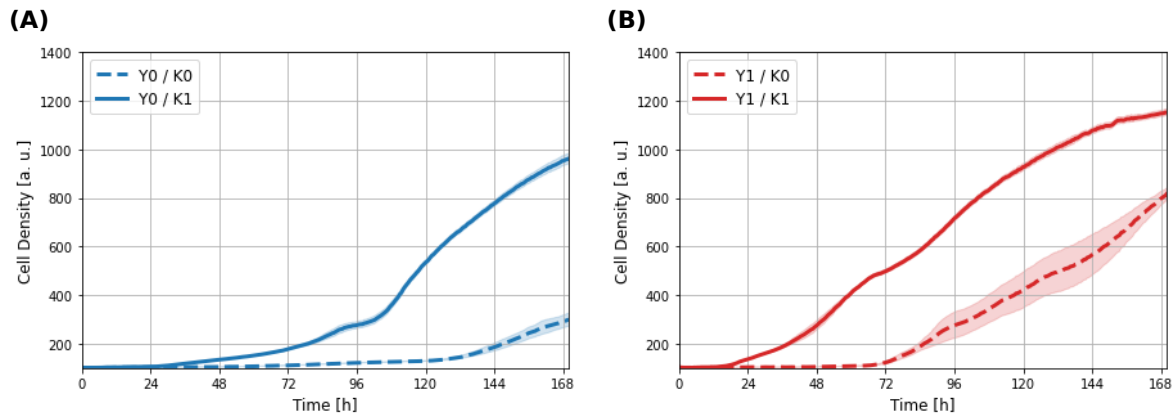
Figure 3.15: Growth performance of co-cultures using an evolved lysine producer strain. Figures **(A)** and **(B)** depict consortia development when the tyrosine producer strain is unevolved and evolved, respectively. Both scenarios test evolved and unevolved lysine donors as well. Lines and shaded areas represent means and standard error of triplicate measurements, respectively. Fermentations used SCD-tyr-lys media.

matter which strain is used as tyrosine-donor. In this sense, including a parasitic strain produces results opposite to what was expected, favouring growth rather than acting as a constraint, as presented in section 3.6.1.

A new co-culture was devised to evaluate this hypothesis further, replacing the parasitic strain with a CEN.PK 2-1c *pgi1*Δ mutant. The gene *PGI1* encodes for a phosphoglucose isomerase that converts glucose-6-phosphate to fructose-6-phosphate, whose deletion disrupts glycolysis (Aguilera 1986; Boles et al. 1993). Therefore, this strain would not be able to grow in an SCD media, nor benefit from the amino acid exchange produced during co-culture development.

(A)   **(B)**
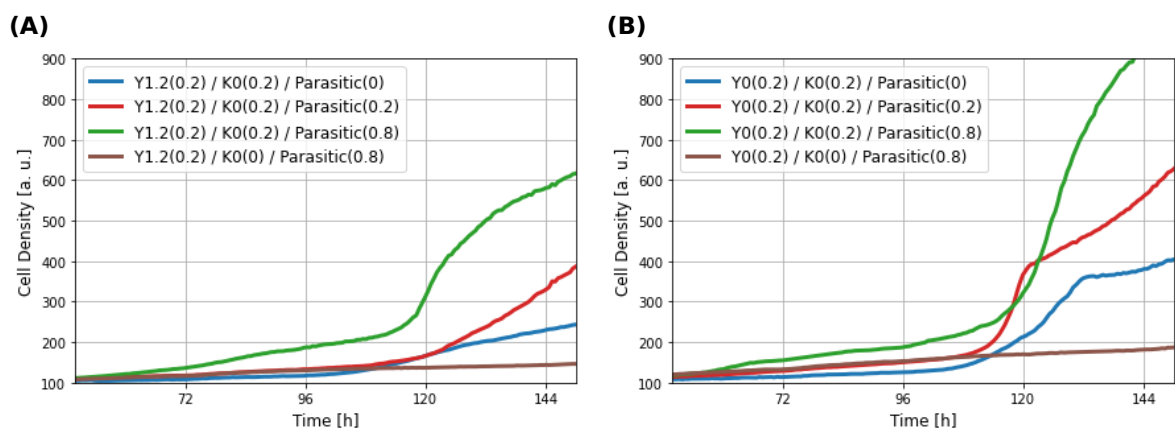
Figure 3.16: Effect of increasing parasitic strain proportion on consortia development. **(A)** and **(B)** display consortia development under four different concentrations of parasitic strain, using Y1.2 and Y0 strains as tyrosine donors, respectively. In every comparison, the strain K0 was used as lysine donor. Parasitic refers to the strain LBGY002. Values in parenthesis next to the names of the strains represent the cell concentrations expressed in OD_{600} values. The experiment used SCD-tyr-lys media.

Results depicted in figure 3.17 agree with the hypothesis that the presence of a third strain improves co-culture development. A possible explanation for this phenomenon would lie in the extra nutrients that this strain brings to the co-culture in terms of biomass. Natural decay on the CEN.PK 2-1c *pgi1Δ* population would eventually enrich the media with debris and intracellular nutrients that would benefit the surviving cells to boost growth.

This new hypothesis would also explain results observed in figure 3.16, where an increasing OD_{600} of the parasitic strain LBGY002 improves co-culture growth. Nevertheless, this growth seems not to be related to a shorter lag phase, but to a faster increase in cell density signal, which suggests that starvation and decay time of the set of strains in the co-culture is set around 115 h. From this moment forward, it is proposed that a fraction of cells die, releasing nutrients to the media, which boosts the development of the surviving cells. The time period from the beginning of the fermentation till co-culture growth would be called "decay time".
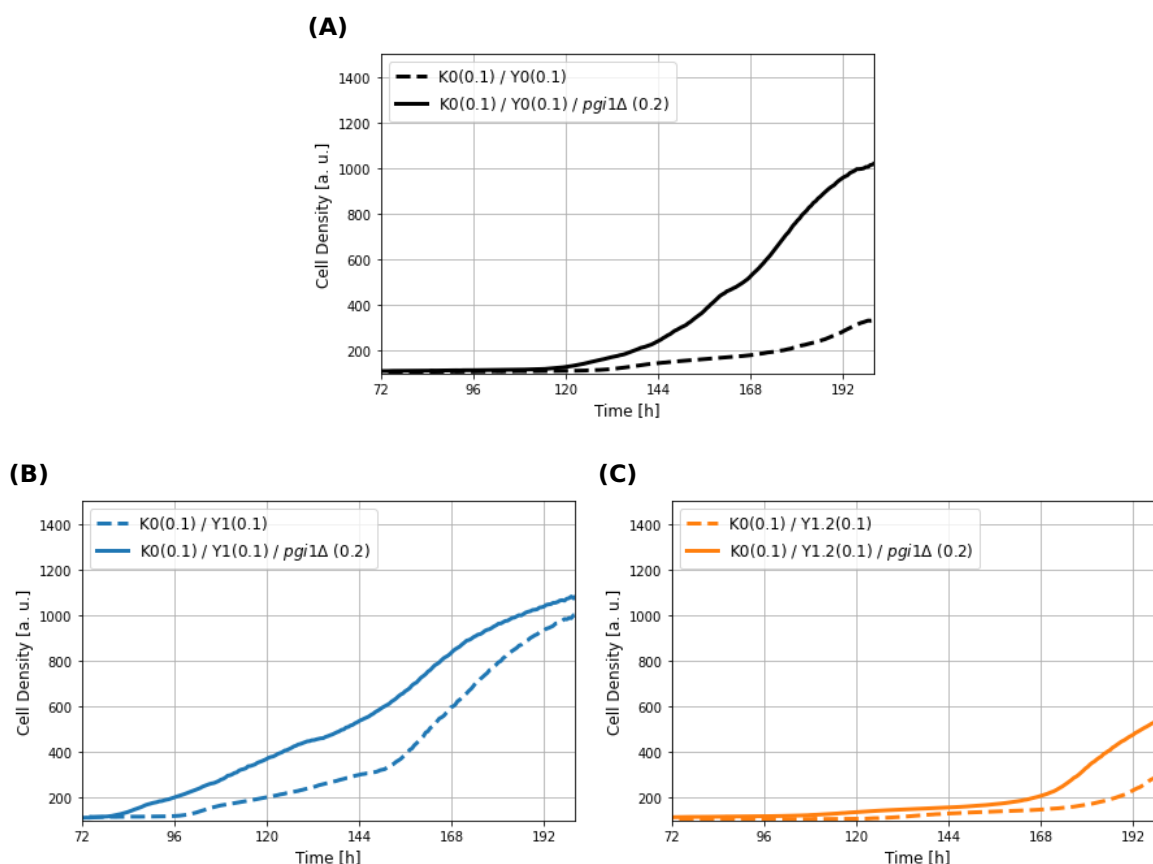
Figure 3.17: Effect of a non-viable strain in co-culture development. For every comparison, the strain K0 was used as lysine donor. OD_{600} values for lysine donor, tyrosine donor, and *pgi1Δ* strain were 0.1, 0.1 and 0.2 respectively. They are expressed in parenthesis next to the strain name for every case. Figures **(A)**, **(B)** and **(C)** depict consortia development using strains Y0, Y1 and Y1.2 as tyrosine donors, respectively. All fermentations used SCD-tyr-lys media.

Differences in the observed decay times appreciated between experiments using LBGY002 and CEN.PK 2-1c *pgi1*Δ (figures 3.16 and 3.17 respectively) could be explained by the strain's genotype and the cell proportion conformation of each experiment. While the former used a cell density of 0.2 OD_{600} per amino acid producer strain and different values for the parasitic strain, the latter used values 0.1 OD_{600} for these strains and always a 0.2 OD_{600} cell density value for the CEN.PK 2-1c *pgi1*Δ.

From this analysis, it could be inferred that the co-culture decay time would also have an impact on fermentations that do not include a parasitic strain. This concept would translate into different dynamics inside co-culture developments, which would result particularly relevant in each passage performed during both adaptive laboratory evolution processes. Nevertheless, co-culture successful growth cannot be reduced just to the effect of nutrients provided by decaying cells, as no co-culture development has been observed when using LBGY002 and LBGY003 strains, both lacking overproducing mechanisms (data not shown) In this sense, an amino acid overproducing phenotype is also crucial for co-culture development.

As a result, the previous hypothesis should be corrected, proposing that co-culture development depends not just on overproducing phenotypes but also on the total cell density used during fermentation. Recognising that besides the effect of overproducing phenotypes, the decay of a certain cell proportion sustains the growth of the surviving cells.

However, despite an initial growth boost provided by the decaying cells, once co-culture growth is detected, its development is sustained until reaching a growth plateau consistent with a stationary phase. Nutrients released into the media after the lysis of decaying cells would be rapidly depleted and fixed into biomass by surviving cells. This suggests that another type of nutrient release system, different from cell lysis, should sustain continuous growth.

3.9.4   Tracking of strains during co-cultivation

As described in section 3.2, the strains used during the development of this project presented two different fluorescent markers. Lysine producer cells with a tyrosine auxotrophic phenotype presented a *eGFP* marker, while tyrosine producer lysine auxotrophic cells presented a *mRuby2* marker. Both markers were integrated into the *URA3* locus under the same promoter and terminater regions to produce a similar expression pattern.

These fluorescent markers were used to develop calibration lines that would allow a correlation between OD_{600} and fluorescence signal as described in section 2.10.2. Indi-

vidual calibration lines were produced to assess each strain, assuming that evolutionary processes could have affected fluorescence protein expression or even cell morphology.
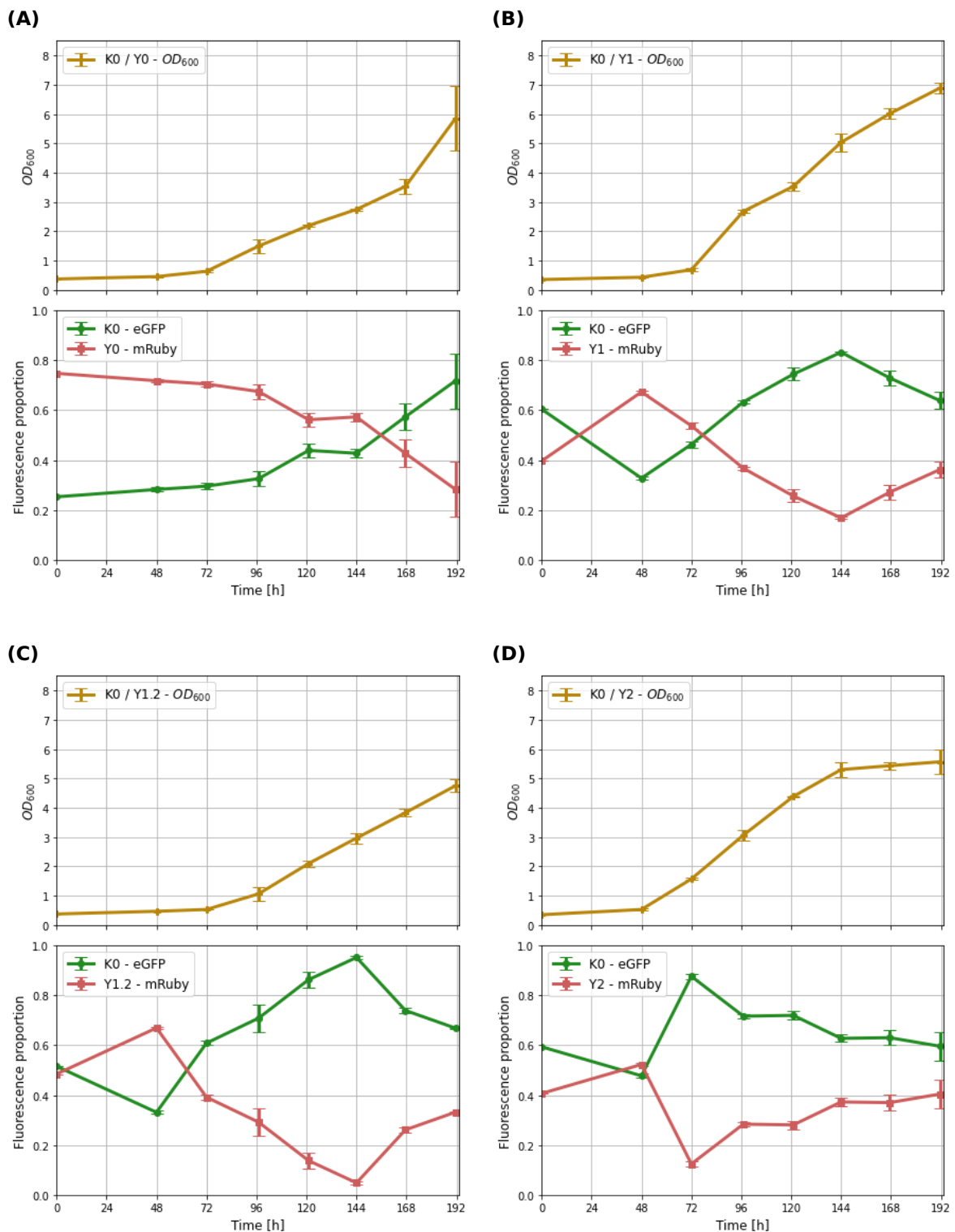
Figure 3.18: Tracking of co-culture strains proportion while using K0 as lysine donor. For each panel, the upper section represents the total OD_{600} of the co-culture while the lower depicts the cell proportion for each population according to the fluorescent marker used, green and red for lysine and tyrosine donors, respectively. Values represent the mean with the standard deviation for each point from triplicates. The experiment employed SCD-tyr-lys media.
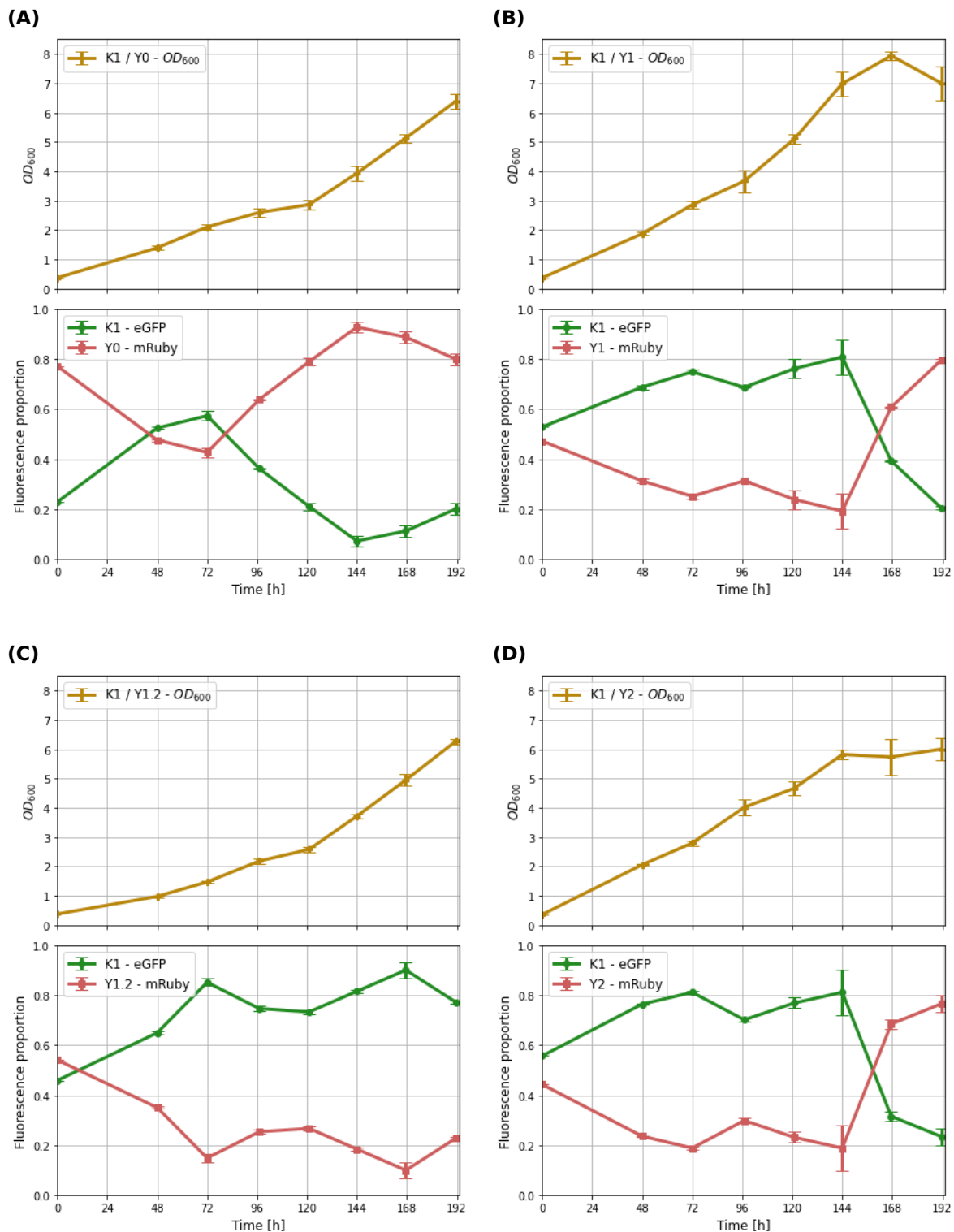
Figure 3.19: Tracking of co-culture strains proportion while using K1 as lysine donor. For each panel, the upper section represents the total OD_{600} of the co-culture while the lower depicts the cell proportion for each population according to the fluorescent marker used, green and red for lysine and tyrosine donors, respectively. Values represent the mean with the standard deviation for each point from triplicates. SCD-tyr-lys media was used for the fermentations.

Fluorescence was determined at different time points as described in section 2.10.2. Briefly, co-cultures featuring lysine and tyrosine overproducer strains were started aiming for a total OD_{600} cell density value of 0.4 using a 1:1 ratio for both species in triplicates. Total OD_{600} estimations were performed from flasks samples using dilutions if necessary. Later, fluorescent determinations of both channels, red and green, were performed in technical triplicates after washing samples to remove cell debris in the media. The raw fluorescence values obtained were used to estimate the individual cell density population from each strain species. These values were combined for a total OD_{600} cell density estimation from each analysed sample. Figures 3.18 and 3.19 depict the cell density population fractions relative to each strain at different time points.

Considering the cell loss during washing cycles and different dilution factors, the total OD_{600} values obtained by spectrophotometric determination were not compared with the total cell density value from the fluorescence determination.

Analysis of figures 3.18 and 3.19 suggest that important OD_{600} increments are most common when lysine-producing cells (green populations) are more abundant than red cells (tyrosine donors), regardless if the lysine donor strain is evolved or not. For instance, figure 3.18B presents a steeped growth period that began at 72 h, the same moment in which the proportion of green cells exceeds the red ones, reverting the decreasing tendency that was observed preceding that time point. Similar tendencies can be observed for subfigures 3.18C and 3.18D when after the low representation pattern of green cells is reverted, important increments on the total co-culture OD_{600} are observed.

Figure 3.19 depicts co-culture development when K1 strain is used as lysine donor. Subfigures 3.19B, 3.19C and 3.19D depict the same pattern discussed above, but interestingly an OD_{600} plateau can be appreciated around the 144 h in subfigures 3.19B and 3.19D, which coincides with the rise of red cell proportion.

Nevertheless, results presented in figures 3.18A and 3.19A are contrary to the previously discussed tendency, with red cells in higher proportion than the green ones during most of the fermentation. Both configurations use the engineered strain Y0 as tyrosine-donor, meaning that these configurations would lack the mutations generated during evolution rounds in the tyrosine donor strain. The individual role of some of the detected mutations will be examined in more detail in subsequent sections; however, their absence could be the reason for the unusual co-culture development.

However, the interaction of both unevolved strains presented in figure 3.18A, describe a

poor co-culture growth until the 72 h time point, at this moment and more clearly from the 96 h, the proportion of green cells slowly increases.

The co-occurrence of both processes could well support the hypothesis behind the relevance of lysine-producing cells for co-culture development. Yet, the same dynamic is not observable in the subfigure 3.19A, when a rising green cell proportion is rapidly overcome in favour of a dominant red cell proportion, dominance that lasts during all the co-culture development time. However, it is important to note that this last configuration involves an evolved lysine producer whose mutations would impact the co-culture development.

As discussed in previous sections, including an evolved strain in the co-culture, either as a lysine donor or a tyrosine donor, positively impacts fast biomass development in terms of OD_{600}. It could be proposed that the adaptations produced during these processes direct the co-culture development in a way that primarily promotes a higher lysine-producer cell proportion. This trend is clearly observable in the analysis of the fastest development co-cultures in figures 3.18 and 3.19.

It is also noticeable that the proportions at the starting point of these co-cultures divert significantly from the targeted 1:1, suggesting an artefact for the determination of Y0 strain presence in the co-cultures as the initial OD_{600} measurements for these. All experiments matched the target value of 0.4 units, disregarding the possibility of over-representation of tyrosine donor over lysine donor strains for this set of experiments. In this sense, assuming an equal strain proportion in these experiments, the analysis of the shifting proportion tendencies still seems relevant to describe the shifting strain representation during culture time.

Nevertheless, reducing a successful co-culture development only to this feature would be incomplete, as it would miss the contribution of decaying cells as previously presented in section 3.9.3. Considering the methodology used for this determination, it was impossible to produce information regarding the viability of cells at each time point. The role of the detected mutations and their possible relation towards a proper description of the observed results will be discussed in later sections.

3.10 Aromatic amino acid compounds production

Preliminary analysis of tyrosine-producer strains used pPET as a proxy molecule to detect increased tyrosine production, as at this point, a direct tyrosine determination protocol

had yet to be fully implemented in our laboratory. By this means, it was possible to establish a production improvement for the strains Y1.2 and Y2 compared to the parental strain Y0 (see figure 3.9B). Increased titers of pPET pointed to an increased carbon flow into the aromatic amino acid pathway, particularly into tyrosine formation, as pPET derives from tyrosine metabolism. Nevertheless, it was still necessary to establish if the increased extracellular presence of pPET was related to an increase in tyrosine production, enhanced activity of the Ehrlich pathway, or more efficient transport (export) mechanisms.

In this regard, several attempts were conducted to investigate an increase in the intracellular or extracellular tyrosine titers.

3.10.1 Betaxanthins production

Tyrosine is produced as one of the end products of the aromatic amino acid pathway (See figure 1.5). Yet, it is not an end metabolite, as it can be degraded via the Ehrlich pathway or incorporated into protein. These constraints would limit the building up of tyrosine titers.

Consequently, an indirect determination method was established to modify tyrosine into a non-metabolizable molecule, for which a betaxanthins-derived analysis was proposed, also motivated by the convenient visual screening strategy it provides.

The betaxanthins correspond to a family of plant-derived pigments exhibiting fluorescence excitation and emissions at 463 nm and 508 nm, respectively, making them distinguishable to the naked eye with a deep-yellow colouration (Gandía-Herrero et al. 2005; Steiner et al. 1999). This approach has been used successfully as a high-throughput method to screen for mutations that would render *S. cerevisiae* strains with improved tyrosine production activity (DeLoache et al. 2015; Mao et al. 2018).

Betaxanthins production depends on the availability of betalamic acid, which is produced from tyrosine after two enzymatic reactions: First, a tyrosine hydroxylase generates L-3,4-dihydroxyphenylalanine (L-DOPA), which finally turns into betalamic acid after the activity of a DOPA dioxygenase (DOD).

To perform both enzymatic reactions, the tyrosine hydroxylase *CYP76AD1* from *Beta vulgaris* and a *DOD* from *Mirabilis jalapa* (DeLoache et al. 2015) were cloned into an episomal plasmid with *URA3* marker to produce the vector LBGV063. The tyrosine hydroxylase used included two substitutions, at W13L and F309L, that reportedly prevent
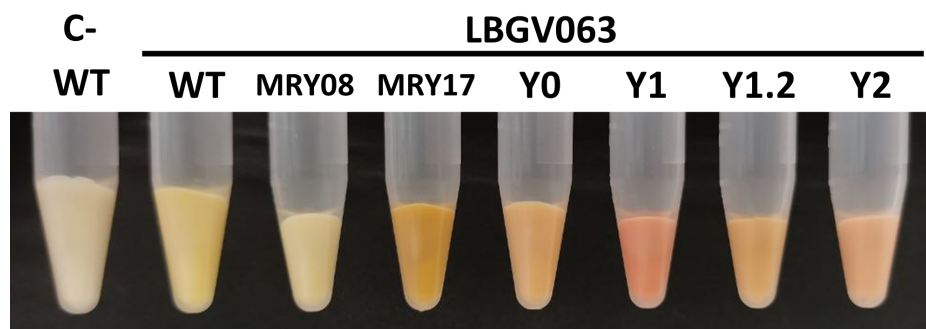
Figure 3.20: Expression of betaxhantins pathway in evolved tyrosine producer strains. Observed phenotypes after transformation of plasmid LBGV063 in evolved tyrosine producer and control strains. C- denotes the empty vector control. Cultures used SCD-tyr media.

undesired L-DOPA oxidase activity. The activity of both enzymes will be referred to as the betaxanthin pathway.

The betaxanthin pathway plasmid was transformed into the most relevant tyrosine producer strains. Additionally, two auxiliary strains were considered as a validation strategy for this system, the strain MRY17 engineered to overproduce tyrosine and its parental strain MRY08 without any optimisation (Reifenrath & Boles 2018).

Interestingly, after being cultured, the strains carrying the LBGV063 plasmid presented a range of colouration from a pale yellow to a soft red, as depicted in figure 3.20. The presence of red colouration was unexpected, as no reaction between betalamic acid and any amino acid is known to produce a reddish colouration (Rodriguez-Amaya 2019; Sunnadeniya et al. 2016) In this context, this colouration would suggest the undesired formation of betanidin-derived molecules, which would have been produced after an unspecific DOPA oxidase activity.

This undesired colouration has been observed as a side product of the wild-type tyrosine hydroxylase CYP76AD1. The enzyme would further oxidise the available L-DOPA to produce L-dopaquinone, which then spontaneously is converted into cyclo-DOPA, reacting with available betalamic acid to produce the betanidin core structure (See figure 3.21) (DeLoache et al. 2015; Sunnadeniya et al. 2016). This structure can, later on, be decorated by a multitude of radicals such as glucosyl, glucuronyl or derivatives groups to produce a wide variety of colourations (Rodriguez-Amaya 2019).

However, the CYP76AD1 enzyme used in this project included two substitutions, W13L and F309L, that reportedly prevent this undesired activity to a point in which no leakage has been evidenced (DeLoache et al. 2015). In *B. vulgaris*, three genes have been described to produce L-DOPA via tyrosine hydroxylation, *CYP76AD6* and *CYP76AD5* and
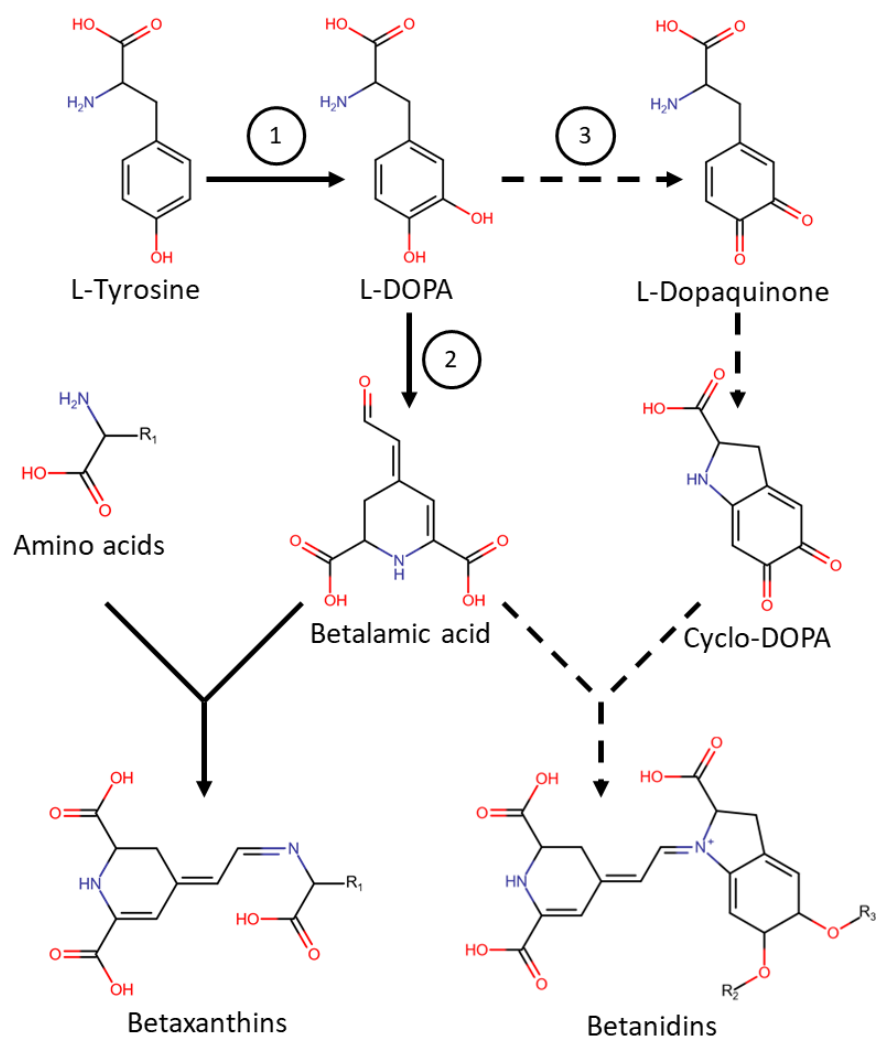
Figure 3.21: Schematic representation of betaxanthins and betanidins production. Processes 1 and 2 represent tyrosine hydroxylation and L-DOPA dioxygenation, respectively. Process 3 depicts a DOPA oxidation process. Unnumbered reactions represent spontaneous conversions. Straight lines mark reactions involved in betaxanthin production, while segmented lines describe steps required for betanidin production. R marks represent variable side chains that might be attached to the respective positions: R1 represents amino acid's radical chains. R2 represents glucosyl, glucuronyl or derivatives groups or Hydrogen atoms. R3 represents glucosyl or derivatives groups. Modified from DeLoache et al. 2015 and Rodriguez-Amaya 2019.

CYP76AD1, but among them, just *CYP76AD1* shows also production of cyclo-DOPA (De-Loache et al. 2015; Sunnadeniya et al. 2016). The presence of a phenylalanine at position 309 in *CYP76AD1* has been described as a vital element in the production of cyclo-DOPA, and its eventual characteristic red colouration, a feature that is absent on the genes *CYP76AD5* and *CYP76AD6*, both of which have a leucine at that position (Sunnadeniya et al. 2016). In this sense, the use of the ancestral natural version with leucine at position 309 was expected to prevent this undesired activity (DeLoache et al. 2015; Sunnadeniya et al. 2016). However just the modified version of *CYP76AD1* has been previously used for betaxanthin screening strategies, which motivated its election.

The pale-yellow and deep-yellow tonalities observed for the control and Y0 strains match the expected betalamic acid colouration in the absence and presence of extra tyrosine, respectively. The system was also validated by using the reference strain MRY17, which has been engineered to overproduce tyrosine, which produces a strong deep-yellow colouration.

These results suggest that the implemented screening system based on betaxanthin production is sensitive to tyrosine concentration and that the red tonalities observed for the evolved strains Y1 and Y2, and in a lesser manner for Y1.2 might be related to enzyme dysfunction, limited to the above mentioned strains. In this sense, the environmental stress endured by these strains during evolution might have constituted a factor that modified intracellular conditions, promoting impaired function of enzymes such as the tyrosine hydroxylase used in this project or any other oxidase, prompting the observed red colouration.

From this perspective, the presence of red colourations would indicate the presence of betanidin structures, which would prevent the use of this screening system to asses tyrosine-improved production in the evolved strains. The presence of betanidin structures would suggest that the tyrosine pool is being depleted from several branches, producing molecules with different properties, making the comparison not meaningful.

The lack of more detailed analytical tools prevented further research into the strange colouration observed by the use of this system. Consequently, alternative approaches were pursued to establish a possible increase in tyrosine intracellular production.

3.10.2 *p*-Coumaric acid

As another alternative to evidence an increased tyrosine production, the use of *p*-coumaric acid (pCA) was chosen, which besides being a stable metabolite not consumed by yeast metabolism, can move freely across the cellular membrane (Jakočiūnas et al. 2015; Rodriguez et al. 2015). *trans-p*-coumaric acid is produced after the elimination of the ammonia group from L-tyrosine by the action of a tyrosine ammonia-lyase enzyme. Tyrosine ammonia-lyase (TAL) enzymes have not been identified in fungi, so for this process the TALp from *Rhodobacter sphaeroides*, which presents the highest specific activity for tyrosine was used (Gold et al. 2015; Louie et al. 2006; Xue et al. 2007).

After transforming the relevant strains with the plasmid LBGV062, which carries the *TAL* gene, titers of pCA and pPET were measured after 70 h, 94 h, 119 h, and 143 h of fermentation. Samples were processed according to a modified protocol from Gottardi,

(A)   **(B)**
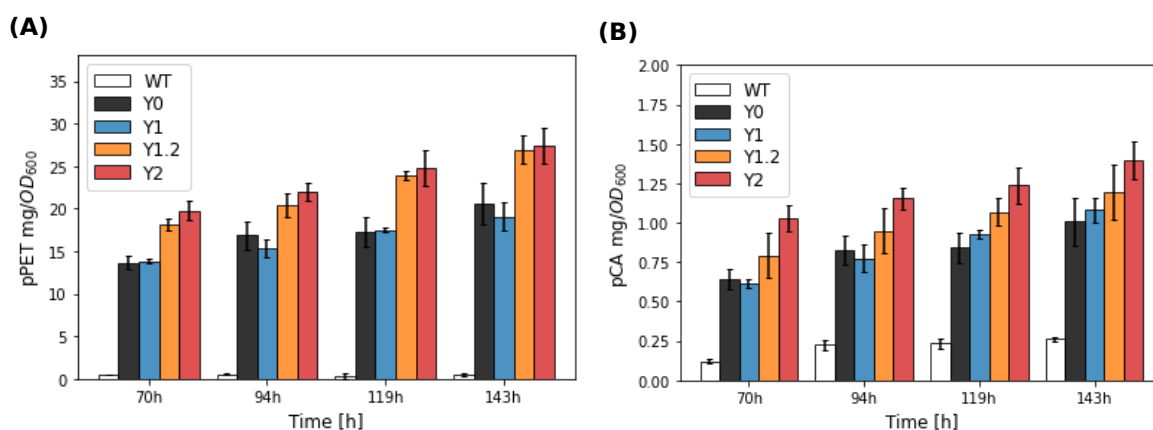
Figure 3.22: Production of pCA and pPET by tyrosine producer evolved strains. Figures **(A)** and **(B)** present the production of pPET and pCA on tyrosine-producing cells, respectively. Bars depict specific normalised titers of triplicates and error bars correspond to the standard deviation. Fermentations were performed using SCD-tyr media.

Reifenrath, et al. 2017 as described in section 2.10.3.2, obtained specific normalised titers are presented in figure 3.22.

The analysed strains showed a time-dependent increment for both molecules, pPET and pCA. The strains Y1.2 and Y2 seem to be the better producers for both molecules across all the time points, at least when compared to the parental strains Y0 or Y1, even though the productivity improvements are limited to 0.2 mg OD_{600}^{-1} for pCA and 5 mg OD_{600}^{-1} for pPET.

Despite the relatively minor improvements, this represents the first evidence of improved intracellular tyrosine production derived from this project's adaptive laboratory evolution processes. Consistently, pPET titer patterns show a similar tendency among the analysed strains, with Y2 and Y1.2 being the strains with higher titers at each time point.

Further sections will explore the possible role of the detected mutations (presented in table 3.2) in the observed phenotypes.

3.10.3 HPLC determination of Tyrosine and pPET

Based on previous results, the increased titers of pCA suggested the increased presence of intracellular tyrosine. Still, it was uncertain if this metabolite was being secreted efficiently into the media to sustain co-culture growth. In this sense, a protocol for directly determining tyrosine was established at a later stage of this project, as a modified version of the protocol presented by Hassing and collaborators (Hassing et al. 2019). The HPLC method is described in section 2.10.3.3.

(A)

(B)
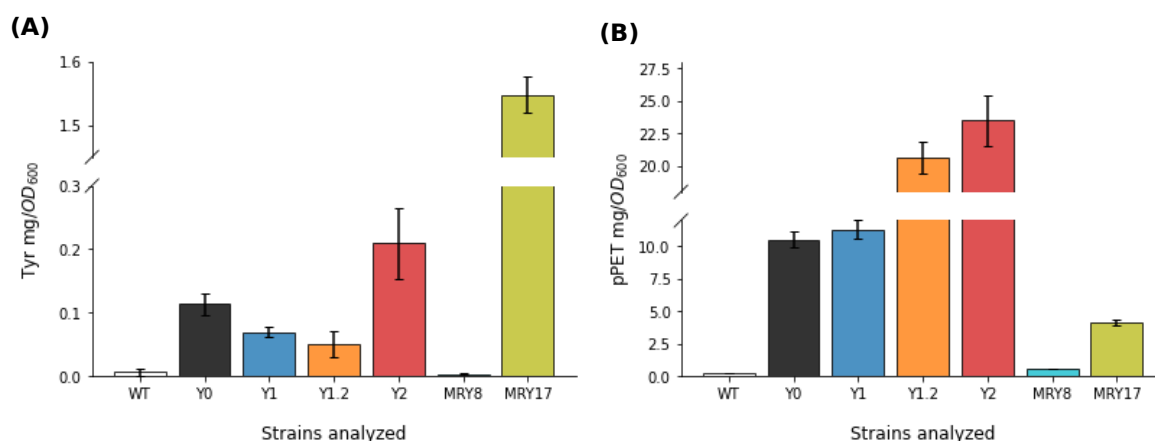
Figure 3.23: Direct determination of tyrosine on evolved producer strains. Bars present averaged values of triplicates with their respective standard deviations. Figures **(A)** and **(B)** describe the normalised extracellular tyrosine and pPET-specific titers produced from evolved strains, respectively. SCD-tyr media was employed for the fermentations.

To evidence the tyrosine production of the analysed strains, all precultures and fermentations were prepared in media lacking tyrosine. The strains MRY17 and MRY8, previously used during the betaxanthin detection assay, were included as tyrosine and pPET production controls. Observed titers after 48h of growth on SCD-tyr media can be observed in figure 3.23.

Tyrosine extracellular production is comparatively high for the control strain MRY17, presumably due to its heavily engineered background. In comparison, evolved strains present low titers, in which the best-producing strain Y2, is nearly one-eighth as efficient as the control strain. The extracellular tyrosine secretion observed in the strains developed in this project was demonstrated to be relatively low, being unlikely that the success in co-culture development is due just to this amino acid secretion. Interestingly, pPET titers from strain Y1.2 and Y2 remain high, suggesting an increased carbon flow into the aromatic amino acid pathway that is being re-routed into the Ehrlich pathway to produce fusel alcohols such as pPET or fusel acids.

One of the most interesting modifications in the strain MRY17 is the deletion of the phenylpyruvate decarboxylase Aro10p, being one of the four enzymes capable of decarboxylating α-keto acids into fusel aldehydes during the second step of the Ehrlich pathway.

Aromatic amino acids degradation into this pathway first involves a transformation into α-keto acids by the action of transaminases such as Aro8p or Aro9p. In this context, Aro8p and Aro9p produce and consume tyrosine, establishing a relative equilibrium delimited by the enzymes' affinity for this amino acid or its α-keto acid form, HPP (see

(A)

(B)
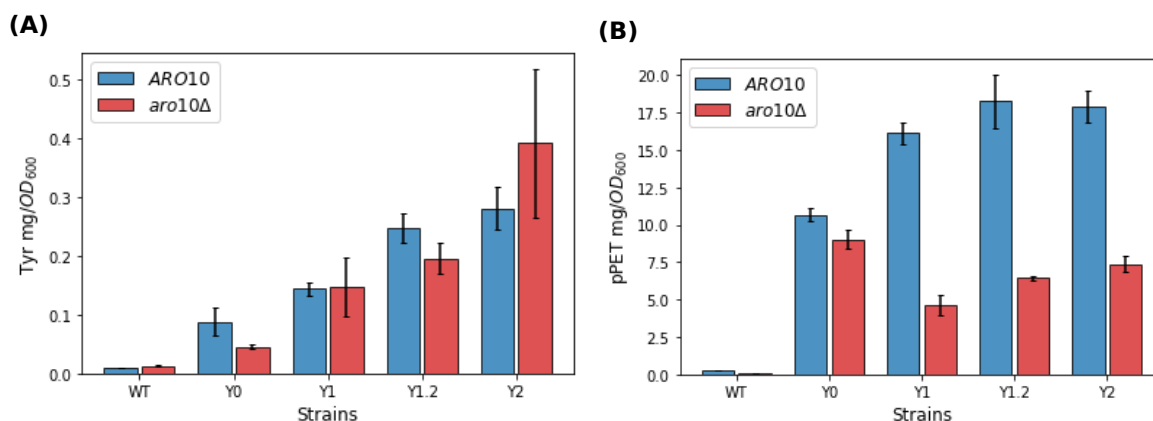
Figure 3.24: Effect of an *aro10Δ* on tyrosine and pPET production in evolved strains. Figures **(A)** and **(B)** depict tyrosine and pPET-specific titers production with corresponding standard deviation from triplicates. Fermentations were performed using SCD-tyr media.

figure 1.5). Such equilibrium would be constantly disrupted due to protein synthesis processes or by decarboxylation of HPP into pPAC by Aro10p (Bulfer et al. 2013; Hazelwood et al. 2008; Karsten et al. 2011). Consequently, suppression of Aro10p is a frequent modification in attempts to increase aromatic amino acids pools, as it prevents their depletion into the Ehrlich pathway (Gold et al. 2015; Kneen et al. 2011; Reifenrath & Boles 2018; Rodriguez et al. 2015). The strain MRY17 in figure 3.23 also demonstrates this concept, producing relatively high tyrosine levels with low pPET titers.

In this light, it was suspected that high pPET titers from tyrosine producers evolved strains established across all the present work could evidence an increased carbon flow into the aromatic amino acid pathway, but whose accumulation in tyrosine form would be prevented by action of decarboxylase enzymes.

To test this theory, an *aro10Δ* was produced in all the relevant tyrosine producer strains developed in this project. After 48 h of culture, tyrosine and pPET titers obtained are presented in figure 3.24.

Even after an *aro10Δ*, tyrosine titers fail to increase in the evolved strains, showing even a decreasing tendency as depicted in figure 3.24A. Interestingly, figure 3.24B shows the desired effect regarding a decrease in pPET titers. Results seem to suggest that tyrosine is still not being accumulated despite deleting the most relevant phenylpyruvate decarboxylase, which, together with the decreasing pPET titers, seems to suggest that *aro10Δ* has a negative impact on carbon flow into the pathway.

In order to further elucidate the impact of this deletion, a new experiment was conducted in which tyrosine production in agar plates will be assessed. Samples from relevant tyro-

sine producer strains were plated in SCD-tyr plates next to areas where the tyrosine aux-
otrophic strain LBGY002 strain was inoculated. The arrangement of the strains in plates
sought to evaluate if evolved strains with an *aro10Δ* could produce tyrosine enough to
sustain the growth of auxotroph strains in the vicinity.

Results after six days of culture at 30°C are presented in figure 3.25. The plate including
evolved strains presented in figure 3.25A fails to show tyrosine production enough to
sustain growth of auxotrophic strains. In this sense, the result is similar to the one
observed in a similar test performed before the evolution process (figure 3.2B).

Nevertheless, plate presenting strains with the *aro10Δ* in figure 3.25B, shows evident
growth of several areas populated with the tyrosine auxotrophic strain LBGY002. This
suggests an effective production and migration of tyrosine or its direct precursor HPP.
Only these two metabolites could be effectively used by the strain LBGY002 to com-
plement its auxotrophy, as it exhibits an *tyr1Δ* (see figure 1.5). However, considering
the consistent results suggesting that tyrosine is not being accumulated in tyrosine pro-
ducer strains, it is more likely to propose HPP as the responsible candidate to sustain the
growth observed in figure 3.25B.

In any case, this represents evidence of an actual improved carbon flow into the aro-
matic amino acid pathway, a phenomenon observed in all the evolved strains, including
Y1.2. Notably, the auxotrophic strain located between Y0 and Y1 in figure 3.25B, shows
growth only on the side closer to the Y1 strain. This suggests that a metabolite is being

(A)   **(B)**
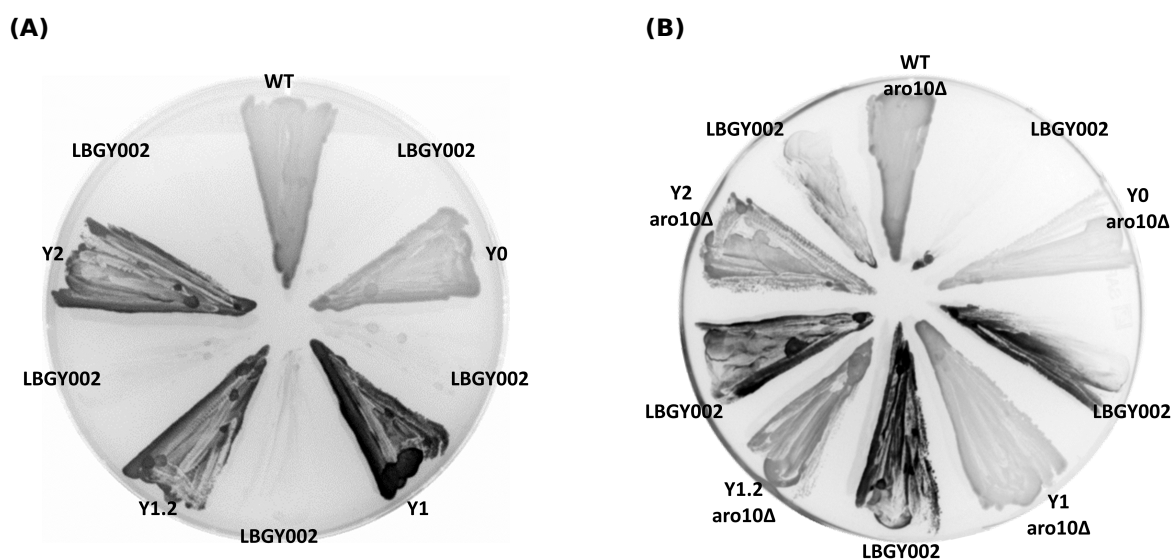
Figure 3.25: Evaluation of tyrosine secretion using solid media on evolved strains.
Tyrosine secretion was assessed by using the tyrosine auxotrophic strain LBGY002 in
SCD-tyr plates. Plates **(A)** and **(B)** depict observed growth by using tyrosine producer
strains with and without Aro10p, respectively.

secreted solely from that direction, implying that the presence of the overproducing vari-ants *ARO3^{fbr}* and *ARO4^{fbr}* integrated on Y0 are not sufficient to produce the observed phenotype after an *aro10Δ*. The auxotrophic strain located between WT and Y2 on the same figure shows an apparent normal growth. However, if observed closely, signs of growth are stronger in the area closer to Y2, suggesting that secretion from this strain is feeding the complete area.

Despite not being able to establish tyrosine increase production on evolved strains by direct or indirect quantification, evolved strains did produce more efficient growth under co-culture conditions. The evidenced increased pPET titers in evolved strains point in the direction of an increased carbon flow into the aromatic amino acid pathway, but no improved accumulation was observed after the deletion of the phenylpyruvate decar-boxylase Aro10p during single fermentations.

Nevertheless, results observed in figure 3.25B indicate a different behaviour on evolved strains without Aro10p. By compromising their ability to produce aromatic alcohols, these strains seem to secrete enough amounts of tyrosine or HPP as to sustain the growth of tyrosine auxotrophic strains in the vicinity. This phenotype is apparently re-vealed after the deletion of *aro10*, but not caused directly by it, as WT or Y0 strains fail to produce growth after introducing this modification.

It is interesting to further speculate on evolution's role over the observed phenotypes, as no direct modification is observed on the aromatic amino acid biosynthesis pathway. Further chapters of this work will discuss in detail the possible affected mechanisms beyond direct genetic modifications.

3.11   Analysis of mutations identified in evolved strains

Previous attempts to measure tyrosine secretion from evolved strains demonstrated that it occurs at very low levels, which suggests this phenomenon is unlikely to be responsible for sustaining the observed improved co-culture growth. Consequently, an analysis of the mutations detected after the evolutionary processes was of great importance to es-tablish improvements in other factors that could help explain the observed phenotypes.

The detailed study of all observed mutations could not be covered in the extent of this project, for this reason, and based on the reported role of each one of these genes, mutations reported in *ASR1*, *ART2*, *LYS9* and *WHI2* where chosen for subsequent study.

3.11.1 Deletion at position 311 in *ASR1*

The gene *ASR1* is located in chromosome XVI in *S. cerevisiae*, first described in Betz et al. 2004 and collaborators as an alcohol sensitive RING/PHD finger protein that shuttles between nucleus and cytoplasm, being accumulated in the cytoplasm upon alcohol stress. The overexpression of this protein has been related to perturbation of septin organisation during cell division, disrupting the G2/M phase transition process and producing an elongated bud phenotype, even though *ASR1* deletion produced no morphological alterations (Zou et al. 2015). Interestingly, it has also been described as a RING finger ubiquitin-ligase protein that binds to the RNA polymerase II, eventually promoting complex disassembly and inactivation (Daulny et al. 2008), associating an *ARS1* deletion to an abnormal accumulation in free amino acids (Mülleder et al. 2016).

A common variation in the gene *ASR1* was observed in the three strains isolated after the first evolutionary round Y0*1, Y0*2 and Y0*5, a nucleotide deletion at position 311 that renders an early stop codon shortening the protein to 121 amino acids from its original 310 residues. As consequence, this mutation is expected to remove the plant homeodomain (PHD) of this protein, localised between the residues 121 to 167 (Betz et al. 2004; Zou et al. 2015). Consequently, it was theorised that the observed mutation would render an inactive protein, which could produce an accumulation of alpha amino acids as reported by Daulny et al. 2008. An intracellular accumulation of amino acids could benefit co-culture development, as they would be realised into the media upon cell death, thereby feeding surviving cells.
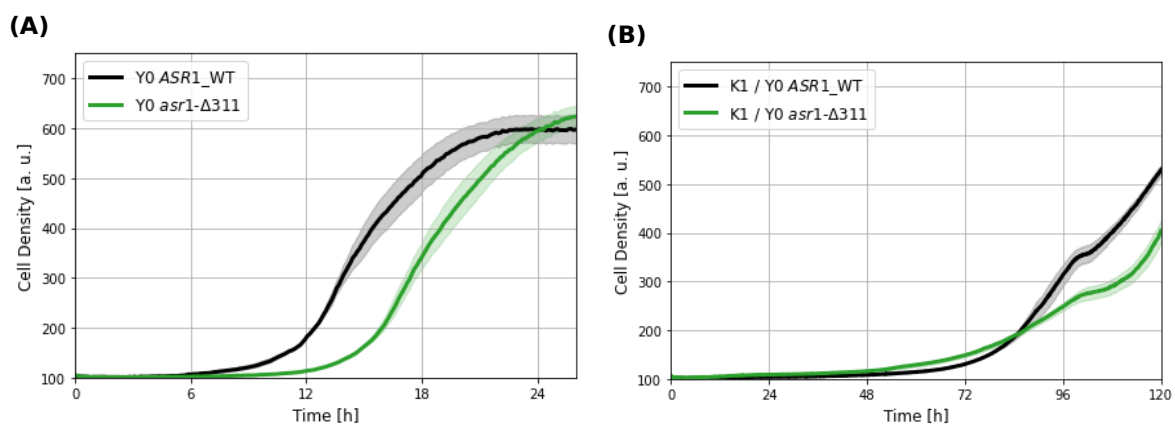
Figure 3.26: Role of mutation in *ASR1* during single and co-culture development. **(A)** Single-growth of mutated and control strain using SCD-tyr media. **(B)** Co-culture development of mutated and control strain using strain K1 as lysine donor. Green line represents the strain LBGY60 (Y0 *asr1*-Δ311), while black line represents the control strain Y0 with an unmodified *ASR1* using SCD-tyr-lys media. Shaded areas represent the standard error of triplicates.

In order to test this theory, the reported mutation was introduced into a Y0 strain using a CRISPR/Cas9-assisted strategy (see section 2.8.11), producing the strain LBGY60, whose growth was evaluated in a single and co-culture fermentation compared to an unmodified Y0 strain.

Results are presented in the figure 3.26, where the deletion at position 311 of *ASR1* seems related to a later development during single fermentation but has no significant effect during co-culture fermentation development.

Complete deletion of *asr1* has been reported to produce up-regulation of genes related to the cell cycle, suggesting some sort of perturbation on this process (Zou et al. 2015). If the shortened protein produced after the deletion at position 311 renders an inactive protein, it could be expected that the strains exhibiting this mutation present some developmental abnormality, which could explain the more prolonged lag phase of the strain LBGY60. But more importantly, the similar growth observed under co-culture conditions would suggest that any intracellular amino acid accumulation, if any, caused by a non-functional Asr1p is not enough to speed up the development of a consortium.

Consequently, the mutation observed in the gene *ASR1* seems not to explain the improved growth observed under co-culture conditions when using evolved strains.

3.11.2 Deletion at position 615 in *ART2*

Upon limited nutrient availability, yeast cells undergo fast and controlled adaptation processes, e.g. autophagy and membrane protein degradation, seeking to secure a minimum metabolic activity that would sustain cell transition into the new nutrient conditions (Bianchi et al. 2019; Loewith & Hall 2011; M. Müller et al. 2015). The TORC1 complex (target of rapamycin complex 1) acts as the major regulator system of these processes, being sensitive to a wide range of physiological conditions such as carbon, nitrogen, or amino acid availability (Loewith & Hall 2011). Under abnormal amino acid conditions, TORC1 mediates the endocytosis of amino acid permeases by a ubiquitin-mediated system, efficiently targeting high-affinity amino acid transporters such as Mup1p, Can1p or Lyp1p (Ivashov et al. 2020; Lin et al. 2008; M. Müller et al. 2015). The α-arrestin proteins act as part of this regulatory process as ubiquitin-ligase adaptors, conferring the system some versatility by allowing degradation as a response to different metabolic cues, such as high or low substrate concentrations or even toxicity-derived stress (Ivashov et al. 2020; Lin et al. 2008; Nikko et al. 2008).

The internalisation of the principal lysine transporter Lyp1p is modulated by the action

(A)

(B)
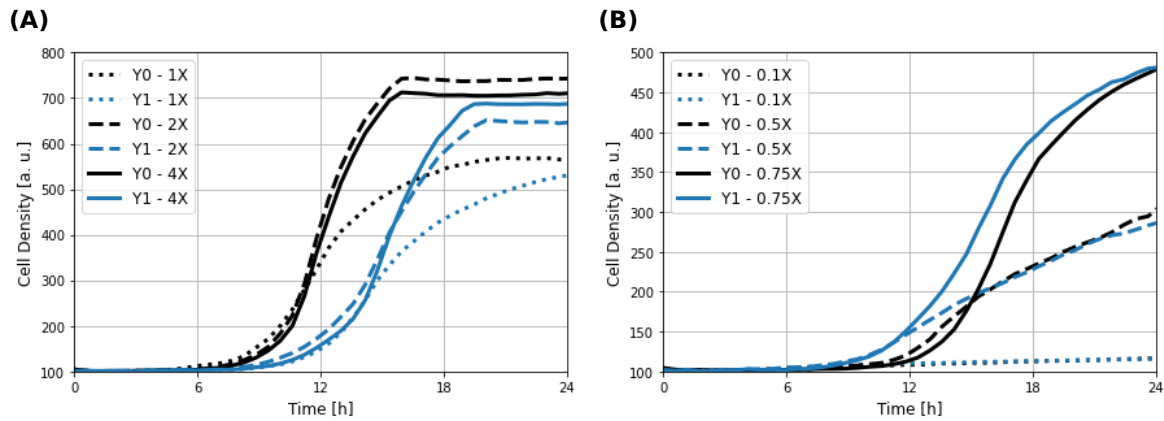
Figure 3.27: Growth behaviour of strains Y0 and Y1 under different lysine concentrations. X represents the normal concentration of Lysine in SCD-tyr media. **(A)** Effect of high lysine concentration on strain development. **(B)** Growth performance under low lysine concentrations. Data presented corresponds to single replicas.

of the α-arrestin proteins Art1p and Art2p, with the latter being involved in transporter degradation under low substrate and stress-toxicity conditions (Ivashov et al. 2020; Lin et al. 2008; Sychrova et al. 1993). Therefore, it was interesting to detect a *art2-Δ615* mutation across the three tyrosine producer strains after the first evolutionary process, causing a frameshift and an early stop codon, which shortens the protein from 1,118 residues to just 218.

It was proposed that such protein disruption would impact the normal functioning of this α-arrestin, particularly under low lysine conditions, affecting the tyrosine producer strains during co-culture. Consequently, an experiment was performed testing the growth performance of the strains Y0 and Y1 under different lysine concentrations.

Growth performances observed in figure 3.27 suggest that high lysine concentrations do not represent an advantage for the development of the strain Y1 which carries the *art2-Δ615* mutation. However, strain Y1 shows faster development under low lysine concentrations than the parental Y0. Observed growth improvement is particularly interesting, as strain Y1 shows a clear growth phenotype compared to Y0 under normal lysine conditions (1x). This suggests that the growth deficit observed after evolution is compensated under low lysine conditions. In this sense, a lysine concentration of 0.75 times the usual concentration in our media (0.75x) was chosen for further analysis of lysine auxotrophic strains as it seems to offer a more evident development difference between wild-type and mutant strains.

A recent report from Ivashov et al. 2020 reports that Art2p negatively regulates the stability of the Mup1p, Can1p and Lyp1p transporters under nitrogen and amino acid starvation conditions. Consequently, it was theorised that the mutation produced after

(A)   **(B)**
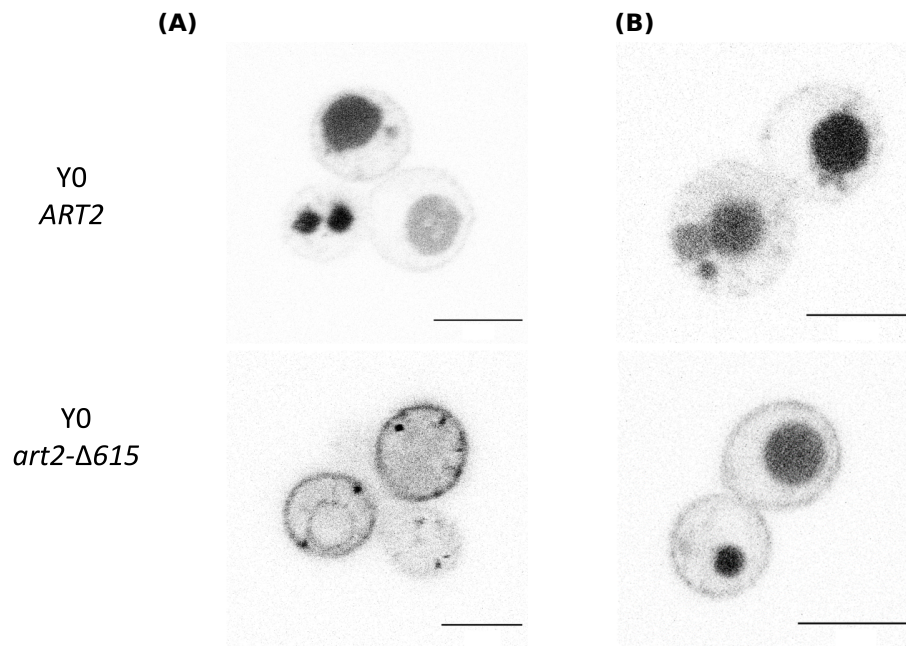
Figure 3.28: Role of the mutation *art2-Δ615* on stability of Lyp1p. All strains express Lyp1p-GFP from a centromeric plasmid (LBGV117). Black lines represent a scale bar of 5 μm for each graph. All cultivations were performed in SCD-tyr-ura media using a 0.75x lysine concentration, and all images represent just the GFP channel. Figures **(A)** and **(B)** show the GFP expression of the strains after 4 h and 72 h of media exposure, respectively.

evolution disrupts Art2p regulation and stabilises the Lyp1p transporter under low lysine conditions, eventually allowing a faster lysine uptake and co-culture development.

To test this theory, a fused *LYP1-GFP* construct was developed in a centromeric plasmid, named LBGV117, and used to evaluate the Lyp1p stability under a mutant and wild-type genotype. Consequently, a Y0 strain with the engineered *art2-Δ615* (LBGY19) modification was transformed with the newly developed plasmid in order to assess the stability of the transporter when compared with a *ART2* genotype.

The results presented in figure 3.28 suggest that after 4 h of growth in fresh media (figure 3.28A), strain Y0 carrying the LBGV117 plasmid shows a relatively low or no existing Lyp1p presence in the plasma membrane, with a high GFP signal coming from the vacuole pointing to the internalisation of this transporter. In contrast, under an *art2-Δ615* genotype, the LBGY19 shows a higher presence of the Lyp1p transporter in the plasma membrane, with partial signs of internalisation, but not as distinctive as observed with the wild type *ART2*. After 72 h (figure 3.28B), no clear sign of Lyp1p presence can be observed in the membrane of the Y0 strain, while all the GFP signal seems concentrated in the vacuole as sign of complete internalisation process. In contrast, when the *art2-Δ615* mutation is present, despite signs of degradation of Lyp1p, the presence of the transporter in the membrane can be clearly seen.

These results suggest that the presence of the *art2-Δ615* mutation helps to stabilise the Lyp1p transporter in the membrane at low lysine concentration conditions (0.75x), which would allow a faster uptake of the amino acid when it becomes available, favouring the strain development. During preculture, lysine auxotrophic strains would deplete the media from this amino acid, reaching a starvation point in which nutrient adaptation mechanisms such as TORC1 complex would internalise specific amino acid transporters such as Lyp1p (Lin et al. 2008; Sychrova et al. 1993). Nevertheless, previous results suggest that strains carrying the *art2-Δ615* mutation fail to completely internalise this transporter.

During co-culture fermentation, nutrients secreted by overproducer cells or released as cell decay products would be quickly uptaken by surviving cells, allowing its growth and consortium development. Strains presenting the *art2-Δ615* mutation would have Lyp1p transporters already present in their membrane, in contrast with *ART2* cells that would be expressing general transporters such as Gap1p (Grenson et al. 1970). Consequently, the better lysine transport efficiency of Lyp1p compared with the general transporters would represent an advantage for those cells, allowing its fast multiplication and prevailing in the population media (Bianchi et al. 2016). In this manner, the *art2-Δ615* mutation would be preserved in the population gene pool, explaining why it was detected in all three strains analysed after the first evolution.

To confirm the hypothesis that a null *art2* genotype will positively affect co-culture development, a full deletion of this gene was engineered into a Y0 background, originating the strain LBGY89. A single and co-culture fermentation between the strains carrying the *art2-Δ615* and *art2Δ* variations was performed on a low-lysine SCD-tyr media (0.75x), using a Y0 *ART2* strain as control.

According to our expectations, figure 3.29 shows that under low lysine concentration, a mutant *ART2* gene confers growth advantages compared to a wild-type gene version. While the *art2-Δ615* mutation seems sufficient to confer a growth advantage, a full *art2* deletion is observed to produce the earliest growth during experiments with low lysine, in this sense, agreeing with the observed results for the strain Y1 in figure 3.27. Although the *art2-Δ615* mutation is expected to produce a non-functional protein, the complete absence of the open reading frame (ORF) seems better for growth under low lysine conditions (0.75x), possibly due to a detrimental effect of the truncated protein or to a reduced metabolic burden associated with the full deletion.

Nevertheless, under co-culture fermentation, the three strains seem to produce similar

(A)

(B)
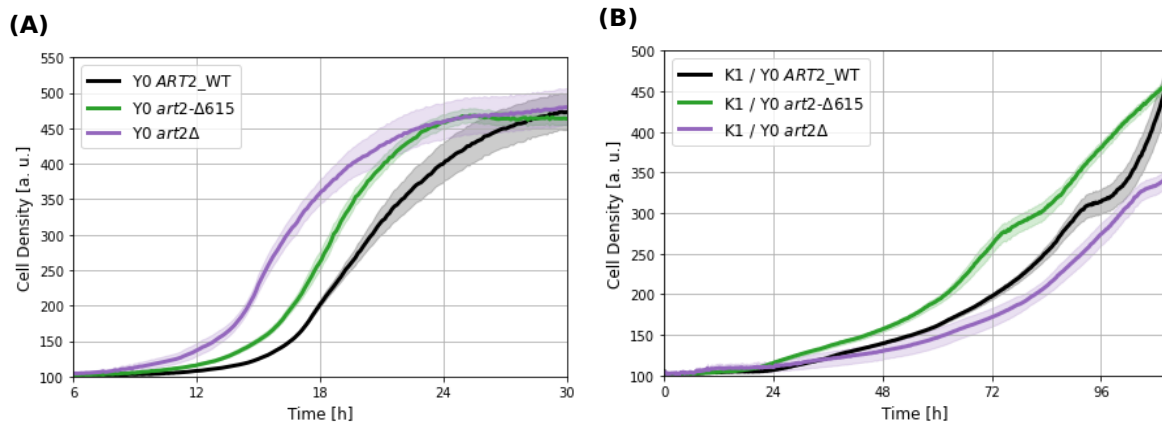
Figure 3.29: Role of *ART2* on strain development during single and co-culture fermentation. The strains analysed are Y0 (*ART2*), LBGY19 (Y0 *art2-Δ615*) and LBGY89 (Y0 *art2Δ*) depicted in black, green and purple respectively. **(A)** Fermentation of the analysed strains in SCD-tyr media, supplemented with just 0.75x of lysine. **(B)** Performance of analysed strains under co-culture fermentation using SCD-lys-tyr media. Lines and shaded areas represent means and standard error of measurements, respectively.

growth, with the strain carrying the *art2-Δ615* variation slightly outperforming strains with wild type or full deletion versions of *ART2*. Unexpectedly, the *art2Δ* genotype produced the worst growth under co-culture conditions.

Stabilisation of the Lyp1p transporter under a deficient Art2p scenario seems to improve single-strain growth, and this holds true for both mutant and full deletion genotypes. Nevertheless, the poor performance of the full deletion under a co-culture scenario suggests that the modification disrupted some other unidentified processes.

It is possible that the CRISPR/Cas9 activity used to produce the full deletion might have exhibited some off-target activity, inserting mutations in an unintended locus that would eventually decrease the fitness of the strain under co-culture conditions. Is also likely that a full deletion of 3,354 nucleotides which encodes for Art2p, might induce alterations in the activity of neighbouring genes, which eventually could induce a growth phenotype under co-culture conditions. This theoretical activity disruption would not be produced during a target engineering of the *art2-Δ615* mutation, preventing in this way undesired further affectation of different metabolic processes. Nevertheless, the detailed analysis of these possibilities was outside the scope of the present project and was not further pursued.

Nevertheless, evidence collected so far seems to strongly demonstrate a positive role of a truncated Art2p for Lyp1p stabilisation, an alteration that proves valuable for early lysine uptake in strains auxotrophic for this amino acid (see section 4.2.1).

3.11.3 Double deletion at position 1013 in *LYS9*

The lysine biosynthesis pathway in yeasts converts 2-oxoglutarate from the tricarboxylic acid (TCA) pathway into lysine and is composed of eight reactions (Lysine biosynthesis pathway is depicted in figure 1.6). Feedback regulation of this pathway has been observed to occur just on its first step, which involves the production of homocitrate by two homocitrate synthases with redundant functions, Lys20p and Lys21p (Bulfer et al. 2010; Feller et al. 1999). However, this is not the only point that can be subject to regulation, as the joint activity of the transcription factor Lys14p together with 2-aminoadipate-6-semialdehyde (ASA), also a byproduct of this pathway, has been observed to upregulate the expression of the genes *LYS20*, *LYS21*, *LYS5*, *LYS9* and *LYS1*. (B. Becker et al. 1998; Borell et al. 1984; Feller et al. 1994; Ramos et al. 1988).

The consortia developed in the present study were built around the exchange of lysine and tyrosine. Consequently, tyrosine producer strains were expected to either generate mutations improving this amino acid production or to control stress mechanisms. In this sense, it was interesting to discover a mutation inside the lysine biosynthesis pathway.

The seventh step in the lysine biosynthesis pathway is performed by Lys9p, a saccharopine dehydrogenase, which converts ASA and glutamate into saccharopine (E. E. Jones & Broquist 1966; Ramos et al. 1988; Storts & Bhattacharjee 1987).

Sequencing analysis revealed a double nucleotide deletion at position 1013 in the *LYS9* gene for all the analysed evolved strains, producing a frameshift since the amino acid 337 and rendering an early stop codon at position 349 from the original 446 residues of this protein. Considering that 75% of the protein sequence was unaffected by this mutation, it was necessary to elucidate the possible functional consequences of this mutation.

According to Andi et al. 2006, Lys9p possess three domains: Domain I, which comprehends residues 1-124 and 387-439 and binds to the NADPH; Domain II, formed by the residues 125-247, 351-386 and 439-446, binds to saccharopine and also participates in the structural dimeric conformation of this protein. Meanwhile, Domain III extends over the residues 248-350 and closes the active site after substrates are attached. In this sense, the *lys9-Δ(1013-1014)* mutation would render a protein with all its domains incomplete or affected by the frameshift produced after the reported mutation. Which suggested that the enzyme would present a drastically reduced or null activity for transforming ASA into saccharophine.

The structural model established by Andi et al. 2006 was used to localise the regions affected by the *lys9-Δ(1013-1014)* mutation. Results of this analysis are presented in figure 3.30. The presented 3D model visualisation was produced using Genious prime protein visualisation feature (Biomatters 2019) It can be appreciated that an important section of the pocket backside would be missing in the mutant genotype, suggesting an important activity disruption. Also, the structural conformation of a protein heavily depends on the stabilising role of nearby structures, suggesting that real alterations for Lys9p under a *lys9-Δ(1013-1014)* genotype could be more drastic than what has been presented, producing a negative impact for protein activity.

To establish the role of a non-functional Lys9p during a single and co-culture development, the *lys9-Δ(1013-1014)* mutation and *lys9Δ* were introduced into a Y0 background, producing the strains LBGY15 and LBGY90 respectively. These strains were tested under single and co-culture growth scenarios to assess their impact on culture development.

The results can be observed in figure 3.31. The presence of a non-functional Lys9p seems to be detrimental to the strain growth on single culture but favourable during a co-culture development. During a single fermentation regimen, the strains displaying the *lys9-Δ1013-1014* and the *lys9Δ* perform worse than the parental strain, with the strain displaying the full deletion being slightly better than the partial mutation (figure 3.31A), probably as a result of reduced metabolic costs as previously described in section 3.11.2. Interestingly, despite not showing any improvement under single growth, mutations on *LYS9* seem to be favourable for co-culture development (figure 3.31B).

(A)   **(B)**
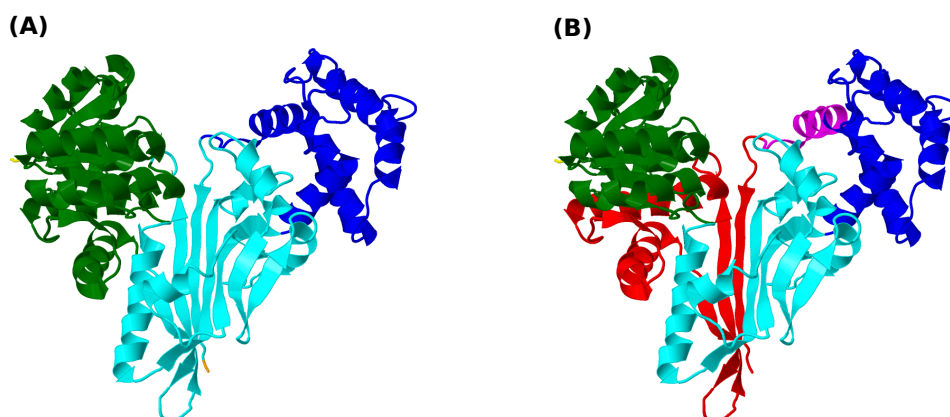
Figure 3.30: Structural 3D representations of Lys9p. Structural model of Lys9p proposed by Andi et al. 2006. Structures coloured in green, cyan and blue represent Lys9p Domains I, II and III, respectively. Figures **(A)** and **(B)** present a front view of a wild-type Lys9p. The region presented in magenta represents the section affected by the frame-shift produced by the *lys9-Δ(1013-1014)* mutation. The section coloured in red represents the protein missing fragment derived from the frameshift.

(A)

(B)
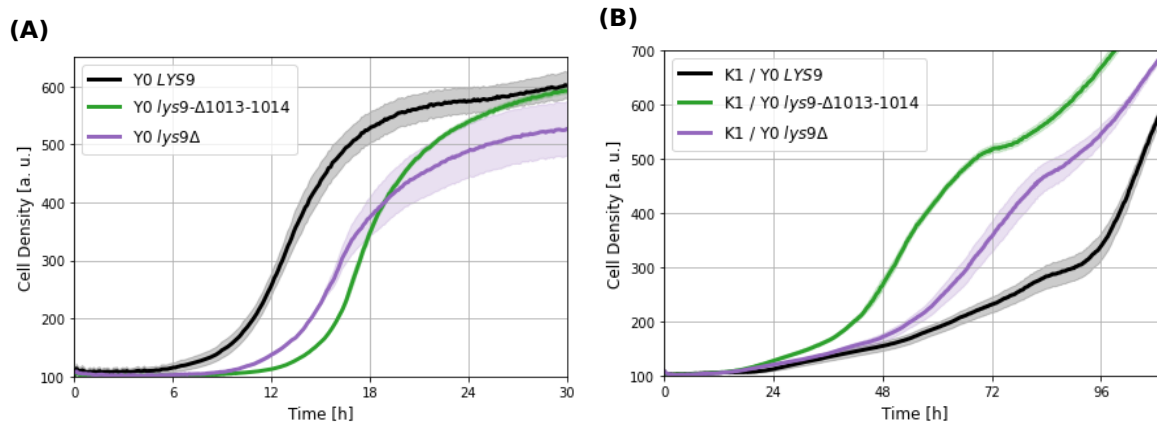
Figure 3.31: Role of *LYS9* on strain development. The strains analysed are LBGY5 (Y0 *LYS9*), LBGY15 (Y0 *lys9-Δ1013-1014*) and LBGY90 (Y0 *lys9Δ*). **(A)** Fermentation of the analysed strains in SCD-tyr media. **(B)** Performance of analysed strains under co-culture fermentation using SCD-tyr-lys media. Lines and shaded areas represent means and standard error of measurements, respectively.

During the lysine biosynthesis pathway, the conversion of 2-oxoadipate into 2-aminoadipate is proposed to be performed by Aro8p, making this enzyme the sole link between the aromatic amino acid and lysine pathways (Karsten et al. 2011). In this sense, we wonder if *ARO8* could be regulated by inducing factors from the lysine biosynthesis pathway, such as the joint activity of Lys14p and ASA (Feller et al. 1999; Ramos et al. 1988). If so, these factors could play a role in the reversible transference of the amino group required to produce tyrosine, possibly producing affectations to this amino acid pool and eventually promoting co-culture growth.

To clarify this possibility, a new fermentation was devised using strains that carried the mutation *lys9-Δ(1013-1014)* in addition to full deletions on genes *LYS2* and *LYS14* (lysine biosynthesis pathway is presented in section 1.6), producing the strains LBGY61 and LBGY62, respectively.

It was theorised that deleting the genes codifying for the inducing factors Lys2p, which is an *α*-aminoadipate reductase in charge of ASA production, and Lys14p would remove the favourable effect of the *lys9-Δ(1013-1014)* mutation. However, results presented in figure 3.32 point in a different direction.

During single cultures, the deletions show to remove the growth constrain related to the *lys9-Δ(1013-1014)* mutation as expected (figure 3.32A), but also show to produce a growth improvement under co-culture conditions (figure 3.32B). If ASA and Lyp14p would induce Aro8p, deletion of *lys14* and *lys2* should down-regulate it, reverting any positive effect shown in figure 3.31. In contrast, the co-culture containing the mutation in *lys9* plus the individual deletions show a performance even better than when just

(A)   **(B)**
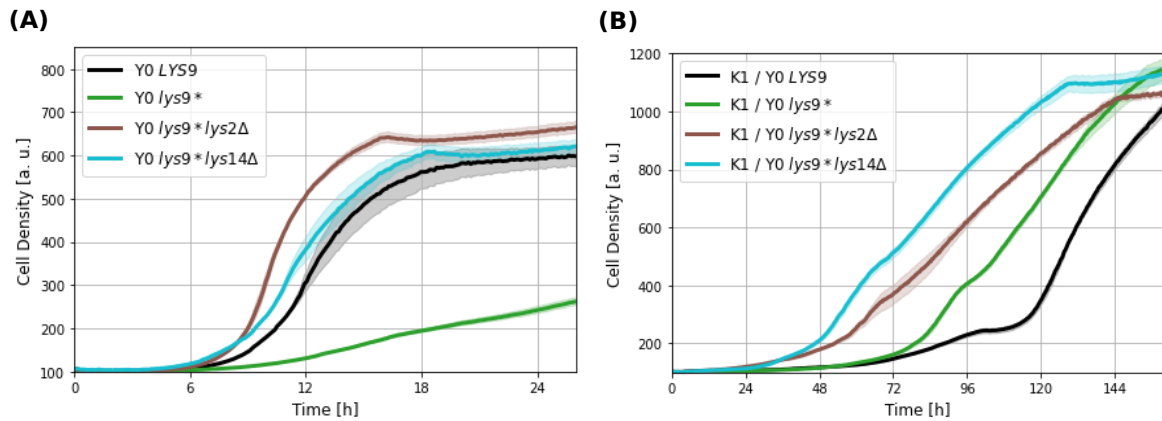
Figure 3.32: Deletion of *lys14* and *lys2* do not restore a Y0 phenotype in co-culture. *
indicates the *lys9-Δ(1013-1014)* mutation. Figures **(A)** and **(B)** present the growth per-
formance of strains during single and co-culture conditions, respectively. Single cultured
used SCD-tyr while co-culture employed SCD-tyr-lys media. Lines and shaded areas rep-
resent means and standard error of triplicate measurements, respectively.

exhibiting the mutation (figure 3.32B). This improved growth under single and co-culture
conditions could be explained by the reduced metabolic burden related to the expression
of enzymes upstream *lys9* position in the lysine biosynthesis pathway.

In order to test this theory, the strain LBGY63 was produced carrying a double deletion
for both homocitrate synthases in an LBGY15 (Y0 *lys9-Δ1013-1014*) background. Growth
patterns depicted in figure 3.33, suggest that the lack of the transcription inducer Lys14p
in an LGBY15 background produces a similar effect to the complete inactivation of the
pathway after removing its first step.

The growth pattern of these strains outperforms the parental and the wild-type strains in
both analysed scenarios. Results suggest that during the development of strains meant

(A)   **(B)**
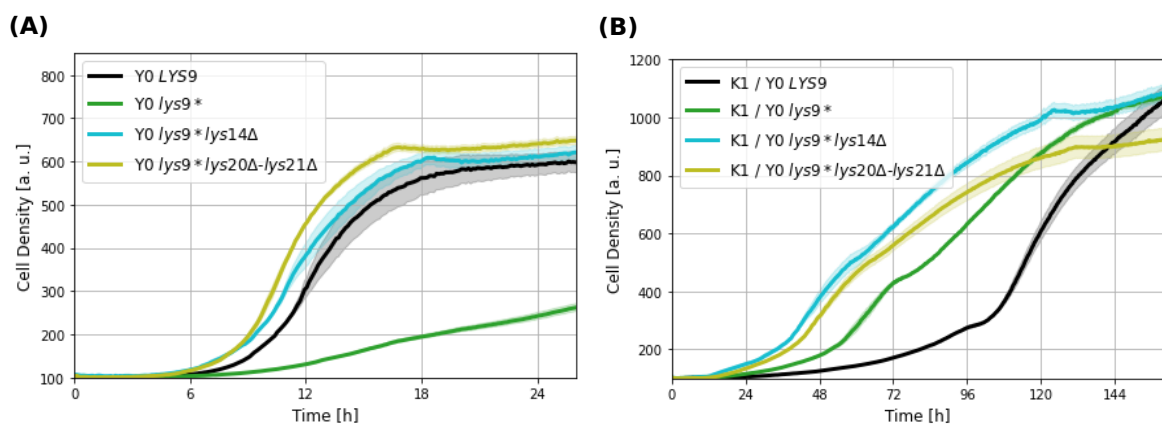
Figure 3.33: Reduced metabolic burden improves co-culture development. Deletion of
both homocitrate synthases, *lys20Δ* and *lys21Δ*, produce similar growth patterns than
when the transcription inducer Lys14p is deleted. * indicates the *lys9-Δ1013-1014* muta-
tion. **(A)** Strains growth under single fermentation using SCD-tyr media. **(B)** co-culture
development using SCD-tyr-lys media. Lines and shaded areas represent means and
standard error of triplicate measurements, respectively.

to be used in synthetic cooperative consortia, it is favourable to produce auxotrophies as early in the target pathway as possible, hence managing to reduce the metabolic burden due to protein synthesis and regulatory mechanisms, and consequently optimising single growth and consortia development.

As previously discussed, Lys9p catalyses the conversion of ASA into saccharophine, a molecule whose accumulation has been observed to produce toxic effects on mitochondria in *Caenorhabditis elegans* (J. Zhou et al. 2019). The missing Lys1p would produce such accumulation in the strain Y0, which could be prevented after disrupting the Lys9p activity. Such disruption could have been provided by the *lys9-Δ(1013-1014)* mutation. In this sense, the evolution process could have favoured a mechanism that prevents saccharopine accumulation in favour of ASA accumulation despite the increased metabolic burdens caused by the later panorama.

To confirm if saccharophine produced any toxic effect, a *LYS9* gene was cloned in a centromeric plasmid under a strong promoter, seeking a stable expression, higher than the one observed under a wild-type phenotype. The resulting plasmid LBGV119 and an empty control were transformed into Y0 *lys9Δ* and the strain Y0 *LYS9* backgrounds to test these strains under a single growth regimen.

Growth performances are displayed in figure 3.34.Even the strain displaying the wild type *LYS9* copy and the LBGV119 plasmid do not show any growth deficit. This suggests that even in a panorama with increased Lys9p activity, accumulation of saccharophine is not toxic for the cell.

In this sense, the reason why the mutation *lys9-Δ(1013-1014)* was selected during the
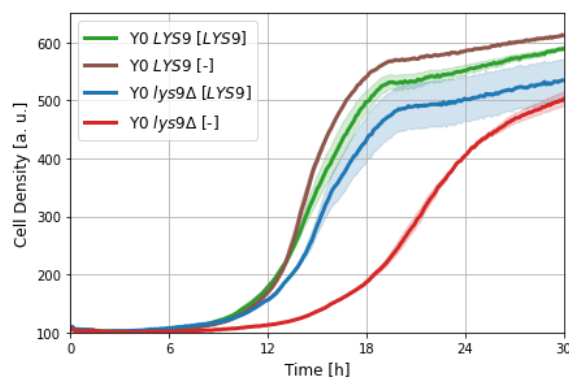
Figure 3.34: Effect of a centromeric *LYS9* expression under a lysine auxotrophic genotype for single strain fermentation. Plasmid expression of *LYS9* was evaluated in lysine auxotrophic strains with and without a wildtype copy of the *LYS9* gene while using SCD-tyr-ura media. Relevant genotypes are described in the figure legend. [-] represents the plasmid basal expression. Lines and shaded areas represent means and standard error of triplicate measurements, respectively.

evolution process, despite producing an ASA accumulation and a detrimental effect upon cell metabolism, cannot be described yet.

Secretion of ASA has been documented, suggesting that it can pass through the cell membrane, even though the secretion mechanisms are not understood (Borell et al. 1984; E. E. Jones & Broquist 1966; Ramos et al. 1988).

Media obtained from *lys9* strains could be assumed to contain ASA, based on literature findings, in which several groups perform studies on ASA present in media after *lys9*Δ genotypes (Borell et al. 1984; E. E. Jones & Broquist 1966; Ramos et al. 1988; Sagisaka & Shimura 1962).

Under this scenario, we wanted to establish if the culture supernatant from *lys9* strains could affect the growth of neighbouring cells. For this, a growth experiment using recycled media was performed. Media from strains Y0 *LYS9* and Y0 *lys9*Δ was collected after 72 h of growth, suspecting that the presence of a functional Lys9p would prevent the accumulation of ASA, intra and extracellularly. Both kinds of media were sterile filtrated and reconstituted with a 10x SMD+ura+lys solution in preparation for a new fermentation. This media was used to conduct a growth comparison between Y0 *LYS9* and Y0 *lys9*Δ.

Results are depicted in the figure 3.35, but show no apparent detrimental effect on growth no matter the media used. In any case, the media that presumably contains ASA produced a minor growth benefit compared to the normal media, which is the opposite effect of what was expected.

Across several experiments, the detrimental effects related to an abnormal *lys9* gene during single growth has been evidenced consistently (see figures 3.31A, 3.33A, 3.34), which makes the results from the recycled media experiment unexpected. From this data, it could be suggested that the amount of ASA secreted to the media does not meet the minimum concentration required to exert metabolic stress on the strains exposed to it or that its import mechanisms are not efficient enough.

Interestingly, this setup has failed to reproduce the previously observed growth defect between the strain Y0 and Y0 *lys9*Δ observed in figure 3.31A or 3.34. This suggests that the fermentation conditions or manipulation during the recycled media preparation could have impacted the usual growth behaviour of the strains. Different nutrient availability and media conditions could have impacted strain development, affecting the characteristic growth difference between Y0 and Y0 *lys9*Δ strains.

(A)

(B)

(C)
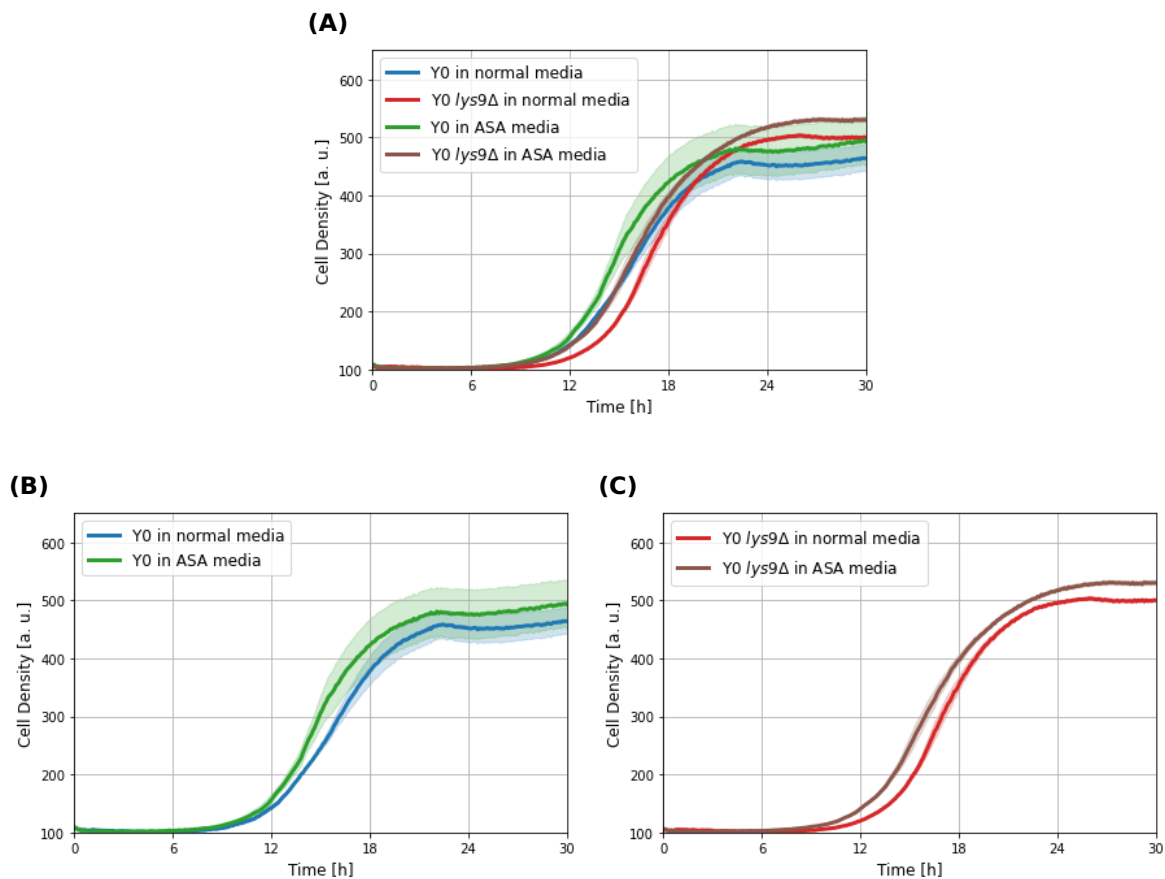
Figure 3.35: Use of recycled media to evaluate the impact of ASA on strains development. Growth of Y0 *LYS9* and Y0 *lys9Δ* strains was evaluated in recycled SCD-tyr media to determine the impact of ASA during development. Normal media refers to media recovered from Y0 a *LYS9* culture, which is suspected not to accumulate ASA due to its functional Lys9p. ASA media was recovered from a Y0 *lys9Δ* culture, expecting it to contain ASA due to the lack of Lys9p. **(A)** Growth performance of all strains. **(B)** Growth of Y0 under normal and ASA media. **(C)** Development a of Y0 *lys9Δ* strain under normal and ASA media. Lines and shaded areas represent means and standard error of triplicate measurements, respectively.

In summary, results suggest that the accumulation of ASA and not of saccharopine is responsible for the observed growth defect of lysine auxotrophic strains. In this sense, the *lys9-Δ(1013-1014)* mutation observed in the evolved strains, even though producing a clear growth defect in comparison with strains carrying a *LYS9* gene, has been positively selected after the evolution process.

If ASA can actually permeate out the cell membrane as suggested by several groups (Borell et al. 1984; Ramos et al. 1988), it could be possible that during a co-culture growth, secreted ASA gets captured by lysine-producing cells, which can readily transform this molecule into the exchange metabolite. All lysine-producer strains developed in this project exhibit a *LYS21*[fbr] variant, allowing an unregulated biosynthesis of this metabolite. This feature may be used by lysine auxotrophic strains with a *lys9* gene populations to outsource lysine production. With more lysine being produced, the co-culture

would grow more efficiently.

3.11.4   Different mutations in *WHI2*

As previously discussed, the TORC1 complex acts as a major regulator of cell metabolism, allowing it to adjust its metabolic functions to resource availability (Beck & Hall 1999; Loewith & Hall 2011). The most well-described pathway for TORC1 regulation is the SEACIT-Gtr1-Gtr2 complex; its active configuration (Gtr1^{GTP}–Gtr2^{GDP}) activates TORC1, allowing protein, lipids and nucleotides synthesis, effectively promoting cell growth. Inactivation of the SEACIT-Gtr1-Gtr2 complex occurs as a response to poor nutrient conditions, prompting an inactivation of TORC1, and leading to a repression of resources demanding processes (Loewith & Hall 2011; Panchaud et al. 2013a).

Nevertheless, the regulatory role of TORC1 has been demonstrated not to depend solely on the SEACIT-Gtr1-Gtr2 gate. Teng et al. 2018, and Teng and Hardwick 2019 described that Whi2p also regulates TORC1 activity independently of the SEACIT-Gtr1-Gtr2 complex, responding to low amino acids, particularly low leucine conditions.

Considering the critical role of *WHI2* in controlling replication under poor nutrient conditions, detecting variation in this gene in strain Y2 and all the evolved lysine producers was interesting. Evolved lysine producers obtained during the first evolution revealed a 535G>T mutation, replacing a glutamic acid with a stop codon, shortening the protein from 487 to 187 residues. The strain Y2 obtained after the second evolution round shows a thymidine deletion at position 227, producing a frameshift that renders a stop codon at position 85. Both detected mutations shorten the protein to less than half its natural extension, suggesting a null or decreased functionality, consequently favouring development under poor media conditions.

A phenotype analysis around the role of Whi2p on single and co-culture development was conducted, for which new strains were developed reverting the observed mutation in the evolved strains and producing full deletions into their parental versions.

A full *whi2* deletion was performed on the strains Y1.2 and K0, producing the strains LBGY51 and LBGY52, respectively. Additionally, the observed mutations on *whi2* gene were reverted for the strains K1 and Y2 using a CRISPR/Cas9 assisted strategy generating the strains LBGY53 and LBGY54, respectively. The newly generated strains were analysed in single and co-culture fermentations using SCD-tyr media to assess the impact of these mutations on the strain's performance.

(A)

(B)
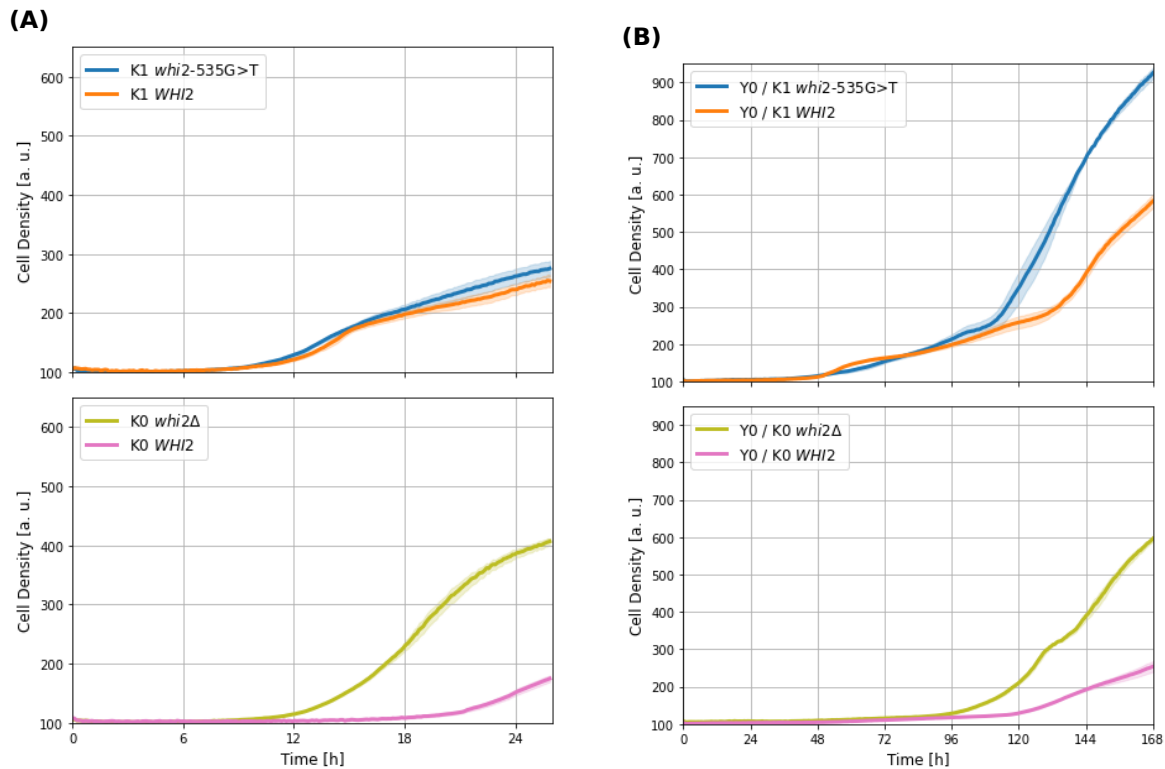
Figure 3.36: Analysis of *WHI2* role on lysine producer strains during single and co-culture conditions. Comparison of mutant versus wildtype versions of *WHI2* in lysine producer strains. Relevant genotypes are described in the figure legends. Panel **(A)** depicts single culture experiments employing SCD-lys media and are depicted on the left panel. Panel **(B)** displays co-culture experiments employing SCD-tyr-lys and are presented on panels at the right. The strain Y0 was employed as lysine donor. Lines and shaded areas represent means and standard error of triplicate measurements, respectively.

It was desirable that co-culture analysis conducted around variations on *WHI2* would present just one gene variation at a time. For this reason, experiments requiring a lysine donor to complement the co-cultures used the unevolved parental strain K0 instead of K1, which has been used to analyse other mutations on tyrosine donor strains. In this sense, to maintain uniformity between the experiments, when a tyrosine producer strain was needed to complement the co-culture, a Y0 strain was used. The performance tests conducted on *WHI2* gene were conducted using triplicates.

A comparison of the newly developed strains was performed grouping them according to the strain in which the mutation was spotted. For instance, the strain K1 that displays the *whi2*-535G>T mutation was compared with its K1 counterpart with the *WHI2* gene reverse-engineered to its wild type sequence. Consequently, K1 parental strain K0, which presents a wildtype *WHI2*, was compared with its K0 version with a *whi2*Δ. The same comparison setting was employed for the tyrosine producer strains Y2 and its parental version Y1.2.
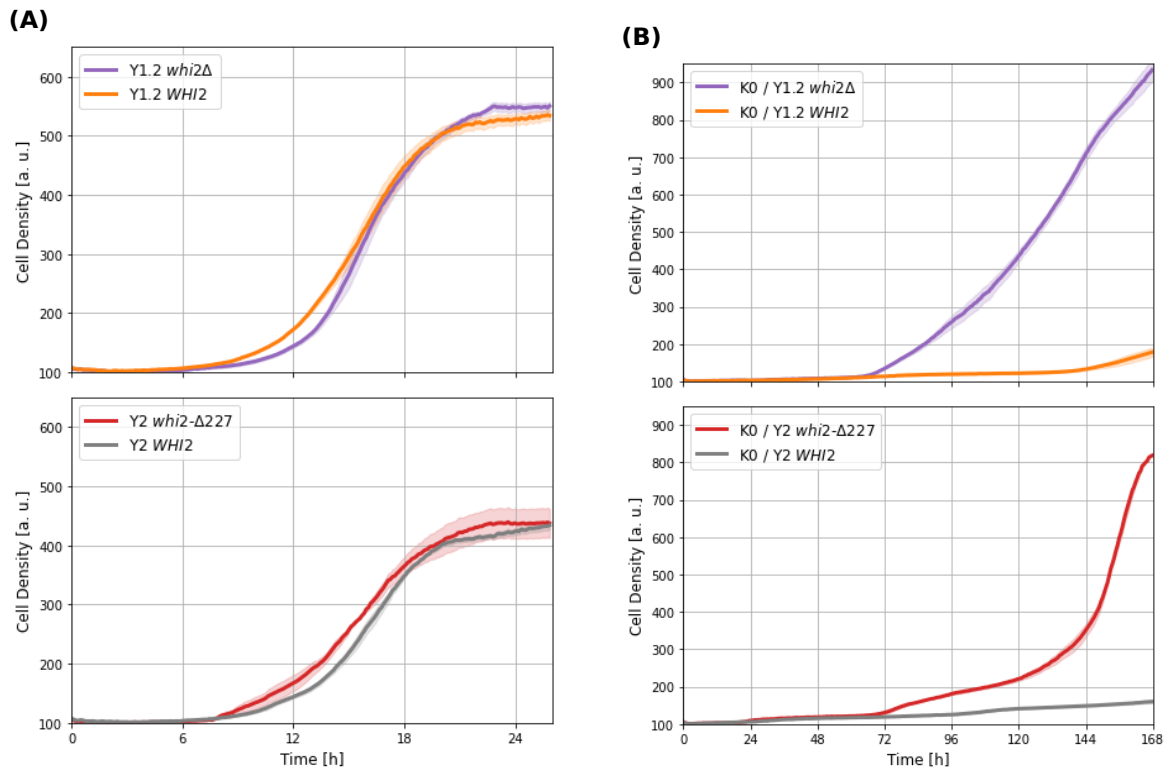
Figure 3.37: Role of *WHI2* on tyrosine producer strains using SCD-tyr media during single and co-culture conditions. Analysis of mutant and wildtype versions of *WHI2* gene on tyrosine producer strains. All relevant genotypes are presented in the figure legends. Panel **(A)** depicts single-strain fermentation using SCD-tyr media. Panel **(B)** displays co-culture comparisons using SCD-tyr-lys. As tyrosine donor, the strain Y0 was employed. Lines and shaded areas represent means and standard error of triplicate measurements, respectively.

Analysis of the mutation *whi2*-535G>T presented in figure 3.36, suggest that this variation does not confer a direct growth advantage under single growth when compared to a wild type version of the gene. On the other hand, deletion of this gene in a K0 background does produce a clear performance improvement under single and co-culture conditions (see figure 3.36A).

Growth improvement for the mutation *whi2*-535G>T can be appreciated in a later stage of development, which differs from the boosting effect related to other mutations in previous experiments such as the ones performed around *LYS9* in figures 3.33B or 3.32B. As it does for the single growth experiment, a full deletion of the mutation *WHI2* also produce a growth-boosting effect during co-culture cultivations (see figure 3.36B).

Analysis of the variation *whi2*-Δ227, observed in the tyrosine producer strain Y2, suggests that *WHI2* does not confer any advantage for growth under single strain conditions. Still, a non-functional *whi2* has a positive impact on consortia development (see figure 3.37).

115
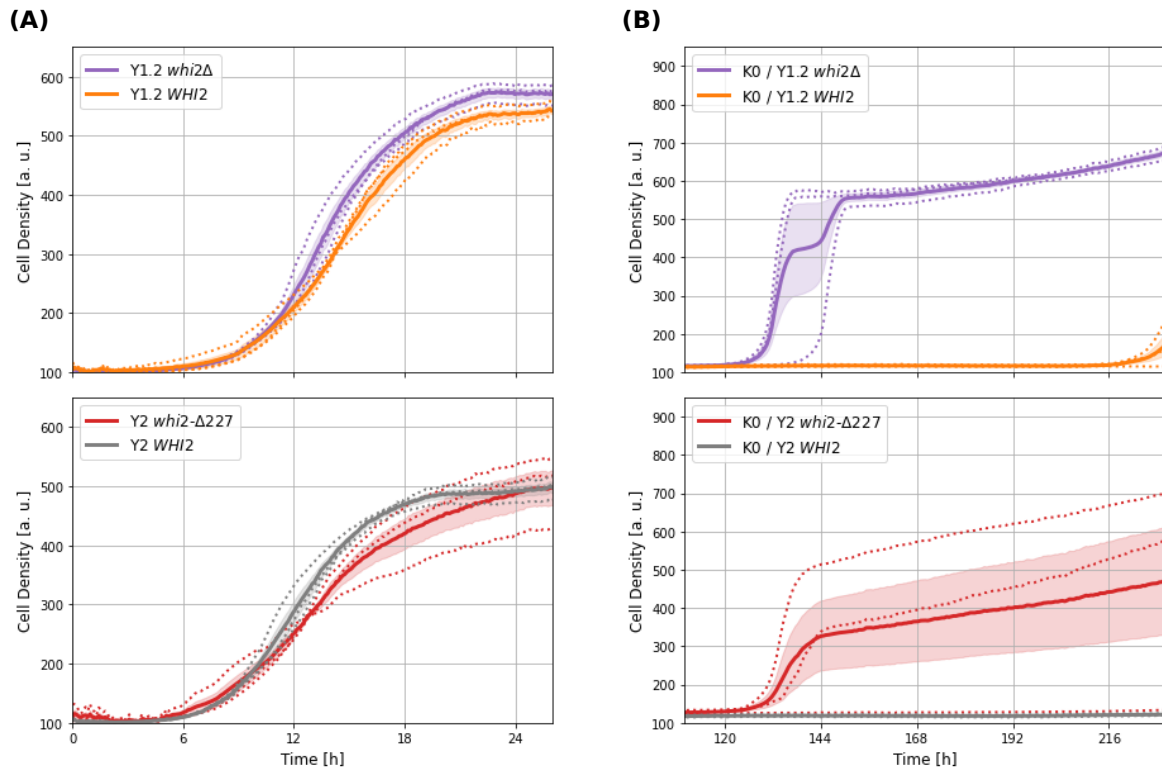
Figure 3.38: Impact of variations on *WHI2* in tyrosine producer strains while using SMD media. Comparison of mutant and wildtype versions of *WHI2* on tyrosine producer strains while using SMD media Figure legends describe all the relevant genotypes used. Panel **(A)** depicts single-strain fermentations while using SMD media supplemented with lysine and uracil for the strain auxotrophies. Panel **(B)** displays co-culture comparisons using SMD media supplemented with uracil. As tyrosine donor, the strain Y0 was employed. Strong lines and shaded areas represent means and standard error of triplicate measurements, respectively. Dotted lines represent individual experiments values according to the colour code described in the figure's legend.

However, as previously discussed in section 3.6.2, the second evolution experiment used SMD+ura media to stress the production and secretion of metabolites, a process that generated the strain Y2 with the mutation *whi2-Δ227*. In this sense, a second experiment was conducted around the mutation obtained in the strain Y2 *whi2-Δ227*, using SMD+ura for the single growth and co-culture experiments.

The results in figure 3.38 again indicate that a non-functional *whi2* offers no advantage for growth under single strain conditions but is favourable for growth under co-culture conditions. The magnitude of the stringent conditions imposed by the minimum media can be observed in the time required for the co-culture to develop. The co-cultures employing a deficient *whi2* showed growth after 120 h of fermentation. Interestingly, the variation between replicas was particularly high under SMD+ura media, i.e. one of the replicas for the role of a *whi2Δ* grew 12 h later than the remaining flasks, and another replica from the analysis of the mutation *whi2-Δ227* did not show any growth during the experiment.

Results suggest that the settings applied during these experiments stress the system close to its limits, producing a considerable variation and even replicas that fail to grow. However, consistently showing that a deficient *whi2* is crucial for the development of co-cultures.

It is particularly interesting that both populations (K and Y donors) developed mutations compromising the function of *WHI2* independently. Considering that the mutation *whi2*-535G>T detected on the K1 strains was generated in a tyrosine auxotrophic strain growing in an SCD-lys-tyr media, it could be argued that either or both of these amino acids are involved in the negative regulatory effect of Whi2p upon TORC1 complex. This possibility implies that a low amount of these amino acids and not just leucine could be involved in the negative regulatory effects that Whi2p exerts over the TORC1 system (Teng & Hardwick 2019; Teng et al. 2018).

Chapter: 4 Discussion

A wider application of microorganisms for industrial processes, especially when foreign metabolic pathways are needed, is constrained by the understanding of the enzymatic steps involved, the required substrates, and optimal environmental conditions for them to perform (S. Y. Lee & Kim 2015; Wu et al. 2016). Among the attempts to address these limitations, the compartmentalisation of steps in different strains has been explored with mixed results (Darvishi et al. 2022; Lyu et al. 2019; Shin et al. 2010), evidencing an insufficient understanding behind the design of stable consortia (Fedorec et al. 2021; Lindemann et al. 2016; Shou et al. 2007).

This project attempts to contribute to this gap of knowledge. By developing a syntrophic consortium around the exchange of two amino acids and submitting them to evolutionary rounds, we aimed to provide information on how to improve the construction of this sort of co-culture and possibly on how to improve the production of aromatic amino acid compounds by naturally occurring mutations during evolution. Although the evolved strains isolated demonstrated an increased ability to promote consortium growth and improved titers of pPET, a tyrosine-derived metabolite, no specific mutation directly related to increased production could be identified. Nevertheless, the analysis of some of the identified mutations allowed us to understand better the stress processes suffered during evolution and how these variations allowed the strains to better cope with selection pressures. The generated information could be helpful for the future design of synthetic consortia.

The present chapter aims to discuss the newly generated information in the context of available literature and speculate on further theories to better understand the design and use of microbial consortia.

4.1 Consortia

A synthetic cooperative consortium was developed using lysine and tyrosine as exchange molecules in *S. cerevisiae* as a model organism. This section covers relevant aspects of consortia's formation, development, and evolution.

4.1.1 Importance of overproducing variants for consortia development

Although the deletions of *LYS1* and *TYR1* successfully rendered strains auxotrophic for lysine and tyrosine, respectively, combinations of these strains failed to show any growth (data not shown), suggesting the need for overproducing mechanisms to compensate for the partner's auxotrophies (M. J. I. Müller et al. 2014; Shou et al. 2007). In this sense, the successful consortia development observed in this project suggested that the selected overproducing variants for lysine (*LYS21*^{Q366R} from Feller et al. 1999), and tyrosine (*ARO3*^{K222L} from Hartmann et al. 2003 and *ARO4*^{K229L} *from Brückner et al. 2018*) were efficient enough for complementing the system's engineered auxotrophies, under the cell density conditions employed.

Interestingly, Campbell et al. 2015 proposed that yeasts can naturally develop complex cooperating communities, capable of exchanging metabolites in sufficient amounts to complement auxotrophies and promote colony growth in a manner similar to fully prototrophic strains. By using LC-MS/MS, the authors could quantify intra- and extracellular metabolites in the colonies at pmol levels, which was sufficient to sustain colony growth at a rate similar to that of a wild-type strain colony.

The methodology employed by Campbell et al. 2015 for amino acid determination prevents the establishment of comparisons between their titers and those obtained in this project. Nevertheless, it is interesting that their complementation findings were reached using solid media, which established reduced and stable distances between cells.

The use of a solid scaffold system has been described to favour the development of consortia and to favour altruistic behaviours inside the colonies, promoting cooperation rather than defection (Lindsay et al. 2018) (see sections 1.2.2 and 4.1.6). Additionally, the consecutive culture and dilution protocol applied by Campbell et al. 2015 to promote plasmid segregation could well be understood as an adaptive laboratory evolution process, which, considering the advantageous effects on solid media usage for cooperative behaviour (Stump et al. 2018), could have favoured over-representation of evolved cooperators, offering more light into their interesting results.

In this sense, the complementation failure observed while using strains without feedback-resistant variants (*ARO3*^{K222L} and *ARO4*^{K229L} for tyrosine and *LYS21*^{Q366R} for lysine production) could well be attributed to the culture system employed, highlighting the importance of overproducing variants for co-culture success in liquid media.

4.1.2 Evolution produces CNV

The results obtained in this study define "evolution" as a crucial factor for successful co-culture development, as it promotes mechanisms to cope with the stress conditions suffered by the strains. After the first round of evolution, all the tyrosine producer strains analysed (figure 3.6), and most of the lysine producers (figure 3.7) promoted faster consortia development.

Data obtained from genome sequencing of the most relevant evolved strains revealed that all presented signs of chromosomal duplication events at several points in their genomes (see section 3.8). Chromosomal duplication events are frequently reported during evolutionary processes in response to selective pressure, producing modifications that are beneficial under the imposed constraint conditions; however, they are lost after the selection pressure is removed (Gresham et al. 2008, 2010; Thierry et al. 2015, 2021).

It is noteworthy that the evolved strain isolation protocol applied after the first evolution (refer to section 2.9) involved subsequent inoculations of a sample obtained from liquid cultures onto SCD-lys-tyr plates, with the expectation that cooperative phenotypes would complement each other, resulting in fast-growing colonies. This approach was intended as a screening system for identifying efficient metabolite producers. However, it also imposed additional stress on the evolved strains by forcing them to grow in solid media.

As previously discussed, consortia growth in solid media tends to favour altruistic behaviour and the presence of cooperator strains (Lindsay et al. 2018; Stump et al. 2018), meaning pressure for developing favourable variations or promote selection of strains that already posses such desirable features.

In this line of thought, it was theorised that the observed chromosomal duplications could be a product of the particular stress on solid media culture. The lack of signals for duplicated chromosomal segments in the strain Y2 helps to sustain this theory, as it was the product of a selection based on dominant markers instead of on consortia complementing properties as during the isolation of the strains obtained after the first evolution.

Establishing the frequency of copy number variation events during yeast evolution is recognised as a technically challenging task (Gresham et al. 2010). Some calculations have labelled these events as rare, placing their occurrence in the order of 10^{-10} events per generation (Dorsey et al. 1992). However, it is recognised that sections of repetitive

DNA, paralogues, tRNA genes or transposons help to increase these low-frequency rates, allowing fast chromosomal recombination or even formation of extrachromosomal bodies (Jordan & McDonald 1999; Putnam et al. 2005; Vitte & Panaud 2005) that could offer performance advantages under selective scenarios (Gresham et al. 2010).

In this way, it seems possible that selection based on consortia complementing properties would favour the presence of improved cooperator strains, which might exhibit chromosomal abnormalities as part of their advantageous modifications.

The initial scope of this project prevented further study into the nature of these chromosomal abnormalities. Due to the short reads employed by the Illumina sequencing methodology for sequencing the evolved strains, extrachromosomal DNA would be invisible during an alignment process. However, techniques such as Pulse field gel electrophoresis (PFGE) would have proved helpful in validating the existence of chromosomal arrangements as independent bodies or as structures fused to existing chromosomes (Dorsey et al. 1992; Koszul et al. 2004).

4.1.3   Duplicated fragment of chromosome XIV

As discussed in section 3.9.1, after discarding the role of the selection marker employed and the occurrence of mutations during the short development time of strain Y1.2, the only difference between it and strain Y1 is the loss of the duplication on chromosome XIV.

Strain Y1.2 displays better growth under single culture conditions (see figure 3.10A), while a worse performance under co-culture conditions (see figures 3.10B and 3.13), in this sense mimicking patterns observed for Y0 strain.

After describing partial chromosomal alterations, gene analysis frequently reveals candidate targets whose duplications may play a role in the observed phenotypes. For instance, an *ace2* mutation in a fully duplicated genome was reported to be sufficient to promote *S. cerevisiae* sedimentation during a study whose design unintendedly favoured fast-sedimenting cells (Oud et al. 2013). In addition, yeast evolution in a nitrogen-limited media produced a section excision from chromosome XI, which was maintained as an extrachromosomal self-replicating body, allowing the presence of multiple copies of the general amino acid permease *GAP1*, proving to be advantageous for the employed culture conditions (Gresham et al. 2010).

Nevertheless, the analysis conducted for the duplicated area in chromosome XIV, com-

mon for all tyrosine-producing strains presenting a favourable co-culture performance (see section 3.9.1), displayed no obvious mutated candidates that could play a role in the observed phenotype. However, this chromosome section includes the *LYP1* gene, regarded as the most relevant lysine transporter in yeast (Bianchi et al. 2016; Sychrova & Chevallier 1993). Increased gene expression could benefit lysine auxotrophic strains, especially if a stabilisation mechanism for this transporter is present, such as the discovered non-functional Art2p previously described (see section 3.11.2).

This scenario predicts that multiple copies of lysine transporters under a deficient Art2p regulation would result in faster development of lysine auxotrophic strains, as it will be more efficient during the uptake process. Nevertheless, figure 3.10A presents a scenario in which strain Y1.2 grows notably better than strain Y1 under single fermentation, opposing this theory, as strain Y1.2 would not exhibit an extra copy of *LYP1*.

Another interesting presence in this section of chromosome XIV is the *AQR1* gene, which has been related to the secretion of homoserine and threonine under high cytosolic concentration scenarios. (Velasco et al. 2004). Additionally, overexpression of *AQR1* has been observed to favour the secretion of amino acids such as aspartate, glutamate and alanine when there is no any overproducing mechanism for these molecules. Consequently, a duplication at chromosome XIV on the evolved strain Y1 would mean an additional copy of *AQR1*, which together with the feedback-resistant variants it possesses, could increase the secretion of aromatic amino acids. This could explain the improved growth observed under consortia conditions.

However, direct tyrosine determination failed to evidence such improvement (see figure 3.23A). It is unlikely that the inability to detect tyrosine derives from a failure to build up intracellular titers as a result of constant degradation into the Ehrlich pathway to produce pPET, as titers obtained from the strain Y1.2 are higher than for Y1, even when the strain Y1.2 lacks the duplication in chromosome XIV. These results suggest that an extra copy of *AQR1* might not by itself play a paramount role during the secretion of tyrosine and the improved growth under consortia conditions.

The extension of the common section of chromosome XIV that is duplicated for all the evolved tyrosine-producer strains covers its first 509,000 nucleotides, a size that is not uncommon for partial chromosomal duplication events in *S. cerevisiae* which seems to be at least in part delimited to the availability of Ty elements (Gresham et al. 2008; Koszul et al. 2004; Thierry et al. 2021). In this sense, it is not possible to narrow down the vital components inside this possible extrachromosomal DNA based on the genes it

contains, particularly if potential epistatic roles are considered (Snitkin & Segrè 2011).

Loss of gene duplications conferring a dosage compensatory effect has been observed to occur relatively quickly, requiring as few as 25 replication events after removing the selective pressure (Naseeb et al. 2017). Therefore, it seems interesting that strains obtained after the first evolution maintained their extrachromosomal DNA after being grown several times on YPD agar during the isolation process prior to their whole-genome sequencing analysis (see section 2.9). However, the homologous recombination event performed during the selection marker replacement seems to have been sufficient to overcome the apparent stability demonstrated by the extrachromosomal DNA in Y1. It is also possible that this event was the product of the random selection of a colony after the dominant marker switch.

Regarding consortia fitness, strain Y2 performed better than strain Y1.2, a feature that apparently does not rely on chromosomal DNA. However, strain Y2 developed a *whi2* variant that was demonstrated to be advantageous under co-culture conditions. This concept is evaluated in figure 3.37 where a non-functional *whi2* demonstrates to be of great importance for co-culture development.

The results from this project suggest that the generation of extrachromosomal bodies as a product of adaptive laboratory evolution processes is highly relevant to the observed phenotypes. The cost–benefit constraints established by a higher protein expression derived from a gene duplication event might represent an immediate advantage under specific stress conditions but represent a burden and will be selected out when the dosage effect conferred by them is no longer beneficial (Ames et al. 2010; Conant & Wolfe 2007; Papp et al. 2003). In this sense, the duplicated fragment reported for chromosome XIV seems to confer a better cooperative phenotype for evolved strains but at the expense of a compromised fitness under single fermentation. Such a phenotype seems unrelated to any mutation or the direct effect of genes comprised in the duplicated fragment but to epistatic interactions unidentified in the present work.

It is remarkable that such beneficial effects for co-culture development, produced at the expense of fitness for single populations, were still positively selected during evolution. This suggests that the feature was developed and sustained for improved consortium fitness, projecting that a benefit for a second population outweighs an extra metabolic burden on the expectation of the benefits further provided by the second population.

4.1.4   Role of cell density for consortia development

This project showed that consortia survival depends additionally on the minimum cell density to sustain growth, as presented in section 3.9.3. Previously, Shou et al. 2007 had described a cell density range that would allow consortia survival, additionally proposing as the key moment for a co-culture development the time required for the cells to enter the death phase as they initiated the nutrient secretion process.

Results from this work complement Shou et al. findings, proposing that consortia survival benefits on a high cell density regardless of overproducing genotypes on either conforming strain (see figures 3.16 and 3.17). The decay time discussed in section 3.9.3 describes the moment at which cells from either population enter the death phase, fueling the growth of surviving cells. This initial nutrient boost is a milestone that prompts co-culture development in both studies, suggesting a release of nutrients that allows the consortium to reach high cell density titers. Such effect is better observed in figure 3.17, where the addition of a strain unable to grow due to a disruption in its glycolysis pathway prompts an early development.

An analysis of figure 3.16 under this premise would explain the rapid growth observed for consortia using high parasitic strain titers, as higher biomass would mean higher nutrients realised at a time, resources that in this experiment are used by consortia, and the parasitic strain alike. Nevertheless, the apparent growth displayed by controls without a lysine producer strain, depicted in both panels of figure 3.16 in brown colour, suggests that nutrients released need to reach a specific concentration before triggering growth, a milestone that is reached at around 120 h.

4.1.5   Consortia survival despite cheater fraction

Successful survival of cooperative consortia depends on the efficient exchange of nutrients, involving the production and secretion of goods that are freely available to any cell in the culture. While the benefit of the availability of such goods is shared by all cells in the culture, the cost of its production resides in single producer cells. This particular scenario represents a controversial topic in evolutionary biology, as it would suggest that by avoiding the production costs, a "cheater" cell can become fitter than cooperating partners while benefiting from common goods available and ultimately compromising the system survival (Konstantinidis et al. 2021; Lindsay et al. 2018; Sanchez et al. 2013; Shou et al. 2007; Stump et al. 2018). Dilemma commonly referred to as "tragedy of the commons" (Hardin 1968; MacLean & Gudelj 2006; West et al. 2007).

When consortia are developed using spatially structured environments, cooperator populations seem to be favoured over cheater factions, as biomass growth tilts in the direction where cooperator cells are present, allowing for the co-culture flourishment (Konstantinidis et al. 2021; Lindsay et al. 2018; Momeni et al. 2013; Stump et al. 2018). While this principle helps to explain the evolution and thriving of microbial consortia in nature, such as microalgae, bacteria interaction (Cooper & Smith 2015) and even far more complex systems such as the human microbiome (Coyte & Rakoff-Nahoum 2019), it cannot be extended to well-mixed environments such as the one employed in this project.

A well-mixed environment for cooperative consortia represents a perfect example of the tragedy of the commons dilemma as common goods produced are expected to be distributed uniformly, making the system vulnerable to cheaters overcome, especially if they are fitter than the cooperating partners (Harrison & Buckling 2005; Shou et al. 2007; Waite & Shou 2012). Such an event is expected to represent the failure of the cooperative system.

The successful completion of the multiple passages to which the consortia developed in this project were submitted, suggests that evolution favoured consortia over individual fitness, as the overrepresentation of cheaters would have produced the failure of co-culture growth. This outcome contradicts what would be expected in a "tragedy of the commons" dilemma.

It is noteworthy that the strains isolation process used after the first evolution round employed a spatial structure environment, as samples from evolved cultures were plated on agar media depleted of lysine and tyrosine, forcing consortia cooperation (see section 3.5.1). In this context, it is possible that the selection process would have played a role during the strains representation, favouring cooperators rather than cheater populations. However, the successful growth of the consortia during ten passages in liquid media suggests that cooperation did play a role in culture survival and that cooperation, even at the expense of individual fitness, was positively selected as a desirable feature, opposing the expected result under a "tragedy of the commons" dilemma.

The results from this project share resemblances with the findings of Waite and Shou 2012, who studied the development of synthetic cooperative consortia employing lysine and adenine as exchange metabolites in a well-mixed environment. They described that after introducing an engineered cheater strain into the cooperative consortia, five out of twelve replicas failed to grow, showing an overrepresentation of death or cheater cells, in contrast with the consortia that grew. It is proposed that the evolution of syntrophic

consortia in well-mixed environments creates an "adaptive race", in which cooperators, as well as cheaters parties, will compete for faster development of features that would allow them to thrive under the established stress conditions (Waite & Shou 2012).

The setup employed by Waite and Shou resembles the second evolution performed in this project, in which two cooperative strains were mixed with an artificial cheater. No culture presented signs of being overcome by a cheater faction in this project, but this could be due to the high cell density employed in contrast with concentrations used by Waite and Shou, who used a ratio of 1:1:1 with an OD_{600} of 0.1 per strain. High cell density would present better chances for favourable mutations to occur in the cooperative cell fraction, increasing the chance of consortia survival.

A genetic analysis of Waite and Shou's lysine auxotrophic cells, of cooperative and cheater nature, revealed mutations affecting the lysine uptake regulatory system, punctually in the genes *ART2*, *DOA4*, and *RSP5*. These mutations would positively affect lysine transport under low-concentration conditions by disrupting ubiquitin regulation of Lyp1p (Waite & Shou 2012).

Strikingly, lysine auxotrophic cells obtained after the first round of evolution in this project also showed a mutation in *ART2*, which stabilised the transporter under low lysine conditions, allowing a positive effect under single and co-culture conditions (see figure 3.29). These results correlate with previous findings positioning Art2p as a key regulatory player of Lyp1p under low lysine conditions (Ivashov et al. 2020; Lin et al. 2008; Waite & Shou 2012).

Analysis of the strains K1 and Y2, produced after the first and second evolution process, identified additional dysfunction mutations in the gene *WHI2*, rendering proteins with decreased or null activity. According to the analysis presented in figures 3.36, 3.37 and 3.38, a nonfunctional *whi2* does not affect fitness during single culture, but represent a clear advantage to achieve fast co-culture development. Whi2p has been described to play a regulatory role in TORC1 as a response to low amino acid conditions, particularly leucine, leading to autophagy or eventual quiescence (X. Chen et al. 2018; Teng & Hardwick 2019). However, results from this work would suggest that besides the described role of leucine on Whi2p over TORC1 regulation, either lysine, tyrosine, or both amino acids might also play a role in its modulation (see section 3.11.4 and 4.2.2). Consequently, it explains why mutations rendering early stop codons for the same gene were developed and selected in independent manners by lysine and tyrosine auxotrophic strains.

In this way, it is proposed that cooperative consortia address the "tragedy of the commons" dilemma by an "adaptive race" strategy, favouring mutations that represent advantages over stress conditions such as the ones found in *ART2* and *WHI2*, which would allow improved stability of lysine transport as well as prompt cell replication under limited nutrient conditions (Waite & Shou 2012). However, this line of reasoning does not seem to explain the selection of the mutation found in *LYS9*, as despite providing growth benefits for co-culture development, it seems to produce an apparent detrimental effect on a single culture (see figure 3.31). This effect can be appreciated even with a *LYS9* full deletion but to a lesser degree than when the mutation is present, suggesting that it is not due to a residual or altered function of native Lys9p.

Lys9p catalyses the transformation of ASA and free L-glutamate into saccharophine, consuming one molecule of NAPDH per reaction (E. E. Jones & Broquist 1966). In this sense, a loss of activity would imply that a NAPDH molecule is not being consumed and would be added to the cell pool, which can be used in plenty of roles (Minard & McAlister-Henn 2005). Cytoplasmic lysine exerts a feedback regulatory effect over its biosynthesis pathway (Feller et al. 1994, 1999); therefore, it is expected that this pathway would not be downregulated under the low-lysine conditions experienced by lysine auxotrophic strains growing in a co-culture regimen. Nevertheless, this lack of regulation is not expected to contribute in a relevant manner to the cell NADPH pool (Minard & McAlister-Henn 2005).

ASA degradation has been described to occur only via Lys9p conversion into saccharopine. In contrast, saccharopine can also be degraded by Cis2p during the glutathione-degrading process besides being converted into lysine by Lyp1p (Kumar et al. 2003; Ubiyvovk et al. 2006). This limitation suggests that a *lys9* genotype results either in ASA accumulation or secretion. Such accumulation is suspected to be the reason for the reduced fitness observed in cells lacking proper Lys9p function (see figures 3.31 and 3.34). In this manner, selecting a *lys9* genotype that results in a fitness cost for the cells makes no sense for natural selection processes unless an unidentified benefit derives from it.

ASA has been shown to permeate across the cell membrane (Borell et al. 1984; Ramos et al. 1988), allowing us to speculate about its traffic to neighbouring cells. If secreted ASA reaches and is processed by lysine-overproducer cells, it would benefit the ASA producer by converting it to lysine. Such a process would mean a higher lysine production than what would be possible by the normal 2-oxoglutarate availability in the overproducer strain. This hypothesis would explain the unusual results observed for the *lys9* genotype, showing improved consortia growth as more lysine would be available in the media.

However, it would be detrimental for single growth as cells and media would experiment with ASA accumulation.

However, the actual evolved consortia probably consisted of multiple additional geno-types, in which it is expected that strains with functional *LYS9* would still be present, especially when considering that they are fitter than the *lys9* variants. Under this panorama, coexisting *LYS9* strains will degrade the available ASA, compromising the system's net lysine production but possibly also playing a protective role against ASA accumulation and its detrimental effects on *lys9* cells. An example of a similar effect has been described previously by Lilja and Johnson, who described that microbial communi-ties can cooperate for faster consumption of toxic intermediates during the degradation of complex substrates (Lilja & Johnson 2016). However, the results in figure 3.31B would argue against the toxic effect of ASA accumulation during co-culture fermentation that included a lysine-producing strain, as the system seems to be efficient enough to con-sume ASA produced by the *lys9* strains.

4.1.6   Quorum sensing role on consortia development

Quorum sensing molecules (QSM) are biochemical signals employed by microorganisms, including *S. cerevisiae*, allowing them to adapt to several environmental conditions such as nitrogen level, pH, oxygen availability, ethanol, and cell density (Jagtap et al. 2020). The Ehrlich pathway contributes to the generation of three of the most relevant QSMs through the catabolism of phenylalanine, tyrosine, and tryptophan, generating PET, pPET, and tryptohol, respectively (Hazelwood et al. 2008; Jagtap et al. 2020). These molecules play a crucial role during the morphological adaptation under low-nitrogen conditions, allowing a transition between mycelium or filamentous and yeast growth forms (H. Chen & Fink 2006; Gimeno et al. 1992; Padder et al. 2018). This phenotype has been described as a scavenging strategy that allows populations to respond to low nitrogen levels and high cell densities, seeking to reach better-supplied areas (Jagtap et al. 2020).

Genetic engineering processes, as well as adaptive laboratory evolution rounds, have been shown to produce strains with increased pPET production titers (see figures 3.9B and 3.23B), which is one of the three QSMs mentioned above. This molecule is described as the QSM with the lowest capacity to induce morphological changes in *S. cerevisiae* (H. Chen & Fink 2006; Christwardana et al. 2019), but the observed titers also suggest an increase in carbon flow into the aromatic amino acid pathway or higher activity in the enzymatic steps related to their production, that is, *ARO8*, *ARO9*, and *ARO10*. In

128

this way, it is possible to speculate that besides the detected pPET titers, there are also higher levels of PE and tryptohol which could play a role in the yeast adaptation to their environmental conditions.

The secretion of QSMs is described as a cell density-related process, first beginning with PET production at the early exponential phase and reaching its peak at the late exponential phase (Avbelj et al. 2015, 2016; Jagtap et al. 2020; Zupan et al. 2013). This process is closely followed by pPET and tryptohol secretion, both reaching their highest production peaks at the late exponential and stationary phases, respectively (see figure 4.1) (Avbelj et al. 2015, 2016; Iraqui et al. 1999; Wuster & Babu 2009; Zupan et al. 2013).

Nevertheless, the strain CEN.PK employed for the present project has been reported to lack some mechanisms for the induction of morphological adaptation, such as the genes *FLO1* and *FLO9* (Nijkamp et al. 2012; Westman et al. 2014). It also possesses a K1876M substitution in the adenylate cyclase Cyr1p, permanently repressing PKA activity and consequently repressing the promoter of *FLO11*. This gene is required for further morphological changes (Torbensen et al. 2012; Vanhalewyn et al. 1999). However, the regulatory mechanisms outside of these genes are still present.

For instance, expression of the genes of *ARO9* and *ARO10* is reported to be cell density-dependent, triggering the production mainly of PET and tryptohol, from which the latter promotes the expression of the transcription factor Aro80p, a positive regulator of the same genes (Avbelj et al. 2015, 2016; H. Chen & Fink 2006; Iraqui et al. 1998; Iraqui et al. 1999; Wuster & Babu 2009). This positive feedback loop would promote increased production of the QSMs derived from aromatic amino acids, including the tyrosine-derived pPET.

Nevertheless, the expression of the genes *ARO8*, *ARO9*, and *ARO10* has been reported to be repressed under high nitrogen conditions, a regulation that is released after a specific cell density has been reached, and nitrogen levels are depleted (Avbelj et al. 2016; H. Chen & Fink 2006; Zupan et al. 2013). Such ammonium sulphate limiting concentration has been described at 66.07 mg L^{-1}, significantly lower than the 5 g L^{-1} employed in the present project, suggesting that the expression of these genes should be repressed.

In agreement with these statements, pPET values described for the wild-type strain used as a control in figures 3.5 and 3.9 always show a marginal pPET mg/OD$_{600}$, suggesting that despite the high cell density values reached, production of higher alcohols through
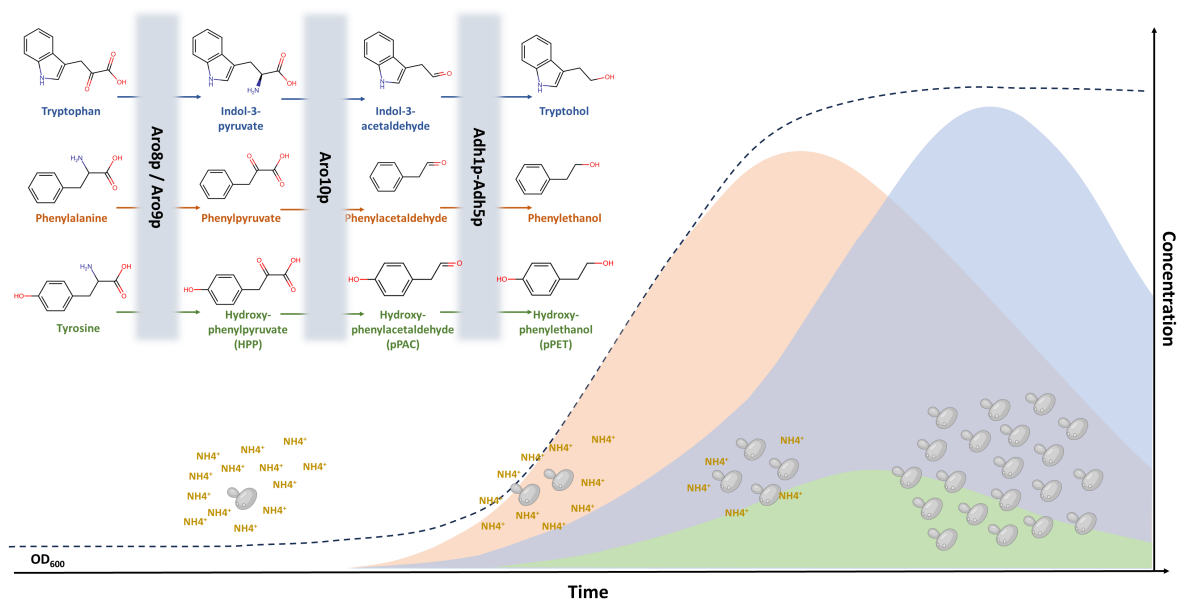
Figure 4.1: Production of QSMs during fermentation. Schematic representation of the conversion of aromatic amino acids into QSMs, proteins involved are described inside grey squares. Colour code represents each one of the QSMs and its relative concentration during fermentation. Ammonia levels (NH4$^+$) decrease through the fermentation as yeast OD$_{600}$ increases. Modified from Avbelj et al. 2016

the Ehrlich pathway is still repressed. Interestingly, the *ARO3^{fbr}* and *ARO4^{fbr}* variants integrated into the strain Y0 were sufficient to release this regulation as they already produced higher titers while using the same ammonium sulfate-rich media.

Considering that the mutations in tyrosine-producing strains identified in this project, such as *art2-Δ615* or *whi2-Δ227*, seem to provide a relative advantage for growth under stress conditions, it is possible that the increased pPET titers observed would be a product of the positive feedback loop created by a high cell density and the presence of tryptohol in the media.

This could also explain the shifting pPET titers observed in the evolved strains, as titers would not depend on specific production mechanisms affected by point mutations but on a more complex regulatory system relying on the gain of cell density, production of QSMs, and their interaction with cell transcription factors such as Aro80p. Even the mutation *lys9-Δ(1013-1014)* would be beneficial for high pPET titers, as it has been demonstrated to promote consortia development, which would consequently induce higher QSMs production titers.

In this sense, aromatic alcohols act as auto-inducing factors, whose titers are also modulated by mutations that impact cell fitness, translating better adaptation into faster biomass development and higher QSMs production. pPET was considered to be an indirect reporter of tyrosine production, as its aromatic alcohol form (Hazelwood et al. 2008;

Jagtap et al. 2020), but could also be considered as an indicator for the production of other QSMs such as PE of tryptohol, which play an important role in the production of more QSMs through the upregulation of *ARO9* and *ARO10*. Deletion of *ARO10* in this context would fail by itself to accumulate aromatic amino acids but restrict the formation of higher alcohols due to the disruption of QSMs stimuli over the transamination and decarboxylation steps of the Ehrlich pathway. Such results can be observed in figure 3.24, where an *aro10Δ* produces no accumulation of tyrosine but a decrease in pPET titers.

Determination of aromatic amino acids and their respective higher alcohol forms would be important to evaluate the arguments presented above, as well as growth analysis under single and co-culture modalities for the *aro10Δ* mutants. Deleting this decarboxylase, which should promote the accumulation of tyrosine and promote faster consortia development, might in fact demonstrate a slower or non-affected growth as it impacts QSMs production and not the effective tyrosine pool available.

4.2 Mutations towards better cell fitness

The adaptive laboratory processes used in the present project produced gene variations that proved to impact cell fitness rather than the overproduction of exchange molecules. This section discusses such adaptations depending on the feature modified.

4.2.1 Stabilisation of lysine import processes

The expression and regulation of high-affinity amino acid permeases allow the cell to respond appropriately to environmental conditions, mainly nutrient availability. Lysine import was particularly relevant for the development of the present project, as cells expected to overproduce tyrosine were built on a lysine auxotrophic genotype. Such a process has been reported to be facilitated by several transporters such as Gap1p, Can1p, Lyp1p and Vba5 (Bianchi et al. 2016; Grenson et al. 1970; Shimazu et al. 2012; Sychrova & Chevallier 1993; Sychrova et al. 1993), but among them, Lyp1p is reported as the most efficient for this amino acid with K_m between 10 and 25 μM (Ghaddar et al. 2014; Grenson et al. 1966).

In this sense, the membrane stability of this transporter is of great importance to respond to extracellular lysine availability. Such process is regulated by two α-arrestins, Art1p and Art2p, the former being described to respond to high concentration stimuli, while the latter for low substrate and toxicity response (Ivashov et al. 2020; Lin et al. 2008).

The present study identified an early stop codon for *ART2* in evolved lysine auxotrophic cells, a mutation that stabilises this transporter under low lysine conditions. Such mutation would represent an advantage under the low lysine concentrations experienced by cells through the evolution process.

Interestingly, mutations in this gene seem to occur relatively frequently in lysine auxotrophic cells growing under limited lysine conditions. In a study analysing the evolution-produced mutations in syntrophic consortia, Waite and Shou discovered that *ART2* was one of the two most frequently mutated genes in lysine auxotrophic strains, producing early stop codons in five out of six mutants (Waite & Shou 2012). Similarly to the results obtained in this project, such mutations would eliminate the C-terminus of the Art2p, which extends from 554 residues of this protein, including at least two described PY motifs, which are required for interaction with Rsp5p, and prevents its normal regulatory function (Baile et al. 2019; Lin et al. 2008; Waite & Shou 2012).

Additionally, Art2p has been described to depend on a basic patch of residues located at its C-terminus to identify its target proteins via interaction with acidic patches at their C-terminus region (Ivashov et al. 2020). In this regard, the early stop codon found on *ART2* would also prevent an interaction with target proteins, disrupting completely its normal regulatory function.

Art2p has been described to mediate, in addition to Lyp1p, the internalisation process for the high-affinity amino acid transporters Mup1p, Can1p, and Tat2p under nitrogen starvation conditions via the interaction mentioned above with common acidic patches at the C-terminus tail of these transporters (Ivashov et al. 2020). In this sense, an Art2p incapable of interacting with Rsp5p would also promote the stabilisation of these transporters with possible consequences for the nutrient traffic processes.

Besides arginine, histidine, and ornithine, Can1p has also been described to transport lysine but with K_m constants relatively higher (150-250μM) than those presented by Lyp1p (10-25μM) (Ghaddar et al. 2014; Grenson et al. 1966), which makes Can1p not so relevant for lysine transport unless relatively larger amounts of this amino acid are present.

Tat2p is another interesting transporter whose stability under starvation is mediated by Art2p, as it has been described to facilitate the trafficking of tryptophan, tyrosine, and phenylalanine (Kanda & Abe 2013). As discussed in section 4.1.6, increased tryptohol could induce faster biomass development during single and co-culture fermentation.

Due to the structural similarities between tryptophan and its higher alcohol form, it could be expected that the same membrane protein would facilitate its import into the cell. In this sense, a more stable Tat2p would add to the effects of QSMs on culture development.

Amino acid secretion in yeast is a recognised phenomenon known to be enhanced upon increased production but remains poorly understood in molecular terms. So far, only some of the proteins of the Drug H^+-Antiporter Family have been related to secretion processes, but only for a few substrates and specific conditions. Secretion of threonine and homoserine has been observed to require the transporter proteins Aqr1p, Qdr2p and Qdr3p. However, the detection was only possible after the use of overproducing mechanisms together with the impairment of the import channels for these amino acids (Kapetanakis et al. 2021; Velasco et al. 2004). A provided explanation to this scenario suggests that overproduced amino acids are re-incorporated via traditional mechanisms after being secreted, preventing an extracellular accumulation (Kapetanakis et al. 2021). Overexpression of the transporter Aqr1p has been reported to favour the secretion of amino acids such as aspartate, glutamate and alanine without employing overproducing mechanisms. However, this report found no detectable amounts of aromatic amino acids or lysine in the supernatant (Velasco et al. 2004).

In a more recent study, Kapetanakis et al. 2023 described that the yeast strain *Ethanol Red* employs the transporters Qdr1p, Qdr2p, and Qdr3p, for the secretion of several amino acids, which undesirably supplement the growth of contaminating lactic acid bacteria during bioethanol production processes. By conducting a series of co-cultures between yeast and bacteria using media that selectively lacked one of the twenty amino acids, they identified thirteen amino acids whose secretion depends on these transporters, including phenylalanine, tyrosine and lysine (Kapetanakis et al. 2023).

It is interesting to speculate on the role of these transporters, especially for tyrosine secretion in the producer strains developed on this project, as they possess overproducing mechanisms that would increase the intracellular concentration and consequently promote secretion. Considering the outcomes reported by Velasco et al. 2004 and Kapetanakis et al. 2021, secreted tyrosine would be rapidly re-assimilated by transporters such as Gap1p, Agp1p, Bap2p, Bap3p, Tat1, Tat2 and Tat3 (Bianchi et al. 2019), which would prevent its extracellular accumulation.

However, this interpretation does not explain the results obtained in the present project. Tyrosine conversion to pCA was intended to evidence its overproduction by converting it into a molecule that can easily permeate the membrane, avoiding its degradation into

the Ehrlich pathway (Jakočiūnas et al. 2015; Rodriguez et al. 2015). In this sense, pCA concentrations were expected to build up according to tyrosine production, replicating in principle the extracellular amino acid concentration expected after impairing tyrosine import mechanisms.

As discussed in section 3.10.2, pCA determination in tyrosine evolved producers identified only a minor improvement between the best producer strains Y1.2 and Y2 in cooperation with the parental strains Y0 and Y1. Additionally, no difference between strains Y1 and Y0 can be appreciated, which does not correlate to the dramatic improvement in consortia development observed between these two strains.

Additionally, as mentioned above, the α-arrestin Art2p has been related to regulating the stability of several transporters proteins as part of the TORC1 regulatory complex (Ivashov et al. 2020). It could be speculated that the *art2-Δ615* mutation, which proved to stabilise Lyp1p, could also exert a similar effect upon other transporters, possibly including proteins that facilitate amino acid secretion, such as the previously mentioned Aqr1, Qdr1p, Qdr2p, and Qdr3p. This would constitute an advantage for consortia development and contribute to explaining the fast development of consortia that include strains with an *art2* genotype.

Nevertheless, the mechanism described for Art2p activity requires the target protein to possess an acidic patch of residues at its C-terminus (Ivashov et al. 2020). The candidate proteins for facilitating the export of amino acids Aqr1, Qdr1p, Qdr2p, and Qdr3p lack such motif of residues at their C-terminus region as depicted in table 4.1. Consequently, it is unlikely that the stability of such transporters is regulated by Art2p, at least utilising the mechanism described so far. Additionally, if amino acid secretion is enhanced on overproducing scenarios (Velasco et al. 2004), it would be more likely that the sta-

Table 4.1: Acidic patches at C-terminus region of transporter proteins. Comparison of the last 60 residues of several protein transporters. Acidic residues are marked in bold and underlined. Stop codons are depicted with the symbol *.

Protein	Residues at C-terminus region
Mup1p	LLPRWGHYKLVSK**D**VLG**ED**GFWRVKIAVY**DD**TIG**D**V**D**TQ**ED**GVI**E**TNII**E**HYKS**E**Q**E**KSL*
Can1p	YISIFLFLAVWILFQCIFRCRFIWKIG**D**V**D**I**D**S**D**RR**D**I**E**AIVW**ED**H**E**PKTFW**D**KFWNVVA*
Lyp1p	YISLILLAVVFIGCQIYYKCRFIWKL**ED**I**D**I**D**S**D**RR**E**I**E**AIIW**EDDE**PKNLW**E**KFWAAVA*
Aqr1p	TFTFLCALVFFFNFLMFIPMKYGMKWR**ED**RLLKQQRQSWLNTLAVKAKKGTKR**D**QN**D**NHN*
Qdr1p	MV**E**KMRYGGVFTFLSAITSSSSLLLFYLLKNGKQLSF**D**RIRAN**D**KSAGRSVGKNS**E**KVST*
Qdr2p	CILSAVFIAALSKMV**E**KMKFGGVFTFLGALTSSSSILLFILLRKGK**E**LAFKRKKQ**E**LGVN*
Qdr3p	LAATAVFVTTPMLNGMGTGWAFTMLAFIVLGASSVLIILKKHG**D**YWR**E**NY**D**LQKLY**D**KI**D***

bility of these transporters is regulated by Art1p rather than by Art2p, as this arrestin is activated upon nutrients excess scenarios (Ivashov et al. 2020). However, no mutation on *ART1* was detected during this project's development, preventing establishing a relation between this arrestin and the improved phenotypes observed under consortia conditions.

Lysine secretion by Lyp1p has also been studied. However, it is described as highly disfavoured when compared to the import efficiency displayed by this transporter, which exhibits far better K_m for import than for export (at least three to four orders of magnitude lower), suggesting an unidirectional transport (Bianchi et al. 2016).

4.2.2   Bypass cell replication restriction under low nutrients

Limited nutrient conditions force cells to modulate their metabolism to face the challenges and ensure survival, which means that the metabolic activity must be diverted from replication and growth into a restricted mode, recycling resources to prioritise survival (Beck & Hall 1999; Loewith & Hall 2011). Such regulation relies mainly on the activity of the TORC1, which, under an active state configuration, promotes the synthesis of lipids, nucleotides, and proteins, thereby promoting growth and replication (Panchaud et al. 2013a). Upon scarcity of nutrients, such as nitrogen or amino acids, TORC1 will become repressed, promoting autophagy, membrane protein degradation and cell arrest into a quiescent state (Loewith & Hall 2011).

TORC1 activity has been described to be regulated most notably by the SEACIT-Gtr1-Gtr2 complex, but this is not the only regulatory system acting in yeast as an independent controller. Whi2p has also been shown to regulate TORC1 activity in a nutrient-dependent manner (Teng & Hardwick 2019). In particular, leucine is highlighted as the most relevant amino acid regarding the regulatory properties of Whi2p (X. Chen et al. 2018; Teng & Hardwick 2019; Teng et al. 2018). Interestingly, response to leucine has been described to be also dependent on other amino acid concentrations, among which tyrosine is described as a candidate (Teng et al. 2018). In this sense, it is interesting to note that single-growth fermentation analysis of lysine producer strains, such as K0, has been performed in SCD media without lysine (as described in section 2.7.2) but supplemented with tyrosine. This latter metabolite is available at a much lower concentration in our SCD media in comparison with the reported value from Teng et al. (14.4 mg L^{-1} versus 30 mg L^{-1}), while our leucine concentration is higher (57.6 mg L^{-1} versus 50 mg L^{-1}) (Teng et al. 2018).
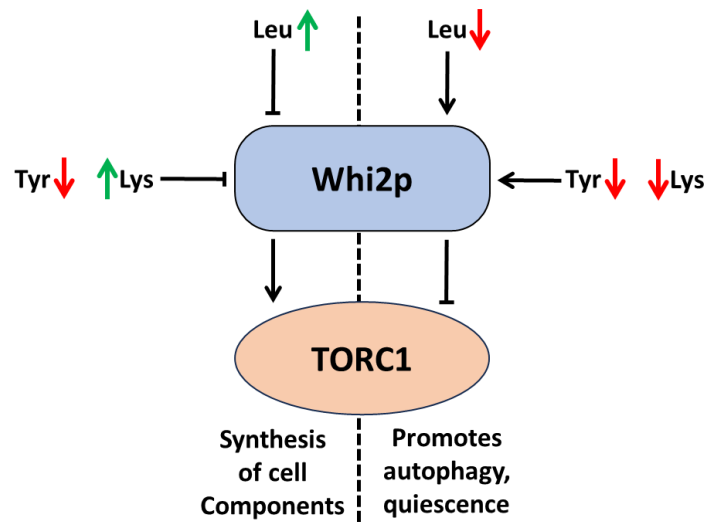
Figure 4.2: Lysine and tyrosine role over Whi2p regulation. Schematic representation of the possible regulatory role of lysine and tyrosine over Whi2p. Left and right sides of the dotted line display inhibition and activation of Whi2p, respectively. Leucine's proportional levels to other media nutrients are alone capable of exerting a regulatory role over Whi2p. Role of lysine and tyrosine in the regulation is proposed as a theory based on results achieved during the present work.

Additionally, the single growth analysis performed on the effect of Whi2p over growth performance in a K0 background (presented in figure 3.36) shows that a non-functional *whi2* improves single growth, stressing the role of low lysine together with low tyrosine on achieving a fast development. Considering this information, the positive effect observed for a non-functional *whi2* seems unrelated to a low leucine concentration but to a low lysine and tyrosine concentration (see figure 4.2).

Strains presenting a tyrosine auxotrophic phenotype, such as K0, have been analysed in an environment lacking lysine and with a low tyrosine concentration, which could possibly promote TORC1 negative regulation mediated by Whi2p. A nonfunctional *whi2* in this scenario would favour growth.

In contrast, strains presenting a lysine auxotrophy were analysed in media depleted of tyrosine but supplemented with a high lysine concentration, which would fail to trigger Whi2p activation, producing no growth difference regardless of the *WHI2* genotype of the strain.

Finally, co-culture experiments were always depleted of lysine and tyrosine, which would successfully exercise a Whi2p regulation of TORC1, despite the high leucine concentration provided by the media.

This theory would explain the growth results obtained in figures 3.36 and 3.37 where a *whi2* genotype seems beneficial for single culture only in a tyrosine auxotrophic (K0)

but no in a lysine auxotrophic (Y0) background, as Whi2p would respond to low levels of both amino acids to trigger its regulatory effect on TORC1. The consistently favourable effects of a *whi2* genotype during consortia fermentations would also be explained as these fermentations are always performed in a media lacking lysine and tyrosine.

However, it is noticeable that this effect is observed only after full deletion of *WHI2* in an unevolved K0 strain, whereas no difference can be observed in an evolved K1 background when comparing a mutated and repaired version of *whi2*. This could be due to additional mutations or adaptations that remain unidentified so far, which prompt a growth performance independent of the role of Whi2p. A residual activity of *whi2-535G>T* seems unlikely as it prompts a growth improvement under co-culture conditions (see figure 3.36B).

Additional experiments are required to elucidate the role of lysine and tyrosine during the Whi2p regulatory process over TORC1. The evidence so far seems to favour the hypothesis that only lysine and no tyrosine are required for Whi2p function, as the regulatory effect upon cell growth is observed only when fermentations are conducted without supplementation of this amino acid. A growth analysis on a K0 background and extra tyrosine would help to elucidate if it is also a factor for Whi2p activation as suggested by Teng et al. 2018.

It is also noticeable that spontaneous mutations are frequently reported to occur in *WHI2* after knockout collections and in genome evolution studies (Teng & Hardwick 2019). For example, a mutation in *WHI2* was reported to rescue a *fis1* knockout, a mitochondrial fission factor that produces a mitochondrial respiratory defect (Cheng et al. 2008). In addition, *WHI2* mutations have been suggested to compensate for the stress-related burden produced after multiple gene deletions (Comyn et al. 2017; Szamecz et al. 2014; Teng et al. 2013) or directly to confer growth advantages under poor nutrient conditions (J. Hong & Gresham 2014; Van Leeuwen et al. 2016).

The mutations obtained in this study point in the same direction, as they apparently conferred mutant strains the capacity to circumvent normal growth regulations imposed by limited nutrients, allowing fast biomass development even in poor media conditions. However, the apparent beneficial effects derived from a *whi2* genotype need to be weighed against the several decreased features it produces, such as increased sensitivity to lower pH, reduced thermo-tolerance, smaller cell size, or increased sensitivity to oxidative stress (Brown et al. 2006; Gibney et al. 2013; Mira et al. 2009; J. Zhang et al. 2002).

Chapter: 5 Conclusions

Developing synthetic consortia for biotechnological production can offer an alternative to traditional limitations, such as metabolic burden and intermediate molecule secretion. However, the mechanisms to achieve a successful implementation are still unclear, particularly regarding how to achieve a steady population distribution or effectively divide labour.

This project aimed to tackle the gaps in knowledge by creating a synthetic cooperative consortium that utilised tyrosine and lysine as exchange metabolites with the help of *S. cerevisiae* as a model organism. Through adaptive laboratory evolution with media that lacked these two amino acids, the project sought to produce better-fit strains adapted to the cooperation dynamic. The hope was to obtain mutations that could later be utilised to improve aromatic compounds derived from yeast's aromatic amino acid biosynthesis pathway.

The evolution process produced several strains with interesting phenotypes. The mutants were primarily chosen for their ability to enhance consortium growth and their capacity to produce pPET, a metabolite derived from tyrosine degradation via the Ehlrich pathway. Interestingly, their genetic analysis did not indicate any clear mutation linked to improved tyrosine synthesis or its secretion.

Among the most relevant variations identified after the whole genome sequencing analysis, highlight the loss of function mutations for the genes *ART2*, *LYS9* and *WHI2*, as well as a partial duplication in chromosome XIV that seems to confer evolved strains an improved capacity for sustaining consortia growth. However, this last modification could not be adequately verified with the methodology employed, and its role remains speculative.

The mutation on gene *ART2* seems to stabilise the lysine transporter Lyp1p under low substrate conditions, promoting a faster uptake of this amino acid. This feature would be advantageous for the conditions endured during the evolution processes.

The role of the mutation on the gene *LYS9* was less clear to attribute to a specific process. It appears to enhance growth in consortia conditions but hinders performance in single-growth conditions. After ruling out the possibility of toxicity from the accumulation of the Lys9p substrate 2-aminoadipate-6-semialdehyde (ASA), it is hypothesised that *lys9* strains are secreting this molecule to be converted into lysine by cells with a wild type

LYS9. This theory would account for the unusual phenotype resulting from this mutation in both single and co-culture conditions and serves as an example of outsourcing the production of a necessary metabolite. Exploiting engineered feedback-resistant variants with metabolites produced from more than one strain could be beneficial for achieving outsourcing production of molecules of interest processes. However, the design of such processes needs to be carefully planned.

Recent studies have identified the protein Whi2p as a negative regulator of TORC1, leading to the suspicion that its loss of function may lead to better growth under low amino acid conditions. However, a thorough analysis of cells with a *whi2* copy indicates that this advantage only applies when cells are grown in media deprived of lysine and with low tyrosine. These two amino acids may represent a previously unknown aspect of Whi2p's role in regulating TORC1 activity.

It is unclear how the improved pPET titters were achieved, as no direct mutations were detected. However, it is speculated that this fusel alcohol and unmeasured PE and tryptophol may influence the consortia development as quorum-sensing molecules (QSMs). As a result, the positive growth effect of the previously discussed mutations could promote increased QSMs production, which in turn would positively impact biomass growth, creating a beneficial cycle.

The variations identified during the present project highlight the importance of individual strain fitness for proper consortia development. The enhanced stability of amino acid transporters and alleviation of growth constraints caused by the TORC1 system can benefit consortia development. Furthermore, targeting genes upstream of metabolic pathways to create auxotrophies can effectively achieve the desired phenotype while minimising the metabolic burden associated with unused pathways.

Chapter: 6 Bibliography

Adrio, J.-L., & Demain, A. L. (2010). Recombinant organisms for production of industrial products. *Bioengineered bugs*, *1*(2), 116–131.

Aguilera, A. (1986). Deletion of the phosphoglucose isomerase structural gene makes growth and sporulation glucose dependent in *Saccharomyces cerevisiae*. *Molecular and General Genetics MGG*, *204*(2), 310–316.

Ajikumar, P. K., Xiao, W.-H., Tyo, K. E. J., Wang, Y., Simeon, F., Leonard, E., Mucha, O., Phon, T. H., Pfeifer, B., & Stephanopoulos, G. (2010). Isoprenoid pathway optimization for taxol precursor overproduction in *Escherichia coli*. *Science (New York, N.Y.)*, *330*(6000), 70–74.

Ames, R. M., Rash, B. M., Hentges, K. E., Robertson, D. L., Delneri, D., & Lovell, S. C. (2010). Gene duplication and environmental adaptation within yeast populations. *Genome Biology and Evolution*, *2*, 591–601.

Andi, B., Cook, P. F., & West, A. H. (2006). Crystal structure of the his-tagged saccharopine reductase from *Saccharomyces cerevisiae* at 1.7-Å Resolution. *Cell Biochemistry and Biophysics*, *46*(1), 17–26.

Andréasson, C., Neve, E. P. A., & Ljungdahl, P. O. (2004). Four permeases import proline and the toxic proline analogue azetidine-2-carboxylate into yeast. *Yeast*, *21*(3), 193–199.

Andrews, S. (2018, January 18). *FastQC: A-Quality control tool for high throughput sequence data*.

Aulakh, S. K., Sellés Vidal, L., South, E. J., Peng, H., Varma, S. J., Herrera-Dominguez, L., Ralser, M., & Ledesma-Amaro, R. (2023). Spontaneously established syntrophic yeast communities improve bioproduction. *Nature Chemical Biology*, *19*(8), 951–961.

Avbelj, M., Zupan, J., Kranjc, L., & Raspor, P. (2015). Quorum-sensing kinetics in *Saccharomyces cerevisiae* : a symphony of *ARO* genes and aromatic alcohols. *Journal of Agricultural and Food Chemistry*, *63*(38), 8544–8550.

Avbelj, M., Zupan, J., & Raspor, P. (2016). Quorum-sensing in yeast and its potential in wine making. *Applied Microbiology and Biotechnology*, *100*(18), 7841–7852.

Babst, M. (2020). Regulation of nutrient transporters by metabolic and environmental stresses. *Current Opinion in Cell Biology*, *65*, 35–41.

Baile, M. G., Guiney, E. L., Sanford, E. J., MacGurn, J. A., Smolka, M. B., & Emr, S. D. (2019). Activity of a ubiquitin ligase adaptor is regulated by disordered insertions in its arrestin domain (H. Riezman, Ed.). *Molecular Biology of the Cell*, *30*(25), 3057–3072.

Bajmoczi, M., Sneve, M., Eide, D. J., & Drewes, L. R. (1998). *Tat1* encodes a low-affinity histidine transporter in *saccharomyces cerevisiae*. *Biochemical and Biophysical Research Communications*, *243*(1), 205–209.

Balagaddé, F. K., Song, H., Ozaki, J., Collins, C. H., Barnet, M., Arnold, F. H., Quake, S. R., & You, L. (2008). A synthetic *Escherichia coli* predator–prey ecosystem. *Molecular Systems Biology*, *4*(1), 187.

Ball, S. G., Wickner, R. B., Cottarel, G., Schaus, M., & Tirtiaux, C. (1986). Molecular cloning and characterization of *ARO7-OSM2*, a single yeast gene necessary for chorismate mutase activity and growth in hypertonic medium. *Molecular & general genetics: MGG*, *205*(2), 326–330.

Beck, T., & Hall, M. N. (1999). The TOR signalling pathway controls nuclear localization of nutrient-regulated transcription factors. *Nature*, *402*(6762), 689–692.

Becker, B., Feller, A., El Alami, M., Dubois, E., & Piérard, A. (1998). A nonameric core sequence is required upstream of the *LYS* genes of *Saccharomyces cerevisiae* for Lys14p-mediated activation and apparent repression by lysine. *Molecular Microbiology*, *29*(1), 151–163.

Becker, J., & Boles, E. (2003). A modified *Saccharomyces cerevisiae* strain that consumes l-Arabinose and produces ethanol. *Applied and Environmental Microbiology*, *69*(7), 4144–4150.

Becuwe, M., Herrador, A., Haguenauer-Tsapis, R., Vincent, O., & Léon, S. (2012). Ubiquitin-mediated regulation of endocytosis by proteins of the arrestin family. *Biochemistry Research International*, *2012*, e242764.

Bertels, L.-K., Fernández Murillo, L., & Heinisch, J. J. (2021). The pentose phosphate pathway in yeasts–more than a poor cousin of glycolysis. *Biomolecules*, *11*(5), 725.

Betz, C., Schlenstedt, G., & Bailer, S. M. (2004). Asr1p, a novel yeast Ring/PHD finger protein, signals alcohol stress to the nucleus. *Journal of Biological Chemistry*, *279*(27), 28174–28181.

Bhatia, S. K., Yoon, J.-J., Kim, H.-J., Hong, J. W., Gi Hong, Y., Song, H.-S., Moon, Y.-M., Jeon, J.-M., Kim, Y.-G., & Yang, Y.-H. (2018). Engineering of artificial microbial consortia of *Ralstonia eutropha* and *Bacillus subtilis* for poly(3-hydroxybutyrate-co-3-hydroxyvalerate) copolymer production from sugarcane sugar without precursor feeding. *Bioresource Technology*, *257*, 92–101.

Bianchi, F., Klooster, J. S. v. t., Ruiz, S. J., Luck, K., Pols, T., Urbatsch, I. L., & Poolman, B. (2016). Asymmetry in inward- and outward-affinity constant of transport explain unidirectional lysine flux in *Saccharomyces cerevisiae*. *Scientific Reports*, *6*(1), 31443.

Bianchi, F., van't Klooster, J. S., Ruiz, S. J., & Poolman, B. (2019). Regulation of amino acid transport in *Saccharomyces cerevisiae*. *Microbiology and Molecular Biology Reviews*, *83*(4), e00024–e00019.

Binda, M., Péli-Gulli, M.-P., Bonfils, G., Panchaud, N., Urban, J., Sturgill, T. W., Loewith, R., & Virgilio, C. D. (2009). The Vam6 GEF controls TORC1 by activating the EGO complex. *Molecular Cell*, *35*(5), 563–573.

Biomatters. (2019, September). *Geneious Prime* (Version 2019.2.3).

Blank, L. M., Kuepfer, L., & Sauer, U. (2005). Large-scale 13C-flux analysis reveals mechanistic principles of metabolic network robustness to null mutations in yeast. *Genome Biology*, *6*(6), R49.

Boles, E., Lehnert, W., & Zimmermann, F. K. (1993). The role of the NAD-dependent glutamate dehydrogenase in restoring growth on glucose of a *Saccharomyces cerevisiae* phosphoglucose isomerase mutant. *European Journal of Biochemistry*, *217*(1), 469–477.

Borell, C. W., Urrestarazu, L. A., & Bhattacharjee, J. K. (1984). Two unlinked lysine genes (*LYS9* and *LYS14*) are required for the synthesis of saccharopine reductase in *Saccharomyces cerevisiae*. *Journal of Bacteriology*, *159*(1), 429–432.

Braus, G. H. (1991). Aromatic amino acid biosynthesis in the yeast *Saccharomyces cerevisiae*: a model system for the regulation of a eukaryotic biosynthetic pathway. *Microbiological Reviews*, *55*(3), 349–370.

Brenner, K., You, L., & Arnold, F. H. (2008). Engineering microbial consortia: a new frontier in synthetic biology. *Trends in biotechnology*, *26*(9), 483–489.

Broach, J. R. (2012). Nutritional control of growth and development in yeast. *Genetics*, *192*(1), 73–105.

Brown, J. A., Sherlock, G., Myers, C. L., Burrows, N. M., Deng, C., Wu, H. I., McCann, K. E., Troyanskaya, O. G., & Brown, J. M. (2006). Global analysis of gene function in yeast by quantitative phenotypic profiling. *Molecular Systems Biology*, *2*, 2006.0001.

Brückner, C., Oreb, M., Kunze, G., Boles, E., & Tripp, J. (2018). An expanded enzyme toolbox for production of *cis, cis*-muconic acid and other shikimate pathway derivatives in *Saccharomyces cerevisiae*. *FEMS yeast research*, *18*(2).

Bruder, S., Reifenrath, M., Thomik, T., Boles, E., & Herzog, K. (2016). Parallelised online biomass monitoring in shake flasks enables efficient strain and carbon source dependent growth characterisation of *Saccharomyces cerevisiae*. *Microbial Cell Factories*, *15*(1), 127.

Bulfer, S. L., Brunzelle, J. S., & Trievel, R. C. (2013). Crystal structure of *Saccharomyces cerevisiae* Aro8, a putative α-aminoadipate aminotransferase: Crystal Structure of Aro8. *Protein Science*, *22*(10), 1417–1424.

Bulfer, S. L., Scott, E. M., Pillus, L., & Trievel, R. C. (2010). Structural basis for L-lysine feedback inhibition of homocitrate synthase. *The Journal of biological chemistry*, *285*(14), 10446–10453.

Bushnell, B. (2015, October). *BBDuk* (Version 1.0).

Cai, M., Wu, Y., Qi, H., He, J., Wu, Z., Xu, H., & Qiao, M. (2021). Improving the level of the tyrosine biosynthesis pathway in *Saccharomyces cerevisiae* through *HTZ1* knockout and atmospheric and room temperature plasma (ARTP) Mutagenesis. *ACS synthetic biology*.

Camilli, A., & Bassler, B. L. (2006). Bacterial small-molecule signaling pathways. *Science (New York, N.Y.)*, *311*(5764), 1113–1116.

Campbell, K., Vowinckel, J., Mülleder, M., Malmsheimer, S., Lawrence, N., Calvani, E., Miller-Fleming, L., Alam, M. T., Christen, S., Keller, M. A., & Ralser, M. (2015). Self-establishing communities enable cooperative metabolite exchange in a eukaryote. *eLife*, *4*, e09943.

Carlson, M., & Botstein, D. (1983). Organization of the *SUC* gene family in Saccharomyces. *Molecular and Cellular Biology*, *3*(3), 351–359.

Carter, B. L. A., & Sudbery, P. E. (1980). Small-sized mutants of *Saccharomyces cerevisiae*. *Genetics*, *96*(3), 561–566.

Cavaliere, M., Feng, S., Soyer, O. S., & Jiménez, J. I. (2017). Cooperation in microbial communities and their biotechnological applications. *Environmental microbiology*, *19*(8), 2949–2963.

Chen, H., & Fink, G. R. (2006). Feedback control of morphogenesis in fungi by aromatic alcohols. *Genes & Development*, *20*(9), 1150–1161.

Chen, X., Wang, G., Zhang, Y., Dayhoff-Brannigan, M., Diny, N. L., Zhao, M., He, G., Sing, C. N., Metz, K. A., Stolp, Z. D., Aouacheria, A., Cheng, W.-C., Hardwick, J. M., & Teng, X. (2018). Whi2 is a conserved negative regulator of TORC1 in response to low amino acids (P. E. Sudbery, Ed.). *PLOS Genetics*, *14*(8), e1007592.

Cheng, W.-C., Teng, X., Park, H. K., Tucker, C. M., Dunham, M. J., & Hardwick, J. M. (2008). Fis1 deficiency selects for compensatory mutations responsible for cell death and growth control defects. *Cell Death & Differentiation*, *15*(12), 1838–1846.

Chinen, A., Kozlov, Y. I., Hara, Y., Izui, H., & Yasueda, H. (2007). Innovative metabolic pathway design for efficient l-glutamate production by suppressing CO2 emission. *Journal of Bioscience and Bioengineering*, *103*(3), 262–269.

Christwardana, M., Frattini, D., Duarte, K. D., Accardo, G., & Kwon, Y. (2019). Carbon felt molecular modification and biofilm augmentation via quorum sensing approach in yeast-based microbial fuel cells. *Applied Energy*, *238*, 239–248.

Compagno, C., Brambilla, L., Capitanio, D., Boschi, F., Maria Ranzi, B., & Porro, D. (2001). Alterations of the glucose metabolism in a triose phosphate isomerase-negative *Saccharomyces cerevisiae* mutant. *Yeast*, *18*(7), 663–670.

Compagno, C., Dashko, S., & Piškur, J. (2014). Introduction to carbon metabolism in yeast. In J. Piškur & C. Compagno (Eds.), *Molecular mechanisms in yeast carbon metabolism* (pp. 1–19). Springer Berlin Heidelberg.

Comyn, S. A., Flibotte, S., & Mayor, T. (2017). Recurrent background mutations in WHI2 impair proteostasis and degradation of misfolded cytosolic proteins in *Saccharomyces cerevisiae*. *Scientific Reports*, *7*(1), 4183.

Conant, G. C., & Wolfe, K. H. (2007). Increased glycolytic flux as an outcome of whole-genome duplication in yeast. *Molecular Systems Biology*, *3*(1), 129.

Concordet, J.-P., & Haeussler, M. (2018). CRISPOR: intuitive guide selection for CRISPR/Cas9 genome editing experiments and screens. *Nucleic Acids Research*, *46*(W1), 242–245.

Cooper, M. B., & Smith, A. G. (2015). Exploring mutualistic interactions between microalgae and bacteria in the omics age. *Current Opinion in Plant Biology*, *26*, 147–153.

Cordente, A. G., Schmidt, S., Beltran, G., Torija, M. J., & Curtin, C. D. (2019). Harnessing yeast metabolism of aromatic amino acids for fermented beverage bioflavouring and bioproduction. *Applied Microbiology and Biotechnology*, *103*(11), 4325–4336.

Coyte, K. Z., & Rakoff-Nahoum, S. (2019). Understanding competition and cooperation within the mammalian gut microbiome. *Current Biology*, *29*(11), 538–544.

Cupp, J. R., & McAlister-Henn, L. (1991). NAD(+)-dependent isocitrate dehydrogenase. Cloning, nucleotide sequence, and disruption of the *IDH2* gene from *Saccharomyces cerevisiae*. *The Journal of Biological Chemistry*, *266*(33), 22199–22205.

Curran, K. A., Leavitt, J. M., Karim, A. S., & Alper, H. S. (2013). Metabolic engineering of muconic acid production in *Saccharomyces cerevisiae*. *Metabolic Engineering*, *15*, 55–66.

Darvishi, F., Rafatiyan, S., Abbaspour Motlagh Moghaddam, M. H., Atkinson, E., & Ledesma-Amaro, R. (2022). Applications of synthetic yeast consortia for the production of native and non-native chemicals. *Critical Reviews in Biotechnology*, 1–16.

Daulny, A., Geng, F., Muratani, M., Geisinger, J. M., Salghetti, S. E., & Tansey, W. P. (2008). Modulation of RNA polymerase II subunit composition by ubiquitylation. *Proceedings of the National Academy of Sciences of the United States of America*, *105*(50), 19649–19654.

DeLoache, W. C., Russ, Z. N., Narcross, L., Gonzales, A. M., Martin, V. J. J., & Dueber, J. E. (2015). An enzyme-coupled biosensor enables (S)-reticuline production in yeast from glucose. *Nature Chemical Biology*, *11*(7), 465–471.

Dickinson, J. R., & Schweizer, M. (Eds.). (2004, April 27). *Metabolism and molecular physiology of Saccharomyces cerevisiae* (0th ed.). CRC Press.

Doebeli, M., & Hauert, C. (2005). Models of cooperation based on the Prisoner's Dilemma and the Snowdrift game. *Ecology Letters*, *8*(7), 748–766.

Donaton, M. C. V., Holsbeeks, I., Lagatie, O., Van Zeebroeck, G., Crauwels, M., Winderickx, J., & Thevelein, J. M. (2003). The Gap1 general amino acid permease acts as an amino acid sensor for activation of protein kinase A targets in the yeast *Saccharomyces cerevisiae*. *Molecular Microbiology*, *50*(3), 911–929.

Dorsey, M., Peterson, C., Bray, K., & Paquin, C. E. (1992). Spontaneous amplification of the *ADH4* gene in *Saccharomyces cerevisiae*. *Genetics*, *132*(4), 943–950.

Dragosits, M., & Mattanovich, D. (2013). Adaptive laboratory evolution – principles and applications for biotechnology. *Microbial cell factories*, *12*, 64.

Düring-Olsen, L., Regenberg, B., Gjermansen, C., Kielland-Brandt, M. C., & Hansen, J. (1999). Cysteine uptake by *Saccharomyces cerevisiae* is accomplished by multiple permeases. *Current Genetics*, *35*(6), 609–617.

Ehmann, D. E., Gehring, A. M., & Walsh, C. T. (1999). Lysine biosynthesis in *Saccharomyces cerevisiae:* mechanism of α-aminoadipate reductase (Lys2) involves posttranslational phosphopantetheinylation by Lys5. *Biochemistry*, *38*(19), 6171–6177.

Entian, K. D., Meurer, B., Köhler, H., Mann, K. H., & Mecke, D. (1987). Studies on the regulation of enolases and compartmentation of cytosolic enzymes in *Saccharomyces cerevisiae*. *Biochimica Et Biophysica Acta*, *923*(2), 214–221.

Ewing, B., & Green, P. (1998). Base-calling of automated sequencer traces using *Phred.* II. error probabilities. *Genome Research*, *8*(3), 186–194.

Fathi, Z., Tramontin, L. R. R., Ebrahimipour, G., Borodina, I., & Darvishi, F. (2021). Metabolic engineering of *Saccharomyces cerevisiae* for production of β-carotene from hydrophobic substrates. *FEMS yeast research*, *21*(1), foaa068.

Fedorec, A. J. H., Karkaria, B. D., Sulu, M., & Barnes, C. P. (2021). Single strain control of microbial consortia. *Nature communications*, *12*(1), 1977.

Feller, A., Dubois, E., Ramos, F., & Piérard, A. (1994). Repression of the genes for lysine biosynthesis in *Saccharomyces cerevisiae* is caused by limitation of Lys14-dependent transcriptional activation. *Molecular and Cellular Biology*, *14*(10), 6411–6418.

Feller, A., Ramos, F., Piérard, A., & Dubois, E. (1999). In *Saccharomyces cerevisae*, feedback inhibition of homocitrate synthase isoenzymes by lysine modulates the activation of *LYS* gene expression by Lys14p. *European journal of biochemistry*, *261*(1), 163–170.

Fierer, N. (2017). Embracing the unknown: disentangling the complexities of the soil microbiome. *Nature Reviews Microbiology*, *15*(10), 579–590.

Finley, D., Ulrich, H. D., Sommer, T., & Kaiser, P. (2012). The ubiquitin–proteasome system of *Saccharomyces cerevisiae*. *Genetics*, *192*(2), 319–360.

Fletcher, T. S., Kwee, I. L., Nakada, T., Largman, C., & Martin, B. M. (1992). DNA sequence of the yeast transketolase gene. *Biochemistry*, *31*(6), 1892–1896.

Forrest, L. R., Krämer, R., & Ziegler, C. (2011). The structural basis of secondary active transport mechanisms. *Biochimica et Biophysica Acta (BBA) - Bioenergetics*, *1807*(2), 167–188.

Furter, R., Paravicini, G., Aebi, M., Braus, G., Prantl, F., Niederberger, P., & Hütter, R. (1986). The TRP4 gene of *Saccharomyces cerevisiae*: isolation and structural analysis. *Nucleic Acids Research*, *14*(16), 6357–6373.

Furter, R., Braus, G., Paravicini, G., Mösch, H.-U., Niederberger, P., & Hütter, R. (1988). Regulation of the *TRP4* gene of *Saccharomyces cerevisiae* at the transcriptional level and functional analysis of its promoter. *Molecular and General Genetics MGG*, *211*(1), 168–175.

Gabba, M., Frallicciardi, J., van 't Klooster, J., Henderson, R., Syga, Ł., Mans, R., van Maris, A. J. A., & Poolman, B. (2020). Weak acid permeation in synthetic lipid vesicles and across the yeast plasma membrane. *Biophysical Journal*, *118*(2), 422–434.

Gandía-Herrero, F., García-Carmona, F., & Escribano, J. (2005). A novel method using high-performance liquid chromatography with fluorescence detection for the determination of betaxanthins. *Journal of chromatography. A*, *1078*(1-2), 83–89.

Ganesan, V., Li, Z., Wang, X., & Zhang, H. (2017). Heterologous biosynthesis of natural product naringenin by co-culture engineering. *Synthetic and Systems Biotechnology*, *2*(3), 236–242.

Gangloff, S. P., Marguet, D., & Lauquin, G. J.-M. (1990). Molecular cloning of the yeast mitochondrial aconitase gene (*ACO1*) and evidence of a synergistic regulation of expression by glucose plus glutamate. *Molecular and Cellular Biology*, *10*(7), 3551–3561.

Garces Daza, F., Haitz, F., Born, A., & Boles, E. (2023). An optimized reverse β-oxidation pathway to produce selected medium-chain fatty acids in *Saccharomyces cerevisiae*. *Biotechnology for Biofuels and Bioproducts*, *16*(1), 71.

Generoso, W. C., Gottardi, M., Oreb, M., & Boles, E. (2016). Simplified CRISPR-Cas genome editing for *Saccharomyces cerevisiae*. *Journal of microbiological methods*, *127*, 203–205.

Ghaddar, K., Krammer, E.-M., Mihajlovic, N., Brohée, S., André, B., & Prévost, M. (2014). Converting the yeast arginine Can1 permease to a lysine permease. *Journal of Biological Chemistry*, *289*(10), 7232–7246.

Gibney, P. A., Lu, C., Caudy, A. A., Hess, D. C., & Botstein, D. (2013). Yeast metabolic and signaling genes are required for heat-shock survival and have little overlap with the heat-induced genes. *Proceedings of the National Academy of Sciences of the United States of America*, *110*(46), 4393–4402.

Gietz, R., & Akio, S. (1988). New yeast-*Escherichia coli* shuttle vectors constructed with in vitro mutagenized yeast genes lacking six-base pair restriction sites. *Gene*, *74*(2), 527–534.

Gimeno, C. J., Ljungdahl, P. O., Styles, C. A., & Fink, G. R. (1992). Unipolar cell divisions in the yeast *S. cerevisiae* lead to filamentous growth: Regulation by starvation and RAS. *Cell*, *68*(6), 1077–1090.

Glick, B. R., Brooks, H. E., & Pasternak, J. J. (1986). Physiological effects of plasmid DNA transformation on *Azotobacter vinelandii*. *Canadian Journal of Microbiology*, *32*(2), 145–148.

Glick, B. R. (1995). Metabolic load and heterologous gene expression. *Biotechnology Advances*, *13*(2), 247–261.

Godard, P., Urrestarazu, A., Vissers, S., Kontos, K., Bontempi, G., van Helden, J., & André, B. (2007). Effect of 21 different nitrogen sources on global gene expression in the yeast *Saccharomyces cerevisiae*. *Molecular and Cellular Biology*, *27*(8), 3065–3086.

Goeddel, D. V., Kleid, D. G., Bolivar, F., Heyneker, H. L., Yansura, D. G., Crea, R., Hirose, T., Kraszewski, A., Itakura, K., & Riggs, A. D. (1979). Expression in *Escherichia coli* of chemically synthesized genes for human insulin. *Proceedings of the National Academy of Sciences of the United States of America*, *76*(1), 106–110.

Gold, N. D., Gowen, C. M., Lussier, F.-X., Cautha, S. C., Mahadevan, R., & Martin, V. J. J. (2015). Metabolic engineering of a tyrosine-overproducing yeast platform using targeted metabolomics. *Microbial Cell Factories*, *14*(1), 73.

Gore, J., Youk, H., & van Oudenaarden, A. (2009). Snowdrift game dynamics and facultative cheating in yeast. *Nature*, *459*(7244), 253–256.

Gottardi, M., Grün, P., Bode, H. B., Hoffmann, T., Schwab, W., Oreb, M., & Boles, E. (2017). Optimisation of trans-cinnamic acid and hydrocinnamyl alcohol production with recombinant *Saccharomyces cerevisiae* and identification of cinnamyl methyl ketone as a by-product. *FEMS yeast research*, *17*(8).

Gottardi, M., Knudsen, J. D., Prado, L., Oreb, M., Branduardi, P., & Boles, E. (2017). De novo biosynthesis of trans-cinnamic acid derivatives in *Saccharomyces cerevisiae*. *Applied Microbiology and Biotechnology*, *101*(12), 4883–4893.

Gottardi, M., Reifenrath, M., Boles, E., & Tripp, J. (2017). Pathway engineering for the production of heterologous aromatic chemicals and their derivatives in *Saccharomyces cerevisiae*: bioconversion from glucose. *FEMS yeast research*, *17*(4).

Gournas, C., Saliba, E., Krammer, E.-M., Barthelemy, C., Prévost, M., & André, B. (2017). Transition of yeast Can1 transporter to the inward-facing state unveils an α-arrestin target sequence promoting its ubiquitylation and endocytosis. *Molecular Biology of the Cell*, *28*(21), 2819–2832.

Graybill, E. R., Rouhier, M. F., Kirby, C. E., & Hawes, J. W. (2007). Functional comparison of citrate synthase isoforms from *S. cerevisiae*. *Archives of Biochemistry and Biophysics*, *465*(1), 26–37.

Greig, D., & Travisano, M. (2004). The Prisoner's Dilemma and polymorphism in yeast *SUC* genes. *Proceedings. Biological sciences*, *271 Suppl 3*, 25–26.

Grenson, M. (1966). Multiplicity of the amino acid permeases in *Saccharomyces cerevisiae*: II. Evidence for a specific lysine-transporting system. *Biochimica et Biophysica Acta (BBA) - General Subjects*, *127*(2), 339–346.

Grenson, M., Hou, C., & Crabeel, M. (1970). Multiplicity of the amino acid permeases in *Saccharomyces cerevisiae* IV. Evidence for a general amino acid permease. *Journal of Bacteriology*, *103*(3), 770–777.

Grenson, M., Mousset, M., Wiame, J., & Bechet, J. (1966). Multiplicity of the amino acid permeases in *Saccharomyces cerevisiae*. *Biochimica et Biophysica Acta (BBA) - General Subjects*, *127*(2), 325–338.

Gresham, D., Desai, M. M., Tucker, C. M., Jenq, H. T., Pai, D. A., Ward, A., DeSevo, C. G., Botstein, D., & Dunham, M. J. (2008). The repertoire and dynamics of evolutionary adaptations to controlled nutrient-limited environments in yeast (M. Snyder, Ed.). *PLoS Genetics*, *4*(12), e1000303.

Gresham, D., Usaite, R., Germann, S. M., Lisby, M., Botstein, D., & Regenberg, B. (2010). Adaptation to diverse nitrogen-limited environments by deletion or extrachromosomal element formation of the *GAP1* locus. *Proceedings of the National Academy of Sciences of the United States of America*, *107*(43), 18551–18556.

Grosskopf, T., & Soyer, O. S. (2014). Synthetic microbial communities. *Current opinion in microbiology*, *18*, 72–77.

Grote, A., Hiller, K., Scheer, M., Munch, R., Nortemann, B., Hempel, D. C., & Jahn, D. (2005). JCat: a novel tool to adapt codon usage of a target gene to its potential expression host. *Nucleic Acids Research*, *33*, 526–531.

Haber, J. E. (2012). Mating-Type genes and MAT switching in *Saccharomyces cerevisiae*. *Genetics*, *191*(1), 33–64.

Hagen, D. C., McCaffrey, G., & Sprague, G. F. (1986). Evidence the yeast *STE3* gene encodes a receptor for the peptide pheromone a factor: gene sequence and implications for the structure of the presumed receptor. *Proceedings of the National Academy of Sciences*, *83*(5), 1418–1422.

Hansen, E. H., Møller, B. L., Kock, G. R., Bünner, C. M., Kristensen, C., Jensen, O. R., Okkels, F. T., Olsen, C. E., Motawia, M. S., & Hansen, J. (2009). De novo biosynthesis of vanillin in fission yeast (*Schizosaccharomyces pombe*) and baker's yeast (*Saccharomyces cerevisiae*). *Applied and Environmental Microbiology*, *75*(9), 2765–2774.

Hardin, G. (1968). The tragedy of the commons. *Science*, *162*(3859), 1243–1248.

Harrison, F., & Buckling, A. (2005). Hypermutability impedes cooperation in pathogenic bacteria. *Current Biology*, *15*(21), 1968–1971.

Hartmann, M., Schneider, T. R., Pfeil, A., Heinrich, G., Lipscomb, W. N., & Braus, G. H. (2003). Evolution of feedback-inhibited / barrel isoenzymes by gene duplication and a single mutation. *Proceedings of the National Academy of Sciences*, *100*(3), 862–867.

Haselbeck, R. J., & McAlister-Henn, L. (1991). Isolation, nucleotide sequence, and disruption of the *Saccharomyces cerevisiae* gene encoding mitochondrial NADP(H)-specific isocitrate dehydrogenase. *The Journal of Biological Chemistry*, *266*(4), 2339–2345.

Haselbeck, R. J., & McAlister-Henn, L. (1993). Function and expression of yeast mitochondrial NAD- and NADP-specific isocitrate dehydrogenases. *The Journal of Biological Chemistry*, *268*(16), 12116–12122.

Hassing, E.-J., Groot, P. A., Marquenie, V. R., Pronk, J. T., & Daran, J.-M. G. (2019). Connecting central carbon and aromatic amino acid metabolisms to improve de novo 2-phenylethanol production in *Saccharomyces cerevisiae*. *Metabolic engineering*, *56*, 165–180.

Hazelwood, L. A., Daran, J.-M., van Maris, A. J. A., Pronk, J. T., & Dickinson, J. R. (2008). The Ehrlich Pathway for fusel alcohol production: a century of research on *Saccharomyces cerevisiae* metabolism. *Applied and Environmental Microbiology*, *74*(8), 2259–2266.

Henderson, R. K., Fendler, K., & Poolman, B. (2019). Coupling efficiency of secondary active transporters. *Current Opinion in Biotechnology*, *58*, 62–71.

Hinnebusch, A. G. (2005). Translational regulation of Gcn4 and the general amino acid control of yeast. *Annual Review of Microbiology*, *59*(1), 407–450.

Hitzeman, R. A., Clarke, L., & Carbon, J. (1980). Isolation and characterization of the yeast 3-phosphoglycerokinase gene (*PGK*) by an immunological screening technique. *The Journal of Biological Chemistry*, *255*(24), 12073–12080.

Ho, P.-W., Swinnen, S., Duitama, J., & Nevoigt, E. (2017). The sole introduction of two single-point mutations establishes glycerol utilization in *Saccharomyces cerevisiae* CEN.PK derivatives. *Biotechnology for Biofuels*, *10*, 10.

Hohmann, S. (1991). Characterization of *PDC6*, a third structural gene for pyruvate decarboxylase in *Saccharomyces cerevisiae*. *Journal of Bacteriology*, *173*(24), 7963–7969.

Hong, J., & Gresham, D. (2014). Molecular specificity, convergence and constraint shape adaptive evolution in nutrient-poor environments (J. C. Fay, Ed.). *PLoS Genetics*, *10*(1), e1004041.

Hong, Y., Pasternak, J. J., & Glick, B. R. (1991). Biological consequences of plasmid transformation of the plant growth promoting rhizobacterium *Pseudomonas putida GR12-2*. *Canadian Journal of Microbiology*, *37*(10), 796–799.

Hou, J., Tyo, K. E., Liu, Z., Petranovic, D., & Nielsen, J. (2012). Metabolic engineering of recombinant protein secretion by *Saccharomyces cerevisiae*. *FEMS Yeast Research*, *12*(5), 491–510.

Hummert, S., Bohl, K., Basanta, D., Deutsch, A., Werner, S., Theissen, G., Schroeter, A., & Schuster, S. (2014). Evolutionary game theory: cells as players. *Molecular bioSystems*, *10*(12), 3044–3065.

Iraqui, I., Vissers, S., Cartiaux, M., & Urrestarazu, A. (1998). Characterisation of *Saccharomyces cerevisiae ARO8* and *ARO9* genes encoding aromatic aminotransferases I and II reveals a new aminotransferase subfamily. *Molecular and General Genetics MGG*, *257*(2), 238–248.

Iraqui, I., Vissers, S., André, B., & Urrestarazu, A. (1999). Transcriptional induction by aromatic amino acids in *Saccharomyces cerevisiae*. *Molecular and Cellular Biology*, *19*(5), 3360–3371.

Isogai, S., Matsushita, T., Imanishi, H., Koonthongkaew, J., Toyokawa, Y., Nishimura, A., Yi, X., Kazlauskas, R., & Takagi, H. (2021). High-level production of lysine in the yeast *Saccharomyces cerevisiae* by rational design of homocitrate synthase. *Applied and Environmental Microbiology*, *87*(15), e00600–21.

Ivashov, V., Zimmer, J., Schwabl, S., Kahlhofer, J., Weys, S., Gstir, R., Jakschitz, T., Kremser, L., Bonn, G. K., Lindner, H., Huber, L. A., Leon, S., Schmidt, O., & Teis, D. (2020). Complementary α-arrestin-ubiquitin ligase complexes control nutrient transporter endocytosis in response to amino acids. *eLife*, *9*.

Jagtap, S. S., Bedekar, A. A., & Rao, C. V. (2020, January). Quorum sensing in yeast. In S. S. Dhiman (Ed.), *Acs symposium series* (pp. 235–250, Vol. 1374). American Chemical Society.

Jakočiūnas, T., Rajkumar, A. S., Zhang, J., Arsovska, D., Rodriguez, A., Jendresen, C. B., Skjødt, M. L., Nielsen, A. T., Borodina, I., Jensen, M. K., & Keasling, J. D. (2015). CasEMBLR: Cas9-facilitated multiloci genomic integration of in vivo assembled DNA parts in *Saccharomyces cerevisiae*. *ACS synthetic biology*, *4*(11), 1226–1234.

Jauniaux, J.-C., & Grenson, M. (1990). *Gap1*, the general amino acid permease gene of *saccharomyces cerevisiae*. *European Journal of Biochemistry*, *190*(1), 39–44.

Jawed, K., Yazdani, S. S., & Koffas, M. A. (2019). Advances in the development and application of microbial consortia for metabolic engineering. *Metabolic engineering communications*, *9*, 00095.

Jones, D. G., Reusser, U., & Braus, G. H. (1991). Molecular cloning, characterization and analysis of the regulation of the *ARO2* gene, encoding chorismate synthase, of *Saccharomyces cerevisiae*. *Molecular Microbiology*, *5*(9), 2143–2153.

Jones, E. E., & Broquist, H. P. (1966). Saccharopine, an intermediate of the aminoadipic acid pathway of lysine biosynthesis. *Journal of Biological Chemistry*, *241*(14), 3430–3434.

Jones, J. A., & Koffas, M. A. G. (2016, January 1). Chapter eight - optimizing metabolic pathways for the improved production of natural products. In S. E. O'Connor (Ed.), *Methods in enzymology* (pp. 179–193, Vol. 575). Academic Press.

Jones, J. A., Vernacchio, V. R., Sinkoe, A. L., Collins, S. M., Ibrahim, M. H. A., Lachance, D. M., Hahn, J., & Koffas, M. A. G. (2016). Experimental and computational optimization of an *Escherichia coli* co-culture for the efficient production of flavonoids. *Metabolic Engineering*, *35*, 55–63.

Jordan, I. K., & McDonald, J. F. (1999). Tempo and mode of Ty element evolution in *Saccharomyces cerevisiae*. *Genetics*, *151*(4), 1341–1351.

Kanda, N., & Abe, F. (2013). Structural and functional implications of the yeast high-affinity tryptophan permease Tat2. *Biochemistry*, *52*(25), 4296–4307.

Kaniak, A., Xue, Z., Macool, D., Kim, J.-H., & Johnston, M. (2004). Regulatory network connecting two glucose signal transduction pathways in *Saccharomyces cerevisiae*. *Eukaryotic Cell*, *3*(1), 221–231.

Kapetanakis, G. C., Gournas, C., Prévost, M., Georis, I., & André, B. (2021). Overlapping roles of yeast transporters Aqr1, Qdr2, and Qdr3 in amino acid excretion and cross-feeding of lactic acid bacteria. *Frontiers in Microbiology*, *12*.

Kapetanakis, G. C., Sousa, L. S., Felten, C., Mues, L., Gabant, P., Van Nedervelde, L., Georis, I., & André, B. (2023). Deletion of *QDR* genes in a bioethanol-producing yeast strain reduces propagation of contaminating lactic acid bacteria. *Scientific Reports*, *13*(1), 4986.

Karsten, W. E., Reyes, Z. L., Bobyk, K. D., Cook, P. F., & Chooback, L. (2011). Mechanism of the aromatic aminotransferase encoded by the *ARO8* gene from *Saccharomyces cerevisiae*. *Archives of Biochemistry and Biophysics*, *516*(1), 67–74.

Kawakami, K., Shafer, B. K., Garfinkel, D. J., Strathern, J. N., & Nakamura, Y. (1992). Ty element-induced temperature-sensitive mutations of *Saccharomyces cerevisiae*. *Genetics*, *131*(4), 821–832.

Keller, L., & Surette, M. G. (2006). Communication in bacteria: an ecological and evolutionary perspective. *Nature Reviews Microbiology*, *4*(4), 249–258.

Kellermann, E., Seeboth, P. G., & Hollenberg, C. P. (1986). Analysis of the primary structure and promoter function of a pyruvate decarbozylase gene (*PDCI*) from *Saceharomyces cerevisiae*. *Nucleic Acids Research*, *14*(22), 8963–8977.

Kennedy, E. J., Pillus, L., & Ghosh, G. (2005). Pho5p and newly identified nucleotide pyrophosphatases/ phosphodiesterases regulate extracellular nucleotide phosphate metabolism in *Saccharomyces cerevisiae*. *Eukaryotic Cell*, *4*(11), 1892–1901.

Kerner, A., Park, J., Williams, A., & Lin, X. N. (2012). A programmable *Escherichia coli* consortium via tunable symbiosis. *PLOS ONE*, *7*(3), e34032.

Kim, K.-S., Rosenkrantz, M. S., & Guarente, L. (1986). *Saccharomyces cerevisiae* contains two functional citrate synthase genes. *Molecular and Cellular Biology*, *6*(6), 1936–1942.

Kirchner, O., & Tauch, A. (2003). Tools for genetic engineering in the amino acid-producing bacterium *Corynebacterium glutamicum*. *Journal of Biotechnology*, *104*(1-3), 287–299.

Kneen, M. M., Stan, R., Yep, A., Tyler, R. P., Saehuan, C., & McLeish, M. J. (2011). Characterization of a thiamin diphosphate-dependent phenylpyruvate decarboxylase from *Saccharomyces cerevisiae*: Characterization of phenylpyruvate decarboxylase. *FEBS Journal*, *278*(11), 1842–1853.

Konstantinidis, D., Pereira, F., Geissen, E.-M., Grkovska, K., Kafkia, E., Jouhten, P., Kim, Y., Devendran, S., Zimmermann, M., & Patil, K. R. (2021). Adaptive laboratory evolution of microbial co-cultures for improved metabolite secretion. *Molecular systems biology*, *17*(8), 10189.

Koszul, R., Caburet, S., Dujon, B., & Fischer, G. (2004). Eucaryotic genome evolution through the spontaneous duplication of large chromosomal segments. *The EMBO Journal*, *23*(1), 234–243.

Kraines, D. P., & Kraines, V. Y. (2000). Natural selection of memory-one strategies for the iterated prisoner's dilemma. *Journal of theoretical biology*, *203*(4), 335–355.

Kumar, C., Sharma, R., & Bachhawat, A. K. (2003). Utilization of glutathione as an exogenous sulfur source is independent of γ-glutamyl transpeptidase in the yeast *Saccharomyces cerevisiae*: evidence for an alternative gluathione degradation pathway. *FEMS Microbiology Letters*, *219*(2), 187–194.

Landrieu, I., Vandenbol, M., Härtlein, M., & Portetelle, D. (1997). Mitochondria1 asparaginyl-tRNA synthetase encoded by the yeast nuclear gene YCR24c. *European Journal of Biochemistry*, *243*(1-2), 268–273.

Lauwers, E., Erpapazoglou, Z., Haguenauer-Tsapis, R., & André, B. (2010). The ubiquitin code of yeast permease trafficking. *Trends in Cell Biology*, *20*(4), 196–204.

Leavitt, J. M., Wagner, J. M., Tu, C. C., Tong, A., Liu, Y., & Alper, H. S. (2017). Biosensor-enabled directed evolution to improve muconic acid production in *Saccharomyces cerevisiae*. *Biotechnology Journal*, *12*(10), 1600687.

Lee, C. R., Kim, C., Song, Y. E., Im, H., Oh, Y.-K., Park, S., & Kim, J. R. (2018). Co-culture-based biological carbon monoxide conversion by *Citrobacter amalonaticus Y19* and *Sporomusa ovata* via a reducing-equivalent transfer mediator. *Bioresource Technology*, *259*, 128–135.

Lee, H.-N., Shin, W.-S., Seo, S.-Y., Choi, S.-S., Song, J.-S., Kim, J.-Y., Park, J.-H., Lee, D., Kim, S. Y., Lee, S. J., Chun, G.-T., & Kim, E.-S. (2018). Corynebacterium cell factory design and culture process optimization for muconic acid biosynthesis. *Scientific reports*, *8*(1), 18041.

Lee, M. E., DeLoache, W. C., Cervantes, B., & Dueber, J. E. (2015). A highly characterized yeast toolkit for modular, multipart assembly. *ACS synthetic biology*, *4*(9), 975–986.

Lee, S. Y., & Kim, H. U. (2015). Systems strategies for developing industrial microbial strains. *Nature Biotechnology*, *33*(10), 1061–1072.

Lee, S., Ho, H.-C., Tumolo, J. M., Hsu, P.-C., & MacGurn, J. A. (2019). Methionine triggers Ppz-mediated dephosphorylation of Art1 to promote cargo-specific endocytosis. *Journal of Cell Biology*, *218*(3), 977–992.

Lee, S., & Kim, P. (2020). Current status and applications of adaptive laboratory evolution in industrial microorganisms. *Journal of Microbiology and Biotechnology*, *30*(6), 793–803.

Li, M., & Borodina, I. (2015). Application of synthetic biology for production of chemicals in yeast *Saccharomyces cerevisiae*. *FEMS yeast research*, *15*(1), 1–12.

Li, Z., Wang, X., & Zhang, H. (2019). Balancing the non-linear rosmarinic acid biosynthetic pathway by modular co-culture engineering. *Metabolic Engineering*, *54*, 1–11.

Liao, M. J., Din, M. O., Tsimring, L., & Hasty, J. (2019). Rock-paper-scissors: Engineered population dynamics increase genetic stability. *Science (New York, N.Y.)*, *365*(6457), 1045–1049.

Lilja, E. E., & Johnson, D. R. (2016). Segregating metabolic processes into different microbial cells accelerates the consumption of inhibitory substrates. *The ISME Journal*, *10*(7), 1568–1578.

Lin, C. H., MacGurn, J. A., Chu, T., Stefan, C. J., & Emr, S. D. (2008). Arrestin-related ubiquitin-ligase adaptors regulate endocytosis and protein turnover at the cell surface. *Cell*, *135*(4), 714–725.

Lindemann, S. R., Bernstein, H. C., Song, H.-S., Fredrickson, J. K., Fields, M. W., Shou, W., Johnson, D. R., & Beliaev, A. S. (2016). Engineering microbial consortia for controllable outputs. *The ISME journal*, *10*(9), 2077–2084.

Lindsay, R. J., Pawlowska, B. J., & Gudelj, I. (2018). When increasing population density can promote the evolution of metabolic cooperation. *The ISME journal*, *12*(3), 849–859.

Liu, Q., Zhang, J., Wei, X.-X., Ouyang, S.-P., Wu, Q., & Chen, G.-Q. (2008). Microbial production of l-glutamate and l-glutamine by recombinant Corynebacterium glutamicum harboring Vitreoscilla hemoglobin gene vgb. *Applied Microbiology and Biotechnology*, *77*(6), 1297–1304.

Liu, Y., Tu, X., Xu, Q., Bai, C., Kong, C., Liu, Q., Yu, J., Peng, Q., Zhou, X., Zhang, Y., & Cai, M. (2018). Engineered monoculture and co-culture of methylotrophic yeast for de novo production of monacolin J and lovastatin from methanol. *Metabolic engineering*, *45*, 189–199.

Lobo, Z. (1984). *Saccharomyces cerevisiae* aldolase mutants. *Journal of Bacteriology*, *160*(1), 222–226.

Lobo, Z., & Maitra, P. K. (1982). Pentose phosphate pathway mutants of yeast. *Molecular & general genetics: MGG*, *185*(2), 367–368.

Loewith, R., & Hall, M. N. (2011). Target of Rapamycin (TOR) in nutrient signaling and growth control. *Genetics*, *189*(4), 1177–1201.

Lõoke, M., Kristjuhan, K., & Kristjuhan, A. (2011). Extraction of genomic DNA from yeasts for PCR-based applications. *BioTechniques*, *50*(5), 325–328.

Louie, G. V., Bowman, M. E., Moffitt, M. C., Baiga, T. J., Moore, B. S., & Noel, J. P. (2006). Structural determinants and modulation of substrate specificity in phenylalanine-tyrosine ammonia-lyases. *Chemistry & Biology*, *13*(12), 1327–1338.

Lu, Y.-M., Lin, Y.-R., Tsai, A., Hsao, Y.-S., Li, C.-C., & Cheng, M. Y. (2003). Dissecting the pet18 mutation in *Saccharomyces cerevisiae*: HTL1 encodes a 7-kDa polypeptide that interacts with components of the RSC complex. *Molecular genetics and genomics: MGG*, *269*(3), 321–330.

Luo, X., Reiter, M. A., d'Espaux, L., Wong, J., Denby, C. M., Lechner, A., Zhang, Y., Grzybowski, A. T., Harth, S., Lin, W., Lee, H., Yu, C., Shin, J., Deng, K., Benites, V. T., Wang, G., Baidoo, E. E. K., Chen, Y., Dev, I., . . . Keasling, J. D. (2019). Complete biosynthesis of cannabinoids and their unnatural analogues in yeast. *Nature*, *567*(7746), 123–126.

Luttik, M., Vuralhan, Z., Suir, E., Braus, G., Pronk, J., & Daran, J. (2008). Alleviation of feedback inhibition in *Saccharomyces cerevisiae* aromatic amino acid biosynthesis: Quantification of metabolic impact. *Metabolic Engineering*, *10*(3-4), 141–153.

Lyu, X., Zhao, G., Ng, K. R., Mark, R., & Chen, W. N. (2019). Metabolic engineering of *Saccharomyces cerevisiae* for de novo production of kaempferol. *Journal of Agricultural and Food Chemistry*, *67*(19), 5596–5606.

MacGurn, J. A., Hsu, P.-C., & Emr, S. D. (2012). Ubiquitin and membrane protein turnover: from cradle to grave. *Annual Review of Biochemistry*, *81*(1), 231–259.

MacGurn, J. A., Hsu, P.-C., Smolka, M. B., & Emr, S. D. (2011). TORC1 regulates endocytosis via Npr1-mediated phosphoinhibition of a ubiquitin ligase adaptor. *Cell*, *147*(5), 1104–1117.

MacLean, R. C., & Gudelj, I. (2006). Resource competition and social conflict in experimental populations of yeast. *Nature*, *441*(7092), 498–501.

Mafakher, L., Mirbagheri, M., Darvishi, F., Nahvi, I., Zarkesh-Esfahani, H., & Emtiazi, G. (2010). Isolation of lipase and citric acid producing yeasts from agro-industrial wastewater. *New Biotechnology*, *27*(4), 337–340.

Maftahi, M., Nicaud, J. M., Levesque, H., & Gaillardin, C. (1995). Sequencing analysis of a 24.7 kb fragment of yeast chromosome XIV identifies six known genes, a new member of the hexose transporter family and ten new open reading frames. *Yeast (Chichester, England)*, *11*(11), 1077–1085.

Mannhaupt, G., Stucka, R., Pilz, U., Schwarzlose, C., & Feldmann, H. (1989). Characterization of the prephenate dehydrogenase-encoding gene, *TYR1*, from *Saccharomyces cerevisiae*. *Gene*, *85*(2), 303–311.

Mao, J., Liu, Q., Li, Y., Yang, J., Song, X., Liu, X., Xu, H., & Qiao, M. (2018). A high-throughput method for screening of L-tyrosine high-yield strains by *Saccharomyces cerevisiae*. *The Journal of general and applied microbiology*, *64*(4), 198–201.

Maragoudakis, M. E., Holmes, H., & Strassman, M. (1967). Control of lysine biosynthesis in yeast by a feedback mechanism. *Journal of Bacteriology*, *93*(5), 1677–1680.

McAlister, L., & Holland, M. J. (1982). Targeted deletion of a yeast enolase structural gene. Identification and isolation of yeast enolase isozymes. *The Journal of Biological Chemistry*, *257*(12), 7181–7188.

McAlister, L., & Holland, M. J. (1985). Isolation and characterization of yeast strains carrying mutations in the glyceraldehyde-3-phosphate dehydrogenase genes. *The Journal of Biological Chemistry*, *260*(28), 15013–15018.

McCarty, N. S., & Ledesma-Amaro, R. (2019). Synthetic biology tools to engineer microbial communities for biotechnology. *Trends in biotechnology*, *37*(2), 181–197.

Minard, K. I., & McAlister-Henn, L. (2005). Sources of NADPH in yeast vary with carbon source. *Journal of Biological Chemistry*, *280*(48), 39890–39896.

Minty, J. J., Singer, M. E., Scholz, S. A., Bae, C. H., Ahn, J. H., Foster, C. E., Liao, J. C., & Lin, X. N. (2013). Design and characterization of synthetic fungal-bacterial consortia for direct production of isobutanol from cellulosic biomass. *Proceedings of the National Academy of Sciences of the United States of America*, *110*(36), 14592–14597.

Miosga, T., & Zimmermann, F. K. (1996). Cloning and characterization of the first two genes of the non-oxidative part of the *Saccharomyces cerevisiae* pentose-phosphate pathway. *Current Genetics*, *30*(5), 404–409.

Mira, N. P., Lourenço, A. B., Fernandes, A. R., Becker, J. D., & Sá-Correia, I. (2009). The RIM101 pathway has a role in *Saccharomyces cerevisiae* adaptive response and resistance to propionic acid and other weak acids. *FEMS yeast research*, *9*(2), 202–216.

Momeni, B., Waite, A. J., & Shou, W. (2013). Spatial self-organization favors heterotypic cooperation over cheating. *eLife*, *2*, e00960.

Moye, W. S., & Zalkin, H. (1985). Deletion mapping the yeast *TRP5* control region. *The Journal of Biological Chemistry*, *260*(8), 4718–4723.

Mülleder, M., Campbell, K., Matsarskaia, O., Eckerstorfer, F., & Ralser, M. (2016). *Saccharomyces cerevisiae* single-copy plasmids for auxotrophy compensation, multiple marker selection, and for designing metabolically cooperating communities. *F1000Research*, *5*, 2351.

Müller, M., Schmidt, O., Angelova, M., Faserl, K., Weys, S., Kremser, L., Pfaffenwimmer, T., Dalik, T., Kraft, C., Trajanoski, Z., Lindner, H., & Teis, D. (2015). The coordinated action of the MVB pathway and autophagy ensures cell survival during starvation. *eLife*, *4*, e07736.

Müller, M. J. I., Neugeboren, B. I., Nelson, D. R., & Murray, A. W. (2014). Genetic drift opposes mutualism during spatial population expansion. *Proceedings of the National Academy of Sciences of the United States of America*, *111*(3), 1037–1042.

Naseeb, S., Ames, R. M., Delneri, D., & Lovell, S. C. (2017). Rapid functional and evolutionary changes follow gene duplication in yeast. *Proceedings of the Royal Society B: Biological Sciences*, *284*(1861), 20171393.

Nash, J. F. (1950). Equilibrium points in n-person games. *Proceedings of the National Academy of Sciences*, *36*(1), 48–49.

Natarajan, K., Meyer, M. R., Jackson, B. M., Slade, D., Roberts, C., Hinnebusch, A. G., & Marton, M. J. (2001). Transcriptional profiling shows that Gcn4p is a master regulator of gene expression during amino acid starvation in yeast. *Molecular and Cellular Biology*, *21*(13), 4347–4368.

Nijkamp, J. F., Van Den Broek, M., Datema, E., De Kok, S., Bosman, L., Luttik, M. A., Daran-Lapujade, P., Vongsangnak, W., Nielsen, J., Heijne, W. H., Klaassen, P., Paddon, C. J., Platt, D., Kötter, P., Van Ham, R. C., Reinders, M. J., Pronk, J. T., De Ridder, D., & Daran, J.-M. (2012). De novo sequencing, assembly and analysis of the genome of the laboratory strain *Saccharomyces cerevisiae* CEN.PK113-7D, a model for modern industrial biotechnology. *Microbial Cell Factories*, *11*(1), 36.

Nikko, E., & Pelham, H. R. B. (2009). Arrestin-mediated endocytosis of yeast plasma membrane transporters. *Traffic*, *10*(12), 1856–1867.

Nikko, E., Sullivan, J. A., & Pelham, H. R. B. (2008). Arrestin-like proteins mediate ubiquitination and endocytosis of the yeast metal transporter Smf1. *EMBO reports*, *9*(12), 1216–1221.

Nogae, I., & Johnston, M. (1990). Isolation and characterization of the *ZWF1* gene of *Saccharomyces cerevisiae*, encoding glucose-6-phosphate dehydrogenase. *Gene*, *96*(2), 161–169.

Nowrouzi, B., Li, R. A., Walls, L. E., d'Espaux, L., Malcı, K., Liang, L., Jonguitud-Borrego, N., Lerma-Escalera, A. I., Morones-Ramirez, J. R., Keasling, J. D., & Rios-Solis, L. (2020). Enhanced production of taxadiene in *Saccharomyces cerevisiae*. *Microbial Cell Factories*, *19*(1), 200.

O'Donnell, A. F., & Schmidt, M. C. (2019). AMPK-mediated regulation of alpha-arrestins and protein trafficking. *International Journal of Molecular Sciences*, *20*(3), 515.

Ogawa, H., & Fujioka, M. (1978). Purification and characterization of saccharopine dehydrogenase from baker's yeast. *The Journal of Biological Chemistry*, *253*(10), 3666–3670.

Omura, F., Hatanaka, H., & Nakao, Y. (2007). Characterization of a novel tyrosine permease of lager brewing yeast shared by *Saccharomyces cerevisiae* strain RM11-1a. *FEMS Yeast Research*, *7*(8), 1350–1361.

Osiro, K. O., Borgström, C., Brink, D. P., Fjölnisdóttir, B. L., & Gorwa-Grauslund, M. F. (2019). Exploring the xylose paradox in *Saccharomyces cerevisiae* through in vivo sugar signalomics of targeted deletants. *Microbial Cell Factories*, *18*(1), 88.

Otero, J. M., Cimini, D., Patil, K. R., Poulsen, S. G., Olsson, L., & Nielsen, J. (2013). Industrial systems biology of *Saccharomyces cerevisiae* enables novel succinic acid cell factory. *PLOS ONE*, *8*(1), e54144.

Oud, B., Guadalupe-Medina, V., Nijkamp, J. F., Ridder, D., Pronk, J. T., van Maris, A. J. A., & Daran, J.-M. (2013). Genome duplication and mutations in *ACE2* cause multicellular, fast-sedimenting phenotypes in evolved *Saccharomyces cerevisiae*. *Proceedings of the National Academy of Sciences of the United States of America*, *110*(45), 4223–4231.

Padder, S. A., Prasad, R., & Shah, A. H. (2018). Quorum sensing: A less known mode of communication among fungi. *Microbiological Research*, *210*, 51–58.

Paluh, J. L., & Zalkin, H. (1983). Isolation of *Saccharomyces cerevisiae TRP3*. *Journal of Bacteriology*, *153*(1), 345–349.

Panaretou, B., & Piper, P. W. (1992). The plasma membrane of yeast acquires a novel heat-shock protein (hsp30) and displays a decline in proton-pumping ATPase levels in response to both heat shock and the entry to stationary phase. *European Journal of Biochemistry*, *206*(3), 635–640.

Panchaud, N., Péli-Gulli, M.-P., & De Virgilio, C. (2013a). Amino acid deprivation inhibits TORC1 through a GTPase-Activating protein complex for the Rag family GTPase Gtr1. *Science Signaling*, *6*(277).

Panchaud, N., Péli-Gulli, M.-P., & De Virgilio, C. (2013b). SEACing the GAP that nEGOCiates TORC1 activation. *Cell Cycle*, *12*(18), 2948–2952.

Papapetridis, I., Verhoeven, M. D., Wiersma, S. J., Goudriaan, M., van Maris, A. J. A., & Pronk, J. T. (2018). Laboratory evolution for forced glucose-xylose co-consumption enables identification of mutations that improve mixed-sugar fermentation by xylose-fermenting *Saccharomyces cerevisiae*. *FEMS Yeast Research*, *18*(6).

Papp, B., Pál, C., & Hurst, L. D. (2003). Dosage sensitivity and the evolution of gene families in yeast. *Nature*, *424*(6945), 194–197.

Pearce, A. K., Crimmins, K., Groussac, E., Hewlins, M. J. E., Dickinson, J. R., Francois, J., Booth, I. R., & Brown, A. J. P. (2001). Pyruvate kinase (Pyk1) levels influence both the rate and direction of carbon flux in yeast under fermentative conditions. *Microbiology*, *147*(2), 391–401.

Péli-Gulli, M.-P., Sardu, A., Panchaud, N., Raucci, S., & De Virgilio, C. (2015). Amino acids stimulate TORC1 through Lst4-Lst7, a GTPase-activating protein complex for the Rag family GTPase Gtr2. *Cell Reports*, *13*(1), 1–7.

Piper, Peter. W., Ortiz-Calderon, C., Holyoak, C., Coote, P., & Cole, M. (1997). Hsp30, the integral plasma membrane heat shock protein of *Saccharomyces cerevisiae*, is a stress-inducible regulator of plasma membrane H+-ATPase. *Cell Stress & Chaperones*, *2*(1), 12–24.

Piškur, J., & Compagno, C. (Eds.). (2014). *Molecular mechanisms in yeast carbon metabolism*. Springer.

Polevoda, B., & Sherman, F. (2001). NatC Nα-terminal acetyltransferase of yeast contains three subunits, Mak3p, Mak10p, and Mak31p. *Journal of Biological Chemistry*, *276*(23), 20154–20159.

Portnoy, V. A., Bezdan, D., & Zengler, K. (2011). Adaptive laboratory evolution—harnessing the power of biology for metabolic engineering. *Current Opinion in Biotechnology*, *22*(4), 590–594.

Prantl, F., Strasser, A., Aebi, M., Furter, R., Niederberger, P., Kirschner, K., & Huetter, R. (1985). Purification and characterization of the indole-3-glycerolphosphate synthase/anthranilate synthase complex of *Saccharomyces cerevisiae*. *European Journal of Biochemistry*, *146*(1), 95–100.

Pronk, J. T., YDE STEENSMA, H., & van DIJKEN, J. P. (1996). Pyruvate metabolism in *Saccharomyces cerevisiae*. *Yeast (Chichester, England)*, *12*(16), 1607–1633.

Putnam, C. D., Pennaneach, V., & Kolodner, R. D. (2005). *Saccharomyces cerevisiae* as a model system to define the chromosomal instability phenotype. *Molecular and Cellular Biology*, *25*(16), 7226–7238.

Quevillon-Cheruel, S., Leulliot, N., Meyer, P., Graille, M., Bremang, M., Blondeau, K., Sorel, I., Poupon, A., Janin, J., & van Tilbeurgh, H. (2004). Crystal structure of the bifunctional chorismate synthase from *Saccharomyces cerevisiae*. *The Journal of Biological Chemistry*, *279*(1), 619–625.

Ramos, F., Dubois, E., & Pierard, A. (1988). Control of enzyme synthesis in the lysine biosynthetic pathway of *Saccharomyces cerevisiae*. Evidence for a regulatory role of gene *LYS14*. *European Journal of Biochemistry*, *171*(1-2), 171–176.

Ramos, F., Verhasselt, P., Feller, A., Peeters, P., Wach, A., Dubois, E., & Volckaert, G. (1996). Identification of a gene encoding a homocitrate synthase isoenzyme of *Saccharomyces cerevisiae*. *Yeast*, *12*(13), 1315–1320.

Regenberg, B., Düring-Olsen, L., Kielland-Brandt, M. C., & Holmberg, S. (1999). Substrate specificity and gene expression of the amino-acid permeases in *Saccharomyces cerevisiae*. *Current Genetics*, *36*(6), 317–328.

Reifenrath, M., Bauer, M., Oreb, M., & Boles, E. (2018). Bacterial bifunctional chorismate mutase-prephenate dehydratase PheA increases flux into the yeast phenylalanine pathway and improves mandelic acid production. *Metabolic engineering communications*, *7*, 00079.

Reifenrath, M., & Boles, E. (2018). Engineering of hydroxymandelate synthases and the aromatic amino acid pathway enables de novo biosynthesis of mandelic and 4-hydroxymandelic acid with *Saccharomyces cerevisiae*. *Metabolic engineering*, *45*, 246–254.

Risinger, A. L., Cain, N. E., Chen, E. J., & Kaiser, C. A. (2006). Activity-dependent reversible inactivation of the general amino acid permease (D. Drubin, Ed.). *Molecular Biology of the Cell*, *17*(10), 4411–4419.

Rodicio, R., Heinisch, J. J., & Hollenberg, C. P. (1993). Transcriptional control of yeast phosphoglycerate mutase-encoding gene. *Gene*, *125*(2), 125–133.

Rodriguez, A., Kildegaard, K. R., Li, M., Borodina, I., & Nielsen, J. (2015). Establishment of a yeast platform strain for production of p-coumaric acid through metabolic engineering of aromatic amino acid biosynthesis. *Metabolic engineering*, *31*, 181–188.

Rodriguez-Amaya, D. B. (2019). Betalains. In *Encyclopedia of food chemistry* (pp. 35–39). Elsevier.

Romeo, M. J., Angus-Hill, M. L., Sobering, A. K., Kamada, Y., Cairns, B. R., & Levin, D. E. (2002). *Htl1* encodes a novel factor that interacts with the rsc chromatin remodeling complex in *saccharomyces cerevisiae*. *Molecular and Cellular Biology*, *22*(23), 8165–8174.

Roy, N., Lapierre, H., & Bernier, J. F. (2000). Whole-body protein metabolism and plasma profiles of amino acids and hormones in growing barrows fed diets adequate or deficient in lysine. *Canadian Journal of Animal Science*, *80*(4), 585–595.

Sabina, J., & Johnston, M. (2009). Asymmetric signal transduction through paralogs that comprise a genetic switch for sugar sensing in *Saccharomyces cerevisiae*. *The Journal of Biological Chemistry*, *284*(43), 29635–29643.

Sáenz, D. A., Chianelli, M. S., & Stella, C. A. (2014). L-phenylalanine transport in *Saccharomyces cerevisiae*: participation of *GAP1, BAP2,* and *AGP1*. *Journal of Amino Acids*, *2014*, e283962.

Sagisaka, S., & Shimura, K. (1962). A method for the quanitative determination of dehydropiperidine carboxylic acid, a reduction product of alpha-aminoadipic acid by yeast enzyme. *Journal of Biochemistry*, *51*, 27–31.

Sahm, H., Eggeling, L., & de Graaf, A. A. (2000). Pathway analysis and metabolic engineering in *Corynebacterium glutamicum*. *Biological Chemistry*, *381*(9-10), 899–910.

Saini, M., Hong Chen, M., Chiang, C.-J., & Chao, Y.-P. (2015). Potential production platform of n-butanol in *Escherichia coli*. *Metabolic Engineering*, *27*, 76–82.

Salazar, A. N., Gorter de Vries, A. R., van den Broek, M., Wijsman, M., La Torre Cortés, P., Brickwedde, A., Brouwers, N., Daran, J.-M. G., & Abeel, T. (2017). Nanopore sequencing enables near-complete de novo assembly of *Saccharomyces cerevisiae* reference strain CEN.PK113-7D. *FEMS Yeast Research*, *17*(7).

Sanchez, A., Alvaro Sanchez, & Gore, J. (2013). Feedback between population and evolutionary dynamics determines the fate of social microbial populations. *arXiv: Populations and Evolution*
MAG ID: 2949862181.

Schaaff, I., Hohmann, S., & Zimmermann, F. K. (1990). Molecular analysis of the structural gene for yeast transaldolase. *European Journal of Biochemistry*, *188*(3), 597–603.

Schmidt, A., Hall, M. N., & Koller, A. (1994). Two FK506 resistance-conferring genes in *Saccharomyces cerevisiae*, *TAT1* and *TAT2*, encode amino acid permeases mediating tyrosine and tryptophan uptake. *Molecular and Cellular Biology*, *14*(10), 6597–6606.

Schnappauf, G., Hartmann, M., Künzler, M., & Braus, G. H. (1998). The two 3-deoxy-D-arabino-heptulosonate-7-phosphate synthase isoenzymes from *Saccharomyces cerevisiae* show different kinetic modes of inhibition. *Archives of microbiology*, *169*(6), 517–524.

Schrader, J., Schilling, M., Holtmann, D., Sell, D., Filho, M. V., Marx, A., & Vorholt, J. A. (2009). Methanol-based industrial biotechnology: current status and future perspectives of methylotrophic bacteria. *Trends in Biotechnology*, *27*(2), 107–115.

Schuster, S., Kreft, J.-U., Schroeter, A., & Pfeiffer, T. (2008). Use of game-theoretical methods in biochemistry and biophysics. *Journal of Biological Physics*, *34*(1-2), 1–17.

Seeboth, P. G., Bohnsack, K., & Hollenberg, C. P. (1990). pdc1(0) mutants of *Saccharomyces cerevisiae* give evidence for an additional structural *PDC* gene: cloning of *PDC5*, a gene homologous to *PDC1*. *Journal of Bacteriology*, *172*(2), 678–685.

Sgobba, E., Stumpf, A. K., Vortmann, M., Jagmann, N., Krehenbrink, M., Dirks-Hofmeister, M. E., Moerschbacher, B., Philipp, B., & Wendisch, V. F. (2018). Synthetic *Escherichia coli-Corynebacterium glutamicum* consortia for l-lysine production from starch and sucrose. *Bioresource Technology*, *260*, 302–310.

Sgobba, E., & Wendisch, V. F. (2019). Synthetic microbial consortia for small molecule production. *Current opinion in biotechnology*, *62*, 72–79.

Shelton, N., Tokach, M., Goodband, R., Nelssen, J., DeRouchey, J., & Dritz, S. (2008). Effects of increasing standardized ileal digestible lysine:calorie ratio on gilts grown in a commercial finishing environment. *Kansas Agricultural Experiment Station Research Reports*, (10), 82–92.

Shepelin, D., Hansen, A. S. L., Lennen, R., Luo, H., & Herrgård, M. J. (2018). Selecting the best: evolutionary engineering of chemical production in microbes. *Genes*, *9*(5), 249.

Shimazu, M., Itaya, T., Pongcharoen, P., Sekito, T., Kawano-Kawada, M., & Kakinuma, Y. (2012). Vba5p, a novel plasma membrane protein involved in amino acid uptake and drug sensitivity in *Saccharomyces cerevisiae*. *Bioscience, Biotechnology, and Biochemistry*, *76*(10), 1993–1995.

Shin, H.-D., McClendon, S., Vo, T., & Chen, R. R. (2010). *Escherichia coli* binary culture engineered for direct fermentation of hemicellulose to a biofuel. *Applied and environmental microbiology*, *76*(24), 8150–8159.

Shou, W., Ram, S., & Vilar, J. M. G. (2007). Synthetic cooperation in engineered yeast populations. *Proceedings of the National Academy of Sciences of the United States of America*, *104*(6), 1877–1882.

Sinha, A. K., Kurtz, M., & Bhattacharjee, J. K. (1971). Effect of hydroxylysine on the biosynthesis of lysine in saccharomyces. *Journal of Bacteriology*, *108*(2), 715–719.

Sinha, A. K., & Bhattacharjee, J. K. (1971). Lysine biosynthesis in Saccharomyces. Conversion of α-aminoadipate into α-aminoadipic δ-semialdehyde. *Biochemical Journal*, *125*(3), 743–749.

Snitkin, E. S., & Segrè, D. (2011). Epistatic interaction maps relative to multiple metabolic phenotypes (T. F. C. Mackay, Ed.). *PLoS Genetics*, *7*(2), e1001294.

Stalidzans, E., & Dace, E. (2021). Sustainable metabolic engineering for sustainability optimisation of industrial biotechnology. *Computational and Structural Biotechnology Journal*, *19*, 4770–4776.

Stanford, D. R., Whitney, M. L., Hurto, R. L., Eisaman, D. M., Shen, W.-C., & Hopper, A. K. (2004). Division of labor among the yeast sol proteins implicated in tRNA nuclear export and carbohydrate metabolism. *Genetics*, *168*(1), 117–127.

Steiner, U., Schliemann, W., Böhm, H., & Strack, D. (1999). Tyrosinase involved in betalain biosynthesis of higher plants. *Planta*, *208*(1), 114–124.

Stenuit, B., & Agathos, S. N. (2015). Deciphering microbial community robustness through synthetic ecology and molecular systems synecology. *Current Opinion in Biotechnology*, *33*, 305–317.

Stewart, A. J., & Plotkin, J. B. (2012). Extortion and cooperation in the Prisoner's Dilemma. *Proceedings of the National Academy of Sciences*, *109*(26), 10134–10135.

Storts, D. R., & Bhattacharjee, J. K. (1987). Purification and properties of saccharopine dehydrogenase (glutamate forming) in the *Saccharomyces cerevisiae* lysine biosynthetic pathway. *Journal of Bacteriology*, *169*(1), 416–418.

Strassman, M., & Ceci, L. N. (1965). Enzymatic formation of alpha-ketoadipic acid from homoisocitric acid. *The Journal of Biological Chemistry*, *240*(11), 4357–4361.

Stucka, R., Dequin, S., Salmon, J.-M., & Gancedo, C. (1991). DNA sequences in chromosomes II and VII code for pyruvate carboxylase isoenzymes in *Saccharomyces cerevisiae*: analysis of pyruvate carboxylase-deficient strains. *Molecular and General Genetics MGG*, *229*(2), 307–315.

Stump, S. M., Johnson, E. C., & Klausmeier, C. A. (2018). Local interactions and self-organized spatial patterns stabilize microbial cross-feeding against cheaters. *Journal of The Royal Society Interface*, *15*(140), 20170822.

Sundström, M., Lindqvist, Y., Schneider, G., Hellman, U., & Ronne, H. (1993). Yeast *TKL1* gene encodes a transketolase that is required for efficient glycolysis and biosynthesis of aromatic amino acids. *The Journal of Biological Chemistry*, *268*(32), 24346–24352.

Sunnadeniya, R., Bean, A., Brown, M., Akhavan, N., Hatlestad, G., Gonzalez, A., Symonds, V. V., & Lloyd, A. (2016). Tyrosine hydroxylation in betalain pigment biosynthesis is performed by cytochrome P450 enzymes in beets (Beta vulgaris). *PLOS ONE*, *11*(2), e0149417.

Suvakov, M., Panda, A., Diesh, C., Holmes, I., & Abyzov, A. (2021). CNVpytor: a tool for copy number variation detection and analysis from read depth and allele imbalance in whole-genome sequencing. *GigaScience*, *10*(11), giab074.

Sychrova, H., & Chevallier, M. R. (1993). Cloning and sequencing of the *Saccharomyces cerevisiae* gene *LYP1* coding for a lysine-specific permease. *Yeast (Chichester, England)*, *9*(7), 771–782.

Sychrova, H., Matejckova, A., & Kotyk, A. (1993). Kinetic properties of yeast lysine permeases coded by genes on multi-copy vectors. *FEMS Microbiology Letters*, *113*(1), 57–61.

Szamecz, B., Boross, G., Kalapis, D., Kovács, K., Fekete, G., Farkas, Z., Lázár, V., Hrtyan, M., Kemmeren, P., Groot Koerkamp, M. J. A., Rutkai, E., Holstege, F. C. P., Papp, B., & Pál, C. (2014). The genomic landscape of compensatory evolution (N. H. Barton, Ed.). *PLoS Biology*, *12*(8), e1001935.

Tamayo Rojas, S. A., Schmidl, S., Boles, E., & Oreb, M. (2021). Glucose-induced internalization of the *S. cerevisiae* galactose permease Gal2 is dependent on phosphorylation and ubiquitination of its aminoterminal cytoplasmic tail. *FEMS yeast research*, *21*(3).

Teng, X., Dayhoff-Brannigan, M., Cheng, W.-C., Gilbert, C. E., Sing, C. N., Diny, N. L., Wheelan, S. J., Dunham, M. J., Boeke, J. D., Pineda, F. J., & Hardwick, J. M. (2013). Genome-wide consequences of deleting any single gene. *Molecular Cell*, *52*(4), 485–494.

Teng, X., & Hardwick, J. M. (2019). Whi2: a new player in amino acid sensing. *Current Genetics*, *65*(3), 701–709.

Teng, X., Yau, E., Sing, C., & Hardwick, J. M. (2018). Whi2 signals low leucine availability to halt yeast growth and cell death. *FEMS Yeast Research*, *18*(8).

Thierry, A., Khanna, V., Créno, S., Lafontaine, I., Ma, L., Bouchier, C., & Dujon, B. (2015). Macrotene chromosomes provide insights to a new mechanism of high-order gene amplification in eukaryotes. *Nature Communications*, *6*(1), 6154.

Thierry, A., Khanna, V., & Dujon, B. (2021). The formation of neochromosomes during experimental evolution in the yeast *Saccharomyces cerevisiae*. *Genes*, *12*(11), 1678.

Toda, T., Cameron, S., Sass, P., Zoller, M., Scott, J. D., McMullen, B., Hurwitz, M., Krebs, E. G., & Wigler, M. (1987). Cloning and characterization of *BCY1*, a locus encoding a regulatory subunit of the cyclic AMP-dependent protein kinase in *Saccharomyces cerevisiae*. *Molecular and Cellular Biology*, *7*(4), 1371–1377.

Toh-e, A., & Sahashi, Y. (1985). The *PET18* locus of *Saccharomyces cerevisiae*: a complex locus containing multiple genes. *Yeast (Chichester, England)*, *1*(2), 159–171.

Torbensen, R., Møller, H. D., Gresham, D., Alizadeh, S., Ochmann, D., Boles, E., & Regenberg, B. (2012). Amino acid transporter genes are essential for FLO11-dependent and FLO11-independent biofilm formation and invasive growth in *Saccharomyces cerevisiae* (M. Polymenis, Ed.). *PLoS ONE*, *7*(7), e41272.

Ubiyvovk, V. M., Blazhenko, O. V., Gigot, D., Penninckx, M., & Sibirny, A. A. (2006). Role of γ-glutamyltranspeptidase in detoxification of xenobiotics in the yeasts Hansenula polymorpha and *Saccharomyces cerevisiae*. *Cell Biology International*, *30*(8), 665–671.

Urano, J., Tabancay, A. P., Yang, W., & Tamanoi, F. (2000). The *Saccharomyces cerevisiae* Rheb G-protein is involved in regulating canavanine resistance and arginine uptake. *Journal of Biological Chemistry*, *275*(15), 11198–11206.

Urban, J., Soulard, A., Huber, A., Lippman, S., Mukhopadhyay, D., Deloche, O., Wanke, V., Anrather, D., Ammerer, G., Riezman, H., Broach, J. R., Virgilio, C. D., Hall, M. N., & Loewith, R. (2007). Sch9 is a major target of TORC1 in *Saccharomyces cerevisiae*. *Molecular Cell*, *26*(5), 663–674.

Urrestarazu, A., Vissers, S., Iraqui, I., & Grenson, M. (1998). Phenylalanine- and tyrosine-auxotrophic mutants of *Saccharomyces cerevisiae* impaired in transamination. *Molecular and General Genetics MGG*, *257*(2), 230–237.

Van Belle, D., & André, B. (2001). A genomic view of yeast membrane transporters. *Current Opinion in Cell Biology*, *13*(4), 389–398.

Van Dien, S. (2013). From the first drop to the first truckload: commercialization of microbial processes for renewable chemicals. *Current Opinion in Biotechnology*, *24*(6), 1061–1068.

Van Leeuwen, J., Pons, C., Mellor, J. C., Yamaguchi, T. N., Friesen, H., Koschwanez, J., Ušaj, M. M., Pechlaner, M., Takar, M., Ušaj, M., VanderSluis, B., Andrusiak, K., Bansal, P., Baryshnikova, A., Boone, C. E., Cao, J., Cote, A., Gebbia, M., Horecka, G., . . . Boone, C. (2016). Exploring genetic suppression interactions on a global scale. *Science*, *354*(6312), aag0839.

Van Zeebroeck, G., Bonini, B. M., Versele, M., & Thevelein, J. M. (2009). Transport and signaling via the amino acid binding site of the yeast Gap1 amino acid transceptor. *Nature Chemical Biology*, *5*(1), 45–52.

Van Zeebroeck, G., Rubio-Texeira, M., Schothorst, J., & Thevelein, J. M. (2014). Specific analogues uncouple transport, signalling, oligo-ubiquitination and endocytosis in the yeast Gap1 amino acid transceptor. *Molecular Microbiology*, *93*(2), 213–233.

van Dijken, J. P., Bauer, J., Brambilla, L., Duboc, P., Francois, J. M., Gancedo, C., Giuseppin, M. L. F., Heijnen, J. J., Hoare, M., Lange, H. C., Madden, E. A., Niederberger, P., Nielsen, J., Parrou, J. L., Petit, T., Porro, D., Reuss, M., van Riel, N., Rizzi, M., . . . Pronk, J. T. (2000). An interlaboratory comparison of physiological and genetic properties of four *Saccharomyces cerevisiae* strains. *Enzyme and Microbial Technology*, *26*(9), 706–714.

Vanhalewyn, M., Dumortier, F., Debast, G., Colombo, S., Ma, P., Winderickx, J., Van Dijck, P., & Thevelein, J. M. (1999). A mutation in *Saccharomyces cerevisiae* adenylate cyclase, Cyr1K1876M, specifically affects glucose- and acidification-induced cAMP signalling and not the basal cAMP level. *Molecular Microbiology*, *33*(2), 363–376.

Velasco, I., Tenreiro, S., Calderon, I. L., & André, B. (2004). *Saccharomyces cerevisiae* Aqr1 is an internal-membrane transporter involved in excretion of amino acids. *Eukaryotic Cell*, *3*(6), 1492–1503.

Vitte, C., & Panaud, O. (2005). LTR retrotransposons and flowering plant genome size: emergence of the increase/decrease model. *Cytogenetic and Genome Research*, *110*(1-4), 91–107.

Vuralhan, Z., Morais, M. A., Tai, S.-L., Piper, M. D. W., & Pronk, J. T. (2003). Identification and characterization of phenylpyruvate decarboxylase genes in *Saccharomyces cerevisiae*. *Applied and Environmental Microbiology*, *69*(8), 4534–4541.

Wagner, A. (2005). Energy constraints on the evolution of gene expression. *Molecular Biology and Evolution*, *22*(6), 1365–1374.

Waite, A. J., & Shou, W. (2012). Adaptation to a new environment allows cooperators to purge cheaters stochastically. *Proceedings of the National Academy of Sciences of the United States of America*, *109*(47), 19079–19086.

Walker, M. E., Val, D. L., Rohde, M., Devenish, R. J., & Wallace, J. C. (1991). Yeast pyruvate carboxylase: Identification of two genes encoding isoenzymes. *Biochemical and Biophysical Research Communications*, *176*(3), 1210–1217.

Walker, R. S. K., & Pretorius, I. S. (2018). Applications of yeast synthetic biology geared towards the production of biopharmaceuticals. *Genes*, *9*(7), 340.

Wang, Z., Bai, X., Guo, X., & He, X. (2017). Regulation of crucial enzymes and transcription factors on 2-phenylethanol biosynthesis via Ehrlich pathway in *Saccharomyces cerevisiae*. *Journal of Industrial Microbiology and Biotechnology*, *44*(1), 129–139.

Weber, C., Brückner, C., Weinreb, S., Lehr, C., Essl, C., & Boles, E. (2012). Biosynthesis of *cis*, *cis* -muconic acid and its aromatic precursors, catechol and protocatechuic acid, from renewable feedstocks by *Saccharomyces cerevisiae*. *Applied and Environmental Microbiology*, *78*(23), 8421–8430.

Wegner, A., Meiser, J., Weindl, D., & Hiller, K. (2015). How metabolites modulate metabolic flux. *Current Opinion in Biotechnology*, *34*, 16–22.

West, S. A., Diggle, S. P., Buckling, A., Gardner, A., & Griffin, A. S. (2007). The social lives of microbes. *Annual Review of Ecology, Evolution, and Systematics*, *38*(1), 53–77.

West, S. A., Griffin, A. S., Gardner, A., & Diggle, S. P. (2006). Social evolution theory for microorganisms. *Nature Reviews Microbiology*, *4*(8), 597–607.

Westman, J. O., Mapelli, V., Taherzadeh, M. J., & Franzén, C. J. (2014). Flocculation causes inhibitor tolerance in *Saccharomyces cerevisiae* for second-generation bioethanol production. *Applied and Environmental Microbiology*, *80*(22), 6908–6918.

Wickner, R. B., Fujimura, T., & Esteban, R. (1986). Overview of double-stranded RNA replication in *Saccharomyces cerevisiae*. In R. B. Wickner, A. Hinnebusch, A. M. Lambowitz, I. C. Gunsalus, A. Hollaender, J. R. Preer, L. Mets, R. I. Gumport, C. M. Wilson, & G. Kuny (Eds.), *Extrachromosomal elements in lower eukaryotes* (pp. 149–163). Springer US.

Wu, G., Yan, Q., Jones, J. A., Tang, Y. J., Fong, S. S., & Koffas, M. A. G. (2016). Metabolic burden: cornerstones in synthetic biology and metabolic engineering applications. *Trends in biotechnology*, *34*(8), 652–664.

Wuster, A., & Babu, M. M. (2009). Transcriptional control of the quorum sensing response in yeast. *Mol. BioSyst.*, *6*(1), 134–141.

Xue, Z., McCluskey, M., Cantera, K., Sariaslani, F. S., & Huang, L. (2007). Identification, characterization and functional expression of a tyrosine ammonia-lyase and its mutants from the photosynthetic bacterium *Rhodobacter sphaeroides*. *Journal of industrial microbiology & biotechnology*, *34*(9), 599–604.

Young, E. T., & Pilgrim, D. (1985). Isolation and DNA sequence of *ADH3*, a nuclear gene encoding the mitochondrial isozyme of alcohol dehydrogenase in *Saccharomyces cerevisiae*. *Molecular and Cellular Biology*, *5*(11), 3024–3034.

Zabriskie, T. M., & Jackson, M. D. (2000). Lysine biosynthesis and metabolism in fungi. *Natural Product Reports*, *17*(1), 85–97.

Zalkin, H., Paluh, J. L., van Cleemput, M., Moye, W. S., & Yanofsky, C. (1984). Nucleotide sequence of *Saccharomyces cerevisiae* genes *TRP2* and *TRP3* encoding bifunctional anthranilate synthase: indole-3-glycerol phosphate synthase. *The Journal of Biological Chemistry*, *259*(6), 3985–3992.

Zalkin, H., & Yanofsky, C. (1982). Yeast gene *TRP5*: structure, function, regulation. *The Journal of Biological Chemistry*, *257*(3), 1491–1500.

Zhang, H., Li, Z., Pereira, B., & Stephanopoulos, G. (2015). Engineering *E. coli-E. coli* cocultures for production of muconic acid from glycerol. *Microbial cell factories*, *14*, 134.

Zhang, H., Pereira, B., Li, Z., & Stephanopoulos, G. (2015). Engineering *Escherichia coli* coculture systems for the production of biochemical products. *Proceedings of the National Academy of Sciences of the United States of America*, *112*(27), 8266–8271.

Zhang, H., & Stephanopoulos, G. (2016). Co-culture engineering for microbial biosynthesis of 3-amino-benzoic acid in *Escherichia coli*. *Biotechnology Journal*, *11*(7), 981–987.

Zhang, H., & Wang, X. (2016). Modular co-culture engineering, a new approach for metabolic engineering. *Metabolic Engineering*, *37*, 114–121.

Zhang, J., Schneider, C., Ottmers, L., Rodriguez, R., Day, A., Markwardt, J., & Schneider, B. L. (2002). Genomic scale mutant hunt identifies cell size homeostasis genes in *S. cerevisiae*. *Current biology: CB*, *12*(23), 1992–2001.

Zhao, W., Zhai, F., Zhang, D., An, Y., Liu, Y., He, Y., Ge, K., & Scrimshaw, N. S. (2004). Lysine-fortified wheat flour improves the nutritional and immunological status of wheat-eating families in Northern China. *Food and Nutrition Bulletin*, *25*(2), 123–129.

Zhou, J., Wang, X., Wang, M., Chang, Y., Zhang, F., Ban, Z., Tang, R., Gan, Q., Wu, S., Guo, Y., Zhang, Q., Wang, F., Zhao, L., Jing, Y., Qian, W., Wang, G., Guo, W., & Yang, C. (2019). The lysine catabolite saccharopine impairs development by disrupting mitochondrial homeostasis. *Journal of Cell Biology*, *218*(2), 580–597.

Zhou, K., Qiao, K., Edgar, S., & Stephanopoulos, G. (2015). Distributing a metabolic pathway among a microbial consortium enhances production of natural products. *Nature biotechnology*, *33*(4), 377–383.

Zhou, K., Zou, R., Stephanopoulos, G., & Too, H.-P. (2012). Metabolite profiling identified methylerythritol cyclodiphosphate efflux as a limiting step in microbial isoprenoid production. *PLOS ONE*, *7*(11), e47513.

Zou, W., Yan, J., Zhao, N., Niu, S., & Huang, X. (2015). A novel role for the alcohol sensitive ring/PHD finger protein Asr1p in regulating cell cycle mediated by septin-dependent assembly in yeast. *Biochemical and Biophysical Research Communications*, *458*(1), 208–213.

Zupan, J., Avbelj, M., Butinar, B., Kosel, J., Šergan, M., & Raspor, P. (2013). Monitoring of quorum-sensing molecules during minifermentation studies in wine yeast. *Journal of Agricultural and Food Chemistry*, *61*(10), 2496–2505.

Chapter: 7 Summaries

7.1 Summary in English language

Microbial consortia represent a promising alternative to tackle traditional problems in industrial biotechnology, such as low titers and increased metabolic burden derived from complex metabolic pathways. Nevertheless, achieving and maintaining a proper balance within these consortia can be challenging due to various factors, including differences in growth rates and response to toxins. In this sense, cooperative cross-feeding systems allow for an alternative, as mutually dependent strains can promote mutual survival and stability while taking advantage of their natural or engineered metabolic capacities.

Several studies have investigated cooperative systems using *S. cerevisiae* as a model organism. This yeast is well understood, making it an ideal choice to gain insights into cross-feeding systems' development, regulation, and population control processes. However, traditional engineering approaches are limited by the available knowledge of its metabolic pathways and regulatory processes. Adaptive laboratory evolution (ALE) offers an interesting alternative to tackle these limitations. By harnessing the mutation capacity and short replication times of *S. cerevisiae*, ALE produces better-adapted strains to particular environmental conditions, allowing innovative solutions to otherwise complex limitations.

By using ALE as a tool to induce mutations that would improve consortia cooperation, this project aimed to advance our understanding of the conformation of microbial cooperative systems while using *S. cerevisiae* as a model organism. After developing a synthetic cooperative consortium centred around the exchange of lysine and tyrosine, ALE was employed to promote the generation of mutations that would positively impact the system's fitness. The most relevant variations produced were analysed to establish their role in the newly developed phenotypes, either by improving production or enhancing stress resistance.

A cooperative system using *S. cerevisiae* was built around the exchange of two amino acids. In this sense, two strains were developed: K0, a tyrosine auxotrophic lysine overproducer with a deletion in the gene *TYR1* and a feedback-resistant variant of *LYS21* for lysine overproduction, and Y0, an aromatic amino acid overproducing lysine auxotrophic strain with a *LYS1* deletion and feedback-resistant variants for the DAHP synthases *ARO3* and *ARO4*.

The newly developed strains failed to demonstrate successful complementarity in SCD-lys-tyr agar media. However, they successfully sustain growth while using liquid media under high cell density conditions. The co-culture was submitted to ten ALE rounds of consecutive growth and dilution to accumulate mutations that could improve system fitness.

Evolved tyrosine producer strains isolated after the evolution were assessed for their ability to produce p-hydroxyphenyl ethanol (pPET), a direct tyrosine metabolite through the Ehrlich pathway. Interestingly, normalised titers from isolated strains presented continuous variations between fermentations. From this batch of evolved strains, three were randomly selected for subsequent analysis, being the most relevant Y1. They all showed to promote co-culture development more efficiently than their parental strain Y0. However, they showed a worse performance during single cultures.

Lysine-overproducer evolved strains were assessed solely based on their ability to promote fast co-culture development. Three strains were selected for further analysis.

The Y1 strain was modified to express a specific dominant marker to simplify the isolation process, creating the Y1.2 strain. However, pPET titters from this strain were higher than those observed in Y1. Growth behaviours were also unexpected, making it more similar to its unevolved ancestor, Y0, than to its direct predecessor, Y1.

A second round of evolution was planned to increase the likelihood of obtaining favourable mutations. This involved creating a new co-culture consisting of a tyrosine overproducer evolved strain (Y1.2), an unevolved K0 strain, and a tyrosine auxotrophic strain without a lysine overproducing mechanism. The goal was to have the strain without the lysine overproducing mechanism act parasitically, reducing the tyrosine pool in the media and hindering the consortia's survival. This increased selective pressure was expected to promote mutations that would improve amino acid production or its uptake.

After ten passages using SMD+ura media, tyrosine-producer evolved strains were assessed by their pPET titers, obtaining the strain Y2. Although this strain showed a slight increase in its ability to produce pPET, it also revealed to have regained some of the characteristic growth phenotype from Y1. However, the differences were less pronounced than those obtained during the first evolution process.

The survival and thriving of cooperative consortia remain a controversial topic in biology. Evolution and selection for cooperative behaviours seem to contradict the best interest of individual cells, as systems that depend on the production of "common goods" are ex-

pected to favour the evolution of cheater cells that feed from available resources without incurring the cost of generating them. The results obtained in this project align with the theory of the "adaptive race," which suggests that the development and evolution of a cooperative system involves competition between parasitic and cooperative factions. In this sense, it is theorised that variations promoting increased resistance appeared first in cooperator strains rather than in cheating mutants, which enabled the successful development of the consortia studied in this project.

A whole-genome sequencing analysis was performed for the representative strains obtained after the first evolution process, derived from K0 and Y0, together with the strains Y1.2 and Y2. The study revealed no relevant mutations that could be linked to an increase in amino acid production for either population. To further elucidate the increased output of pPET on the evolved tyrosine producer strains, other proxy molecules were studied, such as betaxanthins and p-coumaric acid.

Betaxanthins are plant-derived pigments that produce a clear, deep-yellow colouration visible to the naked eye. However, the evolved strains presented an unexpected red colouration pattern after transforming the required heterologous pathways. Such colouration is suspected to be caused by an unspecific oxidase activity, which is alleged to derive from the stress conditions experienced by the evolved strains during the evolution passages.

p-Coumaric acid, a deaminated form of tyrosine, was also employed as an additional proxy molecule to establish tyrosine overproduction. Its determination failed to evidence increased tyrosine production from evolved strains, mimicking the results obtained for pPET determination. Direct tyrosine determination on all the interest strains also failed to evidence increased tyrosine secretion.

Despite these results, a clear indication of increased carbon flow into the aromatic amino acids pathway was observed after the deletion of *ARO10*. This phenylpyruvate decarboxylase transforms p-hydroxyphenylpyruvate (HPP) into phenylacetaldehyde in the second step of the Ehrlich pathway. During an agar plate feeding experiment, this deletion showed that all the evolved tyrosine producer strains successfully sustained the growth of tyrosine auxotrophic strains. However, it is suspected that HPP was the molecule responsible for these results, which, after being imported by *tyr1* strains, could allow them to supplement their auxotrophy.

A possible explanation for the increased production of pPET in evolved strains came from

the role of fusel alcohols as quorum sensing molecules (QSMs). It was theorised that the feedback-resistant DAHP synthase variants integrated into these strains, besides pPET would also produce other fusel alcohols such as phenylethanol or tryptophol. These molecules, particularly tryptophol, have been reported to exert a positive effect upon cell density during cultures, acting as inducers of several genes in the aromatic amino acid and Ehrlich pathway, promoting a positive feedback loop over the production of fusel alcohols. In this context, any favourable mutations present in evolved tyrosine producer strains that would prompt a faster biomass development will amplify the production of fusel alcohols. This theory could explain the variation in pPET titers observed in evolved strains, as they would be product not only from overproducing mechanisms but also as a loop response tied to biomass growth.

The data obtained from the whole genome analysis of the evolved strains was used to establish copy number variation analysis. The results suggested that the evolved tyrosine-producer cells share a partial duplication for chromosome XIV. This abnormality is suggested as a factor for the improved co-culture performance demonstrated by the evolved tyrosine producer strains, as it is the only relevant difference between the strain Y1.2 and its parental Y1.

Additionally, several interesting variations that improve cell fitness were identified. Such as a loss of function mutation on the *ART2* gene, common for all evolved tyrosine producers obtained after the first round. This gene codes for an α-arrestin involved in the endocytosis process of several amino acid transporters, especially under low substrate conditions. Cells expressing this mutation showed a more stable Lyp1p lysine transporter under low lysine conditions, which was beneficial for fast single and consortia growth. The α-arrestin Art2p also participates in the ubiquitination process of other transporters, such as Can1p or Tat2p, whose stability is also expected to improve under low lysine conditions.

Another interesting mutation in evolved tyrosine producer strains was a loss of function mutation in the *LYS9* gene, located in a non-functional biosynthetic pathway, as these strains cannot synthesise lysine. This mutation produces improved growth under consortia conditions but a growth deficit under single-strain growth conditions. However, this phenotype could not be related to a reduced metabolic burden, a remanent function of the mutant Lys9p, the accumulation of toxic intermediate metabolites, or a possible cross-effect modulation over other metabolic pathways. A theory was proposed to explain this unusual phenotype, which involved the secretion of the Lys9p substrate, 2-

aminoadipate-6-semialdehyde (ASA), a molecule that could later be fed into the lysine biosynthesis pathway in prototrophic cells, increasing its global production.

Another relevant mutation detected during the evolution processes involved a loss of function in the *WHI2* gene. Whi2p is a negative regulator for the TORC1 system, a major regulatory complex that modulates cell response to different environmental conditions. Low nitrogen and amino acid conditions, particularly leucine, have been observed to trigger the regulatory role of Whi2p over the TORC1 complex. In this context, it was interesting to obtain two loss of function mutations on *WHI2* in response to different conditions: one was detected in the evolved lysine producer strains after the first evolution round, while the second variation was discovered in the strain Y2, an evolved tyrosine producer isolated after the second evolution round. Growth analysis performed on this mutation suggests that the regulatory role of Whi2p upon TORC1 seems not to depend solely on leucine but also on a low lysine and tyrosine concentration in the media.

The variations observed during the current project highlight the importance of individual strain fitness for the proper development of consortia. Improved stability of amino acid transporters and reduced growth constraints caused by the TORC1 system can benefit consortia development.

7.2   Summary in German Language

Mikrobielle Konsortien stellen eine vielversprechende Alternative dar, um traditionelle Probleme in der industriellen Biotechnologie zu bewältigen, wie geringe Titer und erhöhte metabolische Belastungen aufgrund komplexer Stoffwechselwege. Dennoch kann es herausfordernd sein, ein angemessenes Gleichgewicht in diesen Konsortien zu erreichen und aufrechtzuerhalten, aufgrund verschiedener Faktoren, einschließlich Unterschieden in Wachstumsraten und Reaktionen auf toxische oder inhibierende Substanzen. In diesem Sinne ermöglichen kooperative Konsortien eine Alternative, da voneinander abhängige Stämme gegenseitig das Überleben und die Stabilität fördern können, während sie von ihren natürlichen oder modifizierten Stoffwechselkapazitäten profitieren.

Mehrere Studien haben kooperative Systeme unter Verwendung von *S. cerevisiae* als Modellorganismus untersucht. Diese Hefe ist gut verstanden und eignet sich daher ideal, um Einblicke in die Entwicklung, Regulation und Populationskontrollprozesse von Konsortien zu gewinnen. Traditionelle *Metabolic Engineering* Ansätze sind jedoch durch das verfügbare Wissen über Stoffwechselwege und regulatorische Prozesse begrenzt. Die *Adaptive Laboratory Evolution* (ALE) bietet eine interessante Alternative, um diese Einschränkungen zu bewältigen. Durch die Nutzung der Mutationskapazität und kurzen Replikationszeiten von *S. cerevisiae* erzeugt ALE besser angepasste Stämme für bestimmte Umweltbedingungen, was innovative Lösungen für sonst komplexe Einschränkungen ermöglicht.

Durch den Einsatz von ALE als Werkzeug zur Induktion von Mutationen, die die Zusammenarbeit von Konsortien verbessern, sollte dieses Projekt unser Verständnis für die Entwicklung mikrobieller kooperativer Systeme verbessern, wobei *S. cerevisiae* als Modellorganismus diente. Nach der Entwicklung eines synthetischen kooperativen Konsortiums, das sich auf den Austausch von Lysin und Tyrosin konzentriert, wurde ALE eingesetzt, um Mutationen zu selektieren, die sich positiv auf die Fitness des Systems auswirken. Die wichtigsten erzeugten Variationen wurden analysiert, um festzustellen, welche Rolle sie bei den neu evolvierten Phänotypen spielen, indem sie entweder die Produktion verbessern oder die Stressresistenz erhöhen.

Ein kooperatives System unter Verwendung von *S. cerevisiae* wurde rund um den Austausch von zwei Aminosäuren aufgebaut. In diesem Sinne wurden zwei Stämme entwickelt: K0, ein Tyrosin-auxotropher Lysin-Überproduzent mit einer Deletion im Gen *TYR1* und einer konstitutiv aktiven Variante von *LYS21* zur Lysinüberproduktion, und Y0, ein

aromatische Aminosäuren-überproduzierender Lysin-auxotropher Stamm mit einer *LYS1* Deletion und konstitutiv aktiven Varianten der DAHP-Synthasen *ARO3* und *ARO4*.

Die neu evolvierten Stämme zeigten keine erfolgreiche Komplementarität auf SCD-lys-tyr Agarmedien. Sie konnten jedoch unter bestimmten Zelldichtebedingungen erfolgreich im Flüssigmedium wachsen. Die Kokultur wurde zehn aufeinanderfolgenden Wachstums und Verdünnungsrunden (ALE) unterzogen, um Mutationen zu akkumulieren, die die Fitness des Systems verbessern könnten.

Die evolvierten Tyrosin-produzierenden Stämme, die nach der Evolution isoliert wurden, wurden auf ihre Fähigkeit zur Produktion von *p*-Hydroxyphenyl-Ethanol (pPET), einem direkten Tyrosinmetaboliten über den Ehrlich-Weg, überprüft. Interessanterweise zeigten normalisierte Titer-werte von isolierten Stämmen kontinuierliche Variationen zwischen den Fermentationen. Aus dieser Gruppe von evolvierten Stämmen wurden drei zufällig für weitere Analysen ausgewählt, wobei Y1 der relevanteste war. Alle zeigten sich effizienter in der Förderung der Entwicklung der Kokultur im Vergleich zu ihrem Ausgangsstamm Y0. Sie zeigten jedoch ein schlechteres Wachstum, wenn sie alleine kultiviert wurden.

Die evolvierten Lysin-überproduzierenden Stämme wurden allein aufgrund ihrer Fähigkeit zur schnellen Förderung der Kokultur untersucht. Drei Stämme wurden für weitere Analysen ausgewählt.

Der Y1-Stamm wurde modifiziert, um einen spezifischen dominanten Marker zur Vereinfachung des Isolationsprozesses zu exprimieren, was zur Schaffung des Y1.2-Stamms führte. Die pPET-Titer in diesem Stamm waren jedoch höher als die in Y1 beobachteten. Das Wachstumsverhalten war ebenfalls unerwartet und ähnelte eher dem Ausgangsstamm Y0 als seinem direkten Vorgänger Y1.

Ein zweiter Evolutionsprozess wurde geplant, um die Wahrscheinlichkeit günstiger Mutationen zu erhöhen. Dies beinhaltete die Schaffung einer neuen Kokultur, bestehend aus einem evolvierten Tyrosinüberproduzenten (Y1.2), einem nicht evolvierten K0-Stamm und einem Tyrosin-auxotrophen Stamm ohne Lysin-überproduzierenden Mechanismus. Das Ziel war es, den Stamm ohne Lysin-überproduzierenden Mechanismus („*Cheater*") parasitär handeln zu lassen, indem er den Tyrosinpool im Medium reduziert und das Überleben der Konsortien behindert. Es wurde erwartet, dass dieser erhöhte Selektionsdruck Mutationen fördert, die die Aminosäureproduktion oder ihre Aufnahme verbessern.

Nach zehn Passagen unter Verwendung von SMD+ura-Medium wurden die evolvierten

Tyrosin-Produzentenstämme anhand ihrer pPET-Titer bewertet, wodurch der Stamm Y2 erhalten wurde. Obwohl dieser Stamm eine leichte Steigerung seiner Fähigkeit zur Produktion von pPET zeigte, hatte er auch einige der charakteristischen Wachstumsphänotypen von Y1 wiedererlangt. Die Unterschiede waren jedoch weniger ausgeprägt als die während des ersten Evolutionsprozesses beobachteten.

Das Überleben und Gedeihen kooperativer Konsortien bleiben ein umstrittenes Thema in der Biologie. Die Evolution und Auswahl für kooperatives Verhalten scheinen dem besten Interesse einzelner Zellen zu widersprechen, da Systeme, die von der Produktion „gemeinsamer Güter" abhängen, die Evolution von *„Cheater"*-Zellen begünstigen sollen, die von verfügbaren Ressourcen profitieren, ohne die Kosten für deren Erzeugung zu tragen. Die in diesem Projekt erzielten Ergebnisse stimmen mit der Theorie des „adaptiven Rennens" überein, die besagt, dass die Entwicklung und Evolution eines kooperativen Systems einen Wettbewerb zwischen parasitären und kooperierenden Fraktionen beinhaltet. In diesem Sinne wird vermutet, dass Variationen, die eine erhöhte Resistenz fördern, zuerst in Kooperationsstämmen auftraten und nicht in *Cheater* Mutanten, was die erfolgreiche Entwicklung der in diesem Projekt untersuchten Konsortien ermöglichte.

Eine Sequenzierungsanalyse des gesamten Genoms wurde für die repräsentativen Stämme durchgeführt, die nach dem ersten Evolutionsprozess von K0 und Y0 sowie den Stämmen Y1.2 und Y2 erhalten wurden. Die Studie ergab keine relevanten Mutationen, die mit einer Steigerung der Aminosäureproduktion für beide Populationen in Verbindung gebracht werden konnten. Um die erhöhte Produktion von pPET bei den evolvierten Tyrosin-Produzentenstämmen weiter zu klären, wurden auch andere Proxy-Moleküle untersucht, wie Betaxanthin und *p*-Cumarsäure.

Betaxanthine sind pflanzliche Pigmente, die eine tiefgelbe, für das menschliche Auge sichtbare Färbung erzeugen. Nach der Transformation der erforderlichen heterologen Wege zeigten die evolvierten Stämme jedoch ein unerwartetes Muster von roter Färbung. Diese Färbung wird vermutlich durch eine unspezifische Oxidaseaktivität verursacht, die möglicherweise von den evolvierten Stämmen während der Evolutionspassagen aufgrund von Stressbedingungen abgeleitet ist.

p-Cumarsäure, eine deaminierte Form von Tyrosin, wurde ebenfalls als zusätzliches Proxy-Molekül zur Bestimmung der Tyrosinüberproduktion verwendet. Diese Bestimmung konnte keine erhöhte Tyrosin-Produktion von den evolvierten Stämmen nachweisen, was den für die pPET-Bestimmung erhaltenen Ergebnissen ähnelte. Die direkte Tyrosinbestimmung bei allen untersuchten Stämmen ergab ebenfalls keine erhöhte Tyrosinsekretion.

Trotz dieser Ergebnisse wurde ein klarer Anstieg der Kohlenstoffflussrate in den aromatischen Aminosäureweg nach der Deletion von *ARO10* beobachtet. Diese Phenylpyruvat-Decarboxylase wandelt *p*-Hydroxyphenylpyruvat (HPP) während des zweiten Schritts des Ehrlich-Weges in Phenylacetaldehyd um. Während eines Agarplatten-Fütterungsexperiments zeigte diese Deletion, dass alle evolvierten Tyrosin-Produzentenstämme das Wachstum von Tyrosin-auxotrophen Stämmen erfolgreich aufrechterhalten konnten. Es wird jedoch vermutet, dass HPP das Molekül war, das für diese Ergebnisse verantwortlich war und dass, nachdem es von den *tyr1*-Stämmen importiert wurde, diesen erlauben könnte, ihre Auxotrophie zu umgehen.

Eine mögliche Erklärung für die erhöhte Produktion von pPET in den evolvierten Stämmen stammte aus der Rolle der Fuselalkohole als Quorum Sensing Moleküle (QSMs). Es wurde vermutet, dass die Konstitutiv Aktiven DAHP-Synthase-Varianten, die in diese Stämme integriert wurden, neben pPET auch die Produktion anderer Fuselalkohole wie Phenylethanol oder Tryptophol Steigern würden. Es wurde berichtet, dass diese Moleküle, insbesondere Tryptophol, eine positive Wirkung auf die Zelldichte der Kulturen ausüben, indem sie als Induktoren mehrerer Gene im aromatischen Aminosäure- und Ehrlich-Weg wirken.Durch einen positiven *Feedback-Loop* wird die Produktion von Fuselalkoholen gefördert.In diesem Zusammenhang könnten günstige Mutationen in den evolvierten Tyrosin-Produzentenstämmen, die eine schnellere Biomassenentwicklung fördern, die Produktion von Fuselalkoholen verstärken. Diese Theorie könnte die beobachteten Variationen in den pPET-Titern in den evolvierten Stämmen erklären, da diese nicht nur von Überproduktionsmechanismen stammen würden, sondern auch als Reaktion auf das Wachstum der Biomasse.

Die aus der Ganzgenomanalyse der evolvierten Stämme erhaltenen Daten, wurden zur Etablierung einer Analyse von Kopienzahlvariationen verwendet. Die Ergebnisse legten nahe, dass in die evolvierten Tyrosin-Produzentenzellen eine teilweise Duplikation von Chromosom XIV entstanden ist. Diese Anomalie wird als ein Faktor für die verbesserte Leistung der evolvierten Tyrosin-Produzentenstämme vorgeschlagen, da sie der einzige relevante Unterschied zwischen dem Stamm Y1.2 und seinem Elternstamm Y1 ist.

Darüber hinaus wurden mehrere interessante Variationen identifiziert, die die Zellfitness verbessern. Dazu gehörte eine Funktionsverlustmutation im Gen *ART2*, die bei allen evolvierten Tyrosinproduzenten nach der ersten Runde auftrat. Dieses Gen codiert für ein *α*-Arrestin, das am Endozytoseprozess mehrerer Aminosäuretransporter beteiligt ist, insbesondere unter niedrigen Substratbedingungen. Zellen, die diese Mutation exprimie-

ren, zeigten einen stabileren Lyp1p-Transporter unter Bedingungen mit niedrigen Lysin Konzentration, was für ein schnelles Einzel- und Konsortien Wachstum von Vorteil war. Das α-Arrestin Art2p ist auch am Ubiquitinierungsprozess anderer Transporter wie Can1p oder Tat2p beteiligt, deren Stabilität ebenfalls unter geringeren Lysin Konzentration verbessert werden soll.

Eine weitere interessante Mutation in den evolvierten Tyrosin-Produzentenstämmen war ein Funktionsverlust des Gen *LYS9*, das sich in einem nicht funktionellen Biosyntheseweg befindet, da diese Stämme kein Lysin synthetisieren können. Diese Mutation führte zu verbessertem Wachstum unter Konsortienbedingungen, jedoch zu einem Wachstumsdefizit unter Bedingungen mit Einzelstammwachstum. Dieses Phänomen konnte jedoch nicht mit einer reduzierten metabolischen Belastung, einer verbleibenden Funktion des mutierten Lys9p, der Anhäufung toxischer Zwischenmetabolite oder einer möglichen Kreuzeffektmodulation über andere Stoffwechselwege in Verbindung gebracht werden. Es wurde eine Theorie vorgeschlagen, um dieses ungewöhnliche Phänomen zu erklären, die die Ausscheidung des Lys9p-Substrats, 2-Aminoadipat-6-semialdehyd (ASA), einem Molekül, das später in den Lysinbiosyntheseweg in prototrophen Zellen eingeschleust werden könnte, um die globale Produktion zu erhöhen.

Eine weitere relevante Mutation, die während der Evolutionsprozesse festgestellt wurde, war ein Funktionsverlust im Gen *WHI2*. Whi2p ist ein negativer Regulator für das TORC1-System, ein wichtiger Regulierungskomplex, der die Zellantwort auf verschiedene Umweltbedingungen moduliert. Es wurde beobachtet, dass niedrige Stickstoff- und Aminosäurebedingungen, vor allem Leucin, die regulatorische Rolle von Whi2p über den TORC1-Komplex auslösen. In diesem Zusammenhang war es interessant, zwei Funktionsverlustmutationen in *WHI2* als Reaktion auf verschiedene Bedingungen zu erhalten: eine wurde bei den evolvierten Lysin-Produzentenstämmen nach der ersten Runde gefunden, während die zweite Variation im Stamm Y2 entdeckt wurde, einem evolvierten Tyrosin-Produzenten, der nach der zweiten Evolutionsrunde isoliert wurde. Wachstumsanalysen, die an dieser Mutanten durchgeführt wurden, deuten darauf hin, dass die regulatorische Rolle von Whi2p auf den TORC1 scheinbar nicht nur von Leucin, sondern auch von niedriger Lysin- und Tyrosinkonzentration im Medium abhängt.

Die während des aktuellen Projekts beobachteten Variationen unterstreichen die Bedeutung der individuellen Stammfitness für die Entwicklung von Konsortien. Eine verbesserte Stabilität der Aminosäuretransporter und reduzierte Wachstumsbeschränkungen durch das TORC1-System können die Entwicklung von Konsortien begünstigen.

Chapter: 8 List of abbreviations

Abbreviation	Definition
Δ (gene)	deletion
μL	microliter
μM	micro molar
μm	micro meter
%	percent
°C	degrees celcius
F1,6BP	fructose-1,6-biphosphate
6PGA	6-phosphogluconate
6PGL	6-phosphogluconolactone
a.u.	artificial units
ALE	adaptive laboratory evolution
AmpR	β-lactamase gene
ASA	2-aminoadipate-6-semialdehyde
ATP	adenosine triphosphate
b (game theory yield)	benefit
bp	base pair
C (game theory behaviour)	cooperate
c (game theory yield)	cost
CamR	chloramphenicol acetyltransferase gene
ClonNAT	nourseothricin N-acetyltransferase gene
CNV	copy number variations
CO_2	carbon dioxide
CoA	coenzyme A
CRISPR	clustered regularly interspaced short palindromic repeats
D (game theory behaviour)	defect
DAHP	3-deoxy-D-arabino-heptulosonate-7-phosphate
ddH_2O	double distilled water
DHAP	dihydroxyacetone phosphate
DNA	desoxyribonucleic acid
DOD	DOPA dioxygenase
e.g.	exempli gratia, Latin
e.i.	id est, Latin
E4P	erythrose-4-phosphate
EPSP	5-enolpyruvylshikimate-3-phosphate
et al.	et alii, Latin
F (amino acid)	phenylalanine
F6P	fructose-6-phosphate
fw	forward primer
g	centrifugal force
g (mass)	grams
G3P	glyceraldehyde-3-phosphate
G418	geneticin
G6P	glucose-6-phosphate
HPLC	high performance liquid chromatography
HPP	hydroxyphenylpyruvate

Abbreviation	Definition
Hyg	hygromycin B
K (amino acid)	lysine
KanMX	aminoglycoside phosphotransferase gene
Kan	neomycin phosphotransferase II gene
kb	kilo base
L	liter
L-DOPA	L-3,4-dihydroxyphenylalanine
mg	mili gram
min	minute
mM	mili molar
mol	mole
NAD+	nicotinamide adenine dinucleotide, oxidized
NADH	nicotinamide adenine dinucleotide, reduced
NADP+	nicotinamide adenine dinucleotide phosphate, oxidized
NADPH	nicotinamide adenine dinucleotide phosphate, reduced
ng	nano gram
nm	nano meters
OD_{600}	optical density measured at wavelength 600nm
ORF	open reading frame
P (amino acid)	proline
pCA	*p*-coumaric acid
PCR	polymerase chain reaction
PD	prisoner's dilemma
PEP	phosphoenolpyruvate
pH	potential of hydrogen
PHD	plant homeodomain
pPET	*p*-hydroxyphenyl ethanol
PPP	pentose phosphate pathway
QSMs	quorum sensing molecules
R5P	ribose-5-phosphate
RD [CN]	read-depth signal
RNA	ribonucleic acid
rpm	revolutions per minute
rRNA	ribosomal RNA
Ru5P	ribulose-5-phosphate
rv	reverse primer
sec	second
S7P	sedoheptulose-7-phosphate
TAL	tyrosine ammonia-lyase
TCA-cycle	tricarboxylic acid cycle, citric acid cycle
U	unit (enzyme activity)
w/v	weight per volume
WT	wild type
X5P	xylulose-5-phosphate
Y (amino acid)	tyrosine

Chapter: 9 Acknowledgements

I would like to thank Prof. Dr. Eckhard Boles for the opportunity to carry out this passionating project in his group, for all the support with experiments and data interpretation, and for the guidance and openness I found in this group. I will always appreciate this. To Dr. Mislav Oreb for all the valuable discussions, comments and challenges to my interpretations, and to Prof. Dr. Claudia Büchel for participating as the second reviewer for this work.

I would like to thank all the people at AK Boles for being the team that made this project possible. From the discussions during seminars and lunches with fellow PhD and Masters students, postdocs, and technicians came great insights and encouragement to complete this project. Thanks to Sebastian, Sandra, Kilan, Priti, Fernando, Simon, Sina, Julia B., Joanna, Julia H., Johannes, Charlotte, and Christine for your support and friendship that made me feel at home while conducting this project. To my students, Betty, Lukas and Julia, for their hard work and dedication. To Susanne for her friendship and for always being available and willing to help with administrative requirements.

I would like to thank the DAAD (Deutscher Akademischer Austauschdienst) and the SENESCYT (Secretaría de Educación Superior, Ciencia, Tecnología e Innovación) from the Ecuadorian government for the kind sponsorship during this project.

Very special thanks to my parents, Vicente and Mariela, for their unconditional love and support, and to my siblings, Pamela and Paúl, for being my advisors, friends and partners in crime. Growing up at your side has been a privilege. To Cristian and Cristina, more than friends, you were our family in the old continent. But most importantly, to Dianny, my wife, who has been my partner, strength and motor throughout this journey and will continue to be in the years to come. And to Theo, my son, who has been a joy and inspiration since the moment he joined our lives.

A todos ustedes, muchas gracias.

Chapter: 10 Curriculum Vitae

LEONARDO JAVIER BELTRÁN GUZMÁN